



**HAL**  
open science

# Integration of an in vitro blood brain barrier model with organic electrochemical transistors

Manuelle Bongo

► **To cite this version:**

Manuelle Bongo. Integration of an in vitro blood brain barrier model with organic electrochemical transistors. Other. Ecole Nationale Supérieure des Mines de Saint-Etienne, 2014. English. NNT : 2014EMSE0753 . tel-01132605

**HAL Id: tel-01132605**

**<https://theses.hal.science/tel-01132605>**

Submitted on 17 Mar 2015

**HAL** is a multi-disciplinary open access archive for the deposit and dissemination of scientific research documents, whether they are published or not. The documents may come from teaching and research institutions in France or abroad, or from public or private research centers.

L'archive ouverte pluridisciplinaire **HAL**, est destinée au dépôt et à la diffusion de documents scientifiques de niveau recherche, publiés ou non, émanant des établissements d'enseignement et de recherche français ou étrangers, des laboratoires publics ou privés.



NNT : 2014 EMSE 0753

## THÈSE

présentée par

**Manuelle BONGO**

pour obtenir le grade de  
Docteur de l'École Nationale Supérieure des Mines de Saint-Étienne

Spécialité : Bioélectronique

### **Integration of an *in vitro* blood brain barrier model with organic electrochemical transistors**

soutenue à Gardanne, le 29 septembre 2014

#### Membres du jury

Président :	Pierre-Olivier COURAUD	Directeur de Recherche (DRCE) INSERM, Institut Cochin, Paris
Rapporteurs :	Susan DANIEL	Professeur, School of Chemical and Bio molecular Engineering Cornell University , Ithaca
	Noëlle CALLIZOT	Pharmacienne, Neurosys, Gardanne
Co-encadrant :	Roisin OWENS	Maître Assistante , ENSMSE, Gardanne
Directeur de thèse :	George MALLIARAS	Professeur, ENSMSE, Gardanne

*A mes parents, Manuel et Aurélie BONGO  
« Quand on veut, on peut. »*

Spécialités doctorales	Responsables	Spécialités doctorales	Responsables
SCIENCES ET GENIE DES MATERIAUX	K. Wolski Directeur de recherche	MATHEMATIQUES APPLIQUEES	O. Roustant, Maître-assistant
MECANIQUE ET INGENIERIE	S. Drapier, professeur	INFORMATIQUE	O. Boissier, Professeur
GENIE DES PROCÉDES	F. Gruy, Maître de recherche	IMAGE, VISION, SIGNAL	JC. Pinoli, Professeur
SCIENCES DE LA TERRE	B. Guy, Directeur de recherche	GENIE INDUSTRIEL	A. Dolgui, Professeur
SCIENCES ET GENIE DE L'ENVIRONNEMENT	D. Graillot, Directeur de recherche	MICROELECTRONIQUE	S. Dauzere Peres, Professeur

EMSE : Enseignants-chercheurs et chercheurs autorisés à diriger des thèses de doctorat (titulaires d'un doctorat d'État ou d'une HDR)				
ABSI	Nabil	CR		CMP
AVRIL	Stéphane	PR2	Mécanique et ingénierie	CIS
BALBO	Flavien	PR2		FAYOL
BASSEREAU	Jean-François	PR		SMS
BATTON-HUBERT	Mireille	PR2	Sciences et génie de l'environnement	FAYOL
BERGER DOUCE	Sandrine	PR2		FAYOL
BERNACHE-ASSOLLANT	Didier	PR0	Génie des Procédés	CIS
BIGOT	Jean Pierre	MR(DR2)	Génie des Procédés	SPIN
BILAL	Essaid	DR	Sciences de la Terre	SPIN
BOISSIER	Olivier	PR1	Informatique	FAYOL
BORBELY	Andras	MR(DR2)	Sciences et génie des matériaux	SMS
BOUCHER	Xavier	PR2	Génie Industriel	FAYOL
BRODHAG	Christian	DR	Sciences et génie de l'environnement	FAYOL
BRUCHON	Julien	MA(MDC)	Mécanique et ingénierie	SMS
BURLAT	Patrick	PR2	Génie Industriel	FAYOL
COURNIL	Michel	PR0	Génie des Procédés	DIR
DARRIEULAT	Michel	IGM	Sciences et génie des matériaux	SMS
DAUZERE-PERES	Stéphane	PR1	Génie Industriel	CMP
DEBAYLE	Johan	CR	Image Vision Signal	CIS
DELAFOSSÉ	David	PR1	Sciences et génie des matériaux	SMS
DESRAYAUD	Christophe	PR2	Mécanique et ingénierie	SMS
DOLGUI	Alexandre	PR0	Génie Industriel	FAYOL
DRAPIER	Sylvain	PR1	Mécanique et ingénierie	SMS
FEILLET	Dominique	PR2	Génie Industriel	CMP
FEVOTTE	Gilles	PR1	Génie des Procédés	SPIN
FRACZKIEWICZ	Anna	DR	Sciences et génie des matériaux	SMS
GARCIA	Daniel	MR(DR2)	Génie des Procédés	SPIN
GERINGER	Jean	MA(MDC)	Sciences et génie des matériaux	CIS
GOEURIOT	Dominique	DR	Sciences et génie des matériaux	SMS
GRAILLOT	Didier	DR	Sciences et génie de l'environnement	SPIN
GROSSEAU	Philippe	DR	Génie des Procédés	SPIN
GRUY	Frédéric	PR1	Génie des Procédés	SPIN
GUY	Bernard	DR	Sciences de la Terre	SPIN
HAN	Woo-Suck	CR	Mécanique et ingénierie	SMS
HERRI	Jean Michel	PR1	Génie des Procédés	SPIN
KERMOUCHE	Guillaume	PR2	Mécanique et Ingénierie	SMS
KLOCKER	Helmut	DR	Sciences et génie des matériaux	SMS
LAFOREST	Valérie	MR(DR2)	Sciences et génie de l'environnement	FAYOL
LERICHE	Rodolphe	CR	Mécanique et ingénierie	FAYOL
LI	Jean-Michel		Microélectronique	CMP
MALLIARAS	Georges	PR1	Microélectronique	CMP
MOLIMARD	Jérôme	PR2	Mécanique et ingénierie	CIS
MONTHILLET	Frank	DR	Sciences et génie des matériaux	SMS
MOUTTE	Jacques	CR	Génie des Procédés	SPIN
NEUBERT	Gilles			FAYOL
NIKOLOVSKI	Jean-Pierre			CMP
NORTIER	Patrice	PR1		SPIN
PIJOLAT	Christophe	PR0	Génie des Procédés	SPIN
PIJOLAT	Michèle	PR1	Génie des Procédés	SPIN
PINOLI	Jean Charles	PR0	Image Vision Signal	CIS
POURCHEZ	Jérémy	CR	Génie des Procédés	CIS
ROBISSON	Bruno			CMP
ROUSSY	Agnès	MA(MDC)		CMP
ROUSTANT	Olivier	MA(MDC)		FAYOL
ROUX	Christian	PR		CIS
STOLARZ	Jacques	CR	Sciences et génie des matériaux	SMS
TRIA	Assia	Ingénieur de recherche	Microélectronique	CMP
VALDIVIESO	François	MA(MDC)	Sciences et génie des matériaux	SMS
VIRICELLE	Jean Paul	MR(DR2)	Génie des Procédés	SPIN
WOLSKI	Krzystof	DR	Sciences et génie des matériaux	SMS
XIE	Xiaolan	PR1	Génie industriel	CIS
YUGMA	Gallian	CR	Génie industriel	CMP
ENISE : Enseignants-chercheurs et chercheurs autorisés à diriger des thèses de doctorat (titulaires d'un doctorat d'État ou d'une HDR)				
BERGHEAU	Jean-Michel	PU	Mécanique et Ingénierie	ENISE
BERTRAND	Philippe	MCF	Génie des procédés	ENISE
DUBUJET	Philippe	PU	Mécanique et Ingénierie	ENISE
FEULVARCH	Eric	MCF	Mécanique et Ingénierie	ENISE
FORTUNIER	Roland	PR	Sciences et Génie des matériaux	ENISE
GUSSAROV	Andrey	Enseignant contractuel	Génie des procédés	ENISE
HAMDI	Hédi	MCF	Mécanique et Ingénierie	ENISE
LYONNET	Patrick	PU	Mécanique et Ingénierie	ENISE
RECH	Joël	PU	Mécanique et Ingénierie	ENISE
SMUROV	Igor	PU	Mécanique et Ingénierie	ENISE
TOSCANO	Rosario	PU	Mécanique et Ingénierie	ENISE
ZAHOUANI	Hassan	PU	Mécanique et Ingénierie	ENISE

# Table of Contents

Table of Contents.....	4
Acknowledgements.....	9
Abbreviations.....	11
List of Tables and Figures.....	14
Abstract.....	22
Aim of the Thesis.....	25
1/ Chapter 1: Introduction to OEET for Biological Applications.....	26
1.1 Organic Electrochemical Transistor.....	28
1.1.1 General Consideration.....	28
1.1.2 Configuration.....	29
1.1.3 Advantages.....	29
1.1.4 Conducting Polymers.....	30
1.1.5 Operational Principle.....	31
1.2 Applications in Biology.....	33
1.2.1 OEETs coupled with biological moieties for sensing.....	33
1.2.2 OEET coupled with whole cells for electrophysiology .....	41
1.3 Conclusion.....	49
1.4 Bibliography.....	50
2/ Chapter 2: Blood Brain Barrier Characterisation .....	57
2.1 Introduction.....	58
2.2 History of the Blood Brain Barrier.....	58
2.3 Structure.....	59
2.3.1 A Biological Barrier.....	59
2.3.1.1 Brain Endothelial Cells.....	60
2.3.1.2 Astrocytes .....	61

2.3.1.3 Pericytes .....	61
2.3.1.4 Neurons .....	62
2.3.2 A Physical Barrier.....	62
2.3.2.1 Tight Junctions.....	63
2.3.2.2 Adherens Junctions.....	64
2.3.3 A Physiological Barrier.....	64
2.3.3.1 The Paracellular Pathways.....	65
2.3.3.2 Transcellular Pathways.....	66
2.3.4 A Metabolic Barrier.....	67
2.3.4.1 Enzymes.....	67
2.3.4.2 Efflux Pumps.....	68
2.4 <i>In vitro</i> Model of Blood Brain Barrier.....	71
2.4.1 Parameters Used to Assess <i>in vitro</i> Model of Blood Brain Barrier.....	71
2.4.1.1 Permeability Measurement.....	71
2.4.1.2 Measurement of TER.....	72
2.4.2 Different Type of Cell Culture.....	77
2.4.3 Different Type of Blood Brain Barrier Model.....	77
2.4.3.1 Bovine Model.....	77
2.4.3.2 Rat and Mouse Model.....	78
2.4.3.3 Porcine Model.....	79
2.4.3.4 Human Model.....	79
2.5 Conclusion.....	80
2.6 Bibliography.....	80
3/ Chapter 3: Development and Characterisation of Different Types of <i>in vitro</i> BBB Models .....	88
3.1 Introduction.....	89
3.2 <i>In vitro</i> BBB Model Using Bovine Brain Endothelial Cells .....	89

3.2.1 Generality on Bovine Brain Endothelial Cells.....	89
3.2.2 Materials and Methods .....	90
3.2.3 Results and Discussion.....	92
3.2.3.1 Experiment 1: Observation of BBECs Morphology.....	92
3.2.3.2 Experiment 2: Measurement Integrity of BBECs using Permeability Assays.....	93
3.2.3.3 Experiment 3: Integrity of BBECs and Biocompatibility with PEDOT(TOS) Using Collagen Coating.....	94
3.2.3.4 Experiment 4: Integrity of BBECs and Biocompatibility with PEDOT(TOS) Using Gelatin Coating.....	96
3.2.4 Conclusion.....	97
3.3 <i>In vitro</i> BBB Model Using Human Brain Microvascular Endothelial Cells (HBMEC) .....	98
3.3.1 Generality on Human Brain Microvascular Endothelial Cells.....	98
3.3.2 Materials and Methods.....	98
3.3.3 Results and Discussion.....	101
3.3.3.1 Experiment 1: Immunofluorescence Time Course of HBMEC.....	101
3.3.3.2 Experiment 2: Integrity of Monoculture and Contact Co-culture of HBMEC.....	102
3.3.3.3 Experiment 3: Integrity of Monoculture Conditioned, Contact and No Contact Co-culture of HBMEC.....	104
3.3.3.4 Experiment 4: Impact of endogenous extracellular matrix on the integrity of Monoculture Conditioned, Contact and No Contact Co- culture of HBMEC.....	107
3.3.3.5 Experiment 5: Impact of Hydrocortisone on Integrity of Monoculture Conditioned, Contact and No Contact Co-culture of HBMEC.....	110
3.3.4 Conclusion.....	112
3.4 <i>In vitro</i> BBB Model Using Immortalized Human Cerebral Microvascular Endothelial Cells (hCMEC/D3) .....	112

3.4.1 Generality on Immortalized Human Cerebral Microvascular Endothelial Cell (hCMEC/D3).....	112
3.4.2 Materials and Methods.....	113
3.4.3 Results and Discussion.....	114
3.4.3.1 Experiment 1: Immunofluorescence Time Course of hCMEC/D3.....	114
3.4.3.2 Experiment 2: Integrity of Monoculture Conditioned, Contact and No Contact Co-culture of hCMEC/D3.....	116
3.4.3.3 Experiment 3: Impact of Neuron on Integrity of Monoculture Conditioned, Contact and No Contact Co-culture of hCMEC/D3...	119
3.4.4 Conclusion.....	121
3.5 Integration of hCMEC/D3 with OECT.....	121
3.5.1 Materials and Methods.....	121
3.5.2 Results and Discussion of Integrity of hCMEC/D3 Using OECT Measurement.....	122
3.5.3 Conclusion.....	123
3.6 Conclusion.....	124
3.7 Bibliography.....	124
4/ Chapter 4: PEDOT:gelatin composites mediate brain endothelial cell adhesion.....	126
4.1 Introduction.....	128
4.2 Materials and Methods.....	129
4.2.1 Material .....	129
4.2.2 Vapor Phase Polymerisation of PEDOT(TOS) and PEDOT(TOS) Composite Films.....	130
4.2.3 Characterisation of PEDOT(TOS) and PEDOT(TOS) Composite Films.....	130
4.2.4 Cell Culture and Characterisation of Cell Growth and Proliferation ...	131
4.3 Results and discussion.....	132

4.3.1 Preparation and Characterisation of PEDOT(TOS):gelatin Composites.....	132
4.3.2 Growth of bovine BBCEC on PEDOT(TOS) Composite Films.....	139
4.4 Conclusion.....	142
4.5 Bibliography.....	143
5/ Chapter 5: Integration of an <i>in vitro</i> Model of the Blood Brain Barrier with the OECT.....	146
5.1 Introduction.....	148
5.2 Materials and Methods.....	149
5.2.1 OECT Fabrication.....	149
5.2.2 OECT Measurement.....	151
5.2.3 Cell Culture.....	151
5.3 Results and Discussion.....	153
5.3.1 Microscale OECT for Monitoring BBB Toxicology .....	153
5.3.2 OECT as a Better Sensing Methods for Monitoring BBB Cells.....	160
5.4 Conclusion.....	163
5.5 Bibliography.....	163
6/ Chapter 6: Conclusion and Outlook.....	165

# Acknowledgements

The present work was carried out at Department of Bioelectronics (BEL), in the Center of Microelectronics in Provence (CMP), a Research and Education center of the École des Mines de Saint-Étienne, located in Gardanne. This work has been funded by the European Research Council (ERC).

First, I want to express my gratitude to my principle supervisor, Associate Professor Dr. Roisin Owens, for giving me the opportunity to work in her research group and for giving me the possibility to grow into an independent scientist. I am thankful for her encouragement, support and invaluable advice during these years. Without her, this thesis would not have been completed.

I also need to extend my gratitude to my director Pr. George Malliaras who has provided invaluable insight, fresh perspectives and incredible opportunities for the members of his research groups over the years. I am thankful for his enthusiasm about research. I wish to the BEL group the best of luck in the years to come.

I am honoured to have Pr. Pierre-Olivier Couraud in the public examination of this thesis. I am grateful to the official reviewers of this thesis, Pr. Susan Daniel and Pr. Noelle Callizot for their careful review and valuable comments.

In the BEL group, I have had the opportunity to work with many talented scientists and good people:

I am very grateful to the talented Dr. Marc Ramuz (Marcus), for his huge help for this thesis, teaching me “electronics” and always available to explain and guide me in my experiments. Thanks you for all these electronics devices!

Next, I need to thank the best engineer, Adel Hama, (Adeligno) for his help, advice in biology and availability during these 3years.

I would also like to thank Dr. Miriam Huerta (Mimi) for her help and encouraging discussion about blood brain barrier (and her amazing guacamole!).

Then I need to thank the future Dr. Xenofon Strakosas, the happy face of my office, born 1 day before me, for his huge help on paper and explanation about electronic field (and this beautiful and enjoyable Greece trip!).

I would like to thanks Dr. Eleni Stavriniidou, the best officemate, for her smile every day, her help and all our “very interesting” conversations.

After I would like to thanks Dr. Scherrine Tria, the first PhD student that I met, for her help in several protocol during this thesis.

I need to thank Dr Leslie Jimison, (Lady Leslie), for teaching me “the secret” of pedot.

Then I would like to thanks Cassandre Vuillaume, for all the good time spent together and her delicious cakes.

Thanks very much to the BioDiagnostic Group to make this three years so pleasant!

I also need to extend my gratitude to the Neuro Group:

I would like to thank Dr. Pierre Leleux (Peio), I will never forget this crazy Atlanta trip!!! Thanks you for all these electronic advice even 24h before my defence!

Next I would like to thank Dr. Jonathan Rivnay (JonnyJonny), thank you so much for your help and make the bandwidth fit for BBB!!

I would also like to thanks Dr. Esma Ismalova Bernard Salas (Mme BS), for her smily angel face every day and her help and support during these three years.

I would also like to thanks Liza Klots-Rivnay for her careful revision of the language of the thesis (and her amazing Chili!).

I would also like to thanks Dr. Thomas Doublet (Mister T.) for his happiness and funny jokes!

I need to thanks Dr. Dion Khodagholy for his explanation about electronics and these great moments in New York.

And all PhD students, post doc, Dr. for all these enjoyable moment during this thesis: Marc, Michele, Dimitri, Thomas L, Sahika, Ilke, Sylvain, Duc, Bartek,, Mary, Eloise.

I also wish to thank all the personnel in Center of Microelectronics in Provence (CMP): Veronique Villareal, Michel Fiocchi, Thierry Camilloni, Jessica Mazuir, Sabine Salmeron, Barbara Bruno, Michelle Gillet and Gracien Counot. And also all PhD student and people of other department SAS and PS2 where I met many nice people.

Life is more than just work or science. I wish to thank my friends who always supported me: Claire (you and me in the same boat, like the fingers of a hand!), Laure-Helene (my best!), Vero (marousse), Nicolas (monbichon), Ludovic, Assa, , Alio (mablond), Aude, Nelly (magrosse), Zouzou, Hajer, Bertrand, Gizou, Benjamin (beninoi), mon jaki, Nadou, Isa, Magno and all....

And Arnaud (namour), for love and cooking every night when I arrive late!

Thanks you all.

From the bottom of my heart, I would like to express my gratitude to my blood, BONGO Family:

To my grandmothers, Mouabouere Bongo and Gueli Awa, to my uncle and aunties, tonton Patty, tonton Dydime, tantine Elise, tonton Kadjou, tonton Jo, tantine Chanel, tantine Melas, tonton Aristide, and all my cousins, I have made your proud.

To my parents Manuel Bongo and Aurelie Bongo who have always loved and supported me, and constantly inspired me to reach even higher goals in my life “when you want you can”, I will never forget . Thanks to my brothers and sisters, Andre-July, Idrysse-Antoine, Diane-Aurelie, Lucas-Loic and Oceane, I love you.

# Abbreviations

ABC: ATP-Binding Cassette  
AC: Alternating Current  
ACM: Astrocyte Conditioned Media  
AFM: Atomic Force Microscopy  
AJ: Adherent Junction  
AGS: Astrocyte Growth Supplement  
AM: Astrocyte Media  
AMP: Adenosine Monophosphate  
ATP: Adenosine Triphosphate  
BBB: Blood Brain Barrier  
BBEC: Bovine Brain Endothelial Cells  
BBCEC: bovine brain capillary endothelial cell  
BBMEC: Bovine Brain Microvessel Endothelial Cell  
BDNF: Brain Derived Neurotrophic Factor  
BMECs: Brain Microvascular Endothelial Cells  
BSA: Bovine Serum Albumin  
BCRP: Breast Cancer Resistance Protein  
CN: Cortical Neurons  
CNS: Central Nervous System  
CPs: Conducting polymers  
CS: Calf Serum  
CV: Cyclic Voltammetry  
DBSA: Dodecyl Benzene Sulfonic Acid  
DC: Direct Current  
DMEM: Dulbecco's Modified Eagle Medium  
EBM: Endothelial Basal Medium  
ECIS: Electric Cell substrate Impedance Sensing  
ECM: Extra Cellular Matrix  
ECoG: Electrocorticography  
ECGS: Endothelial Cell Growth Supplement

EDOT: 3,4-Ethylenedioxythiophene  
EDTA: Ethylenediaminetetraacetic acid  
EEG: Electroencephalography  
EGT: Electrolyte Gated Transistor  
EGTA: Ethylene Glycol Tetraacetic Acid  
EGOFET: Electrolyte Gated Organic Field Effect Transistor  
EVOM: Epithelial Voltohmmeter  
FCS: Fetal Calf Serum  
FGF: Fibroblast Growth Factor  
GOPS: 3-glycidoxypropyltrimethoxysilane  
 $\gamma$ -GT: Gamma Glutamyl Transpeptidase  
HA: Human Astrocyte  
HBMEC: Human Brain Microvascular Endothelial Cells  
h CMEC/D3: Immortalized Human Brain Endothelial Cell Line  
HIV: Human Immunodeficiency Virus  
HS: Horse Serum  
ID: drain current  
IG: gate current  
IgG: Immunoglobulin G  
JAM: Junctional Adhesion Molecule  
LY: Lucifer Yellow  
MCF: Michigan Cancer Foundation  
MDCK: Madin Darby Canine Kidney  
MOA: Mono Amine Oxidase  
MRP: Multidrug Resistance-associated Protein  
MW: Molecular Weight  
NR: Normalized Response  
NVU: Neurovascular Unit  
OAT: Organic Anion Transporters  
OATP: Organic Anion Transporters Polypeptide  
OECT: Organic Electrochemical Transistor  
PAL: Phosphatase Alkaline  
Papp or Pe: Apparent Permeability

PBMEC: Porcine Brain Microvessel Endothelial Cell  
PBS : Phosphate Buffered Saline  
PDMS : Polydiméthylsiloxane  
PEDOT: Poly 3-4 EthyleneDiOxyThiophene  
PEG: Poly(ethyleneglycol)  
P-gp: P-glycoprotein  
Pt: Platinum  
PSS: Polystyrene sulfonate  
QCM: Quartz Crystal Microbalance  
RBMEC: Rat Brain Microvessel Endothelial Cell  
RBE4: Rat Brain Endothelial  
RTIL: Room Temperature Ionic Liquid  
SEM: Scanning Electron Microscopy  
SNR: Signal-to-Noise Ratio  
SLC: Solute Carrier Transporter  
TER or TEER: Trans Electrical Endothelial Resistance  
TJ: Tight Junctions  
TOS: Tosylate  
Vg: Gate Voltage  
VPP: Vapor Phase Polymerisation  
XPS: X-ray Photoelectron Spectroscopy

# List of Tables and Figures

## **Chapter 1: Introduction to OECT for Biological Applications**

**Figure 1.1:** The organic electrochemical transistor: a. schematic cross-section of an OECT b. PEDOT:PSS structure. (a, b reproduced from [5], with permission from [Nature Publishing Group]) c. Ionic circuit of an OECT (c reproduced from [6], with permission from [Wiley-VCH ])...28

**Figure 1.2:** Robust micrometer scale, high amplification OECTs: a. an array of OECTs on a thin flexible substrate: scale bar = 1 cm b. the array is extensively crumpled c. transfer characteristics of device before (red) and after (blue) crumpling b. transconductance and time response for devices before (red) and after (blue) crumpling. (a, b, c reproduced from [5], with permission from [Nature Publishing Group])...32

**Figure 1.3:** OECTs used as ion sensors a. Transfer characteristics of an OECT for different concentrations of KCl solutions ( $V_d = -0.1$  V). (reproduced from [31], with permission from [ACS Publications]). b. Wheatstone bridge circuit diagram. c. The peak-to-peak voltage difference as a function of concentration difference of NaCl solution, inset curve shows the raw data. (b, c reproduced from [33], with permission from [American Institute of Physics]). d. schematic of Ion-selective OECT. e. Calibration curves ( $I_d$ ,  $V_{g,m}$  vs concentration) of pure KCl and NaCl solutions performed using ion selective OECT (IS-OECT). (d, e reproduced from [34], with permission from [Wiley Online Library])...34

**Figure 1.4:** OECTs used as enzymatic sensors: a. i) Transfer of electron from glucose to the gate through the biological reaction catalyzed by glucose oxidase ii) de-doping mechanism of PEDOT:PSS at the channel b. Drop of potential at the interfaces and its dependence to the gate/ channel size ratio. (b, is reproduced and modified from [42] with permission from [Wiley Online Library]) c. Schematic layout of an OECT glucose sensor with the gate modified with Pt NPs, MWCTS and GOx f. The dependence of  $\Delta V_{g,eff}$  as a function of  $\log[C_{glucose}]$  for CHIT/GOx/Pt (line I), MWCNT-CHIT/GOx/Pt (line II) and CHIT/GOx/Pt-NPs/Pt (line III) gate electrodes. (c, d are reproduced from [44] with permission from [Wiley – VCH]). e. Schematic layout of an OECT lactate sensor with solid state ionogel electrolyte. f. Normalized response of the OECT vs. lactate concentration. (e, f are reproduced from [47] with permission from [RSC Publishing])...38

**Figure 1.5:** OECTs as Immunosensors and nucleotide sensors: a. Schematic of an E. coli O157:H7 sensor based on an OECT. b. Schematic diagram of potential drops in

the electric double layers (EDL), including the channel/electrolyte and electrolyte/gate interfaces, in the OECT before and after the immobilization of *E. coli* O157:H7 on the PEDOT:PSS surface. (a, b, reproduced from [50], with permission from [RSC Publishing]) c. Schematic of an OECT integrated in a flexible microfluidic system, which is characterized before and after the modification and the hybridization of DNA on the surface of Au gate electrode. d. Transfer characteristics of OECTs measured in microfluidic channels before and after the immobilization and the hybridization of DNA on Au gate electrodes.  $V_{ds} = -0.1$  V. The inset shows the horizontal shifts of the transfer curves. (c, d, reproduced from [52], with permission from [Wiley Online Library]).....41

**Figure 1.6 :** Barrier tissue integrity at the interface with an OECT: a. Layout of an OECT with an integrated barrier tissue b. Equivalent circuit describing ionic transport between gate electrode and transistor channel. TER refers to the transepithelial resistance of the cell layer, C<sub>cell</sub> refers to the capacitance of the cell layer, R<sub>filter</sub> and C<sub>filter</sub> refer to the resistance and capacitance of the porous filter, respectively, R<sub>med</sub> refers to the resistance of the media, and C<sub>cp</sub> refers to the capacitance at the CP and electrolyte layer c. Cartoon showing polarized Caco-2 cells with tight junctions (left) and without (right), sitting on a porous cell culture membrane, above a PEDOT:PSS transistor channel. Tight junctions are shown in yellow. d. OECT Id transient response with cells before (left) and after (right) the addition of 100 mM H<sub>2</sub>O<sub>2</sub>, (solid lines). OECT Id response in the absence of cells is overlaid (dashed lines) (a, b, c, d, reproduced from [56], with permission from [Wiley Online Library]) e. Picture of the multiplex device shown on a Petri dish inside the cell-culture incubator. The cell culture insert is shown suspended in the plastic holder affixed to the glass slide. The Ag/AgCl gate electrode is shown immersed in the apical media, while source and drain cables are attached to their respective positions on the glass slide g. Kinetics of polarized epithelial monolayer infected with *Salmonella typhimurium*. Cartoon illustrating infection with wildtype (WT) (left) and non-invasive *S. typhimurium* (right). Mean normalized response ( $\tau$ ) of the OECT in the presence of WT (left) and non-invasive *S. typhimurium* (right) at different MOI over 4 h, bacteria were added at  $t = 0$ . Non-infected represents OECT + cells with no added bacteria. Non-infected cells are in cyan, MOI: 10 in blue, MOI: 100 in purple, and MOI: 1000 in red. (e, f, g, reproduced from [57], with permission from [Wiley Online Library])**Figure 1.7:** (a). Recordings from an OECT (pink), a PEDOT:PSS surface electrode (blue) and an Ir-penetrating electrode (black). The transistor was biased with  $V_D = -0.4$  V and  $V_G = 0.3$  V, and the scale of 10 mV is for both surface and penetrating electrodes. Note the superior SNR of the OECT as compared with the surface electrode (b). Time-frequency analysis of epileptiform activity during a short period, recorded by an OECT (top), a PEDOT:PSS surface electrode (middle) and an Ir-penetrating electrode (bottom).....42

**Figure 1.7:** Non electrogenic cells in direct contact with OECTs: a. view of polarized Calu-3 cells with tight junction sitting on the PEDOT:PSS transistor channel of an

OECT b. In situ OECT response with (red) and without (black) Calu-3 cells upon the addition of 1  $\mu\text{M}$  CFTR agonist forskolin. Transistor channel current change was converted to effective gate voltage change. (a, b reproduced from [62], with permission from [Wiley Online Library]). c. Micro-optical images of MDCK-I on top of the OECT channel area (the darker horizontal line in the middle of the picture corresponds to the PEDOT:PSS channel) and corresponding electrical characteristics with a measurement taken every 3h. d. Illustrative example of high resolution fluorescence imaging possible on PEDOT:PSS devices. HeLa cells (left) and immortalized human fibroblasts (right) (c, d, reproduced from [63], with permission from [Wiley Online Library]).....46

**Figure 1.8:** OECTs for measuring electrogenic cells: a. ECG recording with an OECT operated in direct contact with the skin. b. Photograph of the device showing its transparency and adaptability when attached to human skin. (a, b, reproduced from [65], with permission from [Wiley Online Library]) c. Optical micrograph of the ECoG probe placed over the somatosensory cortex, with the craniotomy surrounded by dashed lines. Scale bar, 1mm d. Recordings from an OECT (pink), a PEDOT:PSS surface electrode (blue) and an Ir-penetrating electrode (black). The transistor was biased with  $V_d = -0.4 \text{ V}$  and  $V_g = 0.3 \text{ V}$ , and the scale of 10mV is for both surface and penetrating electrodes. Note the superior SNR of the OECT as compared with the surface electrode. (c, d, reproduced from [28], with permission from [Nature Publishing Group]). e. Wiring configuration chosen for the EOG measurement, recording of electrical activity during left/ right eyeball movements, recording of electrical activity during up/down eyeball movements. Both up/ down (red) and left/ right (blue) activities are measured. f. Wiring configuration used for the EEG measurement, along with recording of spontaneous brain activity (top) showing the alpha rhythm, and associated time-frequency spectrogram (bottom), Fourier analysis of a 3min recording. (e, f, reproduced from [68], with permission from [Wiley – VCH]).....48

**Chapter 2: Blood Brain Barrier Characterisation**

**Figure 2.1:** Historical research on the blood-brain barrier.....59

**Figure 2.2:** Schematic representation of a blood-brain barrier.....60

**Figure 2.3:** Representation of a section of brain capillaries with tight and adherens junctions present between endothelial cells.....62

**Figure 2.4:** Diagram of the different transport processes involved in the permeability of brain capillaries.....65

**Figure 2.5:** Representation of the metabolic activity of the blood-brain barrier.....69

**Figure 2.6:** Impedance measurements with chopstick-like electrodes. The chopstick-like electrodes (E1, E2) are traditionally used to determine the electric resistance of cells grown on filter inserts. The ohmic resistance of the cell layer (TER), the cell culture medium in the upper and lower compartment ( $R_{Med}$ ), the membrane of the filter inserts ( $R_{pm}$ ) and electrode-medium interface ( $R_E$ ) all contribute to the total electric resistance.  $I_{AC}$ : alternating current.....73

**Figure 2.7:** The CellZscope (a). CellZscope device (b). Equivalent circuit for cell layer grown on porous filter (c). Impedance frequency scan (d). Overview of CellZscope data acquisition window. Adapted from technical bulletin, Nanoanalytics.com.....74

**Figure 2.8:** Schematic drawing of an ECIS array and principle of the electric cell-substrate impedance sensing (ECIS) method. (a) Cell layers are grown to confluence on integrated gold-film electrodes. An applied AC current flows between small working electrodes and the larger counter electrode using normal culture medium as an electrolyte. By a variation of the frequency  $\omega$ , a spectrum can be obtained. Applying higher frequencies the current flow is dominated by the capacity of the total system, at mid-range frequencies the ohmic resistance of the total system is mirrored. (b) The current pathway at low frequencies on a cerebral endothelial cell monolayer (ECIS method, 400 Hz). At low frequencies the current predominantly flows paracellular (through extracellular matrix proteins) and between adjacent cells (through tight junctions) and the electrolyte (medium). (c) Application of high frequencies (ECIS method, > 40 kHz), the capacitive amount of measured impedance is especially sensitive for adhered cells. The current passes through the insulating cell monolayer, especially through cell membranes.....75

**Figure 2.9:** Schematic of planar OECT device which consists of a PEDOT:PSS channel and gate patterned onto a glass slide.....76

### **Chapter 3: Development and Characterisation of different types of *in vitro* BBB Models**

**Figure 3.1:** Light Microscope images of BBECs on well coated with gelatin.....92

**Figure 3.2:** SEM of a confluent monolayer of BBECs on filter coated with gelatin...93

**Table 3.1:** Details of BBECs culture for experiment 1.....93

**Table 3.2:** Permeability of the BBECs culture for experiment 2.....94

**Table 3.3:** Details of the BBEC culture for experiment 3.....95

**Table 3.4:** Permeability and TER results of the BBECs culture for experiment 3.....95

**Table 3.5:** Details of the BBEC culture for experiment 4.....96

<b>Table 3.6:</b> Permeability and TER results of the BBECs culture for experiment 4.....	96
<b>Figure 3.3:</b> Immunofluorescence staining of BBECs. (a). Immunofluorescence of BBECs on gelatin coated filter, stained with antibodies against apical junction proteins ZO-1 (green), occludin (red) and nucleus (blue). (b). Immunofluorescence of BBECs on gelatin on top of PEDOT(TOS) coated filter, stained with antibodies against apical junction proteins claudin-1 (green), ZO-1 (red) and nucleus (blue)...	97
<b>Figure 3.4:</b> A scheme of the different <i>in vitro</i> BBB models.....	99
<b>Figure 3.5:</b> Cells cultured on the underside of the filter membrane. (a) 24well filter is upside down in 12 well plate containing water. (b) Cells are seeded onto the underside of the membrane for 2h in the incubator. (c) The filter is placed in 24 well plates for the rest of experiment.....	100
<b>Figure 3.6:</b> Immunofluorescence of HBMEC of ZO-1 (red) and claudin 5 proteins (green) at day 2, 4 and 6. Nucleus is stained with DAPI (blue).....	101
<b>Figure 3.7:</b> Schematic for the HBMEC experiment 2.....	102
<b>Figure 3.8:</b> (a).TER recorded by the CellZscope system of contact co-culture at 8 days (black), contact co-culture at 6 days (red) and monoculture at 10 days (blue). (b). Apparent permeability of contact co-culture at 8 days (black), contact co-culture at 6 days (red) and monoculture at 10 days (blue).....	103
<b>Figure 3.9:</b> (a).TER recorded by the CellZscope system of contact co-culture at 8 days (black), contact co-culture at 6 days (red) and monoculture at 10 days (blue). (b). Apparent permeability of contact co-culture at 8 days (black), contact co-culture at 6 days (red) and monoculture at 10 days (blue).....	104
<b>Figure 3.10:</b> (a).TER recorded by the CellZscope system of contact co-culture at 8 days (black), no contact co-culture at 8 day (red) and monoculture conditioned at 8 days (blue). (b). Apparent permeability of contact co-culture at 8 days (black), no contact co-culture at 8 days (red) and monoculture conditioned at 8 days (blue)....	105
<b>Figure 3.11:</b> Actin staining by phalloidin examined by fluorescence microscopy. Nuclei were counterstained with DAPI. (a) Control of HBMEC cultured in monoculture in well. (b). HBMEC cultured in contact co-culture. (c) HBMEC cultured in non contact co-culture. (d). HBMEC cultured in monoculture with HA's conditioned media. ....	106
<b>Figure 3.12:</b> Schedule organization of the HBMEC experimentation 4. (a). Establishment of endogenous extracellular matrices derived from HBMEC and HA, adapted from experimental cell research, Hartmann C et al., [2]. (b). Organization of the experiment.....	107

<b>Figure 3.13:</b> (a).TER recorded after deposition of endogenous extracellular matrix by the CellZscope system of monoculture conditioned (black), and contact co-culture (red). (b). Apparent permeability of monoculture conditioned (black), and contact co-culture (red).....	109
<b>Figure 3.14:</b> Details of the HBMEC experiment 5.....	110
<b>Figure 3.15:</b> (a).TER recorded by the CellZscope system of contact co-culture supplemented with hydrocortisone at 8 days (black), contact co-culture at 8 days (red), no contact supplemented with hydrocortisone at 8 days (blue), no contact co-culture at 8 days (purple), monoculture conditioned supplemented with hydrocortisone at 8 days (green) and monoculture conditioned at 8 days (dark blue). (b). Apparent permeability of system of contact co-culture supplemented with hydrocortisone at 8 days (black), contact co-culture at 8 days (red), no contact supplemented with hydrocortisone at 8 days (blue), no contact co-culture at 8 days (purple), monoculture conditioned supplemented with hydrocortisone at 8 days (green) and monoculture conditioned at 8 day (dark blue).....	111
<b>Figure 3.16:</b> Immunofluorescence of hCMEC/D3 of ZO-1 (red) and claudin 5 proteins (green) at day 2, 4 and 6.....	115
<b>Figure 3.17:</b> Details organization of the hCMEC/D3 experimentation 2.....	116
<b>Figure 3.18:</b> (a).TER recorded by the CellZscope system of contact co-culture at 8 days (black), no contact co-culture at 8 days (red) and monoculture conditioned at 8 days (blue). (b). Apparent permeability of contact co-culture at 8 days (black), no contact co-culture at 8 days (red) and monoculture conditioned at 8 days (blue).....	117
<b>Figure 3.19:</b> Actin staining by phalloidin examined by fluorescence microscopy. Nuclei were counterstained with DAPI. (a). hCMEC/D3 cultured in contact co-culture. (b) hCMEC/D3 cultured in non contact co-culture. (c). hCMEC/D3 cultured in monoculture with HA's conditioned media.....	118
<b>Figure 3.20:</b> Details organization of the hCMEC/D3 experimentation 3.....	119
<b>Figure 3.21:</b> (a).TER recorded by the CellZscope system of contact co-culture with CN (black), contact co-culture with CN (red), no contact co-culture with CN (blue), no contact co-culture with HA (purple) and monoculture conditioned HA media (dark blue). (b). Apparent permeability of contact co-culture with CN (black), contact co-culture with CN (red), no contact co-culture with CN (blue), no contact co-culture with HA (purple) and monoculture conditioned HA media (dark blue).....	120
<b>Table 3.7:</b> Summarize TER and Papp data obtained on <i>in vitro</i> BBB model.....	121
<b>Figure 3.22:</b> OECT transconductance response versus frequency, of the device alone (black), the hCMEC/D3 cells co-cultured in contact with HA (blue), after scratch the filter (red).....	123

## **Chapter 4: PEDOT:gelatin Composites Mediate Brain Endothelial Cell Adhesion**

**Figure 4.1:** XPS of PEDOT(TOS) top and PEDOT(TOS):gelatin (bottom) films...134

**Table 4.S1:** XPS of PEDOT (TOS) films.....134

**Figure 4.2:** NanoSIMS of PEDOT(TOS):gelatin films. Panels A, B and C show elemental analysis for nitrogen, carbon and sulphur respectively.....135

**Figure 4.3:** Immunofluorescence images of substrates stained with anti-gelatin antibodies (red). (A) PEDOT(TOS), (B) gelatin coated on well, (C) PEDOT(TOS) + gelatin, and (D) PEDOT(TOS):gelatin. Scale bar = 100  $\mu\text{m}$ .....136

**Figure 4.4:** CVs of PEDOT(TOS), PEDOT (TOS): gelatin 1 : 1 and PEDOT(TOS):gelatin 1 : 2 in 0.05 M NaTOS, pH 6.9 at 20  $\text{mV s}^{-1}$ .....137

**ESI, Figure 4. 1:** SEM of PEDOT(TOS) and PEDOT(TOS):gelatin.....138

**Table 4.1:** Contact angles and roughness values (obtained from AFM measurements) for PEDOT(TOS) and PEDOT(TOS) composite films. Data presented are mean SD, n = 3.....139

**Figure 4.5:** Initial adhesion (1) and viability (2) of BBCECs observed 3 hours and 5 days after seeding on 96-well plates  $\pm$  polymer composite coating. Wells are as follows: (A) well, (B) PEDOT(TOS), (C) gelatin, (D) BSA, (E) PEDOT(TOS) + gelatin, (F) PEDOT(TOS) + BSA, (G) PEDOT(TOS):gelatin, and (H) PEDOT(TOS):BSA. For the initial adhesion study images were taken by phase contrast microscopy. For viability assays, the live cells are stained with calcein-AM (green) and dead cells are stained with propidium iodide (red). Scale bar = 50  $\mu\text{m}$ ..140

**ESI, Figure 4.2:** water uptake.....141

**Figure 4.6:** Viability of BBCECs grown on (1) gelatin, (2) well, (3) BSA, (4) PEDOT(TOS), (5) PEDOT(TOS) + gelatin (6) PEDOT(TOS) + BSA, (7) PEDOT(TOS):gelatin, and (8) PEDOT(TOS):BSA. Gelatin represents the positive control and is used to determine 100% viability.....142

## **Chapter 5: Development of an *in vitro* Model of the Blood Brain Barrier Integrated with the OECT**

**Figure 5.1:** Schematic of the fabrication process for the OECT.....150

**Figure 5.2:** (a). Schematic of the OECT at  $V_g=0$ . PEDOT:PSS conducting polymer is connected by gold source and drain contacts. Ions are present and stay in the

biological media (in pink). (b) At  $V_g > 0$ , the electric field push the positive ions from the media into the PEDOT:PSS. The measured source drain current ( $I_{DS}$ ) is thus decreased. (c). Pictures of the OECT made on a 3 x 1 inches glass substrates. A dedicated 3D printed holder with embedded pogo pin was used to probe the OECTs.....153

**Figure 5.3:** Electrical modeling of the OECT with and without cell layer.....154

**Figure 5.4:** OECT frequency response. (a) Monitoring of frequency, without cells (purple), with cells (black), on addition of 40mM of EGTA (red), on addition of 0.25% of trypsin (blue). (b) Table of frequency cut off values.....156

**Figure 5.5:** Light microscope images of device at day 8 (a). without h CMEC/D3 cells (b). with healthy h CMEC/D3 cells (c). after EGTA (d). after Trypsin.....157

**Figure 5.6:** Immunofluorescence of proteins in BBB monolayer upon exposure to EGTA. (a) Monolayers were exposed to 40mM of EGTA for and then stained with antibodies against apical junction proteins. (b) Monolayers non exposed to EGTA.....158

**Figure 5.7:** TER of h CMEC/D3 cells and the filter alone using the CellZscope at day 8 (N=3). (a) TER at day 7 for monoculture (red), co culture with neuron (blue) and without cells (black). (b) Table of TER values.....161

**Figure 5.8:** OECT frequency response at day 8. (a) Monitoring of frequency, without cells (black), in monoculture condition (red), in co culture with neuron (blue). (b) Table of frequency cut off values.....162

NNT : 2014 EMSE 0753

**Manuelle BONGO**

***Integration of an in vitro blood brain barrier model with organic electrochemical transistors***

Speciality: Bioelectronics

Keywords: Blood Brain Barrier, Integrity, OECT

Abstract:

In biological systems many tissue types have evolved a barrier function to selectively allow the transport of matter from the lumen to the tissue beneath; one example is the Blood Brain Barrier (BBB). The BBB protects the brain from the blood and maintains homeostasis of the brain microenvironment, which is crucial for neuronal activity and function. Characterization of the BBB is very important as its disruption or malfunction is often indicative of toxicity/disease. Though the number of published papers in the field of *in vitro* BBB has multiplied in recent years, the validity of the models used is still a subject of debate.

The advent of organic electronics has created a unique opportunity to interface the worlds of electronics and biology, using devices such as the Organic ElectroChemical Transistor (OECT), which provide a very sensitive way to detect minute ionic currents in an electrolyte as the transistor amplifies the gate current.

In this study, we test three different type of BBB in order to develop a stable BBB model. We optimize the adhesion of brain endothelial cell on OECT conducting polymer. We show the integration of OECTs with immortalized human cerebral microvascular endothelial cells as a model of human blood brain barrier, and demonstrate that the barrier tissue function can be detected. Moreover, by this technique, a disruption in the barrier (e.g. caused by a toxic compound) is assessed electrically through a measurement of the drain current.

Results show the successful development and validation of an *in vitro* BBB model. Dynamic monitoring of the barrier properties of the BBB barrier tissue was possible using the OECT.

NNT : 2014 EMSE 0753

**Manuelle BONGO**

***Intégration d'un model in vitro de barrière hémato-encéphalique avec des transistors organiques électrochimiques.***

Spécialité: Bioélectronique

Mots clefs : Barrière hémato-encéphalique, intégrité, OECT

Résumé :

Dans les systèmes biologiques, les barrières tissulaires permettent le transport sélectif de molécules du sang au tissu approprié. Un exemple de barrière tissulaire est la barrière hémato-encéphalique (BHE). La BHE protège le cerveau du sang et maintient l'homéostasie du microenvironnement du cerveau, ce qui est essentiel à l'activité et à la fonction neuronale. La caractérisation de cette BHE est importante, car un dysfonctionnement de cette barrière est souvent révélateur de toxicité ou de maladie. Bien que le nombre d'articles publiés dans le domaine du développement et de la caractérisation de la BHE ait été multiplié ces dernières années, la validité des modèles utilisés est encore un sujet de débat.

L'avènement de l'électronique organique a créé une occasion unique pour coupler les mondes de l'électronique et de la biologie, à l'aide de dispositifs tels que le transistor électrochimique organique (OECT). OECT constitue un outil très sensible et économique pour diagnostiquer l'intégrité d'une barrière tissulaire.

Dans cette étude, nous avons tout d'abord développé trois différents modèles de BHE. Nous avons optimisé l'adhésion des cellules endothéliales cérébrales sur la matière active du transistor. Nous avons ainsi pu établir l'intégration des OECTs avec des cellules immortalisées humaines micro vasculaires cérébrales endothéliales (h CMEC/D3) en tant que modèle *in vitro* de BHE. Nous avons démontré que la fonction de tissu de la BHE peut être détectée en utilisant cette nouvelle technique. En outre, par cette technique, une perturbation de la barrière (par exemple, provoquée par un composé toxique) pourra être détectée électriquement au moyen d'une mesure de courant.

# Aim of Thesis

The Blood Brain Barrier (BBB) is a highly selective membrane which separates the peripheral blood and the central nervous system (CNS). This barrier greatly restricts the passage of almost every compound into the brain. However some pathogen or toxin can enter and cause brain dysfunction. A variety of techniques are used to assess *in vitro* BBB models, including immunofluorescence staining of proteins related to BBB function, permeability assays and measurements of TER. The aim of these measurements is twofold: 1. To assess the accuracy or physiological relevance of a model under development, and 2. For use in diagnostics for determining compounds/pathogens that disrupt the barrier function of the BBB. Several different *in vitro* BBB models have been developed however the experimental format of most models does not allow for high throughput screening to access barrier integrity.

Current biological methods for evaluating barrier property are often expensive and time consuming. Electronic devices like the OECT create an opportunity to generate a low cost technique, both rapid and adaptable to high throughput screening methods for measuring barrier tissue integrity. Importantly, the transistor geometry permits to get an inherent amplification resulting in much more sensitive device.

The aim of this thesis is to integrate the barrier function of BBB with the ability of OECTs to detect minute ionic currents in order to assess barrier integrity. We first try to develop a stable BBB model using human brain endothelial cells. Then we combine the OECT with live BBB cell layers, thereby creating a device that will allow the evaluation of barrier properties in *in vitro* BBB models and the future detection of pathogens and toxins.

# Chapter 1

---

## Introduction to OECT for Biological Applications

---

This first chapter is a description of the state of art of the function and the properties of the OECT. Here we describe the configuration and the operational principle of the device. We demonstrate the possibility to integrate the OECT device with biological elements and the multiple advantages of this device for biological sensing.

In this chapter, my role was to describe the general consideration of the OECT and the application in biology and more specifically in the monitoring cellular integrity.

***This chapter corresponds to a review in preparation:***

Strakosas, Xenofon, Bongo, Manuelle and Owens, Roisin.M. *OECT for biological applications*. *APL Materials*'s special topic on **Biomaterials and Bioelectronics** to be published in December 2014

## 1.1 The Organic Electrochemical Transistor

### 1.1.1 General considerations

The coupling of organic electronics with biology is an emerging and continuously growing field [1]. The motivation for organic bioelectronics is to address and anticipate the current and future diagnostic and therapeutic needs of the biomedical community [2]. These needs include detecting low concentrations of biological analytes, low amplitude brain activity, and pathogens, as well as improving compatibility with the biological environment [3]. Electrical methods for biological sensing are considered advantageous, in particular due to the fact that they are label-free, not requiring expensive and time consuming techniques involving fluorophores or chromophores (optical methods). Current diagnostic approaches using electrical sensors involve electrochemical biosensors, passive metal electrodes, and/or large scale integrated systems, in which the operating principle is based on redox reactions, changes in the local potential or impedance. However, for electrochemical sensors and passive recording sites for electrophysiology the biological signals are often challenging to record and require further amplification to become detectable, necessitating a push towards more active, sensitive and biocompatible devices [4]. A promising technology that has the potential to overcome such limitations and respond to these specific requirements is the organic electrochemical transistor (OECT).

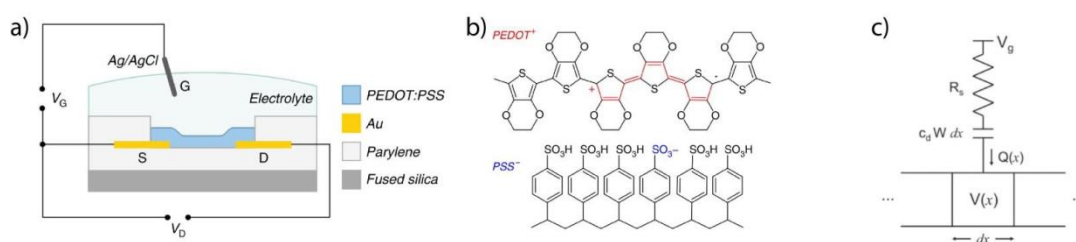


**Figure 1.1:** The organic electrochemical transistor: a. schematic cross-section of an OECT b. PEDOT:PSS structure. (a, b reproduced from [5], with permission from [Nature Publishing Group]) c. Ionic circuit of an OECT (c reproduced from [6], with permission from [Wiley-VCH]).

### 1.1.2 Configuration

The OEET, first reported by White et al., [7] is a three terminal device in a transistor configuration (source, gate, and drain) (figure 1a). The source and drain are connected by an organic conducting material in which an electronic current is generated ( $I_d$ ) in response to a potential difference. A variable potential at the gate controls the magnitude of the drain current ( $I_d$ ) by doping and de-doping the channel.

The OEET belongs to a broader class of transistors called electrolyte gated transistors (EGTs), in which the electrolyte is an integral part of the device [8]. This property makes the EGT compatible with aqueous environments. Apart from OEETs, a major subclass of the EGT is the electrolyte gated organic field effect transistor (EGOFET) [9], which has also been used as a diagnostic tool [10]. The difference between OEETs and EGOFETs lies in the interface between the channel and the electrolyte [11]. Specifically, in EGOFETs the ions of the electrolyte create an electrical double layer (EDL) with the charges (electrons/holes) of the channel. In contrast, in OEETs, ions from the electrolyte can penetrate the whole bulk of the polymeric channel. This key difference enables the OEET to exhibit high amplification properties in sub-volt operation regimes, preventing electrolysis, and extending operating times necessary for in-vitro and in-vivo applications [5]. The latter affords high sensitivity sensing for a wide spectrum of applications without additional amplification.

### 1.1.3 Advantages

The OEET offers a unique set of advantages for biomedical tools. One notable advantage includes adaptability to a wide variety of fabrication methods, from simple to complex; OEETs have been fabricated using low-cost printing techniques, [12] and exhibit high stability, high current modulation and fast response [13]. Simple, planar, all Poly 3,4-EthyleneDiOxyThiophene Polystyrene sulfonate (PEDOT:PSS) transistors on the macroscale have been shown to be capable of detecting glucose levels that exist in human saliva [14, 15]. For more challenging applications, OEETs are equally compatible with ongoing miniaturization techniques to the micro-scale, necessitated for the fabrication of high density electrode arrays for better interfacing with single neurons [16], integration with microfluidics for detection of multiple analytes [17], and lab on chip technologies [17b]. The use of robust and versatile organic materials has also facilitated the fabrication of conformal OEETs (figure 1.2a) for non-invasive, long term, continuous recordings [18]. Additionally, OEETs have been integrated with natural and synthetic fibers for fully integrated sensors and

wearable circuits compatible with human skin [19]. Although OECTs could be fabricated using a variety of organic conducting materials including small molecules, graphene or nanotubes, the majority of OECTs have been fabricated with conducting polymers (CPs) as active materials in the channel.

#### 1.1.4 Conducting Polymers

CPs, first discovered in 1976 by Alan MacDiarmid, Hideki Shirakawa and Alan Heeger, exhibit a wide spectrum of desired characteristics [20]. Of particular interest to biomedical applications, they exhibit mixed conductivity; ionic and electronic. Some of the first applications of CPs in the biomedical arena, were their use as coatings on metal electrodes, where they were shown to improve recordings of brain activity by lowering the impedance of the electrode [14, 21]. CPs are chemically tuneable, and can be designed according to the needs of each application. For instance, CPs have been designed to entrap enzymes and mediators [22]. Direct electrical connection of enzymes to electrodes has been explored, using polyelectrolytes with redox active groups, and conducting polymers [23]. Electrochemical biosensors have enlisted these types of CPs to improve stability and sensitivity. Finally, CPs have been shown repeatedly to be biocompatible, hosting a wide variety of cell types [24]. Part of their compatibility with live cells, may be due to the fact that these polymeric materials are oxide-free, resulting in a closer interaction with cells hosted on their surface possibly facilitating adhesion and promoting ionic interactions [24b,25]. Other advantages of CPs that will be highlighted below include their optical transparency and their mechanical flexibility akin to tissue, providing benefits for tissue engineering.

A well-studied and widely used CP is poly(3,4-ethylenedioxythiophene) doped with poly(styrene sulfonate) (PEDOT:PSS). PEDOT:PSS is a p-type conducting polymer, in which the negative charge of PSS is compensated by a hole in the PEDOT backbone (figure 1.1b). This conducting polymer exhibits high electronic conductivities, with typical conductivity values of commercially available PEDOT:PSS reaching approximately 1000 S/cm. Furthermore, PEDOT:PSS shows high ionic conductivities: ionic mobilities for small ions migrating in PEDOT:PSS can reach values that exist in dilute electrolytes [26]. Indeed, a novel class of devices based on PEDOT:PSS have been reported, which have ions as their main charge carrier (Iontronics), with subsequent development of ion transistors and ion pumps demonstrated for delivery of ions, neurotransmitters and other small molecules [27]. The combined high ionic and electronic mobilities are key reasons for PEDOT:PSS emerging as the champion material for devices such as OECTs.

### 1.1.5 Operational Principle

Apart from choosing the optimal materials for an OECT, it is important to understand its operating principle. Bernardis and Malliaras [6], have reproduced the transient, the speed with which the transistor responds to external changes such as biological signals, and the steady state behavior of an OECT by modeling it as an ionic and electronic circuit (figure 1.1c). The electronic circuit refers to the current flux of holes inside the channel and the changes of its magnitude upon de-doping. The ionic circuit (figure 1.1c), has been modeled as a capacitor and resistor in series. For simplicity, the capacitance of the gate has been neglected. The resistor in the model refers to the ionic strength of the electrolyte and the capacitor to the amount of ions that can be stored in the bulk of the channel. The model explains the operating principle of the OECT which is affected by the interplay between the ionic and electronic currents. Thus, an understanding of the parameters that influence these properties must be taken into consideration and tuned according to the specific applications at hand. These parameters include: the material / size of the gate, the resistance of the electrolyte, and the size and geometry of the channel. Once defined, optimal parameters must be weighed with considerations such as fabrication - for instance, micrometer scale transistors exhibit fast responses which are stable for higher frequencies, making them suitable and more specific for fast biological events (such as neuronal signaling), however, scaling down the dimensions requires somewhat complex lithographic techniques (figure 1.2a).

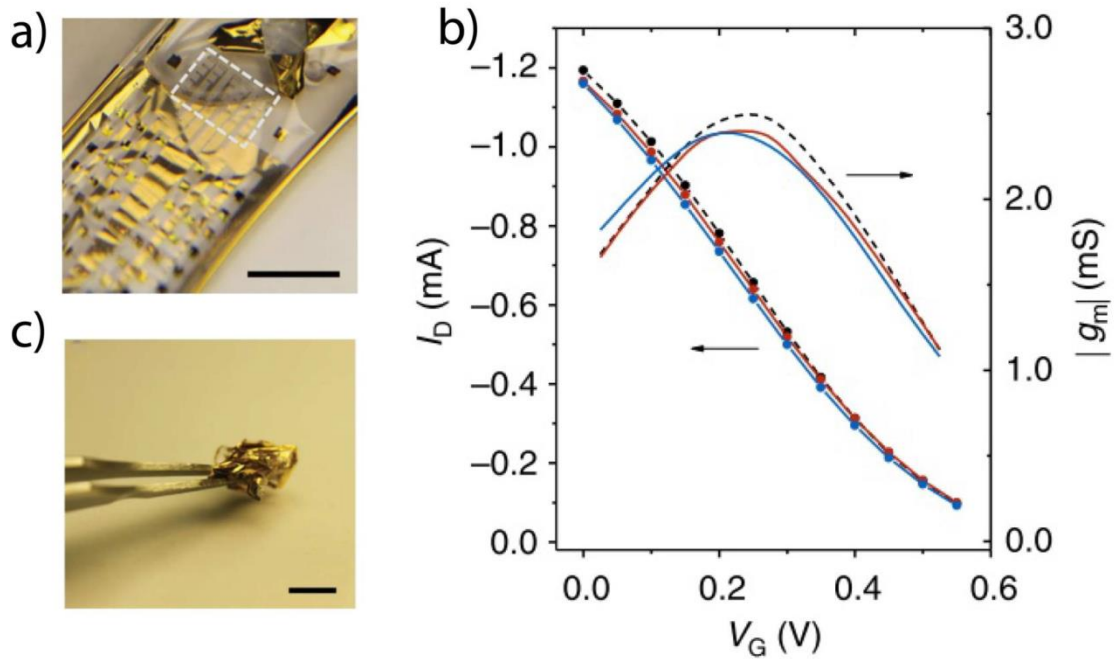


**Figure 1.2:** Robust micrometer scale, high amplification OEETs: a. an array of OEETs on a thin flexible substrate: scale bar = 1 cm b. the array is extensively crumpled c. transfer characteristics of device before (red) and after (blue) crumpling b. transconductance and time response for devices before (red) and after (blue) crumpling. (a, b, c reproduced from [5], with permission from [Nature Publishing Group])

Arguably, the most important device property of the OEET is related to its amplification properties. High amplification is a common necessity for unraveling biological information; to increase signal to noise ratio and to lower detection limits thus increasing sensitivity. For example, in electrophysiology it is important to record brain activity that has a wide spectrum of frequencies and amplitudes. The potential difference of this activity is on the order of a few micro volts, and by taking advantage of its inherent transistor properties, OEETs can be used to locally amplify the signal [28]. The efficiency of the amplification can be measured by the transconductance, which is defined as  $g_m = \frac{\Delta I_d}{\Delta V_g}$ . Therefore, the higher the value of the transconductance, the better the gain. Khodagholy et al.,[5] have shown that the OEET reaches transconductance values in the miliSiemens range, outperforming traditional and other organic transistors (figure 1.2b), an impressive feat for a device fabricated based with solution processed materials at room temperature. Furthermore, as shown in figure 2b and c, the transconductance and the time characteristics are not affected even after extensive use and harsh manipulation. Finally, by carefully selecting and varying geometrical characteristics such as channel length, width and thickness, Rivnay et al.,[29] have engineered OEETs with peak transconductance values at zero gate voltage. This is of importance in many applications where very

low voltages are required, for example when cell or lipid bilayer integrity has to be maintained over an extended period of biasing [30]. Moreover, omitting additional biasing facilitates simpler integration to circuits and recording systems, something desirable for lab on chip applications. From the above, we see how individual properties and characteristics of an OECT may be tuned for a broad range of biological applications.

## 1.2 Applications in Biology

### 1.2.1 OECTs coupled with biological moieties for sensing.

In this section work related to the coupling of OECTs with a variety of different biological molecules and macromolecules will be discussed, including ions, proteins (enzymes and antibodies), lipids and nucleic acids. These devices have been reported for applications in basic research but particularly as new alternatives for low-cost diagnostics.

#### *OECTs as ion sensors*

The electrolyte is an integral part of an OECT; variations in its ionic concentration affect the device properties. Therefore, sensing of ions, which is of great importance in healthcare diagnostics, has been possible with the OECT. Lin et al.,[31] have shown that altering the ionic concentration of an electrolyte affects its channel current ( $I_d$ ). Figure 1.3a shows a transfer curve, which is a function of the drain current with respect to the sweep of the gate voltage, for a range of concentrations of a potassium chloride (KCl) electrolyte. The transfer characteristics display the decrease in  $I_d$  with increase of the  $V_g$ , with a shift of these curves to lower values of  $V_g$  when the ionic concentration increases. This behavior can be simply explained by the ionic circuit in figure 1c; the higher the ionic concentration in the electrolyte the higher the ionic charge at the interface between PEDOT:PSS. So, the increase of the charge shifts the effective gate voltage ( $V_{g,eff}$ ) (constituting the potential drop to the channel) to higher values and in turns de-dopes the channel. Apart from changes in electrolytes concentration, changes in electrolyte composition can shift the  $V_{g,eff}$  in the OECT, a principle used by Tarabella et al.,[32] for sensing liposomes and micelle formation of cetyltrimethylammonium bromide (CTAB).

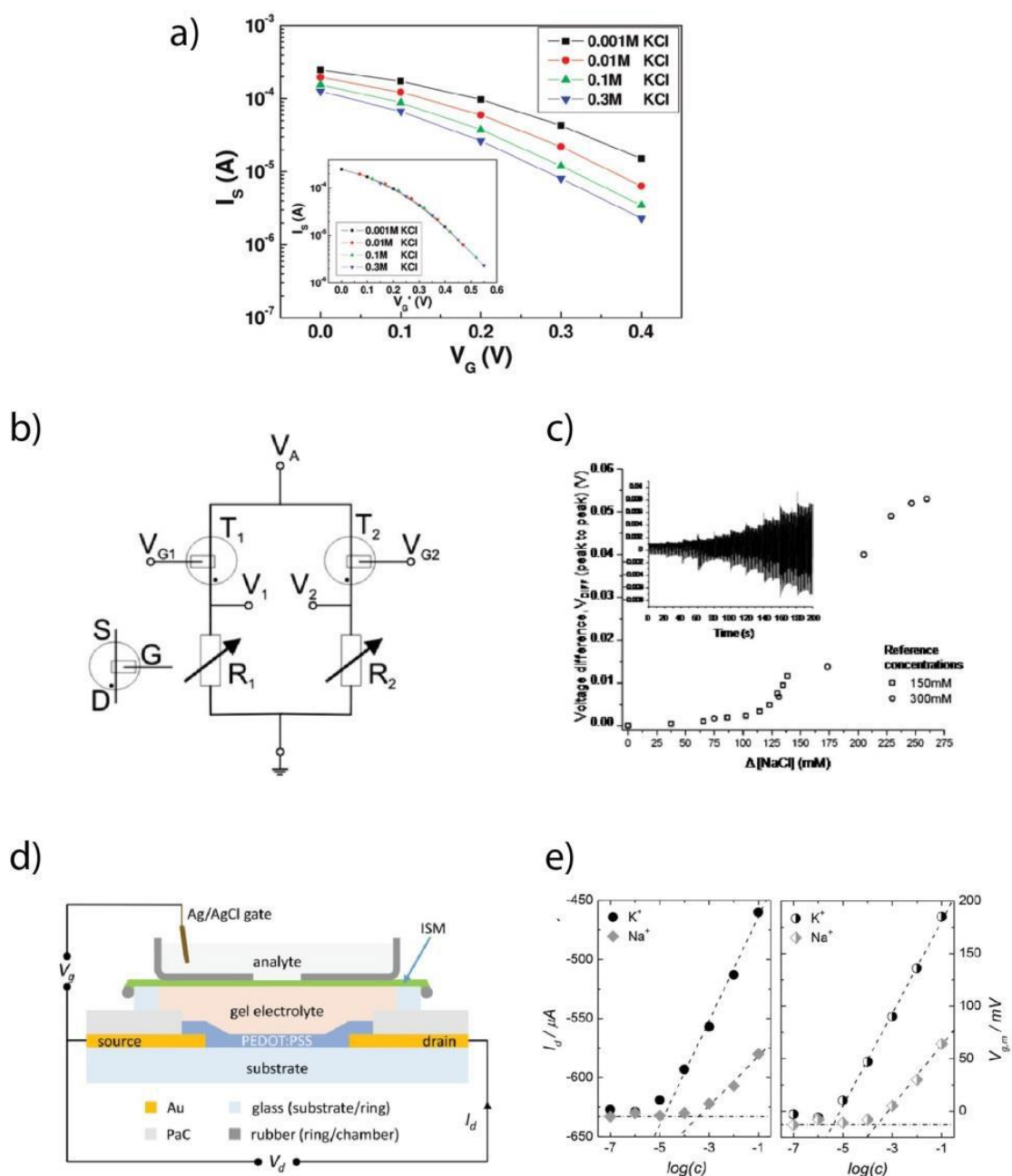


**Figure 1.3:** OECTs used as ion sensors a. Transfer characteristics of an OECT for different concentrations of KCl solutions ( $V_d = -0.1$  V). (reproduced from [31], with permission from [ACS Publications]). b. Wheatstone bridge circuit diagram. c. The peak-to-peak voltage difference as a function of concentration difference of NaCl solution, inset curve shows the raw data. (b, c reproduced from [33], with permission from [American Institute of Physics]). d. schematic of Ion-selective OECT. e. Calibration curves ( $I_d$ ,  $V_{g,m}$  vs concentration) of pure KCl and NaCl solutions performed using ion selective OECT (IS-OECT). (d, e reproduced from [34], with permission from [Wiley Online Library]).

Svensson et al.,[33] have integrated OECTs in circuits for ion sensing in order to improve the sensitivity. In this case, two transistors were connected with two resistors in a Wheatstone bridge circuit configuration (figure 1.3b). After application of a small constant drain voltage the transistors operate in a resistive mode and the potential difference ( $V_{diff}$ ) between the two transistors is continuously recorded. By additional application of a sinusoidal gate voltage of 10 Hz, a change of the resistance in the electrolyte and thus the  $V_{diff}$  can be measured. When the ionic concentration of the electrolyte in both transistors is the same, no potential difference is observed. By changing however the concentration of the electrolyte in the second transistor, a potential difference is observed. In figure 1.3c (inset; raw data), we see how the phase of the potential between the two transistors shifts versus the concentration difference in the two electrolytes.

The importance of sensing specific ions has prompted the development of ion-selective OECT sensors (IS-OECT). Sessolo et al.,[34] as well as Mousavi et al.,[35] have combined OECTs with polymeric membranes that permit the passage of specific ions. In figure 1.3d the lay-out of an ion-selective OECT is shown. Briefly, a polyvinylchloride (PVC) based potassium-selective membrane was placed between a gel electrolyte and the electrolyte of interest, separating the channel from the gate of the OECT. By increasing the concentration of the electrolyte, a decrease in the drain current which is proportional to the  $[K^+]$  is observed. This is attributed to the increase number of  $K^+$  ions penetrating the channel and de-doping it, or to the decrease of the electrolyte resistance. Figure 1.3e shows the calibration curve of drain current and effective membrane voltage versus ion concentration for pure KCl and NaCl solutions. The sensitivity to  $K^+$  ions is an order of magnitude higher than that of  $Na^+$  ions, and this confirms the ion selectivity of the membrane. In a similar configuration, Bernards et al.,[30] have placed a lipid bilayer with and without embedded proteins, in this case bacterial gramicidin ion pores, selective for monovalent cations, as a selective membrane instead of a polymeric one. In the absence of gramicidin no  $I_d$  modulation was observed when a gate potential was applied, whereas in the presence of gramicidin channels a clear modulation was observed in the presence of gramicidin, although only in the presence of KCl, not in the presence of  $CaCl_2$ , demonstrating the selectivity of the bilayer lipid membrane. A 1V pulse was demonstrated to disrupt the bilayer membrane, underlying the importance of operation at low voltages when interfacing with biological systems.

### *OECTs as enzymatic sensors*

One of the first applications of the OECT for interfacing with biology was as an enzymatic sensor [36]. The operating principle of an OECT enzymatic sensor involves either a change in a local pH upon oxidation of species or transfer of electrons to the gate of the device (figure 1.4a). By measuring changes in pH Nishizawa et al., have used polypyrrole based OECTs to sense penicillin [37]. They

immobilized the enzyme on top of the channel and upon oxidation of the penicillin to penicilloic acid; the change of the local pH increased the conductivity of the polypyrrole. A major drawback, however, is that the conductivity of polypyrrole drops in physiological conditions, creating a mismatch between the device's operation regime and the optimal physiological environment of enzymes and proteins. In contrast, by measuring electron transfer, Zhu et al.,[38] demonstrated the use of a PEDOT: PSS based OECT for glucose sensing in a wide range of pH environments. The sensing mechanism is as follows: glucose oxidase catalyzes the conversion of glucose to gluconolactone in the presence of oxygen forming hydrogen peroxide ( $H_2O_2$ ) as a byproduct. The  $H_2O_2$  in turn transfers an electron to the gate of the OECT (figure 1.5a(i)). In order for charge neutrality to be maintained in the electrolyte, a positive ion penetrates the OECT and compensates the PSS anion (figure 1.4a(ii)) , which in turn causes a shift of the  $V_{g,eff}$  and thus a decrease of the source–drain current, proportional to the glucose concentration [39]. Platinum (Pt) has been extensively used as a gate in OECT-based glucose sensors [40] because of its good catalytic performance for the oxidation and reduction of  $H_2O_2$  and other biomolecules of interest such as dopamine and adrenaline [41]. The sensitivity of OECT devices, after optimization, can detect levels of glucose that exist in human saliva (as low as  $8\mu M$ ), and sweat ( $\sim 150\mu M$ ), leading to non – invasive measurement systems [40].

The geometry of an OECT-based enzymatic sensor affect its sensitivity and a systematic study has been performed by Cicoira et al.,[42] who measured the decomposition of  $H_2O_2$ , mentioned above as the byproduct of the enzymatic reaction, for devices with the same channel, but different gate area (figure 1.4b). They showed that the sensitivity of the device increased as the gate size decreased. Such optimization is confirmed by modeling the behavior of the OECT and optimizing it for two types of applications: for electrochemical sensing and for ion to electron conversion [43]. This can be explained by the potential drop at the two interfaces: the gate/electrolyte and electrolyte/channel interface (Figure 1.4b). For ion to electron conversion, after application of  $V_g$ , the necessity of a high driving force to push the ions to the channel requires that most of the potential drops at the channel, therefore a non-polarizable gate or a gate bigger than the channel is needed (figure 1.4b). Conversely, for enzymatic sensors such as the glucose sensor, most of the driving force comes from the electron transfer to the gate, which in turns shifts the  $V_{g,eff}$  at the gate/electrolyte interface; hence if the potential drops at the electrolyte / channel interface, the change will be negligible. This is the case when the gate is smaller and the material is polarizable.

The inherent amplification afforded by the OECT coupled with the optimization of the geometrical characteristics have resulted in highly sensitive enzymatic sensors. However, further modification of the gate with novel materials, such as Pt nanoparticles, has pushed the limit of detection to the nanomolar range. Tang et al.,[44] modified a Pt gate with Pt nanoparticles (Pt - NPs) and carbon nanotubes (figure 1.4c). Moreover, the enzyme was entrapped on the gate by a chitosan

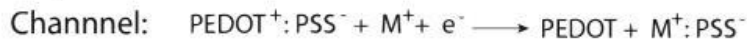
membrane. Owing to their high electrocatalytic activity and the high surface to volume ratio, the Pt - NP modified gate showed an increased sensitivity compared to the pristine Pt gate and the gate modified with carbon nanotubes, and increased the limit of detection for glucose to 10 nM (figure 1.4d). By using the same concept, Liao et al.,[45] used graphene and reduced graphene oxide flakes at the gate and pushed the sensitivity to a similar range while simultaneously improving the selectivity of sensing by adding a Nafion membrane. Negatively charged acids, such as ascorbic acid and uric acid commonly found in biological media, create interference in the measurements by direct oxidation at the gate. However, the use of a Nafion membrane or chitosan functionalization can repel and attract respectively these species while the neutral hydrogen peroxide can diffuse to the gate unimpeded. Finally, Kergoat et al.,[46] have blended Pt nanoparticles with PEDOT:PSS. By using the modified PEDOT:PSS:Pt-NPs, they have successfully fabricated OEECTs in order to sense glutamate and acetylcholine, which are important neurotransmitters.

a)

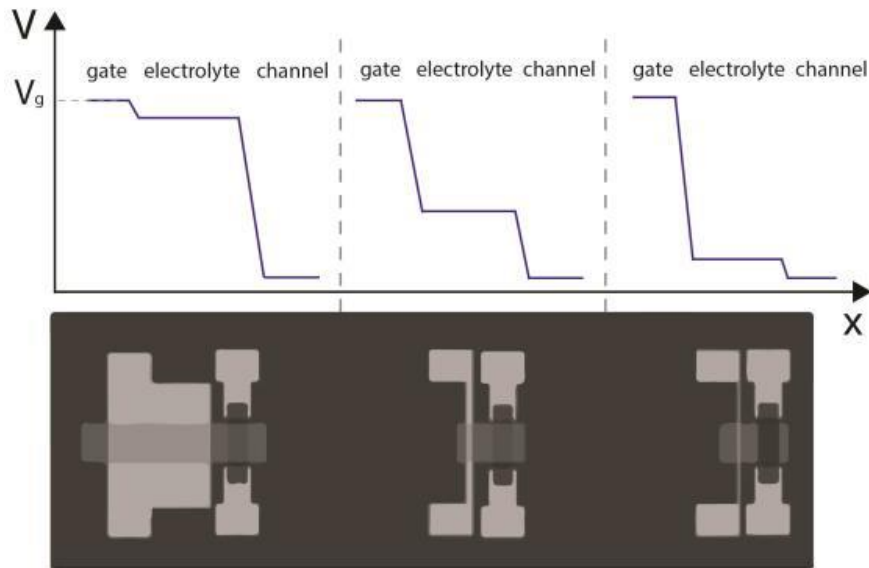
i)



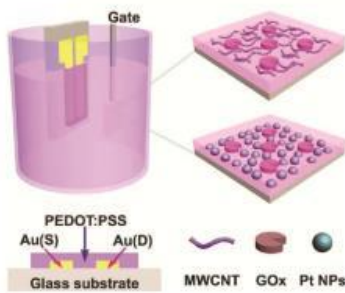
ii)



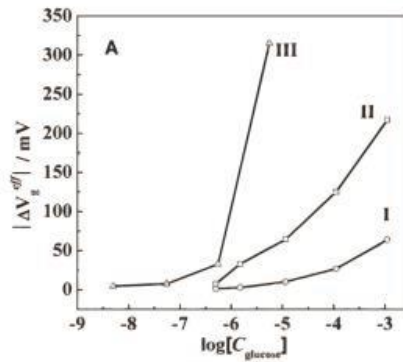
b)



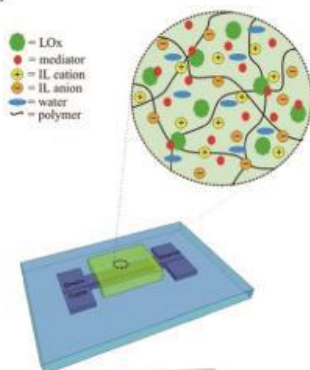
c)



d)



e)



f)

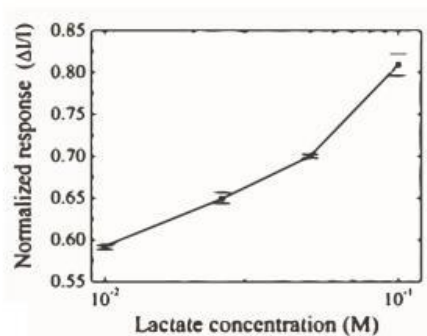


**Figure 1.4:** OECTs used as enzymatic sensors: a. i) Transfer of electron from glucose to the gate through the biological reaction catalyzed by glucose oxidase ii) de-doping mechanism of PEDOT:PSS at the channel b. Drop of potential at the interfaces and its dependence to the gate/ channel size ratio. (b, is reproduced and modified from [42] with permission from [Wiley Online Library]) c. Schematic layout of an OECT glucose sensor with the gate modified with Pt NPs, MWCTS and GOx f. The dependence of  $\Delta V_{g,eff}$  as a function of  $\log[C_{glucose}]$  for CHIT/GOx/Pt (line I), MWCNT-CHIT/GOx/Pt (line II) and CHIT/GOx/Pt-NPs/Pt (line III) gate electrodes. (c, d are reproduced from [44] with permission from [Wiley – VCH]). e. Schematic layout of an OECT lactate sensor with solid state ionogel electrolyte. f. Normalized response of the OECT vs. lactate concentration. (e, f are reproduced from [47] with permission from [RSC Publishing]).

Apart from high sensitivity, the need for low cost and stable biosensors requires the use of alternative materials and simple fabrication techniques. Towards that goal, Shim et al.,[14] developed an all-PEDOT OECT for glucose sensing. PEDOT:PSS, however, exhibits low catalytic properties for the oxidation of  $H_2O_2$ . Therefore, owing to its low redox potential, ferrocene has been used as a mediator for the transfer of electrons to the gate. This facilitates a single step fabrication of low cost OECT based enzymatic sensors. Yang et al.,[15] have successfully demonstrated an all plastic OECT glucose sensor using room temperature ionic liquids (RTILs) as an electrolyte, thus solving issues related to long term stability of the OECTs for use in biosensing. Liquid electrolytes are unstable for long term applications, since they are susceptible to evaporation, and thus destabilization of ionic concentration. RTILs, molten salts at room temperature, have gained significant attention in electrochemistry as alternatives to aqueous electrolytes [48]. This is due to their desired characteristics, such as wide electrochemical window of operation, high ionic strength, low or zero evaporation rates, and for biological applications stabilization of enzyme conformation and function. For this application Yang and co-workers dissolved both the mediator and the enzyme in the RTIL and drop casted on top of a hydrophobic virtual well. The glucose sensor showed sensitivities in the micromolar range. Subsequently, Khodagholy et al.,[47] combining ionic liquids with cross linkable polymers, developed an OECT lactate sensor integrated with a solid state electrolyte. The ionic liquid gel electrolyte included: lactate oxidase and the ferrocene mediator for sensing, IL for its high ionic conductivity and for the stabilization of enzyme's conformation, and photo-crosslinkable monomer and photo-initiator for creating the solid state electrolyte (figure 1.5c). Drop-casting and subsequent polymerization under UV resulted in a gel-like electrolyte. Figure 1.5d shows the normalized response of the OECT for a concentration range of lactate that exists in human sweat. This type of device was proposed as a wearable long term sensor for continuous monitoring of lactate levels in athletes. Finally, OECTS have been integrated with microfluidics for the fabrication of multi-analyte sensors: Yang et al.,[17a] demonstrated surface

directed microfluidic that uses capillarity forces to drive a sample consisting of glucose and lactate to an array of OECTs for simultaneous measurement of glucose and lactate.

#### *OECTs as immunosensors/ nucleotide sensors*

OECTs can detect the presence of cells and biomolecules. Specifically, when a cell is in the proximity of an OECT channel, its membrane is polarized, resulting in an additional potential. The cause for the polarization of the cell is the potential difference between the channel and cell [49]. This additional potential shifts the effective gate voltage to lower values affecting the de-doping of the channel. Using this principle, He et al.,[50] have fabricated an OECT that detects the presence of the pathogenic bacteria *E. coli*. In more detail, an immobilization step of the anti-*E. Coli* antibody took place through biofunctionalization on the OECT channel (figure 1.5a). The *E. coli* bacteria were then captured through antibody antigen interactions. When the bacteria are in a low ionic concentration media they exhibit a negative charge in their membrane, thus immobilized bacteria on top of the OECT channel form a negatively charged layer. Consequently, upon application of a gate voltage the negatively charged layer of bacteria attracts positive ions in the electrolyte, resulting in a shift of the  $V_{g,eff}$  to lower values (proportional to the bacteria concentration), which means that fewer ions are de-doping the channel or a higher voltage has to be applied in order to de-dope the same magnitude of current in the absence of bacteria (figure 1.5b). Similarly, Kim et al.,[51] fabricated an OECT based immunosensor for prostate specific antigen (PSA), by immobilizing a PSA specific antibody on the channel. The shift of the  $V_{g,eff}$  to the channel is proportional to the captured PSA antigen concentration. A secondary antibody conjugated with Au nanoparticles was then used in a typical sandwich-ELISA format, thereby resulting in an increased sensitivity, mostly likely due to the fact that Au-NPs are negatively charged in suspension.

Finally, an OECT DNA sensor has been developed by Lin et al.[52]. Figure 1.5c shows the layout of the device, which consists of an OECT with integrated microfluidics on top of a flexible polyethylene terephthalate (PET) substrate. Single stranded DNA was immobilized on the gate, with a second gate was used as a control. Figure 5d shows a transfer curve, in which the gate voltage needed to de-dope the channel shifts to higher values after immobilization and hybridization of the complementary DNA strand. The mechanism of sensing is as described above; owing to its charge, the DNA affects the capacitance at the interface between gate and electrolyte, and thus shifts  $V_{g,eff}$ . A similar mechanism was also shown by Liao et al., for the detection of diatoms in sea water [53]. An interesting observation was that PEDOT:PSS appeared to promote diatom growth when compared with simple glass slides.

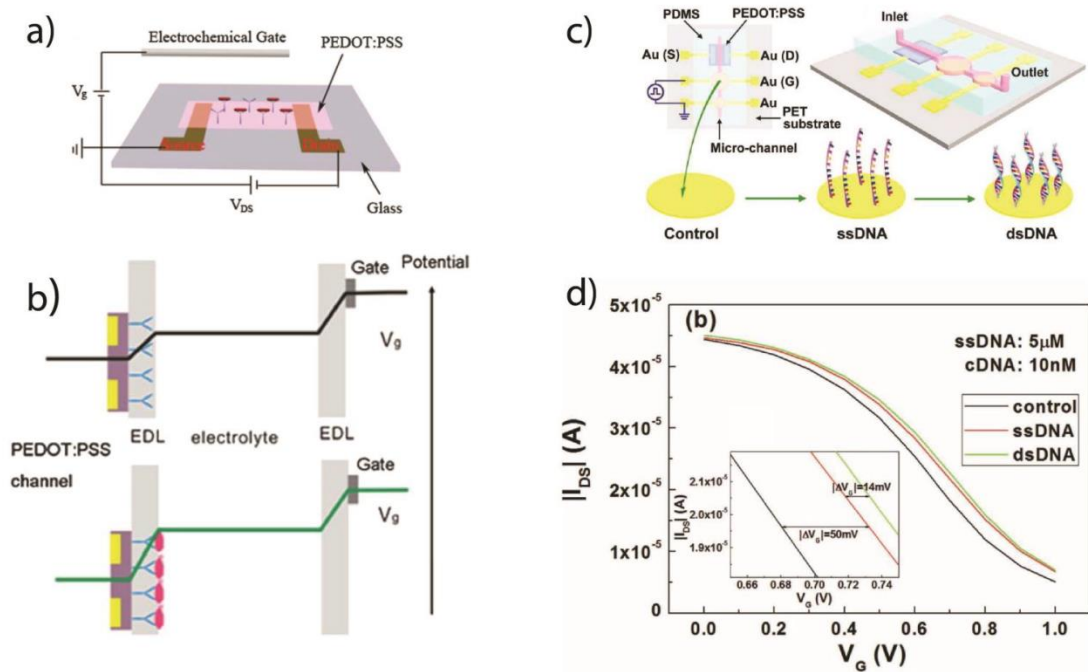


**Figure 1.5:** OECTs as Immunosensors and nucleotide sensors: a. Schematic of an *E. coli* O157:H7 sensor based on an OECT. b. Schematic diagram of potential drops in the electric double layers (EDL), including the channel/electrolyte and electrolyte/gate interfaces, in the OECT before and after the immobilization of *E. coli* O157:H7 on the PEDOT:PSS surface. (a, b, reproduced from [50], with permission from [RSC Publishing]) c. Schematic of an OECT integrated in a flexible microfluidic system, which is characterized before and after the modification and the hybridization of DNA on the surface of Au gate electrode. d. Transfer characteristics of OECTs measured in microfluidic channels before and after the immobilization and the hybridization of DNA on Au gate electrodes.  $V_{ds} = -0.1$  V. The inset shows the horizontal shifts of the transfer curves. (c, d, reproduced from [52], with permission from [Wiley Online Library])

### 1.2.2 OECT coupled with whole cells for electrophysiology

In this section work related to the coupling of OECTs with live mammalian cells will be discussed, rather than individual biomolecules or macromolecules as in the previous section. This section has been split into two sections; integration with non-electrogenic cells for monitoring toxicology/diagnostics, and, integration with electrogenic cells such as cardiomyocytes and neurons. In the former case, the OECT is used to measure a ‘passive’ electrical property of the cells, whereas in the latter, the

OECT is measuring active electrical properties of the cells, with applications both in vitro for toxicology/diagnostics, but also in vivo for potential therapeutics.

### *Integration of OECTs with non-electrogenic cells*

The first report of OECTs with live mammalian cells was by Bolin et al. [54]. MDCK (Madin Darby canine kidney) epithelial cells were seeded along the channel of an OECT and the device was used to bias the channel such that an electrochemical gradient was produced. Depending on the redox potential of discrete areas of the channel, differential cell adhesion was observed, illustrating the potential for conducting polymers with electrically tuneable surface properties in controlling adhesion of cells. A non-trivial issue associated with this work was the demonstration by the authors that live cells grow and proliferate on conducting polymer devices, indicating the biocompatibility of the materials used. Long term stability of these devices in cell culture media has also been demonstrated [55]. Subsequent integration of OECTs with live cells have focused on the sensitivity of the devices to changes in biological ion flux, a parameter which can be used for monitoring the integrity of mammalian cells, as the flow of ions is tightly regulated in tissues and dysregulation is often a sign of disease or dysfunction. In particular, OECTs have been used as an alternative technology for sensing barrier tissue integrity, monitoring variations in paracellular ion flux with state-of-the-art temporal resolution and high sensitivity. Barrier tissue is composed of epithelial or specialized endothelial cells whose role is to modulate ion flux between different bodily compartments. As this role is often compromised during toxic events, monitoring of this tissue is very interesting for diagnostics/toxicology. In a first instance, Jimison et al., [56] integrated epithelial cells grown on filter supports with the OECT, using a model of the gastrointestinal tract Caco-2 cell line which is established as a barrier tissue model (figure 1.6a). This configuration is compatible with existing barrier tissue characterization and toxicology methods and protocols which frequently use filter supports as they mimic the polarized nature of the cells in vivo where they separate different functional compartments (e.g. gastrointestinal tract from blood stream). The OECT ionic circuit on the addition of barrier tissue is shown schematically in figure 1.6b, with the cell layer represented as a resistor and capacitor in parallel. In this way, the OECT uses the ionic to electronic transduction to measure changes in the impedance of the ionic circuit. Application of a positive gate voltage  $V_g$  leads cations from the electrolyte, in this case cell culture media, into the conducting polymer channel thus de-doping it. The transient response, which gives the time of how fast the channel will be dedoped, can be quantified by the time constant ( $\tau = RC$ ). The  $\tau$  depends on the capacitance of the channel and the resistance of the electrolyte. The presence of the barrier tissue modifies the ionic flux, due to the addition of additional capacitor and resistor (figure 1.6b) and the drain current by inducing a slow response thus increase in the  $\tau$  [25b].

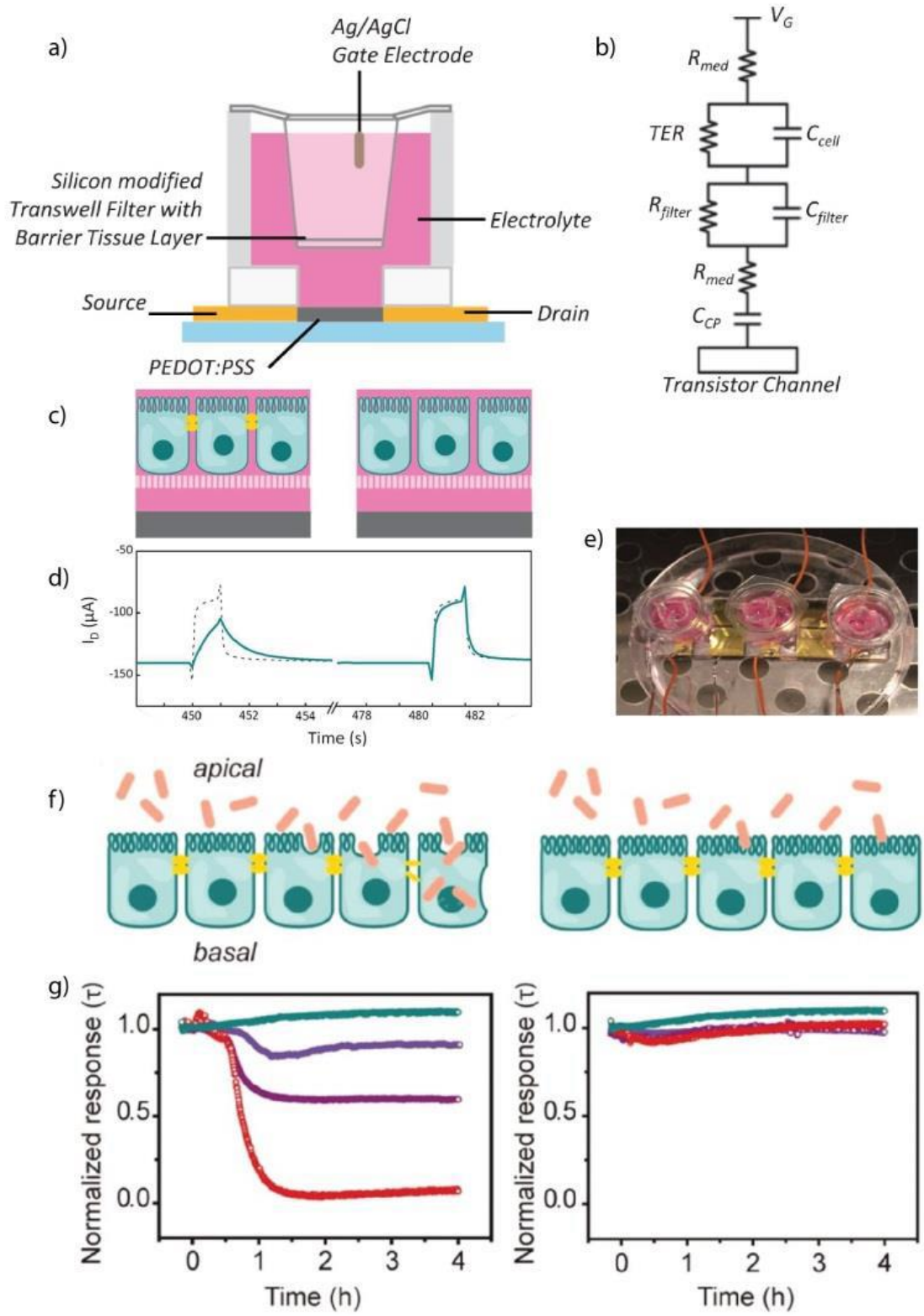


**Figure 1.6:** Barrier tissue integrity at the interface with an OEET: a. Layout of an OEET with an integrated barrier tissue b. Equivalent circuit describing ionic transport between gate electrode and transistor channel. TER refers to the transepithelial resistance of the cell layer,  $C_{cell}$  refers to the capacitance of the cell layer,  $R_{filter}$  and

Cfilter refer to the resistance and capacitance of the porous filter, respectively, Rmed refers to the resistance of the media, and Ccp refers to the capacitance at the CP and electrolyte layer c. Cartoon showing polarized Caco-2 cells with tight junctions (left) and without (right), sitting on a porous cell culture membrane, above a PEDOT:PSS transistor channel. Tight junctions are shown in yellow. d. OECT Id transient response with cells before (left) and after (right) the addition of 100 mM H<sub>2</sub>O<sub>2</sub>, (solid lines). OECT Id response in the absence of cells is overlaid (dashed lines) (a, b, c, d, reproduced from [56], with permission from [Wiley Online Library]) e. Picture of the multiplex device shown on a Petri dish inside the cell-culture incubator. The cell culture insert is shown suspended in the plastic holder affixed to the glass slide. The Ag/AgCl gate electrode is shown immersed in the apical media, while source and drain cables are attached to their respective positions on the glass slide g. Kinetics of polarized epithelial monolayer infected with Salmonella typhimurium. Cartoon illustrating infection with wildtype (WT) (left) and non-invasive S. typhimurium (right). Mean normalized response ( $\tau$ ) of the OECT in the presence of WT (left) and non-invasive S. typhimurium (right) at different MOI over 4 h, bacteria were added at  $t = 0$ . Non-infected represents OECT + cells with no added bacteria. Non-infected cells are in cyan, MOI: 10 in blue, MOI: 100 in purple, and MOI: 1000 in red. (e, f, g, reproduced from [57], with permission from [Wiley Online Library])

The disruption of barrier tissue (illustrated schematically in figure 1.6c), related to the destruction of protein complexes between the cells, was also demonstrated upon addition of hydrogen peroxide (H<sub>2</sub>O<sub>2</sub>), a known toxin. Figure 1.6d illustrates the high temporal resolution of the OECT in monitoring barrier tissue disruption, from one pulse to the next. Monitoring of the Id response to the gate voltage was normalized as a function of time in the presence of both H<sub>2</sub>O<sub>2</sub> and a second toxin, ethanol, and shown to have greater sensitivity than traditional methods. The effect of EGTA (Ethylene glycol-bis(beta-aminoethyl ether)-N,N,N',N'-tetra acetic acid) known to affect paracellular ion transport pathways and trans epithelial resistance of cells has also been demonstrated with the OECT [58]. Dose dependent responses to addition of EGTA were detected and validated against existing commercially available electrical impedance spectroscopy shown significant advantages of the OECT in terms of temporal resolution. A visual demonstration of the OECT fabrication and operation for monitoring barrier tissue disruption by EGTA has also been reported [59].

For non-acute diagnostics applications where time scales for readouts exceed minutes and may actually extend to days or even weeks, not only the stability of the sensor, but also the environmental conditions for measurement must be required. To test the stability of the OECT and assess suitability for long term measurements of an OECT, Tria et al., transitioned the device to a format compatible with operation in

physiological conditions, and to cope with the many varying parameters inherent to biological systems, the number of devices operated simultaneously was scaled-up (Figure 1.6e) [60]. This system was used to successfully monitor the kinetics of integrity of the same gastrointestinal model after infection with the pathogenic organism *Salmonella typhimurium* (illustrated in figure 1.6f), while a non-pathogenic *Salmonella* bacterium showed no response regardless of the concentration added (figure 1.6g). The experiment was also carried out in milk, a complex matrix containing many different compounds including proteins and fats; however the OECT operation and detection of *Salmonella typhimurium* remained robust, unlike a leading commercially available alternative based on electrical impedance scanning using stainless steel electrodes.

OECTs show promise for applications requiring rapid and dynamic detection of variations in ion flow. The examples cited up until now have involved integration of the cells on a filter, physically separated from the device by the electrolyte, using a top-gate format. Another approach to measure the integrity of cells is to seed the cells directly on device, either with a top-gate format, or with a side-gate. This former principle was used by Lin et al., and the device was shown to be able to detect cell attachment and cell detachment by shifting the  $V_g$ ,  $eff$  values, via a mechanism similar to that used by Yan and co-workers for detecting antibody/DNA binding [61]. Again the stable operation of the OECT in cell culture medium was confirmed, as well as the ability to support cell growth, in this case two cell lines: human esophageal squamous epithelial cancer cells and fibroblasts. In a similar configuration, Yao et al., [62] show the integration of human airway epithelial cells with the OECT. Cells were seeded directly on an OECT array, however the cells directly above the PEDOT:PSS channel are postulated to be suspended over the channel with a gap formed below (figure 1.7a). The authors investigated the dose response of transepithelial ion transport to forskolin, an agonist which causes opening of the CFTR (cystic fibrosis transmembrane conductance regulator) channel (figure 1.7b), a major contributor to transcellular ion transport. The transport of  $Na^+$  ions from the basolateral compartment to the apical compartment, result in a change in the channel current, which the authors convert to an effective gate voltage change. Ramuz et al., combined optical and electronic sensing of epithelial cells using OECTs with both the gate and the channel in the same plane, both consisting of PEDOT:PSS [63]. This circumvents an issue for long term operation of devices using Ag/AgCl electrodes which were demonstrated to be toxic to live cells for periods  $> 10$  hours [60]. MDCK I cells were seeded directly over an area comprising both the channel and the gate. The authors demonstrated the possibility for continuous measurements of ion flow in epithelial cells coupled with optical imaging of the cell layer on the device, thanks to the transparent nature of the PEDOT:PSS film (figure 1.7c). Further, the measured electrical signal is demonstrated to be due to tight junction-related barrier tissue formation and not to simple cell coverage as the presence of cells on the active area of the OECT does not change the transistor response to gate pulse voltage unless the cells present barrier tissue properties. A corollary of this work is that high resolution

imaging of cells is possible on PEDOT:PSS films, not only in bright field mode, but also for fluorescence imaging (figure 1.7d), highly valuable for definition of molecular mechanisms in biological systems.

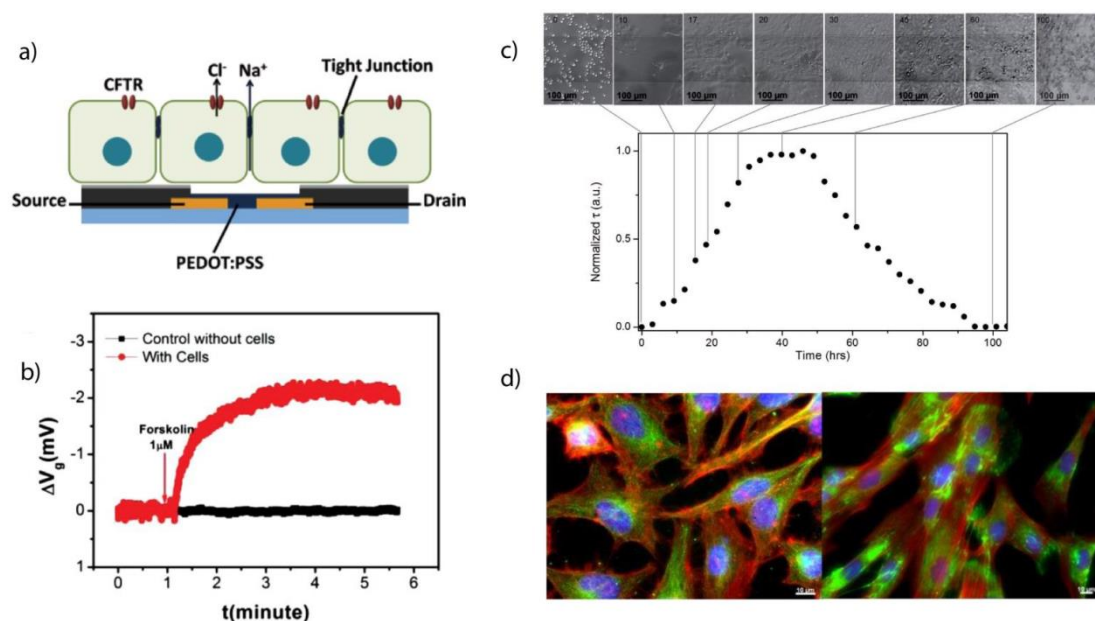


**Figure 1.7:** Non electrogenic cells in direct contact with OECTs: a. view of polarized Calu-3 cells with tight junction sitting on the PEDOT:PSS transistor channel of an OECT b. In situ OECT response with (red) and without (black) Calu-3 cells upon the addition of 1  $\mu$ M CFTR agonist forskolin. Transistor channel current change was converted to effective gate voltage change. (a, b reproduced from [62], with permission from [Wiley Online Library]). c. Micro-optical images of MDCK-I on top of the OECT channel area (the darker horizontal line in the middle of the picture corresponds to the PEDOT:PSS channel) and corresponding electrical characteristics with a measurement taken every 3h. d. Illustrative example of high resolution fluorescence imaging possible on PEDOT:PSS devices. HeLa cells (left) and immortalized human fibroblasts (right) (c, d, reproduced from [63], with permission from [Wiley Online Library]).

### *OECT for stimulation and recording of electrogenic cells*

Electrical stimulation and recording of nerve tissue and neural activity have provided valuable information about physiological and pathological functions of the body and brain. Typically, these recordings are performed with metal electrodes [64]. For example, the main technique to record cardiac activity, electrocardiography (ECG), uses electrodes in contact with the skin which provide information about the normal function or abnormalities of the heart. OECTs include advantages that can overcome many limitations in electrophysiology. First of all, the low temperature fabrication of OECTs enables devices on flexible, biocompatible, and biodegradable substrates. Campana et al., [65] fabricated OECTs on flexible, resorbable poly(L-lactide-co-glycolide) substrates for ECG recordings. Figure 1.8a shows the layout of the measurements and the raw signal compared to the theoretical heart pulse. In this work, the gate of the OECT was placed directly on skin close to the heart at a constant positive potential ( $V_g = 0.5$  V) relative to the ground potential of the body, while the transistor channel was placed on the forearm at a negative potential ( $V_d = -0.3$  V) relative to the ground. Every heartbeat creates an additional potential which modulates the  $V_{g,eff}$  seen by the channel and result in a clear de-doping of the channel. Conductive gels are usually used as an interface between the skin and channel in order to increase the adhesion for long-term measurements. Figure 8b shows how the fabrication of the device on a flexible substrate improves the contact with the skin which is desirable for recordings of freely moving subjects. Furthermore, the use of biodegradable materials can push to implantable devices that can be used for recording or stimulating electrogenic cells.

For the brain, there are three main electrophysiology recording techniques: electroencephalography (EEG) which utilizes electrodes in contact with the skin, electrocorticography (ECoG) which utilizes electrodes in contact with the surface of the brain, and stereoelectroencephalography (SEEG) which utilizes probes that penetrate deep in the brain [66]. Depending on the nature of the signal of interest, or the size of the neural population to be interrogated, or the invasiveness / goal of the measurement, EEG, ECoG or SEEG may be selected. Most of the electrodes currently used are relatively inflexible, anchored in the skull, and do not follow the movements of the brain. Moreover, the recording quality usually deteriorates over time, due to the tissue injury and reaction of the immune system to the electrode [67]. A primary challenge is to, to form a good contact with the brain. This can be achieved by using flexible electrodes that conform to the shape of the brain surface [18]. Other requirements are to obtain high quality and stable overtime recordings, i.e through the use of more biocompatible materials, and of course amplification of neuronal signals necessary to detect low magnitude signals of interest. As a proof of concept, Khodagholy et al., [28] demonstrated implantable OECTs for ECoG recordings. A conformal device, consisting of integrated electrodes and OECTs array, was placed on the surface of the brain of an epileptic rat (figure 1.8c). The dimensions of the devices are on the order of few micrometers, fabricated on top of a 2  $\mu$ m polymer substrate.

Figure 8d shows that the signal to noise ratio of the organic electrochemical transistor was far superior compared to the electrodes. Furthermore, the OEET could record low amplitude signals and fast signals from the interior of the brain that the electrodes were unable to detect, hitherto only recordable by depth probes (SEEG). Finally, a recent publication has demonstrated the use of an OEET to monitor cardiac rhythm, eye movement, and brain activity in a human volunteer (figure 1.8e-f) [68]. The device showed a high transconductance operation at low gate voltage, which simplified the wiring, as it necessitated only one power supply to bias the drain.

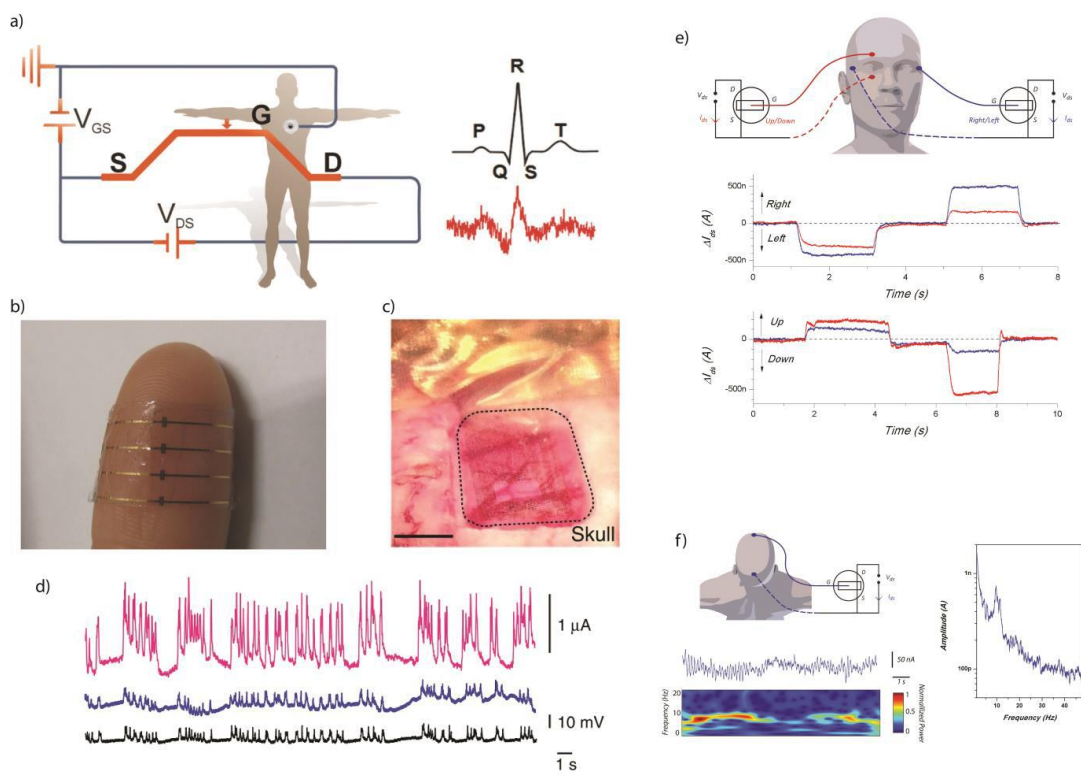


**Figure 1.8:** OEETs for measuring electrogenic cells: a. ECG recording with an OEET operated in direct contact with the skin. b. Photograph of the device showing its transparency and adaptability when attached to human skin. (a, b, reproduced from [65], with permission from [Wiley Online Library]) c. Optical micrograph of the ECoG probe placed over the somatosensory cortex, with the craniotomy surrounded by dashed lines. Scale bar, 1mm d. Recordings from an OEET (pink), a PEDOT:PSS surface electrode (blue) and an Ir-penetrating electrode (black). The transistor was biased with  $V_d = -0.4$  V and  $V_g = 0.3$  V, and the scale of 10mV is for both surface and penetrating electrodes. Note the superior SNR of the OEET as compared with the surface electrode. (c, d, reproduced from [28], with permission from [Nature Publishing Group]). e. Wiring configuration chosen for the EOG measurement,

recording of electrical activity during left/ right eyeball movements, recording of electrical activity during up/down eyeball movements. Both up/ down (red) and left/ right (blue) activities are measured. f. Wiring configuration used for the EEG measurement, along with recording of spontaneous brain activity (top) showing the alpha rhythm, and associated time-frequency spectrogram (bottom), Fourier analysis of a 3min recording. (e, f, reproduced from [68], with permission from [Wiley – VCH]).

### 1.3 Conclusion

Bioelectronics is a growing interdisciplinary field which aims to interface electronics and biology, improving current biomedical tools. The particular niche for organic electronic materials in integration with biological materials or use in biomedical applications comes from a host of beneficial properties unique to these materials in contrast to traditional electronic materials. The underlying notion of amplification, a pre-requisite in biosensing, pushes towards active devices (transistors) rather than passive devices (electrodes). The organic electrochemical transistor lies at the heart of this field principally because of the intimate nature of the interface with biological components, where the biological milieu comprises an integral part of the device, and ions from this milieu are the key to the operation mechanism of the OECT. Improved signal transduction and amplification are common themes in the research cited above, demonstrated repeatedly for the OECT in a wide variety of formats and applications. Stability is a highly valued characteristic for biosensing, and the OECT has been shown to operate stably in a variety of different electrolytes, include complex cell media, seawater and even milk. Long term operation in these electrolytes on the scale of days to weeks has also been possible.

The OECT is a current to voltage transducer; small changes at the input ( $\Delta V_{g,eff}$ ) result in big changes at the output ( $\Delta I_d$ ). OECTs exhibit high transconductance values, essentially high gain, and by tuning the geometry and the size of the channel, the transconductance and the time response can be optimized. Different modes of operation depend on how the effective gate voltage ( $V_{g,eff}$ ) shifts. For example, the  $V_{g,eff}$  can be modulated by changes in the resistance of the electrolyte, charge transfer to the gate, or sensing of an additional external  $\Delta V_g$  signal. Using this principle, OECTs have been used as ion-sensors, enzymatic sensors, DNA sensors, immunosensors, and pathogen sensors. Further, OECTs have been integrated with individual cells, tissues, and even whole organs. Application dependent tuning is a very important benefit of the use of conducting polymers, which are amenable to chemical modification, biofunctionalisation, and fabrication using a wide variety of techniques on different substrates. Compatibility with photolithographical techniques

also facilitates fabrication of micron-scale devices, particularly interesting for monitoring of cells in vitro and in vivo, as well as for high-throughput device arrays.

Future applications for OECTs are expected to further exploit the beneficial properties of these devices, with significant potential in tissue engineering for in vivo applications. The first wave of industrial prototypes in the biomedical arena is anticipated imminently.

OECT has been successfully used in a wide spectrum of biological applications. From simple enzymatic sensing, in which you require large scale devices, to more sophisticated applications, in which the use of micro-scale devices with faster responses and better interface with cells is mandatory. This increased biocompatibility can be used in order to monitor more fragile cells such as primary neuron, astrocytes, and brain endothelial cells.

## 1.4 Bibliography

1. Berggren, M.; Richter-Dahlfors, A., *Organic Bioelectronics, Adv. Mater.* **2007**, *19*, 3201.
2. (a) Svennersten, K.; Larsson, K. C.; Berggren, M.; Richter-Dahlfors, A., *Organic bioelectronics in nanomedicine, Biochimica et biophysica acta* **2011**, *1810*, 276(b) Owens, R.; Kjall, P.; Richter-Dahlfors, A.; Cicoira, F., *Organic bioelectronics - novel applications in biomedicine, Biochimica et biophysica acta* **2013**, *1830*, 4283.
3. Owens, R. M.; Malliaras, G. G., *Organic Electronics at the Interface with Biology. MRS Bulletin* **2010**, *35*, 449.
4. (a) Buzsáki, G.; Anastassiou, C. a.; Koch, C., *The origin of extracellular fields and currents — EEG, ECoG, LFP and spikes, Nature reviews. Neuroscience* **2012**, *13*, 407(b) Rivnay, J.; Owens, R. M.; Malliaras, G. G., *The rise of organic bioelectronics, Chemistry of Materials* **2013**, *26*, 679.
5. Khodagholy, D.; Rivnay, J.; Sessolo, M.; Gurfinkel, M.; Leleux, P.; Jimison, L. H.; Stavriniidou, E.; Herve, T.; Sanaur, S.; Owens, R. M.; Malliaras, G. G., *High transconductance organic electrochemical transistors, Nature communications* **2013**, *4*, 2133.
6. Bernards, D. a.; Malliaras, G. G., *Steady-state and transient behavior of organic electrochemical transistors, Advanced Functional Materials* **2007**, *17*, 3538.
7. White, H. S.; Kittlesen, G. P.; Wrighton, M. S., *Chemical derivatization of an array of three gold microelectrodes with polypyrrole: fabrication of a molecule-based transistor, J. Am. Chem. Soc.*, **1984**, 5375.
8. Kim, S. H.; Hong, K.; Xie, W.; Lee, K. H.; Zhang, S.; Lodge, T. P.; Frisbie, C. D., *Electrolyte-gated transistors for organic and printed electronic, Advanced materials (Deerfield Beach, Fla.)* **2013**, *25*, 1822.

9. Crone, B.; Dodabalapur, a.; Gelperin, a.; Torsi, L.; Katz, H. E.; Lovinger, a. J.; Bao, Z., *Electronic sensing of vapors with organic transistors*, *Applied Physics Letters* **2001**, 78, 2229.
10. (a) Magliulo, M.; Mallardi, A.; Mulla, M. Y.; Cotrone, S.; Pistillo, B. R.; Favia, P.; Vikholm-Lundin, I.; Palazzo, G.; Torsi, L., *Electrolyte-gated organic field-effect transistor sensors based on supported biotinylated phospholipid bilayer*, *Advanced materials (Deerfield Beach, Fla.)* **2013**, 25, 2090(b) Hammock, M. L.; Knopfmacher, O.; Naab, B. D.; Tok, J. B. H.; Bao, Z., *Investigation of protein detection parameters using nanofunctionalized organic field-effect transistors*, *ACS Nano* **2013**, 7, 3970(c) Torsi, L.; Magliulo, M.; Manoli, K.; Palazzo, G., *Organic field-effect transistor sensors: A tutorial review*, *Chemical Society Reviews* **2013**, 42, 8612.
11. Kergoat, L.; Piro, B.; Berggren, M.; Horowitz, G.; Pham, M.-C., *Advances in organic transistor-based biosensors: from organic electrochemical transistors to electrolyte-gated organic field-effect transistors*, *Analytical and bioanalytical chemistry* **2012**, 402, 1813.
12. (a) Blaudeck, T.; Ersman, P. A.; Sandberg, M.; Heinz, S.; Laiho, A.; Liu, J.; Engquist, I.; Berggren, M.; Baumann, R. R., *Simplified large-area manufacturing of organic electrochemical transistors combining printing and a self-aligning laser ablations step*, *Advanced Functional Materials* **2012**, 22, 2939(b) Basiricò, L.; Cosseddu, P.; Fraboni, B.; Bonfiglio, A., *Inkjet printing of transparent, flexible, organic transistors*, *Thin Solid Films* **2011**, 520, 1291(c) Basiricò, L.; Cosseddu, P.; Scidà, A.; Fraboni, B.; Malliaras, G. G.; Bonfiglio, A., *Electrical characteristics of ink-jet printed, all-polymer electrochemical transistors*, *Organic Electronics* **2012**, 13, 244(d) Kaihovirta, N.; Mäkelä, T.; He, X.; Wikman, C.-j.; Wilén, C.-e.; Österbacka, R., *Printed All-Polymer Electrochemical Transistors on Patterned Ion Conducting Membranes*, *Organic Electronics* **2010**, 11, 1207(e) Nilsson, D.; Kugler, T.; Svensson, P.-o.; Berggren, M., *An all-organic sensor–transistor based on a novel electrochemical transducer concept printed electrochemical sensors on paper*, *Sensors and actuators b: chemical* **2002**, 86, 193.
13. Andersson Ersman, P.; Nilsson, D.; Kawahara, J.; Gustafsson, G.; Berggren, M., *Fast-switching all-printed organic electrochemical transistors*, *Organic Electronics* **2013**, 14, 1276.
14. Shim, N. Y.; Bernards, D. a.; Macaya, D. J.; DeFranco, J. a.; Nikolou, M.; Owens, R. M.; Malliaras, G. G., *All-plastic electrochemical transistor for glucose sensing using a ferrocene mediator*, *Sensors* **2009**, 9, 9896.
15. Yang, S. Y.; Cicoira, F.; Byrne, R.; Benito-Lopez, F.; Diamond, D.; Owens, R. M.; Malliaras, G. G., *Electrochemical transistors with ionic liquids for enzymatic sensing*, *Chemical communications (Cambridge, England)* **2010**, 46, 7972.
16. (a) Sessolo, M.; Khodagholy, D.; Rivnay, J.; Maddalena, F.; Gleyzes, M.; Steidl, E.; Buisson, B.; Malliaras, G. G., *Easy-to-fabricate conducting polymer microelectrode arrays*, *Advanced Materials* **2013**, 25, 2135(b) Khodagholy, D.; Gurfinkel, M.; Stavriniidou, E.; Leleux, P.; Herve, T.; Sanaur, S. b.; Malliaras, G. G., *High speed and high density organic electrochemical transistor arrays*, *Applied Physics Letters* **2011**, 99, 163304.
17. (a) Yang, S. Y.; Defranco, J. a.; Sylvester, Y. a.; Gobert, T. J.; Macaya, D. J.; Owens, R. M.; Malliaras, G. G., *Integration of a surface-directed microfluidic system with an organic electrochemical transistor array for multi-analyte*

- biosensors, Lab on a chip* **2009**, *9*, 704(b) Mabeck, J. T.; DeFranco, J. a.; Bernards, D. a.; Malliaras, G. G.; Hocdé, S.; Chase, C. J., *Microfluidic gating of an organic electrochemical transistor, Applied Physics Letters* **2005**, *87*, 013503.
18. Khodagholy, D.; Doublet, T.; Gurfinkel, M.; Quilichini, P.; Ismailova, E.; Leleux, P.; Herve, T.; Sanaur, S.; Bernard, C.; Malliaras, G. G., *Highly conformable conducting polymer electrodes for in vivo recordings, Advanced materials (Deerfield Beach, Fla.)* **2011**, 268.
  19. (a) Hamed, M.; Forchheimer, R.; Inganäs, O., *Towards woven logic from organic electronic fibres, Nature materials* **2007**, *6*, 357(b) Mattana, G.; Cosseddu, P.; Fraboni, B.; Malliaras, G. G.; Hinestroza, J. P.; Bonfiglio, A., *Organic electronics on natural cotton fibres, Organic Electronics* **2011**, *12*, 2033(c) Müller, C.; Hamed, M.; Karlsson, R.; Jansson, R.; Marcilla, R.; Hedhammar, M.; Inganäs, O., *Woven electrochemical transistors on silk fibers, Advanced materials (Deerfield Beach, Fla.)* **2011**, *23*, 898.
  20. (a) Heeger, A. J., *Semiconducting and metallic polymers: the fourth generation of polymeric materials, The Journal of Physical Chemistry B* **2001**, *105*, 8475(b) Heeger, A. J.; MacDiarmid, A. G.; Shirakawa, H., *Conductive polymers, Stockholm, Sweden: Royal Swedish Academy of Sciences* **2000**.
  21. Sessolo, M.; Khodagholy, D.; Rivnay, J.; Maddalena, F.; Gleyzes, M.; Steidl, E.; Buisson, B.; Malliaras, G. G., *Easy-to-fabricate conducting polymer microelectrode arrays, Advanced materials (Deerfield Beach, Fla.)* **2013**, *25*, 2135.
  22. (a) Guimard, N. K.; Gomez, N.; Schmidt, C. E., *Conducting polymers in biomedical engineering, Progress in Polymer Science* **2007**, *32*, 876(b) Asplund, M.; Nyberg, T.; Inganäs, O., *Electroactive polymers for neural interfaces, Polym Chem-Uk* **2010**, *1*, 1374.
  23. (a) Thompson, B. C.; Winther-Jensen, O.; Vongsvivut, J.; Winther-Jensen, B.; MacFarlane, D. R., *Conducting polymer enzyme alloys: Electromaterials exhibiting direct electron transfer, Macromolecular Rapid Communications* **2010**, *31*, 1293(b) Heller, A., *Electrical connection of enzyme redox centers to electrodes, The Journal of Physical Chemistry* **1992**, *96*, 3579(c) McQuade, D. T.; Pullen, A. E.; Swager, T. M., *Conjugated polymer-based chemical sensors, Chemical Reviews* **2000**, *100*, 2537.
  24. (a) Owens, R. M.; Malliaras, G. G., *Organic electronics at the interface with biology, Mrs Bull* **2010**, *35*, 449(b) Jimison, L. H.; Rivnay, J.; Owens, M., *Conducting polymers to control and monitor cells, Organic electronics: Emerging concepts and technologies* **2013**.
  25. (a) Bongo, M.; Winther-Jensen, O.; Himmelberger, S.; Strakosas, X.; Ramuz, M.; Hama, A.; Stavriniidou, E.; Malliaras, G. G.; Salleo, A.; Winther-Jensen, B.; Owens, R. M., *PEDOT: Gelatin composites mediate brain endothelial cell adhesion, Journal of Materials Chemistry B* **2013**, *1*, 3860(b) Jimison, L. H.; Hama, A.; Strakosas, X.; Armel, V.; Khodagholy, D.; Ismailova, E.; Malliaras, G. G.; Winther-Jensen, B.; Owens, R. M., *PEDOT:TOS with PEG : a biofunctional surface with improved electronic characteristics, Journal of Materials Chemistry* **2012**, *22*, 19498(c) Strakosas, X.; Sessolo, M.; Hama, A.; Rivnay, J.; Stavriniidou, E.; Malliaras, G. G.; Owens, R. M., *A facile biofunctionalisation route for solution processable conducting polymer devices, Journal of Materials Chemistry B* **2014**, *2*, 2537.

26. Stavrinidou, E.; Leleux, P.; Rajaona, H.; Khodagholy, D.; Rivnay, J.; Lindau, M.; Sanaur, S.; Malliaras, G. G., *Direct measurement of ion mobility in a conducting polymer*, *Advanced materials (Deerfield Beach, Fla.)* **2013**, *25*, 4488.
27. (a) Simon, D. T.; Kurup, S.; Larsson, K. C.; Hori, R.; Tybrandt, K.; Goiny, M.; Jager, E. W. H.; Berggren, M.; Canlon, B.; Richter-Dahlfors, A., *Organic electronics for precise delivery of neurotransmitters to modulate mammalian sensory function*, *Nat Mater* **2009**, *8*, 742(b) Isaksson, J.; Kjall, P.; Nilsson, D.; Robinson, N.; Berggren, M.; Richter-Dahlfors, A., *Electronic control of Ca<sup>2+</sup> signalling in neuronal cells using an organic electronic ion pump*, *Nat Mater* **2007**, *6*, 673(c) Tybrandt, K.; Forchheimer, R.; Berggren, M., *Logic gates based on ion transistors*, *Nat Commun* **2012**, *3*, 871.
28. Khodagholy, D.; Doublet, T.; Quilichini, P.; Gurfinkel, M.; Leleux, P.; Ghestem, A.; Ismailova, E.; Hervé, T.; Sanaur, S.; Bernard, C.; Malliaras, G. G., *In vivo recordings of brain activity using organic transistors*, *Nature communications* **2013**, *4*, 1575.
29. Rivnay, J.; Leleux, P.; Sessolo, M.; Khodagholy, D.; Hervé, T.; Fiocchi, M.; Malliaras, G. G., *Organic electrochemical transistors with maximum transconductance at zero gate bias*, *Advanced materials (Deerfield Beach, Fla.)* **2013**, *25*, 7010.
30. Bernards, D. a.; Malliaras, G. G.; Toombes, G. E. S.; Gruner, S. M., *Gating of an organic transistor through a bilayer lipid membrane with ion channels*, *Applied Physics Letters* **2006**, *89*, 053505.
31. Lin, P.; Yan, F.; Chan, H. L. W., *Ion-sensitive properties of organic electrochemical transistors*, *ACS applied materials & interfaces* **2010**, *2*, 1637.
32. (a) Tarabella, G.; Balducci, A. G.; Coppedè, N.; Marasso, S.; D'Angelo, P.; Barbieri, S.; Cocuzza, M.; Colombo, P.; Sonvico, F.; Mosca, R.; Iannotta, S., *Liposome sensing and monitoring by organic electrochemical transistors integrated in microfluidics*, *Biochimica et biophysica acta* **2013**, *1830*, 4374(b) Tarabella, G.; Nanda, G.; Villani, M.; Coppedè, N.; Mosca, R.; Malliaras, G. G.; Santato, C.; Iannotta, S.; Cicoira, F., *Organic electrochemical transistors monitoring micelle formation*, *Chemical Science* **2012**, *3*, 3432.
33. Svensson, P.-O.; Nilsson, D.; Forchheimer, R.; Berggren, M., *A sensor circuit using reference-based conductance switching in organic electrochemical transistors*, *Applied Physics Letters* **2008**, *93*, 203301.
34. Sessolo, M.; Rivnay, J.; Bandiello, E.; Malliaras, G. G.; Bolink, H. J., *Ion-selective organic electrochemical transistors*, *Advanced Materials* **2014**, *26*, 4803.
35. Mousavi, Z.; Ekholm, A.; Bobacka, J.; Ivaska, A., *Ion-selective Organic Electrochemical Junction Transistors Based on Poly(3,4-ethylenedioxythiophene) Doped with Poly(styrene sulfonate)*, *Electroanalysis* **2009**, *21*, 472.
36. Lin, P.; Yan, F., *Organic Thin-Film Transistors for Chemical and Biological Sensing*, *Advanced materials (Deerfield Beach, Fla.)* **2012**, *24*, 34.
37. Nishizawa, M.; Matsue, T.; Uchida, I., *Penicillin sensor based on a microarray electrode coated with pH-responsive polypyrrole*, *Analytical Chemistry* **1992**, *64*, 2642.

38. Zhu, Z.-T.; Mabeck, J. T.; Zhu, C.; Cady, N. C.; Batt, C. A.; Malliaras, G. G., *A simple poly(3,4-ethylene dioxythiophene)/poly(styrene sulfonic acid) transistor for glucose sensing at neutral pH*, *Chemical Communications* **2004**, 1556.
39. Bernards, D. a.; Macaya, D. J.; Nikolou, M.; DeFranco, J. a.; Takamatsu, S.; Malliaras, G. G., *Enzymatic sensing with organic electrochemical transistors*, *Journal of Materials Chemistry* **2008**, *18*, 116.
40. Macaya, D. J.; Nikolou, M.; Takamatsu, S.; Mabeck, J. T.; Owens, R. M.; Malliaras, G. G., *Simple glucose sensors with micromolar sensitivity based on organic electrochemical transistors*, *Sensors and Actuators B: Chemical* **2007**, *123*, 374.
41. (a) Tang, H.; Lin, P.; Chan, H. L. W.; Yan, F., *Highly sensitive dopamine biosensors based on organic electrochemical transistors*, *Biosensors & bioelectronics* **2011**, *26*, 4559(b) Tarabella, G.; Pezzella, A.; Romeo, A.; D'Angelo, P.; Coppedè, N.; Calicchio, M.; d'Ischia, M.; Mosca, R.; Iannotta, S., *Irreversible evolution of eumelanin redox states detected by an organic electrochemical transistor: en route to bioelectronics and biosensing*, *Journal of Materials Chemistry B* **2013**, *1*, 3843(c) Coppede, N.; Tarabella, G.; Villani, M.; Calestani, D.; Iannotta, S.; Zappettini, A., *Human stress monitoring through an organic cotton-fiber biosensor*, *Journal of Materials Chemistry B* **2014**, *2*, 5620.
42. Cicoira, F.; Sessolo, M.; Yaghmazadeh, O.; DeFranco, J. a.; Yang, S. Y.; Malliaras, G. G., *Influence of device geometry on sensor characteristics of planar organic electrochemical transistors*, *Advanced materials (Deerfield Beach, Fla.)* **2010**, *22*, 1012.
43. (a) Tarabella, G.; Santato, C.; Yang, S. Y.; Iannotta, S.; Malliaras, G. G.; Cicoira, F., *Effect of the gate electrode on the response of organic electrochemical transistors*, *Applied Physics Letters* **2010**, *97*, 123304(b) Yaghmazadeh, O.; Cicoira, F.; Bernards, D. A.; Yang, S. Y.; Bonnassieux, Y.; Malliaras, G. G., *Optimization of organic electrochemical transistors for sensor applications*, *Journal of Polymer Science Part B: Polymer Physics* **2011**, *49*, 34.
44. Tang, H.; Yan, F.; Lin, P.; Xu, J.; Chan, H. L. W., *Highly sensitive glucose biosensors based on organic electrochemical transistors using platinum gate electrodes modified with enzyme and nanomaterials*, *Advanced Functional Materials* **2011**, *21*, 2264.
45. Liao, C.; Zhang, M.; Niu, L.; Zheng, Z.; Yan, F., *Highly selective and sensitive glucose sensors based on organic electrochemical transistors with graphene-modified gate electrodes*, *Journal of Materials Chemistry B* **2013**, *1*, 3820.
46. Kergoat, L.; Piro, B.; Simon, D. T.; Pham, M.-C.; Noël, V.; Berggren, M., *Detection of glutamate and acetylcholine with organic electrochemical transistors based on conducting polymer/platinum nanoparticle composites*, *Advanced materials (Deerfield Beach, Fla.)* **2014**, *1*.
47. Khodagholy, D.; Curto, V. F.; Fraser, K. J.; Gurfinkel, M.; Byrne, R.; Diamond, D.; Malliaras, G. G.; Benito-Lopez, F.; Owens, R. M., *Organic electrochemical transistor incorporating an ionogel as solid state electrolyte for lactate sensing*, *J. Mater. Chem.* **2012**, *22*, 4440.

48. Lee, K. H.; Kang, M. S.; Zhang, S.; Gu, Y.; Lodge, T. P.; Frisbie, C. D., "Cut and Stick" Rubbery Ion Gels as High Capacitance Gate Dielectrics, *Advanced materials (Deerfield Beach, Fla.)* **2012**, *24*, 4457.
49. Lin, P.; Yan, F.; Yu, J.; Chan, H. L.; Yang, M., *The Application of Organic Electrochemical Transistors in Cell-Based Biosensors*, *Adv Mater* **2010**, *22*, 3655.
50. He, R.-X.; Zhang, M.; Tan, F.; Leung, P. H. M.; Zhao, X.-Z.; Chan, H. L. W.; Yang, M.; Yan, F., *Detection of bacteria with organic electrochemical transistors*, *Journal of Materials Chemistry* **2012**, *22*, 22072.
51. Kim, D.-J.; Lee, N.-E.; Park, J.-S.; Park, I.-J.; Kim, J.-G.; Cho, H. J., *Organic electrochemical transistor based immunosensor for prostate specific antigen (PSA) detection using gold nanoparticles for signal amplification*, *Biosensors & bioelectronics* **2010**, *25*, 2477.
52. Lin, P.; Luo, X.; Hsing, I. M.; Yan, F., *Organic electrochemical transistors integrated in flexible microfluidic systems and used for label-free DNA sensing*, *Advanced materials (Deerfield Beach, Fla.)* **2011**, *23*, 4035.
53. Liao, J.; Lin, S.; Liu, K.; Yang, Y.; Zhang, R.; Du, W.; Li, X., *Organic electrochemical transistor based biosensor for detecting marine diatoms in seawater medium*, *Sensors and Actuators B: Chemical* **2014**, *203*, 677.
54. Bolin, M. H.; Svennersten, K.; Nilsson, D.; Sawatdee, A.; Jager, E. W. H.; Richter-Dahlfors, A.; Berggren, M., *Active Control of Epithelial Cell-Density Gradients Grown Along the Channel of an Organic Electrochemical Transistor*, *Adv. Mater.* **2009**, *21*, 4379.
55. Khodagholy, D.; Doublet, T.; Quilichini, P.; Gurfinkel, M.; Leleux, P.; Ghestem, A.; Ismailova, E.; Herve, T.; Sanaur, S.; Bernard, C.; Malliaras, G. G., *High transconductance organic electrochemical transistors*, *Nat Commun* **2013**, *4*, 1575.
56. Jimison, L. H.; Tria, S. A.; Khodagholy, D.; Gurfinkel, M.; Lanzarini, E.; Hama, A.; Malliaras, G. G.; Owens, R. M., *Measurement of barrier tissue integrity with an organic electrochemical transistor*, *Adv Mater* **2012**, *24*, 5919.
57. Tria, S. a.; Ramuz, M.; Huerta, M.; Leleux, P.; Rivnay, J.; Jimison, L. H.; Hama, A.; Malliaras, G. G.; Owens, R. M., *Dynamic monitoring of Salmonella typhimurium infection of polarised epithelia using organic transistors*, *Advanced healthcare materials* **2014**, *1*.
58. Tria, S.; Jimison, L. H.; Hama, A.; Bongo, M.; Owens, R. M., *Sensing of EGTA mediated barrier tissue disruption with an organic transistor*, *Biosensors* **2013**, *3*, 44.
59. Tria, S. A.; Ramuz, M.; Jimison, L. H.; Hama, A.; Owens, R. M., *Sensing of barrier tissue disruption with an organic electrochemical transistor*, *Journal of visualized experiments : JoVE* **2014**, e51102.
60. Tria, S. A.; Ramuz, M.; Huerta, M.; Leleux, P.; Rivnay, J.; Jimison, L. H.; Hama, A.; Malliaras, G. G.; Owens, R. M., *Dynamic monitoring of Salmonella typhimurium infection of polarised epithelia using organic transistors*, *Adv Healthc Mater* **2014**, *3*, 1053.
61. Lin, P.; Yan, F.; Yu, J. J.; Chan, H. L. W.; Yang, M., *The Application of Organic Electrochemical Transistors in Cell-Based Biosensors*, *Adv. Mater.* **2010**, *22*, 3655.

62. Yao, C.; Xie, C.; Lin, P.; Yan, F.; Huang, P.; Hsing, I. M., *Organic Electrochemical Transistor Array for Recording Transepithelial Ion Transport of Human Airway Epithelial Cells*, *Advanced Materials* **2013**, *25*, 6575.
63. Ramuz, M.; Hama, A.; Huerta, M.; Rivnay, J.; Leleux, P.; Owens, R. M., *Combined optical/electronic monitoring of epithelial cells in vitro*, *Advanced Materials* **2014**, DOI:10.1002/adma.201401706.
64. Buzsáki, G.; Anastassiou, C. A.; Koch, C., *The origin of extracellular fields and currents--EEG, ECoG, LFP and spikes*, *Nat Rev Neurosci* **2012**, *13*, 407.
65. Campana, A.; Cramer, T.; Simon, D. T.; Berggren, M.; Biscarini, F., *Electrocardiographic recording with conformable organic electrochemical transistor fabricated on resorbable bioscaffold*, *Advanced materials (Deerfield Beach, Fla.)* **2014**, *26*, 3874.
66. Jasper, H. H.; Arfel-Capdeville, G.; Rasmussen, T., *Evaluation of EEG and cortical electrographic studies for prognosis of seizures following surgical excision of epileptogenic lesions*, *Epilepsia* **1961**, *2*, 130.
67. Gilletti, A.; Muthuswamy, J., *Brain micromotion around implants in the rodent somatosensory cortex*, *Journal of neural engineering* **2006**, *3*, 189.
68. Leleux, P.; Rivnay, J.; Lonjaret, T.; Badier, J.-M.; Bénar, C.; Hervé, T.; Chauvel, P.; Malliaras, G. G., *Organic electrochemical transistors for clinical applications*, *Advanced Healthcare Materials* **2014**, n/a.

# Chapter 2

---

## Blood Brain Barrier Characterisation

---

## 2.1 Introduction

The brain is the body's control center. When this organ is healthy, it works very quickly and automatically. It operates for speech, thinking, memory and movement. However, the brain can default when diseases appear. The brain's inflammation results in disorder-like weakness, vision loss, paralysis, and syndromes such as sclerosis, Alzheimer's, and Parkinson's [1]. Brain disorders are the largest cause of hospitalization, more than cancer and heart disease. Brain illnesses touch at least 50 million people per year for an amount of \$500 billion to treat [2]. The complexity of the central nervous system (CNS) and the role of its specific protection, called the Brain Blood Barrier (BBB), limit the general treatments [3].

The BBB is a dynamic barrier that isolates the brain from the circulatory system. This barrier protects the brain by strictly controlling transport in and out of the brain, thereby maintaining brain homeostasis [4]. The disadvantage of this tightly controlled barrier is that it also selects the transport of therapeutics into the brain. Drugs that treat the CNS disorders are often unable to penetrate into the brain to perform their actions. Almost 98% of the small molecule drugs and practically 100% of the large molecule pharmaceuticals cannot cross this barrier [5]. The BBB is powerful at protecting the brain against the passage of foreign substances that it often forbids the passage of life-saving drugs able to repair the injured or diseased brain. To find out how pathogens or toxins can skirt BBB protection and disturb the brain, it is essential to further investigate the neurology field.

Our motivation to characterize this barrier is to further our understanding of this interface in contact with toxins and pathogen.

## 2.2 History of the Blood Brain Barrier

In 1885, Paul Ehrlich was the first to discover the presence of a barrier between blood vessels and the brain. After intravenously injecting organic dyes into animals, he noted that the dyes would go out of the capillaries and stain all organs, except the brain. He concluded that the "dyes had a lower affinity for binding to the nervous system as compared to other tissues" [6]. In 1900, Lewandowsky gave the name of the blood-brain barrier after he had demonstrated that neurotoxic agents affected brain function exclusively when these agents are directly injected into the brain and not into the vascular system [7]. In 1913, Edwin Goldmann, a student of Dr. Ehrlich, did the

opposite and injected the dyes directly into the cerebro-spinal fluid of the brain and showed that injection of trypan blue in the cerebrospinal fluid of rabbits stained only the brain [7]. Over the years, this barrier has been subject to controversy. In 1967, Reese and Karnovsky used electron microscopy to show that the endothelium of brain capillaries composed the BBB [8]. In 1969, Siakotos *et al.* isolated brain capillaries [9]. Betz *et al.* isolated endothelial cells and brain capillaries, and they established an *in vitro* model of BBB [10] (Figure 2.1). Since then, many models *in vivo*, *ex vivo* and *in vitro* were adopted in basic research screening and in the drug industry in order to increase drug delivery to the brain [11]. Much research has gone into understanding the molecular mechanisms of development of the BBB. Today, new technologies such as genomics, proteomics and bioelectronics are used to characterize the BBB.

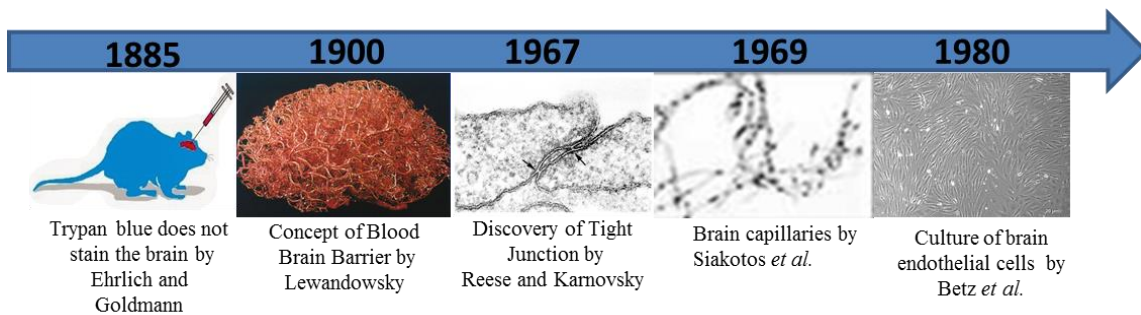


**Figure 2.1:** Historical research on the blood-brain barrier.

## 2.3 Structure

### 2.3.1 A Biological Barrier

The BBB is composed of brain microvascular endothelial cells (BMECs) that line cerebral microvessels along with periendothelial structures, which include pericytes, astrocytes and a basement membrane [12, 13] (Figure 2.2). The basement membrane is a layer of extracellular matrix secreted by the endothelial cells as well as by the perivascular cells, astrocytes and pericytes. It is composed of type IV collagen, fibronectin, and laminin. This layer is important because it give a mechanical support for cell attachment, and cell migration [3].

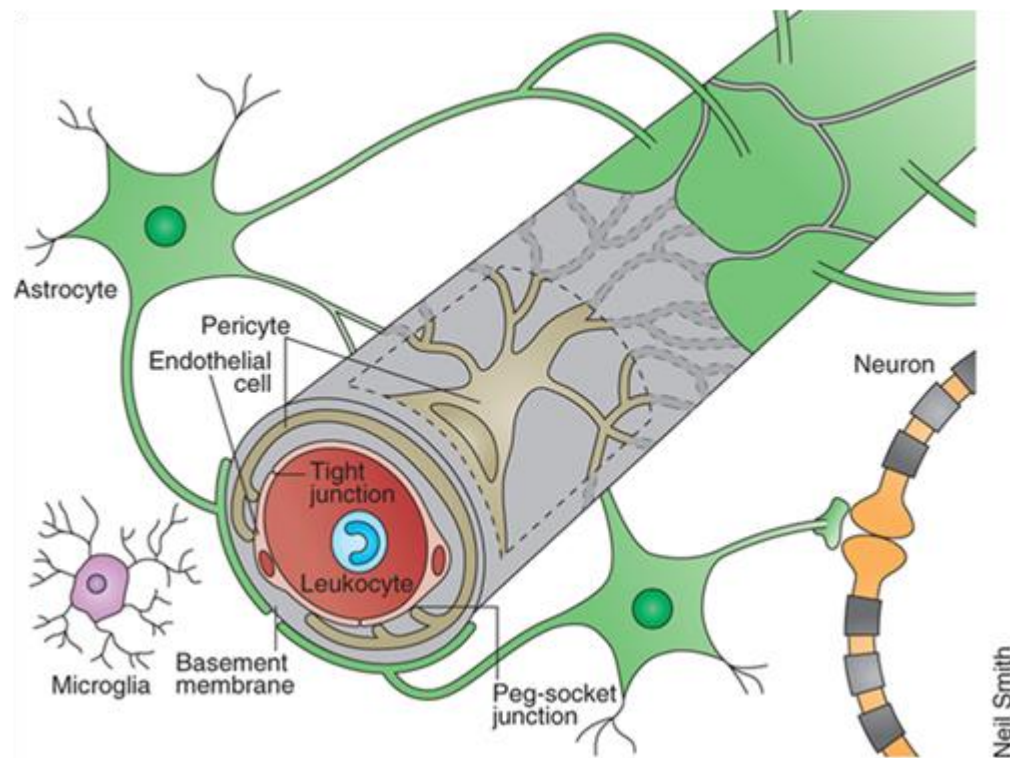


**Figure 2.2:** Schematic representation of a blood-brain barrier (from Nature Medicine Obermeier *et al.* [13]).

### 2.3.1.1 Brain Endothelial Cells

Endothelial cells in brain capillaries are the essential element of the BBB. Brain endothelial cells are distinguished from peripheral endothelial cells by possessing fewer cytoplasmic vesicles [14], more mitochondria, and a large number of intercellular junctions like tight junctions (TJs) that promote an electrical resistance, strongly limit paracellular flux of polar substances, and a high energy metabolism [15]. Brain endothelial cells have several specific markers such as the glucose transporter GLUT-1, that mediates the passage of glucose through the barrier or the glutamyl transpeptidase ( $\gamma$ -GT) involved in the metabolism of amino acids [3]. Due to these characteristics, brain endothelial cells have a decisive role in the selection of substances and cells transported in and out of the CNS.

### 2.3.1.2 Astrocytes

The astrocyte cells are glial cells. These cells cover approximately 99% of the abluminal surface of the brain capillary and induce endothelial cells to differentiate directly through cell to cell communication or indirectly by secreting astrocytic factors [16]. Astrocytes are able to regulate neuronal excitability, and are a source of energy for the brain through the process of degrading glycogen to lactate [17]. Astrocytes are attached to each other by "gap junctions" through which various metabolites can diffuse [18]. Intercellular adhesion between astrocytes in the blood-brain barrier has been observed in the form of gap junctions and adherens junctions [19]. There is significant body of evidence, *in vitro* and *in vivo*, indicating that astrocyte interaction with the cerebral endothelium determine BBB function, morphology (*i.e.* tightness, TER), and protein expression [20].

### 2.3.1.3 Pericytes

Pericytes are mesenchymal cells localized at the abluminal membrane of brain capillary endothelial cells in the basal lamina [21]. These cells have cellular projections, which penetrate the basal lamina and cover approximately 20-30% of the microvascular circumference [22]. It has been reported that there is approximately one pericyte for every three endothelial cells [16]. Pericytes are physically associate to the endothelium by Gap junction communication [23]. In the brain, pericytes are involved in the cerebral vasculature by controlling the diameter of capillaries, blood flow, and also by contributing to the microvascular vasodynamic capacity and structural stability. Lack of pericytes has led to endothelial hyperplasia and abnormal vascular morphogenesis in the brain [24]. The pericytes are also considered the first line of defense during the rupture of the BBB [25] and play an important role in brain homeostasis [3].

### 2.3.1.4 Neurons

The neurovascular unit (NVU) composed by neurons, astrocytes, pericytes, endothelial cells, supports the neurovascular coupling controlling changes in cerebral blood flow in response to the needs of neuronal supply. In spite of their close localization to capillaries, less data is available on the putative direct role of neurons on BBB permeability [26]. Cerebral endothelial cells cultured with cortical neurons have been shown to increase the expression of the BBB marker enzyme  $\gamma$ -glutamyl transpeptidase demonstrating that neurons can induce BBB properties [27]. In 2013, Xue *et al.* demonstrated that the existence of astrocytes and neurons could promote the formation of junction in brain endothelial cells and increase the resistance of these cells [28].

### 2.3.2 A Physical Barrier

The BBB is a physical barrier (Figure 2.3) that prevents entry of large and potentially toxic molecules into the brain, thus separating the central nervous system and systemic circulation. The BBB is composed by adherens junctions (AJ) [29] and tight junctions (TJ), which selectively prevent the diffusion of for example, hydrophilic molecules and pathogens [7].

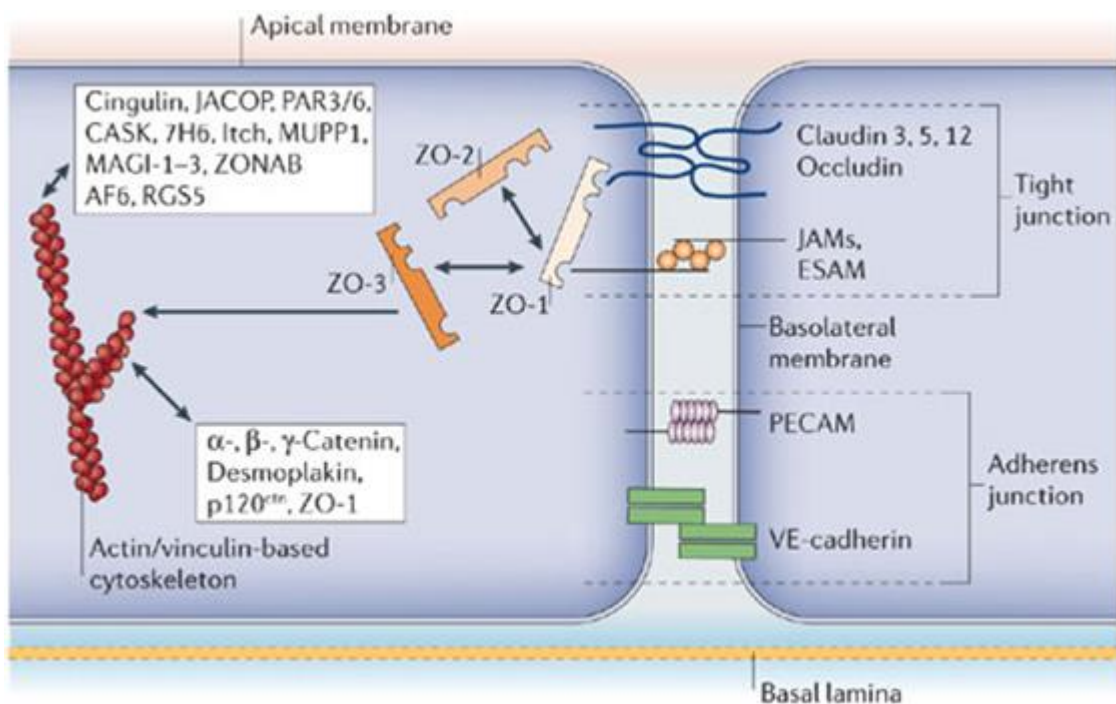


**Figure 2.3:** Representation of a section of brain capillaries with tight and adherens junctions present between endothelial cells (from Nature Reviews Neuroscience, Abbott *et al.*, [49]).

### 2.3.2.1 Tight Junctions

TJs are elaborate structures that span the apical region of the endothelial barrier tissues. They are formed by transcellular proteins, such as occludin [30] and claudins [31]. They join the cytoskeleton via cytoplasmic proteins such as zonula occludens 1 (ZO-1) [32] [33]. TJ are known to prevent the paracellular passage of small molecules and even ions such as Na<sup>+</sup> and Cl<sup>-</sup>. This function leads to high transendothelial electrical resistances (TER) and a very selective transport [34]. Regulation of TJ protein expression and/or subcellular distribution plays a key role in the physiology of the BBB [35]. When TJs are altered, the polarity of the blood-brain barrier decreases [32] [36].

**Occludin** has a molecular mass of 65 kDa, and contains two extracellular loops and four membrane-spanning regions. In 1997, Hirase *et al.* [37] first reported that occludin protein was strongly expressed and distributed continuously at the interface of brain endothelial cells. This protein is specific to tight junctions but several knockout and knockdown experiments have provided evidence that occludin is not essential for the formation of the tight junctions [38] despite the fact that a decrease in occludin expression is associated with a disruption of BBB function in several diseases [39].

**Claudins** are 22 kDa proteins and have four transmembrane domains. At least 24 have been identified in mammals. Claudins are the major components of the TJ and are localized exclusively at TJ strands. These proteins are essential for TJ formation [31]. The expression patterns of claudins vary among different tissues. Most cell types express more than two types of claudins. In brain endothelial cells claudins 3, 5, and 12 are the most expressed [40].

**Junctional Adhesion Molecule** (JAMs) is a group of 40-kDa proteins of the IgG superfamily. It possesses a single transmembrane domain and two immunoglobulin variable domains. JAMs were found to be selectively concentrated at intercellular junctions of endothelial cells where they mediate the early attachment of adjacent cell membranes via homophilic interactions [41]. JAMs are associated with claudins in TJ formation and is involved in the adhesion and the junction between cells [42].

**TJ-associated Proteins** belong to different groups of proteins containing a PDZ domain. Almost 30 additional proteins have been found associated with the cytoplasmic domains of claudins and occludin [43]. They can be grouped into two major categories: The first are the peripherally associated proteins like ZO-1 (ZO-2, ZO-3, AF6, and cingulin) that appear to organize the transmembrane proteins and couple them to other cytoplasmic proteins and to actin microfilaments [44]. The second are numerous “signaling” proteins (ZONAB, RhoA, RalA, and Raf-1) which are involved in junction assembly and gene transcription.

### 2.3.2.2 Adherens Junctions

Besides tight junctions, brain endothelial cells are also joined by adherens junctions. Adherens junctions form an adhesive cell-cell contact [45]. They are located near the basal membrane and consist of catenins and cadherins that interact with each other when calcium ions are present.

**Catenins** ensure adhesive contacts between cells. These accessory proteins mediate the connection between cytoplasmic domain of cadherins and actin cytoskeleton [46].

**Cadherins** belong to a superfamily of cell adhesion molecules, all of which are single transmembrane domain proteins. Vascular endothelial-cadherin (VE-cadherin) is found in endothelial cells and mediates calcium-dependent cell adhesion by binding to actin via catenin accessory proteins [47].

### 2.3.3 A Physiological Barrier

In physiological conditions, BBB is able to control brain homeostasi by specific mechanisms by which solute molecules move across membranes. Several transport mechanisms across the BBB have been identified, including paracellular, between adjacent cells and the transcellular pathway through the cell [48]. The majority of this transport is carried out via the transcellular pathway through transport proteins, receptor-mediated transcytosis, and adsorptive transcytosis (Figure 2.4).

### 2.3.3.1 The Paracellular Pathway

The paracellular pathway is a passive transport driven by electrochemical, hydrostatic and osmotic gradients. This transport is formed by the endothelial tight junction openings. Only some claudin proteins and more specifically claudin-2, allow the passage of ions predominately  $\text{Na}^+$  and  $\text{Cl}^-$  but limit the movement of large molecules and proteins [49]. Water and small hydrophilic solutes can cross the BBB by the paracellular pathway, only when TJs are destabilized by inflammatory or other pathological stimuli [50] (Figure 2.4). The paracellular pathway is characterized by higher conductance and lower selectivity.

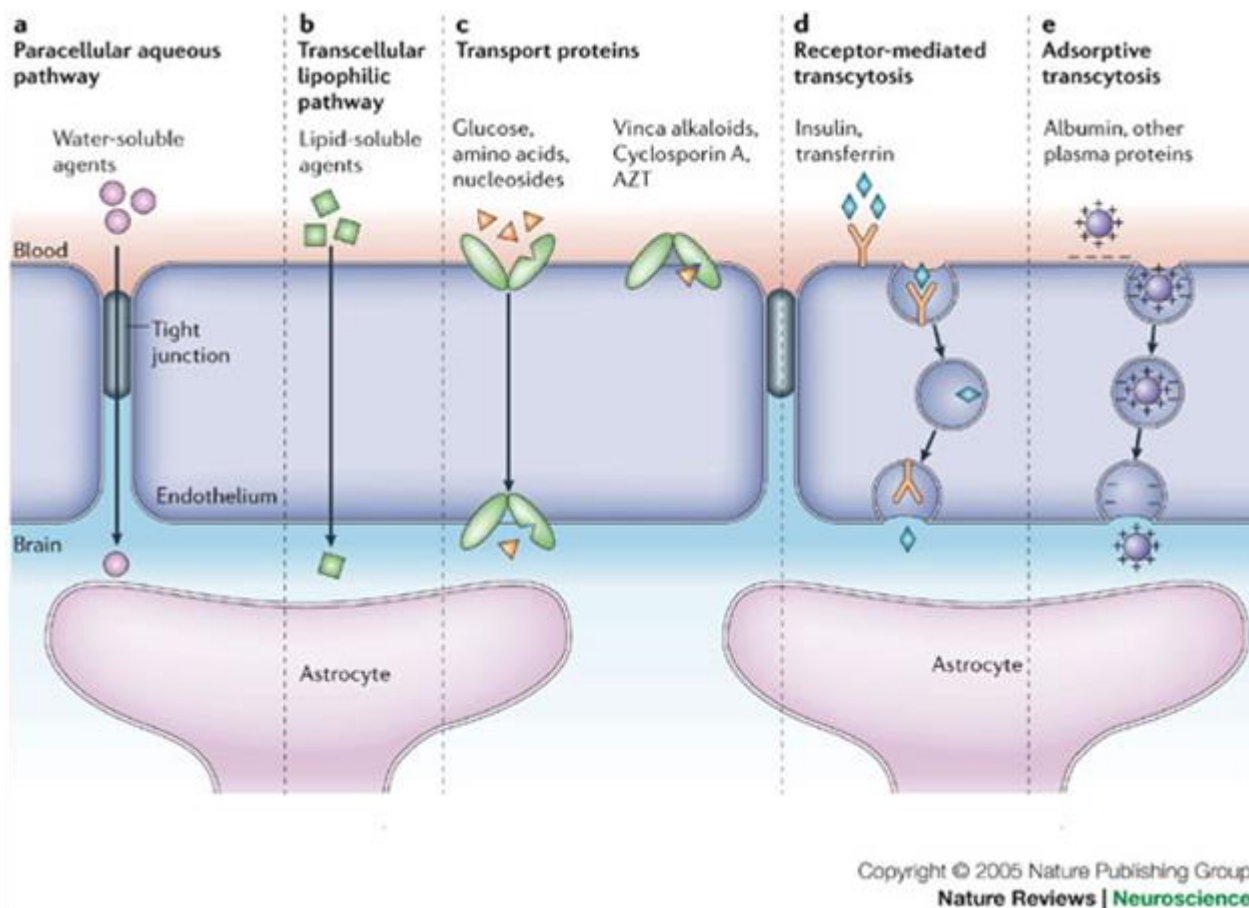


**Figure 2.4:** Diagram of the different transport processes involved in the permeability of brain capillaries (from Nature Reviews Neuroscience, Abbott *et al.*, [49]).

### 2.3.3.2 Transcellular Pathways

Tight junctions restrict the passage of molecules between ECs (paracellular transport), but it is possible to cross the BBB through ECs (transcellular transport). The traffic of molecules via transcellular transport is highly regulated and many mechanisms are involved. The pathway used to cross the BBB is dependent on the type of molecules [51] (Figure 2.4). This transcellular route is tightly regulated with a very high degree of molecular specificity.

**Passive diffusion** is a spontaneous process, without energy. The passage of molecules through the cell membrane by simple diffusion is controlled by the concentration gradient between the blood and brain. Molecules using this transport are small molecules such as carbon dioxide, oxygen, or are highly lipophilic substances such as nicotine and alcohol. In general, molecules that passively diffuse across the BBB have a  $MW < 500$  Da [52].

**Facilitated diffusion** allows the transport of compounds across the BBB by their concentration gradient without energy. This is a passive mechanism and saturated when concentrations exceed the capacity of transporters. Facilitated diffusion allow transport of a wide range of molecules such as glucose and amino acids [53].

**Glucose** is an exclusive substrate of cerebral energy metabolism [54]. Glucose transport by facilitated diffusion is provided by the multigene family coding for GLUT transporters to 12 transmembrane segments. The expression of GLUT-1 transporter is ubiquitous in normal tissues. At the BBB, GLUT-1 is highly expressed on membranes and the luminal and abluminal of brain endothelial cells, which gives high transport capacity of glucose from the blood into the brain [3].

**Amino acids** are essential for the synthesis of neurotransmitters and cerebral protein synthesis. Some amino acids such as glutamate and aspartate are synthesized efficiently by the brain. However, for other amino acids such as arginine, cerebral synthesis is not sufficient. To cover the metabolic needs of the brain, a balance must be made from the blood into the brain. Eleven systems of amino acid transport across the BBB have been described. These systems are differently distributed on luminal and abluminal membranes of the BBB. They are divided into two groups, facilitated transport system independent of the sodium present in luminal and abluminal membranes and sodium-dependent localized exclusively in abluminal face [55]. These pumps regulate ion influx from the blood to the brain and vice versa. Ion concentrations need to be stable since they greatly influence the behavior of neurons.

**Transcytosis** is a selective transport of macromolecules plasma proteins (*eg*: albumin), across a cell by vesicles. This is a slow process which takes place in three steps: binding to the membrane occurs by electrostatic (receptor mediated) at the cell surface, endocytosis followed by migration within vesicles through the cell, and finally, through the vesicular exocytosis at the opposite membrane. There is transcytosis by a receptor where the molecule binds to specific membrane receptor, and induces invagination of the membrane with formation of vesicle by endocytosis [56]. Receptor-mediated transcytosis is specific to a given endogenous macromolecule, while adsorptive transcytosis is non-specific. Under normal physiological conditions, adsorptive vesicles rarely occur [19].

#### 2.3.4 A Metabolic Barrier

The blood-brain barrier is also considered as a metabolic barrier by the presence of several specific enzymes and efflux pumps [3]. Indeed, it is known that the brain, the endothelial cells and astrocytes cells have extracellular and intracellular enzymes which can metabolize and eliminate xenobiotics. Among the systems responsible for the transport of these molecules out of the cell there are P-glycoprotein (P-gp), the multidrug resistance-related proteins (MRP family), and the ABCG2 (breast cancer resistance protein) which plays an important role, notably in humans. These systems are key elements in the BBB as they are able to actively prevent lipophilic molecules to cross the BBB. This mechanism is known as "multidrug resistance". These proteins belong to the superfamily ABC (ATP-binding cassette).

##### 2.3.4.1 Enzymes

Many metabolic enzymes are expressed in brain endothelial cells. The main enzymes involved in this metabolic barrier are alkaline phosphatase (ALP), monoamine oxidase (MAO), and gamma-glutamyl transpeptidase ( $\gamma$ -GT) [57].

**Alkaline phosphatase** is present in many tissues and plays a key role in hydrolysis of phosphorylated metabolites. It also controls the transport of phosphate esters and phosphate ions. Like the  $\gamma$ -GT, this enzyme is expressed at a high level in endothelial cells of brain capillaries [57].

**Monoamines oxidases** are present in the brain tissue. The MAO metabolizes monoaminergic neurotransmitters (dopamine, serotonin, norepinephrine, and epinephrine) and limits the transcellular exchange of these neurotransmitters and their precursors from the blood into the brain [58].

**Gamma-glutamyl transpeptidase enzyme** ( $\gamma$ -GT) is the most characteristic of the BBB. This is a membrane-associated glycoprotein. Although its activity is higher in endothelial cells of the BBB, the  $\gamma$ -GT is not exclusively found in endothelial cells in brain capillaries. This enzyme is also present and functional in pericytes [59]. The  $\gamma$ -GT appears to be involved in the transport of many amino acids across the BBB. This enzyme is also involved in the neuroprotective function of the brain [60].

#### 2.3.4.2 Efflux Pumps

The presence of efflux pumps at the surface of brain endothelial cells highly contributes to the protection of the CNS by the BBB. Many drug transporters are members of the adenosine triphosphate (ATP)-binding cassette (ABC) transporter superfamily or the solute carrier superfamily (SLC) class (Figure 2.5). These pumps participate in the active transport of both endogenous and exogenous molecules and play an important role in the homeostasis of CNS by extruding toxins and xenobiotics out of the brain [3]. In humans, seven families of ABC transporters have been identified (ABCA, ABCB, ABCC, ABCD, ABCE, ABCF, and ABCG) [61]. Three of these seven gene families are particularly important for drug transport and multiple drug resistance in BBB: (1) the ABCB1 gene, encoding MDR1 (also known as P-gp); (2) ABCG2 (breast cancer resistance protein); and (3) the ABCC family (ABCC1 through ABCC6) or multidrug resistance proteins (MRP) [62].

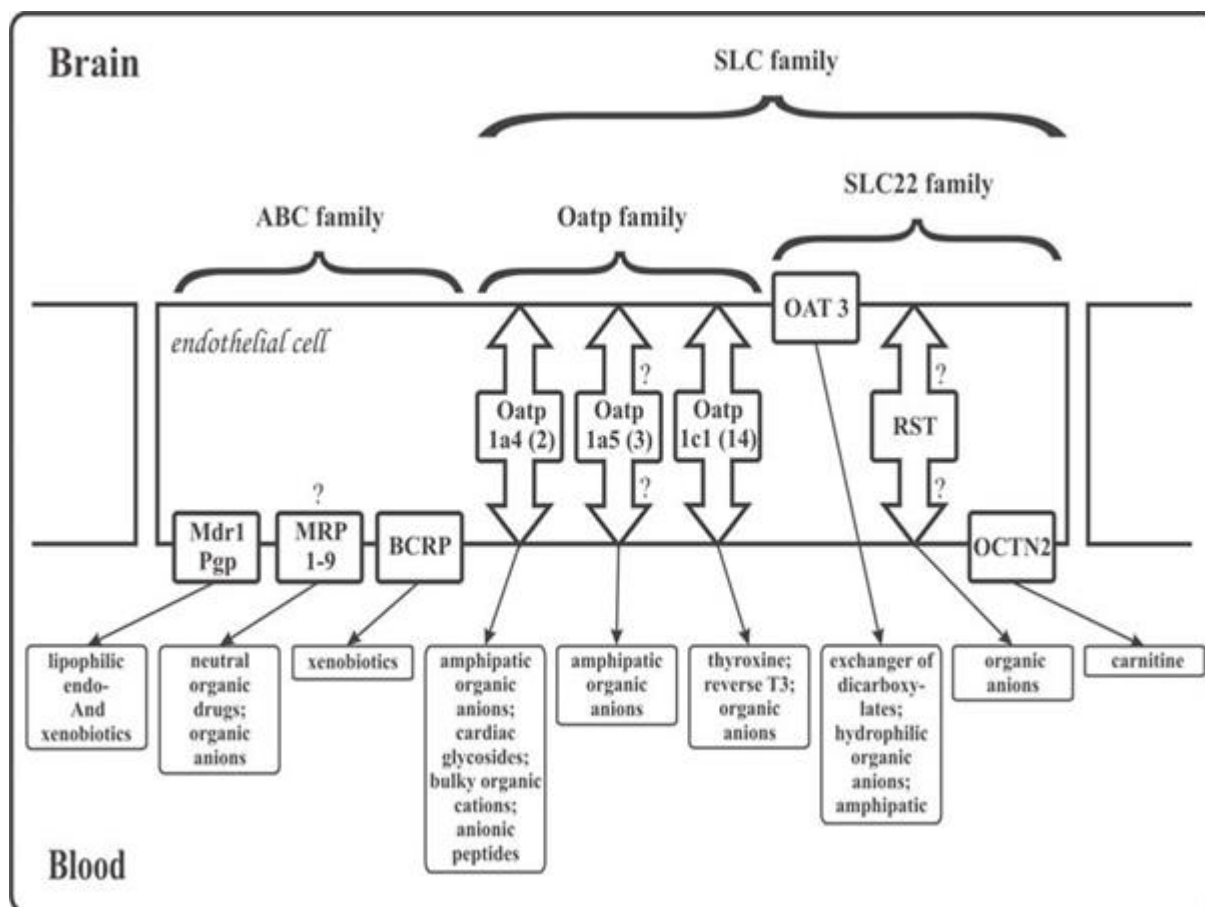


**Figure 2.5:** Representation of the metabolic activity of the blood-brain barrier (from *Pharmacological Reports*, Bernacki *et al.*, [3]).

**P-glycoprotein (P-gp)** is an important individual transport protein at the BBB [63], functioning as an efflux pump and limiting the brain uptake of many lipophilic substances. It was the first efflux transporter to be discovered and is the most extensively studied member of the ABC multidrug transporter family [64]. P-gp was discovered in cancer cells, where it was found to be responsible for causing multiple drug resistances (MDR) [65]. It is located on the luminal side of the BBB [66]. Like other ABC-transporters, this transport protein displays a very broad specificity of substrates. These substrates include anticancer drugs such as vinca alkaloids, anthracycline, and taxanes, and also a large number of other clinically important drugs such as HIV-1 protease inhibitors [67], the immunosuppressive agent cyclosporine A, and the cardiac glycoside digoxin [68]. P-gp decreases the brain concentrations of its substrates and, importantly, protects against possibly toxic substances. At the BBB P-gp is an efflux transporter of particular interest, because it plays a major role in the

phenomenon of multidrug resistance, many pharmaceutical drugs cannot overcome the BBB because they are transported out of the brain capillary endothelial cells back into blood by P-gp [69].

**The Multidrug Resistance Associated Proteins** are involved in the transport of xenobiotics. 9 MRP were detected in various normal tissues in mammals [70]. The MRP 1-6 were found in brain endothelial cells in mice and humans [71]. The MRP transported a wide range of substrates with different chemical structures and different pharmacological properties. Despite this diversity, MRP have specific substrates. The substrates of MRP are generally organic anions of lipophilic compounds conjugated to glutathione [72].

**The Breast Cancer Resistance Protein** was first detected in a chemotherapy-resistant breast cancer cell line MCF-7 but it is expressed in a variety of tissues including the intestine, kidney, placenta, brain endothelium and hematopoietic cells [62] as well as solid tumors [73]. In the brain, BCRP has been detected mainly at the luminal surface of capillary endothelial cells. Murine BCRP is encoded by Bcrp1/Abcg2 gene. It shares some substrates with P-gp and MRPs [62], and the tissue distribution of BCRP shows extensive overlap with that of P-gp [74]. It was recently reported that this overlap is due to an increase in function of P-gp or BCRP rather than an increase in the actual expression levels. In humans, BCRP is more important than P-gp in terms of quantitative expression levels at the BBB [75].

**Organic Anion Transporters** such as OATPs and OATs belong to the family of "Solute Carrier transporters" (SLC). They typically operate as exchangers, using bidirectional transport, which depends on the concentration gradient of the molecule exchanged. They transport bile acids, organic dyes, thyroid hormones, anionic oligopeptides and xenobiotics [76].

## 2.4 *In vitro* Models of the Blood Brain Barrier

### 2.4.1 Parameters Used to Assess *in vitro* Models of Blood Brain Barrier

The tight paracellular barrier is a fundamental characteristic of the BBB. To assess the tightness of a given model, the two most important methods are permeability (Pe) and transendothelial resistance measurement (TER) [11]. All relevant models present tight junction protein and show a sufficient tightness ( $150\text{--}200 \text{ }\Omega\cdot\text{cm}^2$ ) to study permeability or transport of molecules [77]. Further some *in vivo* investigations of the TER of BBB is estimated to average out at  $2000 \text{ }\Omega\cdot\text{cm}^2$  [78] [79].

#### 2.4.1.1 Permeability Measurement

Permeability assay (Pe) are important assay of the quality of BBB models [80]. Pe is expressed in  $\text{cm}\cdot\text{s}^{-1}$ , and illustrates the ability of the molecule to pass through the cell membrane. Methods to determine Pe are based on the cell culture of brain endothelial cells on semipermeable filters which define two compartments: the apical, upper compartment which can be considered as “blood-side” and the basolateral, lower compartment which is the “brain side”. This assay measures the transport of radiolabeled or fluorescent compounds such as Lucifer yellow (LY) across a monolayer. The apparent permeability (Papp) is determined using the following equation:  $P_{app} = dQ/(dT \times A \times C_0)$ , where dQ is the transported amount of the radiolabeled or fluorescent compounds, dT is the incubation time, A is the surface of a filter and C<sub>0</sub> is the initial concentration of the radiolabeled or fluorescent compounds. Permeability values in the order of magnitude of  $1 \cdot 10^{-6} \text{ cm}\cdot\text{s}^{-1}$  for sodium fluorescein are considered good values for tight barrier. Sodium fluorescein is used as an indicator of ion permeability and the common values for low permeability are when  $P_{app} \leq 2 \cdot 10^{-6} \text{ cm}\cdot\text{s}^{-1}$  [81]. In general the ions flux using the paracellular pathway pass by the pore route formed by transmembrane tight junction proteins, or by the non pore way formed by the dynamic opening and closing of tight junction strands [82]. However, the use of tracer molecule like sodium fluorescein for the measurement present some disadvantage because these tracer goes through the non pore way. Therefore, the permeability assay cannot be investigated as a rigorous assessment of the role of the pore pathway [83].

### 2.4.1.2 Measurement of TER

Measurement of the transendothelial resistance (TER) is one of the most important methods to assess barrier tissue integrity [80]. In culture conditions, TER reflects the impedance of ions through the physiological barrier and indicates the integrity of the epithelium and the degree of organization of TJ between cells. TJ has been shown by FRAP technique (fluorescence recovery after photobleaching) to have a permanent and rapid remodelling what suggest a change in their structure upon exposure to extracellular stimuli on the scale of seconds to minutes [84].

The impedance can be monitored by different types of measure, the non-planar method and the planar method.

**The non-planar method:** In the non-planar method, cells grow on permeable supports like filter. This filter configuration is compatible with transport assay because this format permits the access to both the apical and the basolateral compartments.

**Chopstick-type electrodes:** The traditional way to measure TER is the use of simple handheld devices with chopstick-type electrodes. This setup permit to get an approximate determination of the ohmic resistance of the barrier-forming cell layer. The chopstick use a direct current (DC) applied to two electrodes, one on each side of the monolayer. In this method, the TER depends strongly on the position of the probing electrodes. Moreover, DC current can damage both the cells and the electrodes [85].

**Epithelial Voltohmmeter world precision instruments (EVOM):** This method avoids the use of DC current which can damage the cells. In this case, an alternating current (AC) square wave with a low frequency (12.5 Hz) is used to avoid deterioration of the cell layer and the electrodes (Figure 2.6). However, the EVOM method is performed outside the incubator which leads to disorders of physiologic parameters and thus to a variation of TER values.

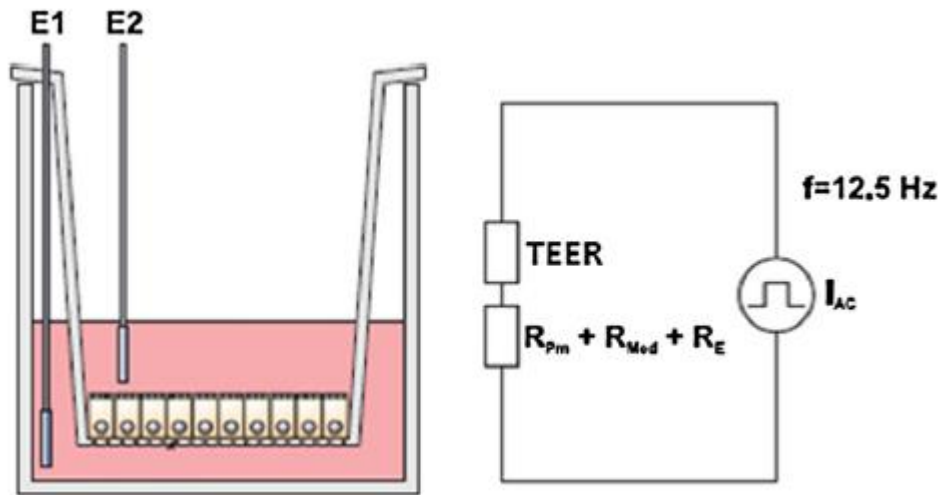


**Figure 2.6:** Impedance measurements with chopstick-like electrodes. The chopstick-like electrodes (E1, E2) are traditionally used to determine the electric resistance of cells grown on filter inserts. The ohmic resistance of the cell layer (TER), the cell culture medium in the upper and lower compartment ( $R_{Med}$ ), the membrane of the filter inserts ( $R_{pm}$ ) and electrode-medium interface ( $R_E$ ) all contribute to the total electric resistance.  $I_{AC}$ : alternating current (from Fluids and Barriers of the CNS, Benson *et al.*, [85]).

**CellZscope:** In the CellZscope method, two electrodes are used; one is placed in the upper and the other in the lower chamber. The electrodes are separated by the endothelial layer seeded on filter, and all measurement is carried out in the incubator (Figure 2.7). The CellZscope (Nanoanalytics) (Figure 5.2a) measures the impedance of barrier forming cell cultures grown on permeable membranes under physiological conditions. The two main parameters directly imputable to the cell layer are the resistance TER and the capacitance Ccl. This tool provides the TER as output. The ohmic resistance, TER, shows the parallel connection of the paracellular pathway, and the capacitance of the apical and the basolateral membranes is described in Ccl. Based on this parallel circuit, TER and Ccl are well suited parameters to describe the integrated cell layer properties. An electrode is placed on each side of the membrane, and a small AC voltage is applied between the two electrodes (Figure 5.2b). The electric impedance of the cell system is measured on a range from 1 to  $10^5$  Hz (Figure 5.2c). The following schematic, an equivalent circuit shows how TER is extracted (Figure 5.2b and 5.2d). TER is commonly expressed as resistance measured multiplied by the area of endothelial monolayer ( $\Omega \cdot \text{cm}^2$ ) and corresponds to  $\text{TER} = (R_{\text{cell}}$

monolayer – R<sub>filtr</sub>) X A where R<sub>cell</sub> is the resistance of the cell monolayer, R<sub>filtr</sub> is the resistance of the membrane filter culture, and A is the surface of the membrane used. Tight models have values in the order of magnitude of hundreds Ω.cm<sup>2</sup> [80]. Tight models are necessary for TJ barrier assembly and cytoskeletal regulation. Usually, a correlation between permeability of a cell layer and the TER exists, with tight cell layers exhibiting high TER and low permeability [86].

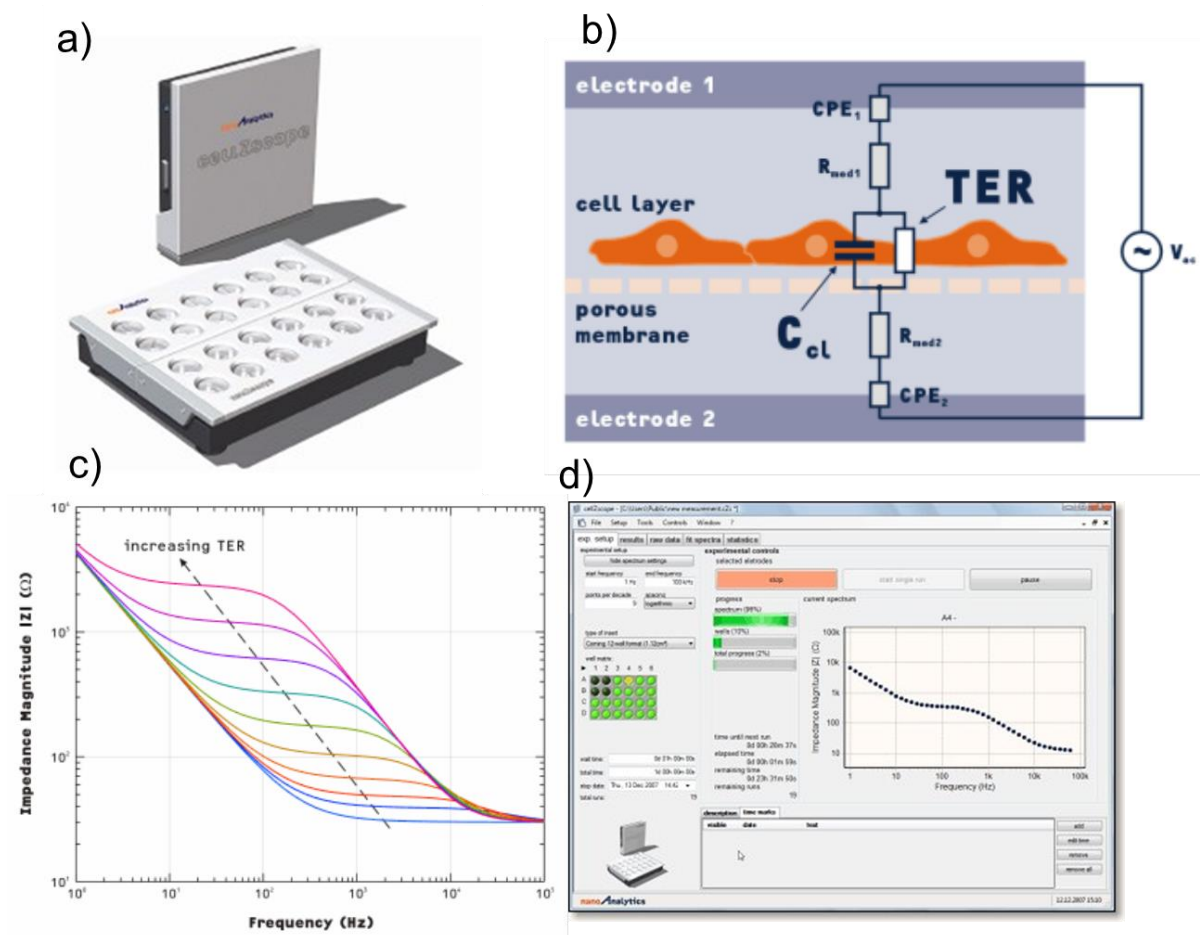


**Figure 2.7:** The CellZscope (a). CellZscope device (b). Equivalent circuit for cell layer grown on porous filter (c). Impedance frequency scan (d). Overview of CellZscope data acquisition window. Adapted from technical bulletin, Nanoanalytics.com.

**Organic electrochemical transistor:** This method using filter was described in detail in chapter 1.

**The planar method:** In this method, cells grow directly on the device. This configuration permits a close proximity of the cell monolayer to the electrodes which results in high sensitivity measurements.

**Electric cell-substrate impedance sensing (ECIS):** ECIS uses small gold film electrodes deposited on the bottom of cell culture dishes and measures the electrode impedance (Figure 2.8a). A constant small AC is applied between the electrodes and the potential across is measured. When cells are seeded on top of the working electrode, the flow is limited and the impedance is modified (Figure 2.8b, 2.8c). This method permits to monitor the TER change in real time [87].

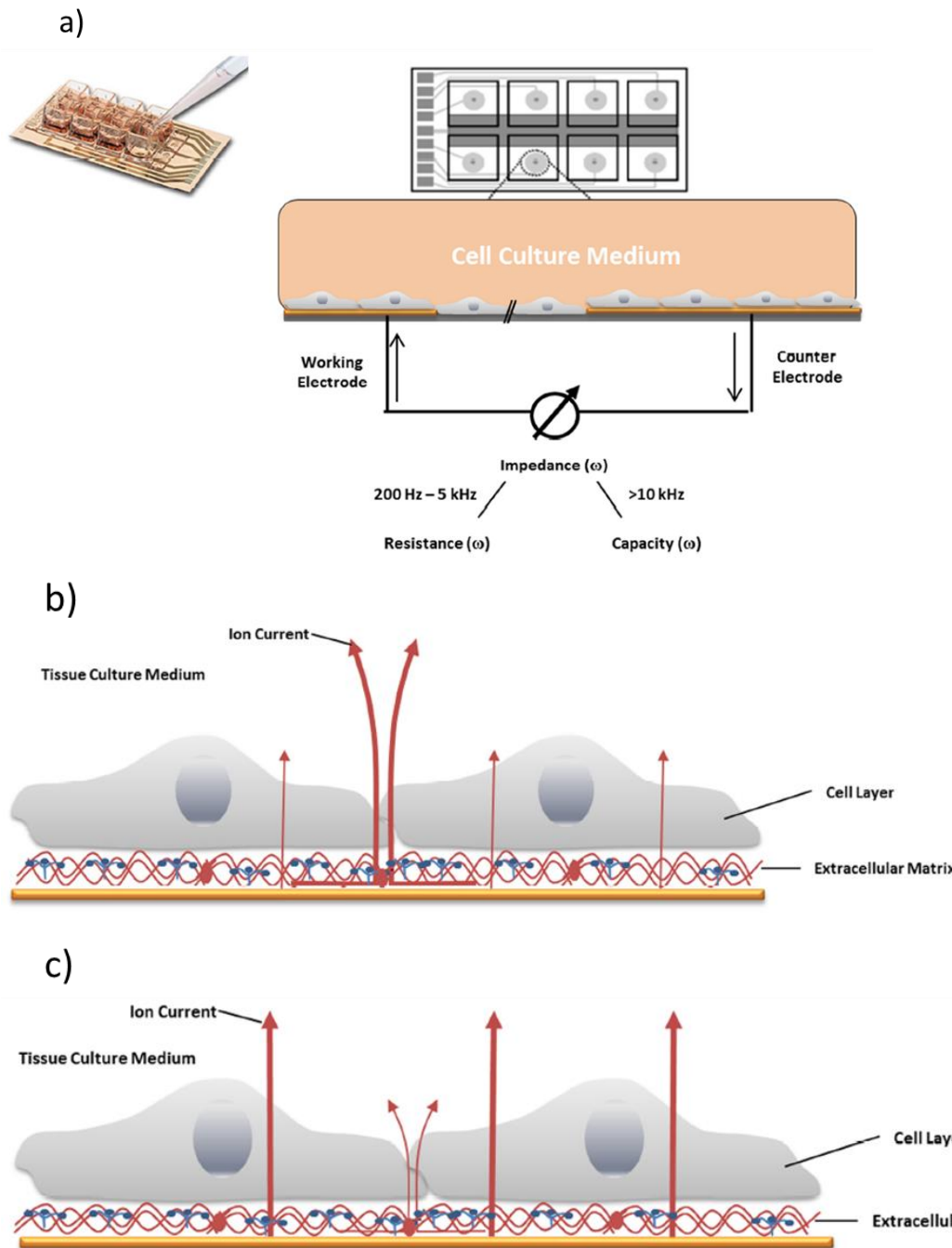


**Figure 2.8:** Schematic drawing of an ECIS array and principle of the electric cell-substrate impedance sensing (ECIS) method. (a) Cell layers are grown to confluence on integrated gold-film electrodes. An applied AC current flows between small working electrodes and the larger counter electrode using normal culture medium as an electrolyte. By a variation of the frequency  $\omega$ , a spectrum can be obtained. Applying higher frequencies the current flow is dominated by the capacity of the total system, at mid-range frequencies the ohmic resistance of the total system is mirrored. (b) The current pathway at low frequencies on a cerebral endothelial cell monolayer (ECIS method, 400 Hz). At low frequencies the current predominantly flows paracellular (through extracellular matrix proteins) and between adjacent cells (through tight junctions) and the electrolyte (medium). (c) Application of high frequencies (ECIS method, > 40 kHz), the capacitive amount of measured impedance is especially sensitive for adhered cells. The current passes through the insulating cell monolayer, especially through cell membranes (from Fluids and Barriers of the CNS, Benson *et al.*, [85]).

**Planar organic electrochemical transistor (OECT):** In the present device architecture of the OECT, the gate and the channel are in the same plane and both composed of PEDOT:PSS (Figure 2.9). Cell monolayers act as a barrier to the ionic current and the channel current is used to detect ion transport through the cell layer [88].

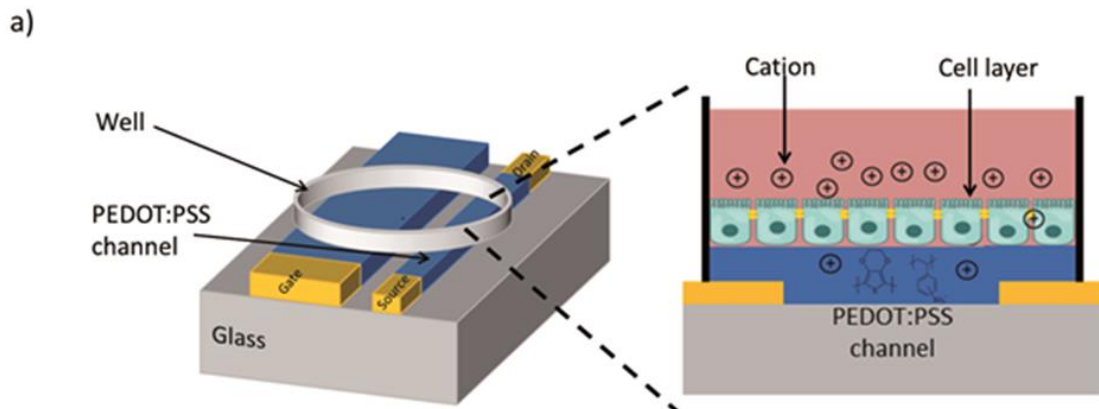


**Figure 2.9:** Schematic of planar OECT device which consists of a PEDOT:PSS channel and gate patterned onto a glass slide (from submitted Advanced Materials, Ramuz *et al.*, [88]).

## 2.4.2 Different Types of Cell Culture

Modelling the BBB is currently a necessity to understand the effect of toxins and pathogen on this barrier. However, developing an accurate and reliable *in vitro* model of BBB which mimics the physiology and the functional response of the BBB *in vitro* is challenging.

The aim of a valid *in vitro* BBB model is to mimic the BBB *in vivo*. The model should display *in vivo* BBB characteristics such as similar cell architecture, tight junctions forming a restrictive paracellular pathway, reproducible solute permeability, functional expression of key transporters such as P-gp, and expression of BBB marker enzymes such as alkaline phosphatase and  $\gamma$ -GT [89]. Additionally, the model should be low cost, allow ease of culture and high throughput screening. *In vitro* BBB models carry some advantages over *in vivo* BBB models, in that they permit the examination of the BBB in isolation and can eliminate compounds prior to *in vivo* studies thereby reducing animal experimentation, and are more cost effective.

In general, *in vitro* BBB models consist of a confluent monolayer of brain endothelial cell grown on a filter in monoculture, or co-culture with an other type of cells like astrocyte or neuron or pericyte and triculture with two other type of cells like astrocyte or neuron or pericyte [90]. Either side of the cell monolayer is a buffer filled compartment, one representing the blood (apical) and the other representing the brain (basolateral).

The extensively used method for studying the BBB is a primary cell culture model using rat, mouse, pig, cow, or human brain endothelial cells from freshly isolated brain microvessels [91].

## 2.4.3 Different Type of Blood Brain Barrier Model

### 2.4.3.1 Bovine Model

Bovine brain microvessel endothelial cells (BBMECs) have been used as an *in vitro* BBB model [92]. BBMECs have been characterized by the expression of the tight junction proteins (occludin, ZO-1, claudin-1 and claudin-5) [93] and efflux transporters (P-glycoprotein, MRP1, MRP4 and MRP5) [94] [95]. The permeability assay have been performed in the BBMEC model, but the tightness of the monocultured BBMECs has been reported to be highly variable ( $4$  to  $80 \times 10^{-6}$  cm.s<sup>-1</sup>)

[96]. Monocultured BBMECs have a rather leaky paracellular barrier which may limit their use in permeability studies. BBMECs have also been seeded with an astrocyte conditioned medium (ACM) [97], co-cultured with rat astrocytes [98] or with agents in order to increase the cyclic adenosine monophosphate (cAMP) levels [97]. The tightness of the co-cultured BBMEC model has been shown to be better (permeability of sucrose  $8.3$  to  $13 \times 10^{-6} \text{ cm.s}^{-1}$ ) than the monocultured BBMEC model (permeability of sucrose  $32 \times 10^{-6} \text{ cm.s}^{-1}$ ) [99]. The TER of BBMECs exhibits better results in co-culture with astrocytes ( $500\text{-}600 \text{ } \Omega.\text{cm}^2$ ) [100]. Further, it has been shown that P-gp expression is increased when BBMECs were co-cultured with astrocytes [101] [102] which indicate the significant effect of astrocytic factors on P-gp expression. Recently, a combination of different culture medium supplements (ACM, hydrocortisone) has been shown to improve the tightness of the BBMEC in co-culture model [103]. This model seems to be a tight *in vitro* BBB model. However, this is still two orders of magnitude leakier than the blood-brain barrier *in vivo* [104].

#### 2.4.3.2 Rat and Mouse Model

The tightness of the monoculture of rat brain microvessel endothelial cells (RBMECs) (permeability of sucrose  $2\text{-}11 \times 10^{-6} \text{ cm.s}^{-1}$ ) [105] [106] is similar to the BBMEC models. However, the disadvantage of the RBMECs is the low numbers of endothelial cells per animal. RBMECs have been used in drug uptake studies and drug transport studies [107] [108]. When RBMECs were co-cultured with astrocytes in presence of hydrocortisone and cAMP supplements, the permeability of sucrose has been reported to be as low as  $1.4 \times 10^{-6} \text{ cm.s}^{-1}$  and the TER around  $350\text{-}500 \text{ } \Omega.\text{cm}^2$  [106] [109] [110].

There are also immortalized rat endothelial cell lines available [111] and the most commonly used is the rat endothelial cell line (RBE4) which has been characterized in terms of the enzymatic activities of  $\gamma$ -GT and the functionality of P-gp [112]. One drawback of RBE4 cells is the poor cell monolayer tightness (permeability of sucrose  $214 \times 10^{-6} \text{ cm.s}^{-1}$ ) [113] which is not adequate for permeability studies. This reduces the feasibility of this model for screening [111] but it can be used for mechanistic studies. Further, several mouse brain endothelial cell lines have been established. Similarly to the rat brain endothelial cell lines, the mouse brain endothelial cell lines do not provide high tightness to permit permeability testing [114].

### 2.4.3.3 Porcine Model

Porcine brain microvessel endothelial cells (PBMECs) were isolated from porcine brain [115]. PBMECs have been used as an *in vitro* BBB model [116]. PBMECs display a very tight intercellular junctions (i.e. very low permeability) when they are cultured in serum-free and hydrocortisone supplemented culture media [117]. PBMECs have also been cultured with ACM [118] and co-cultured with rat astrocytes [80]. Co-culturing with astrocytes has increased the tightness of the paracellular barrier (permeability of sucrose  $0.2 \times 10^{-6} \text{ cm.s}^{-1}$ , TER  $>1000 \text{ } \Omega.\text{cm}^2$ ) [80]. The expressions of some transporters such as BCRP, MRP1 and MRP4 have been reported in the PBMECs cultured with ACM [118]. Nevertheless, the functionality of the transporters has not been sufficiently assessed in PBMECs.

### 2.4.3.4 Human Model

The first isolation of microvessel endothelial cells from human brain was in 1991 [119]. The Human Brain Microvascular Endothelial Cells (HBMECs) have been characterized for the transporter genes (MDR1, MRP2, MRP1, MRP4, MRP5, MRP6). The existence of MRP mediated efflux and functional amino acid transporters has been shown in the HBMECs [120] [121]. The permeability of sucrose was lower in the HBMECs co-cultured with human astrocytes ( $\sim 20 \times 10^{-6} \text{ cm.s}^{-1}$ ) than in the monocultured HBMECs ( $50 \times 10^{-6} \text{ cm.s}^{-1}$ ) [122]. Further, the TER was higher in HBMECs co-cultured with human astrocytes ( $260 \pm 130 \text{ } \Omega.\text{cm}^2$ ) than in the monocultured HBMECs ( $61 \pm 2 \text{ } \Omega.\text{cm}^2$ ) [122] suggesting the important role of astrocytes in the tightness of human brain endothelial cells *in vitro*. The HBMEC model appears to be promising as an *in vitro* model for human blood-brain barrier. However, the disadvantage of this model is the limited availability of the human brain tissue and the cost of these primary cells.

To avoid these concerns, an Immortalized Human Cerebral Microvascular Endothelial Cells, hCMEC/D3, derived from HBMECs, has been developed. hCMEC/D3 possess many blood-brain barrier markers, like tight junction proteins ZO-1 and claudin-5 [123]. Furthermore, expression of the efflux transporters (MDR1, MRP1-5, BCRP) has been reported in the hCMEC/D3 cells at the mRNA level and expression of P-glycoprotein, MRP1, MRP4, BCRP at the protein level [124] [125] [126]. The functionality of the efflux transporters P-glycoprotein, MRP, and BCRP was demonstrated in the absence of astrocytes [126]. The advantage of the hCMEC/D3 cells is that these cells are easy to grow and show a stable normal karyotype at least until the 35th passage [127]. All these characteristics make the hCMEC/D3 an interesting tool for permeability and resistance studies.

## 2.5 Conclusion

Characterisation of *in vitro* models of BBB for future diagnostics with toxins and pathogens is challenging. Traditional biological methods like the permeability assay, TER, or immunofluorescence are necessary to understand the mechanisms that interact in the BBB. However, these tests cannot evaluate the toxic potential, or detect the state of the pathogen (living or dead). Many pathogens are often not detected because they require a specific test or because they are unknown. Therefore, it would be wise to develop a system for the evaluation of new model which have a high throughput screening for drugs and can simultaneously detect a wide range of toxins and pathogens which are cheap, sensitive, and specific. Biosensor systems could provide solutions and become an alternative to traditional methods.

## 2.6 Bibliography

1. Nag, S., *Pathophysiology of blood-brain barrier breakdown*. Methods Mol Med, 2003. **89**: p. 97-119.
2. Lloyd-Jones, D., et al., *Heart disease and stroke statistics--2010 update: a report from the American Heart Association*. Circulation, 2010. **121**(7): p. e46-e215.
3. Bernacki, J., et al., *Physiology and pharmacological role of the blood-brain barrier*. Pharmacol Rep, 2008. **60**(5): p. 600-22.
4. Abbott, N.J., *Blood-brain barrier structure and function and the challenges for CNS drug delivery*. J Inher Metab Dis, 2013. **36**(3): p. 437-49.
5. Pardridge, W.M., *The blood-brain barrier: bottleneck in brain drug development*. NeuroRx, 2005. **2**(1): p. 3-14.
6. Burns, E.M., et al., *Blood-brain barrier: morphology, physiology, and effects of contrast media*. Adv Neurol, 1981. **30**: p. 159-65.
7. Hawkins, B.T. and T.P. Davis, *The blood-brain barrier/neurovascular unit in health and disease*. Pharmacol Rev, 2005. **57**(2): p. 173-85.
8. Reese, T.S. and M.J. Karnovsky, *Fine structural localization of a blood-brain barrier to exogenous peroxidase*. J Cell Biol, 1967. **34**(1): p. 207-17.
9. Siakotos, A.N. and G. Rouser, *Isolation of highly purified human and bovine brain endothelial cells and nuclei and their phospholipid composition*. Lipids, 1969. **4**(3): p. 234-9.
10. Betz, A.L., J.A. Firth, and G.W. Goldstein, *Polarity of the blood-brain barrier: distribution of enzymes between the luminal and antiluminal membranes of brain capillary endothelial cells*. Brain Res, 1980. **192**(1): p. 17-28.
11. Cecchelli, R., et al., *Modelling of the blood-brain barrier in drug discovery and development*. Nat Rev Drug Discov, 2007. **6**(8): p. 650-61.

12. Obermeier, B., R. Daneman, and R.M. Ransohoff, *Development, maintenance and disruption of the blood-brain barrier*. Nat Med, 2013. **19**(12): p. 1584-96.
13. Deli, M.A., *Blood-Brain Barrier Models*, in Handbook of Neurochemistry and Molecular Neurobiology, A. Lajtha and M.A. Reith, Editors. 2007, Springer US. p. 29-55..
14. Begley, D.J. and M.W. Brightman, *Structural and functional aspects of the blood-brain barrier*. Prog Drug Res, 2003. **61**: p. 39-78.
15. Hawkins, R.A., et al., *Structure of the blood-brain barrier and its role in the transport of amino acids*. J Nutr, 2006. **136**(1 Suppl): p. 218S-26S.
16. Pardridge, W.M., *Blood-brain barrier biology and methodology*. Journal of Neurovirology, 1999. **5**(6): p. 556-69.
17. Fellin, T., M. D'Ascenzo, and P.G. Haydon, *Astrocytes control neuronal excitability in the nucleus accumbens*. ScientificWorldJournal, 2007. **7**: p. 89-97.
18. Brown, A.M. and B.R. Ransom, *Astrocyte glycogen and brain energy metabolism*. Glia, 2007. **55**(12): p. 1263-71.
19. Brightman, M.W. and T.S. Reese, *Junctions between intimately apposed cell membranes in the vertebrate brain*. J Cell Biol, 1969. **40**(3): p. 648-77.
20. Cancilla, P.A. and L.E. DeBault, *Neutral amino acid transport properties of cerebral endothelial cells in vitro*. J Neuropathol Exp Neurol, 1983. **42**(2): p. 191-99.
21. Allt, G. and J.G. Lawrenson, *Pericytes: cell biology and pathology*. Cells Tissues Organs, 2001. **169**(1): p. 1-11.
22. Frank, R.N., S. Dutta, and M.A. Mancini, *Pericyte coverage is greater in the retinal than in the cerebral capillaries of the rat*. Invest Ophthalmol Vis Sci, 1987. **28**(7): p. 1086-91.
23. Larson, D.M., M.P. Carson, and C.C. Haudenschild, *Junctional transfer of small molecules in cultured bovine brain microvascular endothelial cells and pericytes*. Microvasc Res, 1987. **34**(2): p. 184-99.
24. Hellstrom, M., et al., *Lack of pericytes leads to endothelial hyperplasia and abnormal vascular morphogenesis*. J Cell Biol, 2001. **153**(3): p. 543-53.
25. Coomber, B.L. and P.A. Stewart, *Morphometric analysis of CNS microvascular endothelium*. Microvasc Res, 1985. **30**(1): p. 99-115.
26. Bauer, H.C. and H. Bauer, *Neural induction of the blood-brain barrier: still an enigma*. Cell Mol Neurobiol, 2000. **20**(1): p. 13-28.
27. Tontsch, U. and H.C. Bauer, *Glial cells and neurons induce blood-brain barrier related enzymes in cultured cerebral endothelial cells*. Brain Res, 1991. **539**(2): p. 247-53.
28. Xue, Q., et al., *A novel brain neurovascular unit model with neurons, astrocytes and microvascular endothelial cells of rat*. Int J Biol Sci, 2013. **9**(2): p. 174-89.
29. Schulze, C. and J.A. Firth, *Immunohistochemical localization of adherens junction components in blood-brain barrier microvessels of the rat*. J Cell Sci, 1993. **104** ( Pt 3): p. 773-82.
30. Furuse, M., et al., *Occludin: a novel integral membrane protein localizing at tight junctions*. J Cell Biol, 1993. **123**(6 Pt 2): p. 1777-88.
31. Furuse, M., et al., *Claudin-1 and -2: novel integral membrane proteins localizing at tight junctions with no sequence similarity to occludin*. J Cell Biol, 1998. **141**(7): p. 1539-50.

32. Persidsky, Y., et al., *Blood-brain barrier: structural components and function under physiologic and pathologic conditions*. J Neuroimmune Pharmacol, 2006. **1**(3): p. 223-36.
33. Persidsky, Y., et al., *Rho-mediated regulation of tight junctions during monocyte migration across the blood-brain barrier in HIV-1 encephalitis (HIVE)*. Blood, 2006. **107**(12): p. 4770-80.
34. Butt, A.M., P.T. Hargittai, and E.M. Lieberman, *Calcium-dependent regulation of potassium permeability in the glial perineurium (blood-brain barrier) of the crayfish*. Neuroscience, 1990. **38**(1): p. 175-85.
35. Afonso, P.V., et al., *Human blood-brain barrier disruption by retroviral-infected lymphocytes: role of myosin light chain kinase in endothelial tight-junction disorganization*. J Immunol, 2007. **179**(4): p. 2576-83.
36. Wolburg, H., et al., *Modulation of tight junction structure in blood-brain barrier endothelial cells. Effects of tissue culture, second messengers and cocultured astrocytes*. J Cell Sci, 1994. **107** ( Pt 5): p. 1347-57.
37. Hirase, T., et al., *Occludin as a possible determinant of tight junction permeability in endothelial cells*. J Cell Sci, 1997. **110** ( Pt 14): p. 1603-13.
38. Saitou, M., et al., *Complex phenotype of mice lacking occludin, a component of tight junction strands*. Mol Biol Cell, 2000. **11**(12): p. 4131-42.
39. Brown, R.C. and T.P. Davis, *Hypoxia/aglycemia alters expression of occludin and actin in brain endothelial cells*. Biochem Biophys Res Commun, 2005. **327**(4): p. 1114-23.
40. Wolburg, H. and A. Lippoldt, *Tight junctions of the blood-brain barrier: development, composition and regulation*. Vascul Pharmacol, 2002. **38**(6): p. 323-37.
41. Dejana, E., et al., *The molecular organization of endothelial junctions and their functional role in vascular morphogenesis and permeability*. Int J Dev Biol, 2000. **44**(6): p. 743-8.
42. Martin-Padura, I., et al., *Junctional adhesion molecule, a novel member of the immunoglobulin superfamily that distributes at intercellular junctions and modulates monocyte transmigration*. J Cell Biol, 1998. **142**(1): p. 117-27.
43. Schneeberger, E.E. and R.D. Lynch, *The tight junction: a multifunctional complex*. Am J Physiol Cell Physiol, 2004. **286**(6): p. C1213-28.
44. Stevenson, B.R., et al., *Identification of ZO-1: a high molecular weight polypeptide associated with the tight junction (zonula occludens) in a variety of epithelia*. J Cell Biol, 1986. **103**(3): p. 755-66.
45. Petty, M.A. and E.H. Lo, *Junctional complexes of the blood-brain barrier: permeability changes in neuroinflammation*. Prog Neurobiol, 2002. **68**(5): p. 311-23.
46. Ballabh, P., A. Braun, and M. Nedergaard, *The blood-brain barrier: an overview: structure, regulation, and clinical implications*. Neurobiology of Disease, 2004. **16**(1): p. 1-13.
47. Brown, R.C. and T.P. Davis, *Calcium modulation of adherens and tight junction function: a potential mechanism for blood-brain barrier disruption after stroke*. Stroke, 2002. **33**(6): p. 1706-11.
48. Pardridge, W.M., *The blood-brain barrier and neurotherapeutics*. NeuroRx, 2005. **2**(1): p. 1-2.
49. Fanning, A.S., L.L. Mitic, and J.M. Anderson, *Transmembrane proteins in the tight junction barrier*. J Am Soc Nephrol, 1999. **10**(6): p. 1337-45.

50. Abbott, N.J., L. Ronnback, and E. Hansson, *Astrocyte-endothelial interactions at the blood-brain barrier*. Nature Reviews Neuroscience, 2006. **7**(1): p. 41-53.
51. Abbott, N.J., et al., *Structure and function of the blood-brain barrier*. Neurobiology of Disease, 2010. **37**(1): p. 13-25.
52. Pardridge, W.M., *Biologic TNF $\alpha$ -inhibitors that cross the human blood-brain barrier*. Bioeng Bugs, 2010. **1**(4): p. 231-4.
53. Ohtsuki, S. and T. Terasaki, *Contribution of carrier-mediated transport systems to the blood-brain barrier as a supporting and protecting interface for the brain; importance for CNS drug discovery and development*. Pharm Res, 2007. **24**(9): p. 1745-58.
54. Simpson, C., et al., *Isolation, purification and characterization of a novel glucose oxidase from Penicillium sp. CBS 120262 optimally active at neutral pH*. Protein Expr Purif, 2007. **51**(2): p. 260-6.
55. O'Kane, R.L., et al., *Cationic amino acid transport across the blood-brain barrier is mediated exclusively by system y(+)*. American Journal of Physiology-Endocrinology and Metabolism, 2006. **291**(2): p. E412-E419.
56. Bickel, U., T. Yoshikawa, and W.M. Pardridge, *Delivery of peptides and proteins through the blood-brain barrier*. Adv Drug Deliv Rev, 2001. **46**(1-3): p. 247-79.
57. Lawrenson, J.G., et al., *Cerebral and pial microvessels: differential expression of gamma-glutamyl transpeptidase and alkaline phosphatase*. Anat Embryol (Berl), 1999. **199**(1): p. 29-34.
58. Betz, A.L. and G.W. Goldstein, *The basis for active transport at the blood-brain barrier*. Adv Exp Med Biol, 1980. **131**: p. 5-16.
59. Frey, A., et al., *Pericytes of the brain microvasculature express gamma-glutamyl transpeptidase*. Eur J Biochem, 1991. **202**(2): p. 421-9.
60. Black, K.L., T. Baba, and W.M. Pardridge, *Enzymatic barrier protects brain capillaries from leukotriene C4*. J Neurosurg, 1994. **81**(5): p. 745-51.
61. Dean, M., Y. Hamon, and G. Chimini, *The human ATP-binding cassette (ABC) transporter superfamily*. J Lipid Res, 2001. **42**(7): p. 1007-17.
62. Sharom, F.J., *ABC multidrug transporters: structure, function and role in chemoresistance*. Pharmacogenomics, 2008. **9**(1): p. 105-27.
63. Tsuji, A., et al., *P-glycoprotein as the drug efflux pump in primary cultured bovine brain capillary endothelial cells*. Life Sci, 1992. **51**(18): p. 1427-37.
64. Schinkel, A.H., *P-Glycoprotein, a gatekeeper in the blood-brain barrier*. Adv Drug Deliv Rev, 1999. **36**(2-3): p. 179-194.
65. Juliano, R.L. and V. Ling, *A surface glycoprotein modulating drug permeability in Chinese hamster ovary cell mutants*. Biochim Biophys Acta, 1976. **455**(1): p. 152-62.
66. Eckford, P.D. and F.J. Sharom, *Interaction of the P-glycoprotein multidrug efflux pump with cholesterol: effects on ATPase activity, drug binding and transport*. Biochemistry, 2008. **47**(51): p. 13686-98.
67. Kim, A.E., et al., *Saquinavir, an HIV protease inhibitor, is transported by P-glycoprotein*. J Pharmacol Exp Ther, 1998. **286**(3): p. 1439-45.
68. Schinkel, A.H., et al., *Multidrug resistance and the role of P-glycoprotein knockout mice*. Eur J Cancer, 1995. **31A**(7-8): p. 1295-8.
69. Volk, H., H. Potschka, and W. Loscher, *Immunohistochemical localization of P-glycoprotein in rat brain and detection of its increased expression by*

- seizures are sensitive to fixation and staining variables.* J Histochem Cytochem, 2005. **53**(4): p. 517-31.
70. Deeley, R.G., C. Westlake, and S.P. Cole, *Transmembrane transport of endo- and xenobiotics by mammalian ATP-binding cassette multidrug resistance proteins.* Physiol Rev, 2006. **86**(3): p. 849-99.
  71. Dauchy, S., et al., *ABC transporters, cytochromes P450 and their main transcription factors: expression at the human blood-brain barrier.* J Neurochem, 2008. **107**(6): p. 1518-28.
  72. Loscher, W. and H. Potschka, *Blood-brain barrier active efflux transporters: ATP-binding cassette gene family.* NeuroRx, 2005. **2**(1): p. 86-98.
  73. Diestra, J.E., et al., *Frequent expression of the multi-drug resistance-associated protein BCRP/MXR/ABCP/ABCG2 in human tumours detected by the BXP-21 monoclonal antibody in paraffin-embedded material.* J Pathol, 2002. **198**(2): p. 213-9.
  74. Schinkel, A.H. and J.W. Jonker, *Mammalian drug efflux transporters of the ATP binding cassette (ABC) family: an overview.* Adv Drug Deliv Rev, 2003. **55**(1): p. 3-29.
  75. Pan, G., N. Giri, and W.F. Elmquist, *Abcg2/Bcrp1 mediates the polarized transport of antiretroviral nucleosides abacavir and zidovudine.* Drug Metab Dispos, 2007. **35**(7): p. 1165-73.
  76. Hagenbuch, B. and P.J. Meier, *The superfamily of organic anion transporting polypeptides.* Biochim Biophys Acta, 2003. **1609**(1): p. 1-18.
  77. Reichel, A., D.J. Begley, and N.J. Abbott, *An overview of in vitro techniques for blood-brain barrier studies.* Methods Mol Med, 2003. **89**: p. 307-24.
  78. Grant, G.A., N.J. Abbott, and D. Janigro, *Understanding the Physiology of the Blood-Brain Barrier: In Vitro Models.* News Physiol Sci, 1998. **13**: p. 287-293.
  79. Forster, C., et al., *Occludin as direct target for glucocorticoid-induced improvement of blood-brain barrier properties in a murine in vitro system.* J Physiol, 2005. **565**(Pt 2): p. 475-86.
  80. Deli, M.A., et al., *Permeability studies on in vitro blood-brain barrier models: physiology, pathology, and pharmacology.* Cell Mol Neurobiol, 2005. **25**(1): p. 59-127.
  81. Wilhelm, I., C. Fazakas, and I.A. Krizbai, *In vitro models of the blood-brain barrier.* Acta Neurobiol Exp (Wars), 2011. **71**(1): p. 113-28.
  82. Gunzel, D. and A.S. Yu, *Claudins and the modulation of tight junction permeability.* Physiol Rev, 2013. **93**(2): p. 525-69.
  83. Van Itallie, C.M. and J.M. Anderson, *Chapter 5 Molecular structure and regulation of tight junctions,* in *Current Topics in Membranes*, M.D. Kim E. Barrett, Editor 2000, Academic Press. p. 163-186.
  84. Shen, L., C.R. Weber, and J.R. Turner, *The tight junction protein complex undergoes rapid and continuous molecular remodeling at steady state.* J Cell Biol, 2008. **181**(4): p. 683-95.
  85. Benson, K., S. Cramer, and H.J. Galla, *Impedance-based cell monitoring: barrier properties and beyond.* Fluids Barriers CNS, 2013. **10**(1): p. 5.
  86. Balda, M.S., et al., *Functional dissociation of paracellular permeability and transepithelial electrical resistance and disruption of the apical-basolateral intramembrane diffusion barrier by expression of a mutant tight junction membrane protein.* J Cell Biol, 1996. **134**(4): p. 1031-49.

87. Wegener, J., C.R. Keese, and I. Giaever, *Electric Cell–Substrate Impedance Sensing (ECIS) as a Noninvasive Means to Monitor the Kinetics of Cell Spreading to Artificial Surfaces*. *Experimental Cell Research*, 2000. **259**(1): p. 158-166.
88. Ramuz, M., et al., *Combined Optical and Electronic Sensing of Epithelial Cells Using Planar Organic Transistors*. *Advanced Materials*, 2014
89. Gumbleton, M. and K.L. Audus, *Progress and limitations in the use of in vitro cell cultures to serve as a permeability screen for the blood-brain barrier*. *J Pharm Sci*, 2001. **90**(11): p. 1681-98.
90. Hatherell, K., et al., *Development of a three-dimensional, all-human in vitro model of the blood-brain barrier using mono-, co-, and tri-cultivation Transwell models*. *J Neurosci Methods*, 2011. **199**(2): p. 223-9.
91. Vernon, H., K. Clark, and J.P. Bressler, *In vitro models to study the blood brain barrier*. *Methods Mol Biol*, 2011. **758**: p. 153-68.
92. Baranczyk-Kuzma, A., K.L. Audus, and R.T. Borchardt, *Catecholamine-metabolizing enzymes of bovine brain microvessel endothelial cell monolayers*. *J Neurochem*, 1986. **46**(6): p. 1956-60.
93. Culot, M., et al., *An in vitro blood-brain barrier model for high throughput (HTS) toxicological screening*. *Toxicol In Vitro*, 2008. **22**(3): p. 799-811.
94. Zhang, Y., et al., *Expression of various multidrug resistance-associated protein (MRP) homologues in brain microvessel endothelial cells*. *Brain Res*, 2000. **876**(1-2): p. 148-53.
95. Zhang, Y., et al., *Plasma membrane localization of multidrug resistance-associated protein homologs in brain capillary endothelial cells*. *J Pharmacol Exp Ther*, 2004. **311**(2): p. 449-55.
96. Cecchelli, R., et al., *In vitro model for evaluating drug transport across the blood-brain barrier*. *Adv Drug Deliv Rev*, 1999. **36**(2-3): p. 165-178.
97. Rubin, L.L., et al., *A cell culture model of the blood-brain barrier*. *J Cell Biol*, 1991. **115**(6): p. 1725-35.
98. Tao-Cheng, J.H., Z. Nagy, and M.W. Brightman, *Tight junctions of brain endothelium in vitro are enhanced by astroglia*. *J Neurosci*, 1987. **7**(10): p. 3293-9.
99. Lundquist, S. and M. Renftel, *The use of in vitro cell culture models for mechanistic studies and as permeability screens for the blood-brain barrier in the pharmaceutical industry--background and current status in the drug discovery process*. *Vascul Pharmacol*, 2002. **38**(6): p. 355-64.
100. Zysk, G., et al., *Pneumolysin is the main inducer of cytotoxicity to brain microvascular endothelial cells caused by Streptococcus pneumoniae*. *Infect Immun*, 2001. **69**(2): p. 845-52.
101. Gaillard, P.J. and A.G. de Boer, *Relationship between permeability status of the blood-brain barrier and in vitro permeability coefficient of a drug*. *Eur J Pharm Sci*, 2000. **12**(2): p. 95-102.
102. Gaillard, P.J., et al., *Astrocytes increase the functional expression of P-glycoprotein in an in vitro model of the blood-brain barrier*. *Pharm Res*, 2000. **17**(10): p. 1198-205.
103. Helms, H.C., et al., *Paracellular tightness and claudin-5 expression is increased in the BCEC/astrocyte blood-brain barrier model by increasing media buffer capacity during growth*. *AAPS J*, 2010. **12**(4): p. 759-70.

104. Ohno, K., K.D. Pettigrew, and S.I. Rapoport, *Lower limits of cerebrovascular permeability to nonelectrolytes in the conscious rat*. Am J Physiol, 1978. **235**(3): p. H299-307.
105. Parkinson, F.E. and C. Hacking, *Pericyte abundance affects sucrose permeability in cultures of rat brain microvascular endothelial cells*. Brain Res, 2005. **1049**(1): p. 8-14.
106. Perriere, N., et al., *A functional in vitro model of rat blood-brain barrier for molecular analysis of efflux transporters*. Brain Res, 2007. **1150**: p. 1-13.
107. Li, Y., et al., *Transport of gatifloxacin involves Na<sup>+</sup>/Ca<sup>2+</sup> exchange and excludes P-glycoprotein and multidrug resistance associated-proteins in primary cultured rat brain endothelial cells*. Eur J Pharmacol, 2009. **616**(1-3): p. 68-72.
108. Perriere, N., et al., *Puromycin-based purification of rat brain capillary endothelial cell cultures. Effect on the expression of blood-brain barrier-specific properties*. J Neurochem, 2005. **93**(2): p. 279-89.
109. Kis, B., et al., *Adrenomedullin regulates blood-brain barrier functions in vitro*. Neuroreport, 2001. **12**(18): p. 4139-42.
110. Hellinger, E., et al., *Comparison of brain capillary endothelial cell-based and epithelial (MDCK-MDR1, Caco-2, and VB-Caco-2) cell-based surrogate blood-brain barrier penetration models*. Eur J Pharm Biopharm, 2012. **82**(2): p. 340-51.
111. Roux, F. and P.O. Couraud, *Rat brain endothelial cell lines for the study of blood-brain barrier permeability and transport functions*. Cell Mol Neurobiol, 2005. **25**(1): p. 41-58.
112. Roux, F., et al., *Regulation of gamma-glutamyl transpeptidase and alkaline phosphatase activities in immortalized rat brain microvessel endothelial cells*. J Cell Physiol, 1994. **159**(1): p. 101-13.
113. Rist, R.J., et al., *F-actin cytoskeleton and sucrose permeability of immortalised rat brain microvascular endothelial cell monolayers: effects of cyclic AMP and astrocytic factors*. Brain Res, 1997. **768**(1-2): p. 10-8.
114. Tatsuta, T., et al., *Functional involvement of P-glycoprotein in blood-brain barrier*. J Biol Chem, 1992. **267**(28): p. 20383-91.
115. Tontsch, U. and H.C. Bauer, *Isolation, characterization, and long-term cultivation of porcine and murine cerebral capillary endothelial cells*. Microvasc Res, 1989. **37**(2): p. 148-61.
116. Zhang, Y., et al., *Porcine brain microvessel endothelial cells as an in vitro model to predict in vivo blood-brain barrier permeability*. Drug Metab Dispos, 2006. **34**(11): p. 1935-43.
117. Lohmann, C., S. Huwel, and H.J. Galla, *Predicting blood-brain barrier permeability of drugs: evaluation of different in vitro assays*. J Drug Target, 2002. **10**(4): p. 263-76.
118. Zhang, Y., et al., *Porcine brain microvessel endothelial cells as an in vitro model to predict in vivo blood-brain barrier permeability*. Drug Metab Dispos, 2006. **34**(11): p. 1935-43.
119. Dorovini-Zis, K. and A.P. Zis, *Innervation of the zona fasciculata of the adult human adrenal cortex: a light and electron microscopic study*. J Neural Transm Gen Sect, 1991. **84**(1-2): p. 75-84.
120. Umeki, N., et al., *mRNA expression and amino acid transport characteristics of cultured human brain microvascular endothelial cells (hBME)*. Drug Metab Pharmacokinet, 2002. **17**(4): p. 367-73.

121. Eilers, M., U. Roy, and D. Mondal, *MRP (ABCC) transporters-mediated efflux of anti-HIV drugs, saquinavir and zidovudine, from human endothelial cells*. *Exp Biol Med* (Maywood), 2008. **233**(9): p. 1149-60.
122. Megard, I., et al., *A co-culture-based model of human blood-brain barrier: application to active transport of indinavir and in vivo-in vitro correlation*. *Brain Res*, 2002. **927**(2): p. 153-67.
123. Weksler, B.B., et al., *Blood-brain barrier-specific properties of a human adult brain endothelial cell line*. *FASEB J*, 2005. **19**(13): p. 1872-4.
124. Ohtsuki, S., et al., *Quantitative targeted absolute proteomic analysis of transporters, receptors and junction proteins for validation of human cerebral microvascular endothelial cell line hCMEC/D3 as a human blood-brain barrier model*. *Mol Pharm*, 2013. **10**(1): p. 289-96.
125. Dauchy, S., et al., *Expression and transcriptional regulation of ABC transporters and cytochromes P450 in hCMEC/D3 human cerebral microvascular endothelial cells*. *Biochem Pharmacol*, 2009. **77**(5): p. 897-909.
126. Poller, B., et al., *The human brain endothelial cell line hCMEC/D3 as a human blood-brain barrier model for drug transport studies*. *J Neurochem*, 2008. **107**(5): p. 1358-68.
127. Weksler, B., I.A. Romero, and P.O. Couraud, *The hCMEC/D3 cell line as a model of the human blood brain barrier*. *Fluids Barriers CNS*, 2013. **10**(1): p. 16.

# Chapter 3

---

## Development and Characterisation of Different Types of *in vitro* BBB Models

---

### 3.1 Introduction

The characterisation of the BBB is primarily carried out in laboratory animals. Although the scientific community encourages animal testing to increase our knowledge of health and medicine, they still agree on the necessity to practice alternatives methods to reduce animal suffering. One major alternative to animal testing is the development of stable and competent valid *in vitro* models [1].

The difficulty to study *in vitro* BBB models is the phenotypes of the existing *in vitro* models which are still very far from those found *in vivo*. The multiple different *in vitro* BBB models come from the complex function of the BBB [2]. On one side, this barrier is really selective and impermeable while on the other hand some pathogen or toxin can penetrate into the CNS and alter BBB properties.

Our goal consists of developing an *in vitro* model of BBB, for later integration with an organic electrochemical transistor, for use in investigating the effect of pathogens or toxins. The first step is to assess the formation of tight confluent monolayer using traditional assays: the permeability assay, measurement of TER and immunofluorescence staining of fixed samples. An '*in vivo*' like barrier is widely thought to be reflected by a low permeability to soluble molecules and by a high TER of the monolayer. We first attempted to get a stable monoculture of Bovine Brain Endothelial Cells (BBECs) and secondly we try to develop a human *in vitro* BBB model.

### 3.2 *In vitro* BBB Model Using Bovine Brain Endothelial Cells

#### 3.2.1 Generality on Bovine Brain Endothelial Cells

The BBEC model consists of microvascular cells derived from bovine brain tissue. This model offers a lot of advantages. First of all, BBECs are easy to obtain. Second, from bovine brain a large amount of cells can be obtained. It is possible to amplify BBECs and in culture which provides cells that can be maintained until passage 7. Further this model can be differentiate in 4 day. BBECs is often used to study transport of drugs across the BBB, because they express tight junctions (ZO-1 and Claudin-1) protein and transport characteristics like P-gp found in the BBB *in vivo* [3].

### 3.2.2 Materials and Methods

**Cell Culture:** Bovine Brain Endothelial Cells (BBECs) were a kind gift of the University Lille Nord de France, U. Artois, BBB Laboratory (LBHE). BBECs were cultured in a petri dish coated with gelatin at 37°C in 5% CO<sub>2</sub> humidified incubators, in DMEM (Dulbecco's Modified Eagle Medium) with 10% Calf Serum (CS), 10% Horse serum (HS), 1% glutamine and 0.5% gentamicin. When cells reached confluence, they were dissociated by enzymatic digestion (1% trypsin EDTA), collected, and 80 µl (= 4.10<sup>4</sup>) of cells are seeded at passage 6 onto filter (Costar or Millipore) coated with collagen (100 µg.ml<sup>-1</sup>) or gelatin (2µg.ml<sup>-1</sup>). The experiment is running during 4 days. To obtain the barrier properties, cells were cultured in DMEM (Dulbecco's Modified Eagle Medium) with 2.5% Calf serum (CS), 2.5% Horse serum (HS), 1% glutamine and 0.5% gentamicin, twenty four hours before the permeability assay and immunofluorescence of tight junction proteins are observed.

**Permeability Assay:** The selective paracellular permeability of BBECs was evaluated by a low permeability to the non-permeant fluorescent marker lucifer yellow (LY) (Sigma Aldrich). When BBECs reach confluency, monolayer was rinsed with Ringer-HEPES solution (150 mmol.L<sup>-1</sup> NaCl, 5.2 mmol.L<sup>-1</sup> KCl, 2.2 mmol.L<sup>-1</sup> CaCl<sub>2</sub>, 0.2 mmol.L<sup>-1</sup> MgCl<sub>2</sub>(6H<sub>2</sub>O), 6 mmol.L<sup>-1</sup>, NaHCO<sub>3</sub>, 5 mmol.L<sup>-1</sup> HEPES, 2.8 mmol.L<sup>-1</sup> glucose, pH 7.4). The permeability marker LY was added to the apical side of the monolayer and fluorescence was measured after 1 h incubation at 37 °C in a humidified CO<sub>2</sub> incubator using a fluorescence spectrophotometer (TECAN). The endothelial permeability coefficient (Pe) was calculated in centimeters per minute. In this calculation, both filter without cells permeability (PSf = insert filter + collagen/gelatin coating) and filter plus cell permeability (PSt = filter + collagen/gelatin + BBECs) were taken into account, following to the formula:  $1/PSe = 1/PSt - 1/PSf$ .

Pe was obtained according to the following relationship:  $Pe = (1/PSe) / A$ , where A is the area of the filter:

BBECs were considered as tight when the Pe value for the marker molecule was below 1.10<sup>-3</sup>cm.min<sup>-1</sup>[3].

**CellZscope Measurements:** The investigation of the TER is measured in cooperation with nanoAnalytics GmbH, the CellZscope. This device (Nanoanalytics) was used to measure the impedance of cell layers grown on inserts under physiological conditions.

**Immunofluorescence:** Cells grown on filters during all experiment. BBECs were next fixed with 4% paraformaldehyde in PBS pH 7.4, 15 min at room temperature. The permeabilization was done in 0.25% Triton in PBS, 10 min at room temperature and the blocking step with 1% BSA in PBST (0.05% Tween 20 in PBS), 30 min at room temperature. Mouse monoclonal anti-ZO-1 and anti-Claudin1 then rabbit polyclonal anti-occludin anti-ZO-1 were used at  $5\mu\text{g}\cdot\text{ml}^{-1}$  (Tight Junction Antibody Sampler Pack, Invitrogen), in 1% BSA in PBST for 1 h at room temperature. BBECs were then incubated for 1 h at room temperature with the secondary antibodies Alexa Fluor 488 goat anti-mouse IgG and Alexa Fluor 568 goat anti-rabbit (Molecular Probes). Lastly, the cells were incubated for 5 min at room temperature with Fluoroshield with DAPI (Sigma Aldrich), mounted and examined with a fluorescent microscope (AxioVision).

**Scanning Electron Microscopy:** To assess the formation of confluent monolayer of BBECs, a scanning electron microscope (SEM, Ultra 55, Carl Zeiss) was used.

**Vapor Phase Polymerisation (VPP) of Poly(3,4-ethylenedioxythiophene):Tosylate (PEDOT(TOS)):** To promote the biocompatibility of PEDOT(TOS) with BBECs , for future use in an *in vitro* model of BBB with integrated OECT devices for measuring the integrity of this tissue layer, a VPP method is done. PEDOT(TOS) (Yacoo Chemical Co., Ltd) was used as the conducting polymer. PEDOT (TOS) composites were prepared by dissolving 0.8 g of Fe(III)TOS in 5 mL of isopropanol (IPA) and 32  $\mu\text{l}$  of pyridine (BDH Chemicals). The oxidant solution was spun onto the filter at 1500 rpm for 30 s and placed directly in the vapor phase polymerisation chamber without a drying step. The vaporization chamber, containing an 3,4-Ethylenedioxythiophene (EDOT) monomer (HD Stark or YacooChemical Co., Ltd.), was kept in an oven at  $70^{\circ}\text{C}$ , at ambient pressure. After polymerization, the film coated filter was cooled to room temperature and washed with ethanol three times to remove excess Fe(III)TOS and unpolymerised EDOT monomer. Protein coated substrates were prepared by depositing collagen ( $0.1\text{ mg}\cdot\text{ml}^{-1}$ ) or gelatin ( $2\mu\text{g}\cdot\text{mL}^{-1}$ ) on top of PEDOT(TOS) and incubating for 1 hour at  $37^{\circ}\text{C}$ .

### 3.2.3 Results and Discussion

#### 3.2.3.1 Experiment 1: Observation of BBECs Morphology

In this first experiment, we observed the morphology of BBECs cultured on well coated gelatin using light microscope and BBECs cultured on filter coated gelatin using SEM.

On wells, a light microscopy observation show a confluent monolayer. In this case, cells are spread out, and elongated (Figure 3.1).

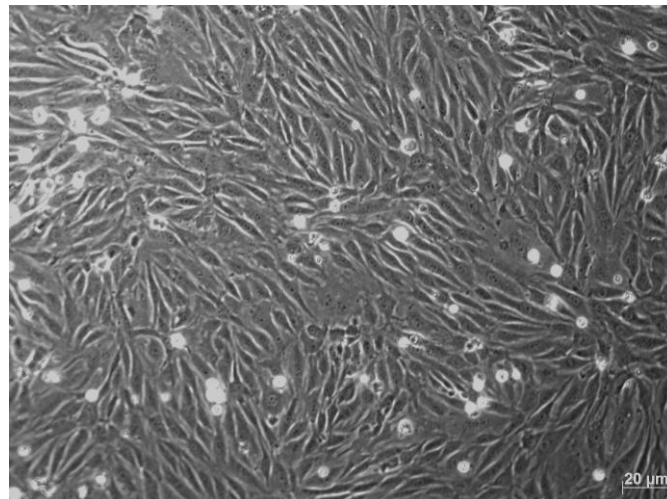


**Figure 3.1:** Light microscope image of BBECs on well coated with gelatin.

The observation of cells by the light microscope on filter cannot be performed because of the high scattering of the light by the filters. Cells cultured on porous polyethylene terephthalate (PET) membrane need to be fixed and stained for observation with microscope. To determine the morphology of cells on filters, we carried out an SEM experiment.

The SEM results show that BBECs retain typical endothelial characteristic such as cobblestone morphology. Like in the case on cells cultured on well, here cells formed a confluent monolayer (Figure 3.2).

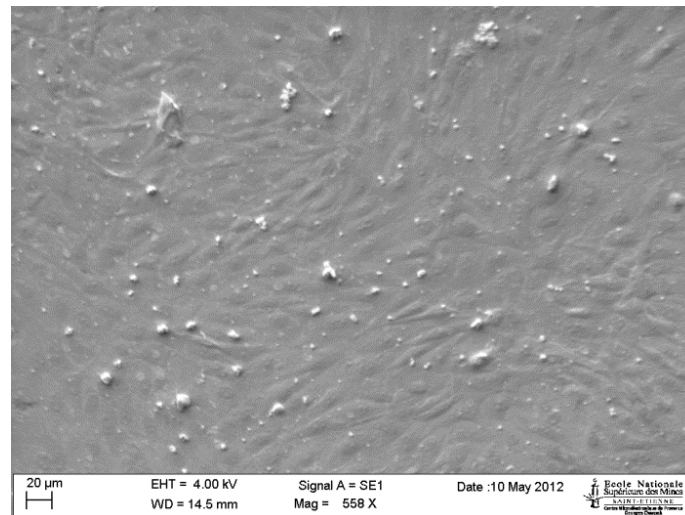


**Figure 3.2:** SEM of a confluent monolayer of BBECs on filter coated with gelatin.

### 3.2.3.2 Experiment 2: Measurement Integrity of BBECs using Permeability Assays

In this experiment, we want to determine the permeability value of BBECs. BBECs were cultured at passage 5, in costar petri dish coated with gelatin, then seeded at passage 6, onto collagen coated 12-well filter with 0.4 µm pore size for 4 days (Table 3.1).

	Size	Coating	Seeding	Passage of cell	Media
<b>Step 1 Petri dish</b>	100 mm	Gelatin	450 µl	P5	HS CS 10% // FGF
<b>Step 2 Filter</b>	12 well // 0.4	Collagen	80 µl	P6	HS CS 10% et HS CS 2.5% // FGF

**Table 3.1:** Details of BBECs culture for experiment 1.

Table 3.2 shows the permeability's results for filters alone, filters coated with collagen and then when BBECs were growing on the filters.

CONDITION			
	FILTER N=1	FILTER + COLLAGEN N=1	FILTER + COLLAGEN + BBECs N=3
Pe ( $10^{-3}$ cm.min <sup>-1</sup> )	8.5	7.3	7.2

**Table 3.2:** Permeability of the BBECs culture for experiment 2.

The filter's permeability to LY is  $8.5 \cdot 10^{-3}$  cm.min<sup>-1</sup> without coating and  $7.3 \cdot 10^{-3}$  cm.min<sup>-1</sup> with collagen coating. These values are very close and suggest that collagen does not obstruct the filter. Also, we observed that the filter is totally non restrictive and does not disturb the assessment of barrier tissue integrity.

### 3.2.3.3 Experiment 3: Integrity of BBECs and Biocompatibility with PEDOT(TOS) Using Collagen Coating

In parallel, we wanted to investigate the possibility to grow BBECs directly on CPs for future integration with electronic devices.

In this experiment, BBECs were cultured at passage 5, in costar petri dishes coated with gelatin, then seeded at passage 6, onto 12-well collagen coated filter with 0.4  $\mu$ m pore size for 4 days (Table 3.3).

We compared BBECs on uncoated filters with filters coated with PEDOT(TOS). This formulation allows easy coating on filters and is explored further in chapter 4.

	Size	Coating	Seeding	Passage of cell	Media
<b>Step 1 Petri dish</b>	60 mm	Gelatin	300 $\mu$ l	P5	HS CS 10% // FGF
<b>Step 2 Filter</b>	12 well // 0.4	Collagen	80 $\mu$ l	P6	HS CS 10% et HS CS 2.5% // FGF

**Table 3.3:** Details of the BBECs culture for experiment 3.

To assess the biocompatibility of PEDOT(TOS) in contact with BBECs, collagen was coated on top of PEDOT(TOS) into filter. Table 3.4 summarizes the results of permeability and TER of each condition.

	CONDITION						
	FILTER N=1	FILTER + COLLAGEN N=1	FILTER + PEDOT: TOS N=1	FILTER + COLLAGEN + PEDOT: TOS N=1	FILTER + COLLAGEN + BBECs N=3	FILTER + COLLAGEN + PEDOT: TOS + BBECs N=3	FILTER + PEDOT: TOS + BBECs N=3
Pe ( $10^{-3}$ cm.min $^{-1}$ )	6.0	7.7	4.0	2.0	21.0 $\pm$ 14.6	1.0 $\pm$ 0.3	2.4 $\pm$ 33.3
TER ( $\Omega$ .cm $^2$ )	22.6	23.0	20.0	17.3	27.0	13.2	19.3

**Table 3.4:** Permeability and TER results of the BBECs culture for experiment 3.

For permeability assays, the presence of PEDOT(TOS) does not change the permeability of filter alone, the value changes from  $6.10^{-3}$  cm.min $^{-1}$  to  $4.10^{-3}$  cm.min $^{-1}$ . This value demonstrates that PEDOT(TOS) cover the filters and makes it impermeable to the passage of LY molecules. The permeability of BBECs on collagen coated filter is still really high and the standard variation too (Table 4). In contrast, the TER of controls are respectively  $22.6 \Omega$ .cm $^2$  for filter,  $23 \Omega$ .cm $^2$  for collagen coated filter and  $20 \Omega$ .cm $^2$  for collagen on top of PEDOT(TOS) coated filter. These results demonstrate that the coating does not change the resistance of filter. TER of BBECs on collagen coated filter is a little bit higher ( $27 \Omega$ .cm $^2$ ), but still low for assessing barrier integrity.

### 3.2.3.4 Experiment 4: Integrity of BBECs and Biocompatibility with PEDOT(TOS) Using Gelatin Coating

In this experiment, to improve the integrity properties of BBECs, we decided not to change the coating of cells during the experiments from gelatin to collagen. We seed cells on gelatin coated filters to minimize changes in the cell environment and increased cell seeding to maximize cell contact (Table 3.5).

	Size	Coating	Seeding	Passage of cell	Media
<b>Step 1 Petri dish</b>	60 mm	Gelatin	300 $\mu$ l	P5	HS CS 10% // FGF
<b>Step 2 Filter</b>	12 well // 0.4	Gelatin	100 $\mu$ l	P6	HS CS 10% et HS CS 2.5% // FGF

**Table 3.5:** Details of the BBEC culture for experiment 4.

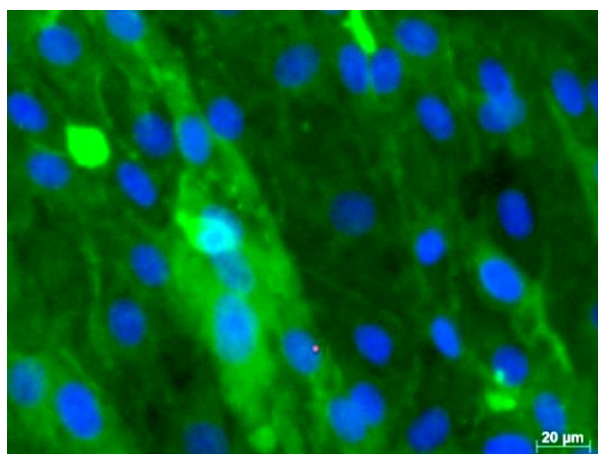
	CONDITION				
	FILTER N=1	FILTER + GELATIN N=1	FILTER + GELATIN + PEDOT: TOS N=1	FILTER + GELATIN + PEDOT: TOS + BBECs N=3	FILTER + GELATIN + BBECs N=3
Pe ( $10^{-3}$ cm.min <sup>-1</sup> )	8.5	7.8	1.0	0.2 $\pm$ 0.0	0.2 $\pm$ 0.1
TER ( $\Omega$ .cm <sup>2</sup> )	19.8	13.7	69.5	32.0	29.3

**Table 3.6:** Permeability and TER results of the BBECs culture for experiment 4.

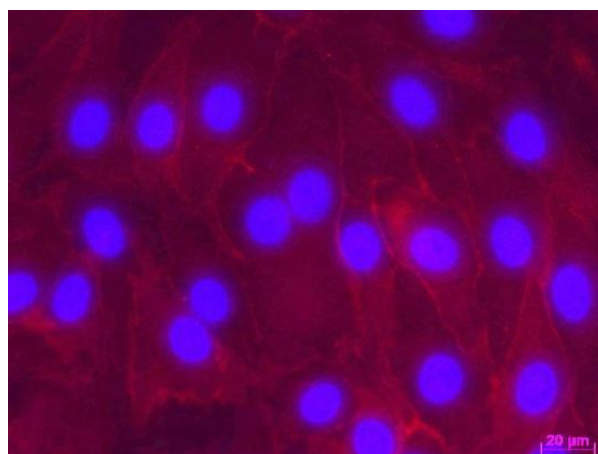
The permeability of BBECs on gelatin coated filter is  $0.2 \cdot 10^{-3}$  cm.min<sup>-1</sup> and the same as BBECs on gelatin on top of PEDOT(TOS) coated filter (Table 3.6). The TER values show that, the control PEDOT(TOS) coated filter is  $69.5 \Omega$ .cm<sup>2</sup>. The presence of PEDOT(TOS) modified the resistance of filters without cells. Further, when cells were added, the resistance was lower, around  $30 \Omega$ .cm<sup>2</sup> in presence of PEDOT(TOS) or not (Table 3.6).

Figure 3.3 shows the immunofluorescence staining of tight junction proteins carried out on BBECs using antibodies against ZO-1, occludin and claudin-1. Control staining of BBECs on gelatin coated filters shows the presence of ZO-1 protein only. There is no staining localization of occludin. However ZO-1 protein is localized on cell periphery. In case of BBECs on gelatin on top of PEDOT(TOS) coated filter, we can observe a nice monolayer but only ZO-1 is also localized.

a)



b)



**Figure 3.3:** Immunofluorescence staining of BBECs. (a). Immunofluorescence of BBECs on gelatin coated filter, stained with antibodies against apical junction proteins ZO-1 (green), occludin (red) and nucleus (blue). (b). Immunofluorescence of BBECs on gelatin on top of PEDOT(TOS) coated filter, stained with antibodies against apical junction proteins claudin-1 (green), ZO-1 (red) and nucleus (blue).

### 3.2.4 Conclusion

BBECs are very sensitive cells. We learned that it is better to grow this cell using a high seeding and a gelatin coating. The PEDOT (TOS) coating of filters shows promising results in term of biocompatibility with BBECs. By SEM, cells appear to form layers on filter, but we cannot take live images because of the refraction of filter on the microscope. The permeability results are high, and the resistance results indicate that BBECs are not forming correct barrier.

To integrate cells with electronic devices in the filter format, we need to get a tight barrier. Together, these conclusions lead us to discontinue the use these cells for our project, so we decided to switch to other model.

### 3.3 *In vitro* BBB Model Using Human Brain Microvascular Endothelial Cells (HBMEC)

#### 3.3.1 Generality on Human Brain Microvascular Endothelial Cells (HBMEC)

To increase awareness of the relevance and the necessity for human models in drug testing and diagnostic, we tried to develop a human cell model for BBB.

Human brain microvascular endothelial cells (HBMECs) were isolated from adult human brain microvessels. HBMECs establish the barrier by forming tight junctions between endothelial cells, limiting the diffusion of proteins, large molecules, and maintaining the stable ionic environment vital to the normal functioning of brain cells [4].

#### 3.3.2 Materials and Methods

**Cell Culture:** HBMEC were purchased from ScienceCell. HBMEC were seeded at  $5.10^4$  cells onto fibronectin coated ( $4 \mu\text{g}\cdot\text{cm}^{-2}$ ), 24 filter  $0.4 \mu\text{m}$  pore size (Millipore), to establish a BBB model. HBMEC were cultured in culture media (ECM, ScienceCell) supplemented with 5% fetal bovine serum, 1% penicillin/streptomycin solution, and 1% growth supplement (ECGS).

For the co-culture model, Human Astrocyte (HA, ScienceCell) were seeded at  $5.10^4$  cells into the poly-l-lysine coated well or filter ( $2 \mu\text{g}\cdot\text{cm}^{-2}$ ). The culture medium (AM) was supplemented with 5% fetal bovine serum, 1% penicillin/streptomycin solution, and 1% growth supplement (AGS). All cells were cultured in a humidified  $37^\circ\text{C}$  incubator with 5%  $\text{CO}_2$ . HA-conditioned medium was collected from confluent HA monolayers. Media was changed every 2 days.

Cortical Neurons (CN) from rat, were kindly donated by Dr. Noelle Callizot of the Neurosys company, Gardanne. These cells were seeded into well or filter at a density of  $3.10^4$  cells (24 plate or filter, Millipore). All well was coated with  $2 \mu\text{g}\cdot\text{cm}^{-2}$  poly-l-lysine (Sigma Aldrich) for 1 h at  $37^\circ\text{C}$ . CN were routinely maintained at  $37^\circ\text{C}$  in a humidified atmosphere of 5%  $\text{CO}_2$  in culture medium containing neurobasal medium (Invitrogen) supplemented with 2% B27 nutrient supplement (Invitrogen), 2 mM l-glutamine (Invitrogen), 1% of Penicillin-Streptomycin (Invitrogen) and 10 ng/ml of

Brain-Derived Neurotrophic Factor (BDNF, Invitrogen). Media was changed every 2 days.

**Permeability assay:** Lucifer yellow is added to the apical side of the membrane and the transport of the compound across the monolayer is monitored after 1 h incubation at 37 °C in a humidified CO<sub>2</sub> incubator. From the fluorescence, the Apparent Permeability (Papp) is obtained from the follow equation:

$$P_{app} = ((Flux \times V_{bas})/t) \times (1/C_0 \times A) \text{ and } Flux = 100 \times (LY_{bas} \times V_{bas}) / (LY_{api} \times V_{api})$$

Where LY<sub>bas</sub> and LY<sub>api</sub> are the concentration of Lucifer Yellow in the basal and apical sides of the hanging porous filter; V<sub>bas</sub> and V<sub>api</sub> are the volume of Lucifer Yellow in the basal and apical sides. The t is the time of incubation, A is the area of the filter and C<sub>0</sub> is the initial concentration in the donor compartment. When the P<sub>app</sub> < or = at 1.10<sup>-6</sup>cm/s, the cells are differentiated, mean that cells become a more specialized cell type.

**BBB *in vitro* model:** As mentioned in chapter 2, co-culture of BBB with HA and CN has been shown to increase brain endothelial cells properties. To monitor barrier integrity of *in vitro* model of BBB, three different models are tested (Figure 3.4). A contact co culture known to increase expression of TJ proteins, and P-glycoprotein (P-gp) on the endothelial cells is used [5]. The HA or CN are cultured onto the membrane underside for few hours in incubator. Then Brain endothelial cells are seeded in apical side of filter for cell-cell contact for the rest of experiment (Figure 3.5).

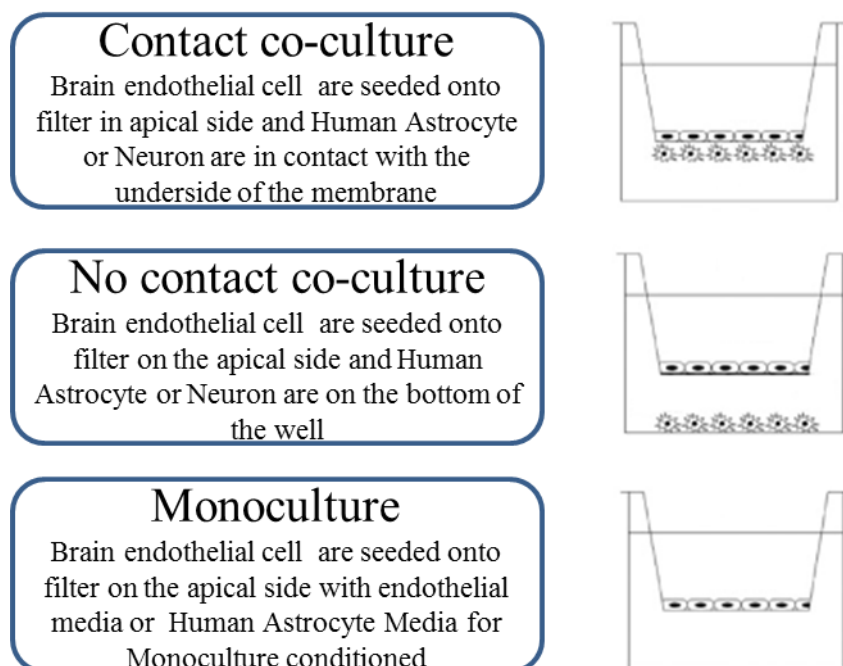


**Figure 3.4:** A scheme of the different *in vitro* BBB models proposed adapted from Journal of Neuroscience Methods, Hatherell K *et al.*, [6].

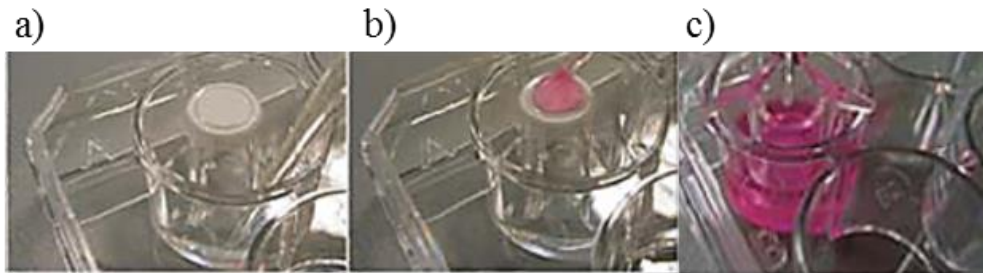


**Figure 3.5:** Cells cultured on the underside of the filter membrane. (a) 24well filter is upside down in 12 well plate containing water. (b) Cells are seeded onto the underside of the membrane for 2h in the incubator. (c) The filter is placed in 24 well plates for the rest of experiment.

A no contact co-culture model of endothelial cells and astrocytes or neuron was tested. The co culture format permits to increase TJ resistance between the endothelial cells compared to endothelial cells grown alone [7]. A monoculture is also used as a control; a simple model cultured with endothelial media and also with astrocyte conditioned media.

**CellZscope Measurements** were carried out as in section 3.2.2.

**Immunofluorescence of tight junction** was carried out as in section 3.2.2.

**Actin staining:** The cytoskeletal organization can be performed by the visualization of the actin cytoskeleton in cells. HBMEC were fixed with 4% formaldehyde in PBS at room temperature for 10 min and then permeabilized for 10 min with 0.1% Triton X-100 in PBS containing 1% BSA. The cells were then incubated with rhodamine-phalloidine (Molecular Probes) for 30 min. After washing, cells were incubated for 5 min at room temperature with Fluoroshield with DAPI (Sigma Aldrich), then mounted and examined with a fluorescent microscope (AxioVision).

### 3.3.3 Results and Discussion

#### 3.3.3.1 Experiment 1: Immunofluorescence Time Course of HBMEC

In order to observe tight junction formation of HBMEC, immunofluorescence staining of ZO-1 and Claudin 5 proteins is done at day 2, 4 and 6. For this experiment, HBMEC were seeded ( $5 \cdot 10^4$  cell/well) on wells at passage 6. Figure 3.6 shows the formation and evolution of tight junctions.

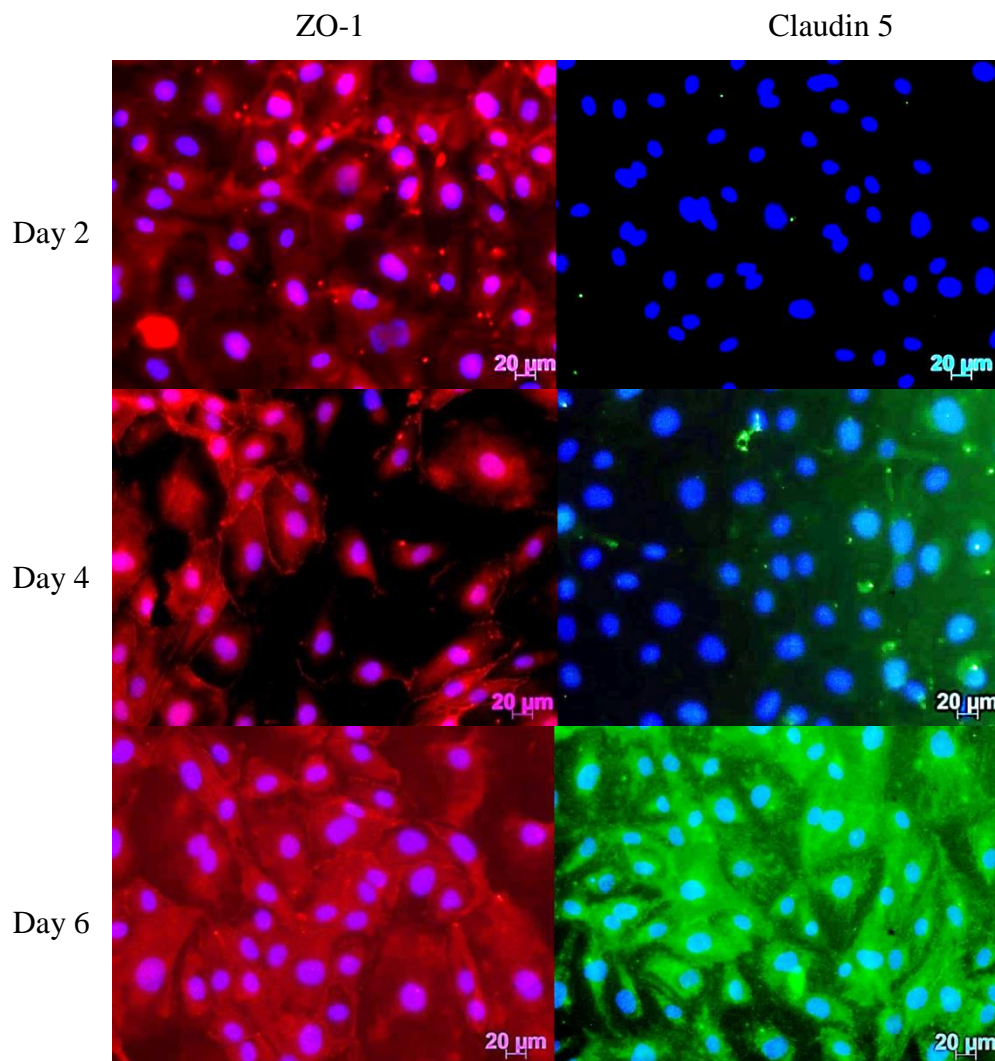


**Figure 3.6:** Immunofluorescence of HBMEC of ZO-1 (red) and claudin 5 proteins (green) at day 2, 4 and 6. Nucleus is stained with DAPI (blue).

At day 2, only ZO-1 is present on the periphery of the cell. At day 4, the presence of claudin 5 protein is observed but the intensity is low compared to ZO-1 on the same day. At day 6, both tight junction proteins are localized with high intensity in HBMEC.

### 3.3.3.2 Experiment 2: Integrity of Monoculture and Contact Co-culture of HBMEC

To establish an *in vitro* model of the BBB, HBMEC and HA were cultured as described in figure 3.7. For co-culture (3 samples are tested for each condition (N=3)) , HA at passage 1 (P1) were seeded ( $5 \cdot 10^4$  cells/filter) in the bottom of inversed 24 filters with  $0.4 \mu\text{m}$  pore size (Millipore), and left for 2h in incubator for adhesion. 2 or 4 days after, HBMEC at passage 5 (P5) were seeded ( $5 \cdot 10^4$  cells/filter) at into filter in apical side. This co-culture is a contact model: there is cell to cell contact between the HBMEC (on the filter) and the HA (on the bottom of the filter). For monoculture (N=3) only HBMEC were seeded with endothelial media on the filter.

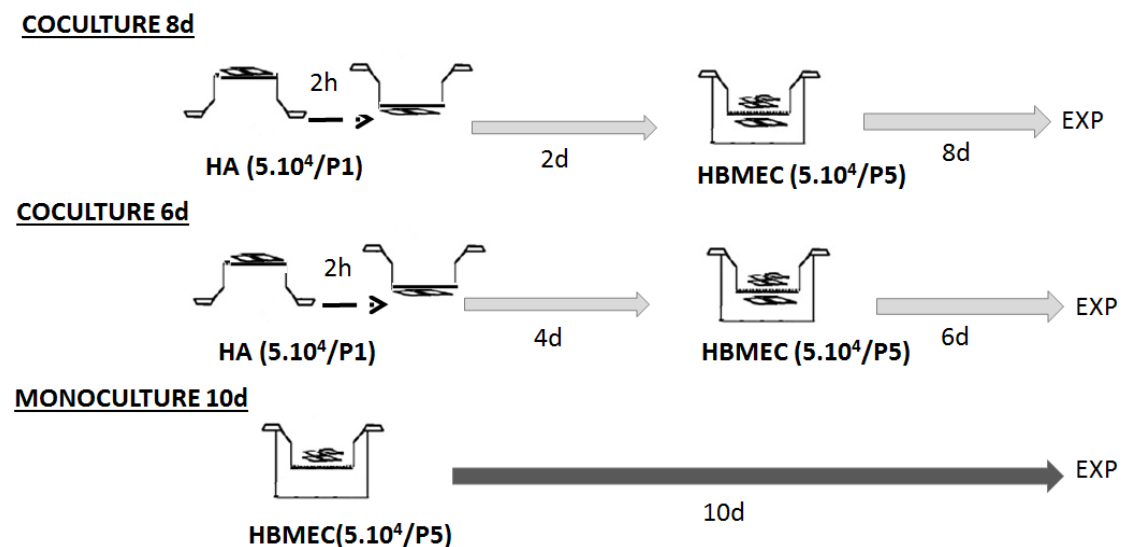
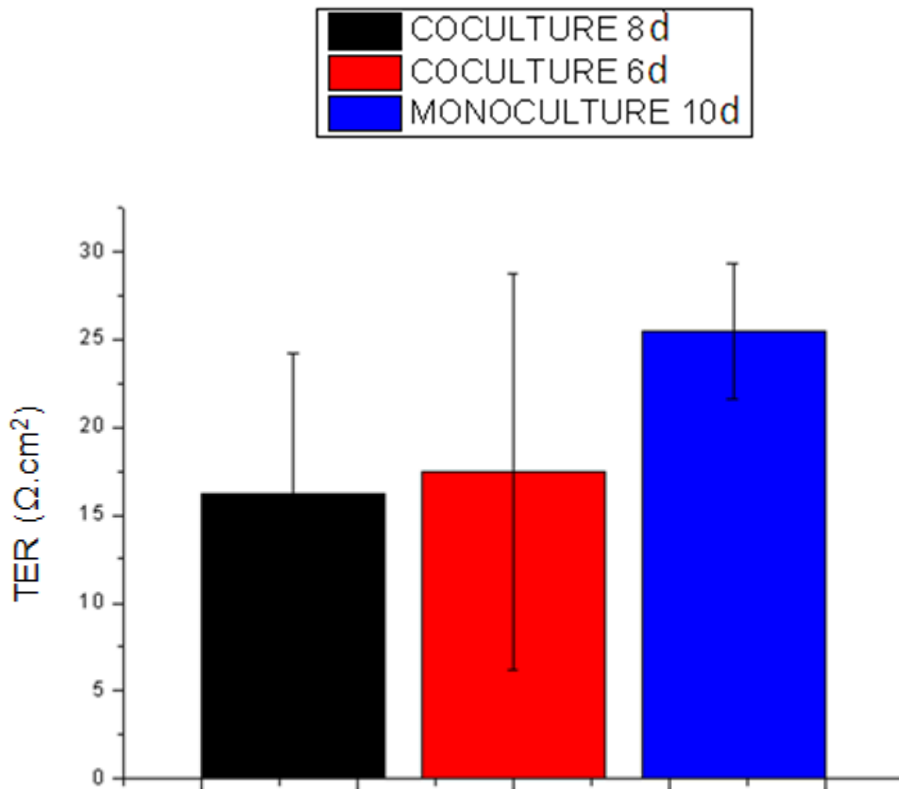


**Figure 3.7:** Schematic for the HBMEC experiment 2.

The TER of HBMEC is low, under  $30 \Omega \cdot \text{cm}^2$ . The maximal TER values measured with the CellZscope were obtained with the monoculture. But the differences of TER between the conditions are not significant. The presence of HA, 2 or 4 days before, in contact with HBMEC did not increase the resistance of the monolayer (Figure 3.8a). For the Papp, the results do not show any difference between the conditions (Figure 3.8b). The Papp of HBMEC is still close to filter alone (range of filter alone is  $10^{-4} \text{cm} \cdot \text{s}^{-1}$ , data not shown).

a)



b)

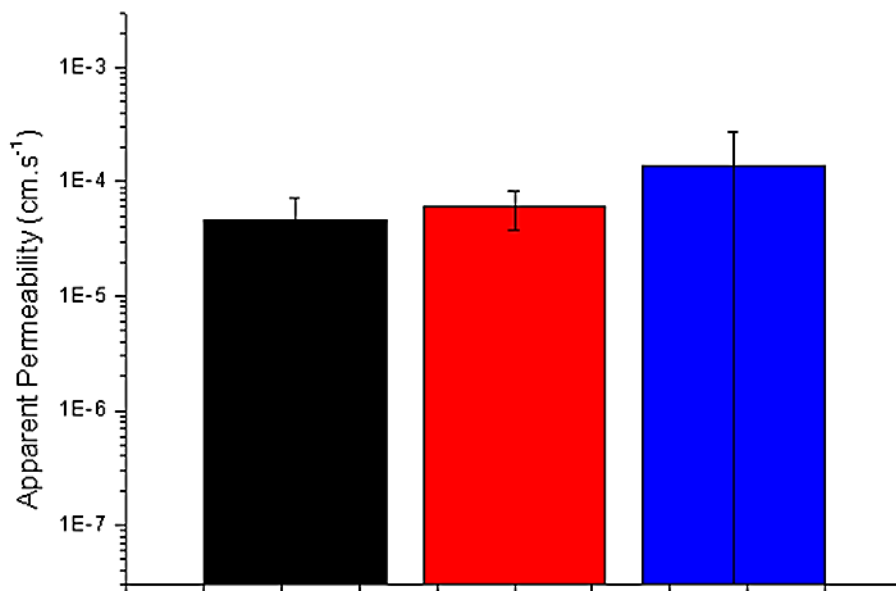


**Figure 3.8:** (a).TER recorded by the CellZscope system of contact co-culture at 8 days (black), contact co-culture at 6 days (red) and monoculture at 10 days (blue). (b). Apparent permeability of contact co-culture at 8 days (black), contact co-culture at 6 days (red) and monoculture at 10 days (blue).

### 3.3.3.3 Experiment 3: Integrity of Monoculture Conditioned, Contact and No Contact Co-culture of HBMEC

In this experiment (Figure 3.9), to get better results on barrier tightness, the seeding concentration were increased and the pore size of filter also in order to have better cell-cell contact. Further, a HA conditioned media is used to improve brain endothelial performance. The contact co-culture (N=3) is composed of HA at passage 2 (P2) seeded ( $2.10^5$ cells/filter) in the bottom of 24 filter with 8  $\mu$ m pore size (Millipore) and HBMEC at passage 9 (P9) seeded ( $2.10^5$ cells/filter) under the filter. The non contact co-culture (N=3) is composed with HA at passage 2 (P2) seeded ( $2.10^5$ cells/well) in the bottom of well and HBMEC at passage 9 (P9) seeded ( $2.10^5$ cells/filter) under the filter. The monoculture conditioned (N=3) is composed with HBMEC at passage 9 (P9) ( $2.10^5$ cells/filter) cultured in HA media on the basal side.

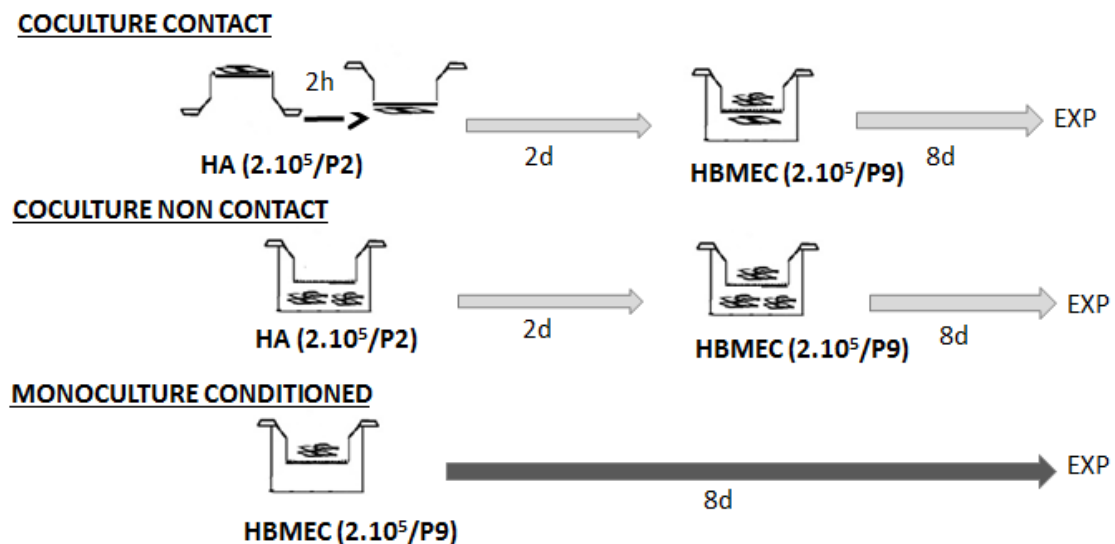


**Figure 3.9:** Schedule organization of the HBMEC experimentation 3.

Figure 3.10 show the results for TER (Figure 3.10a) and Papp (Figure 3.10b) of the experiment3. For the three conditions, the TER data is in the same range and still low, around  $15 \Omega \cdot \text{cm}^2$ . The Papp for each condition stayed in the range of  $10^{-4} \text{cm} \cdot \text{s}^{-1}$ , which confirmed that HBMEC are not differentiated in these three conditions.

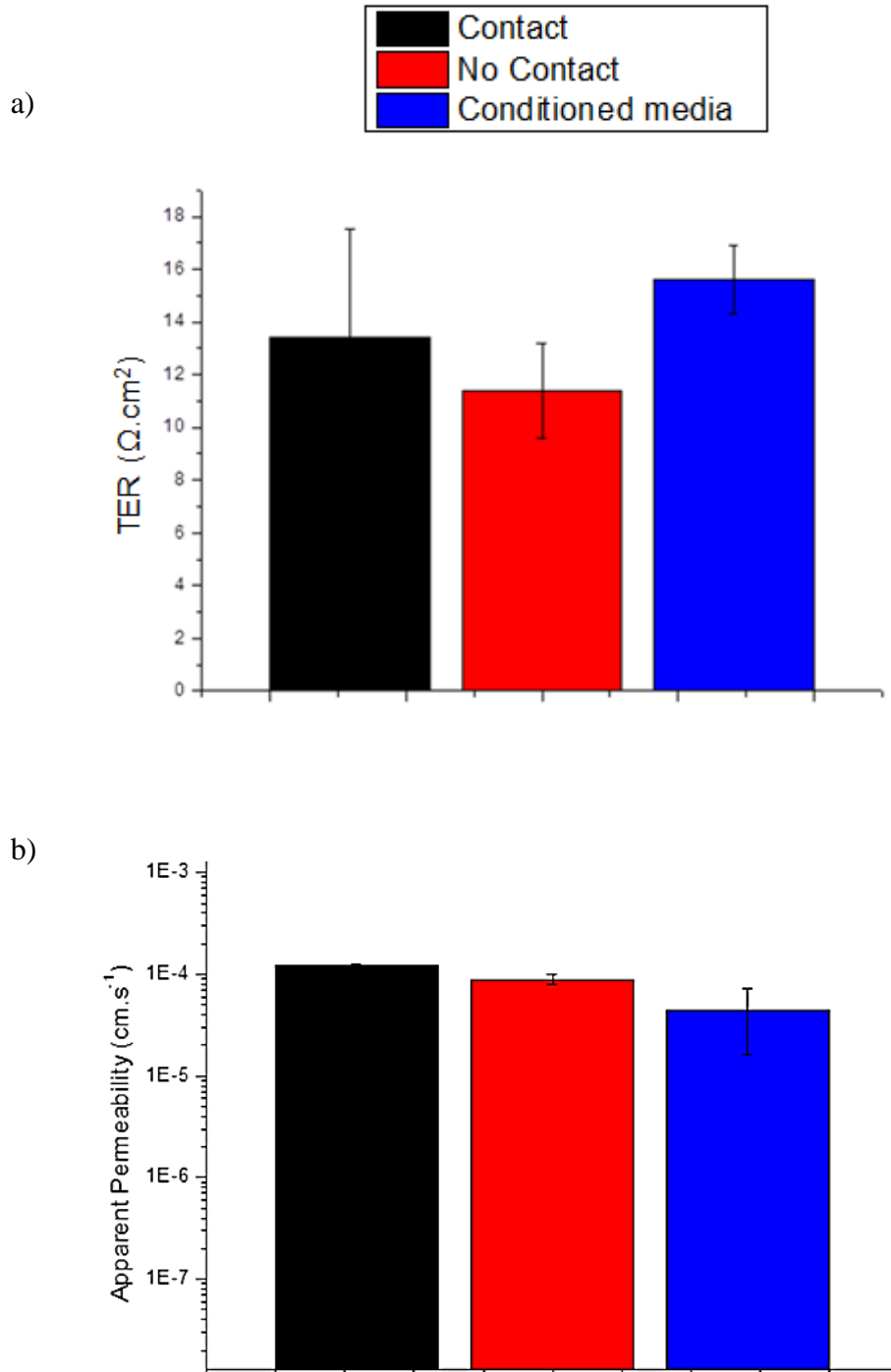


**Figure 3.10:** (a).TER recorded by the CellZscope system of contact co-culture at 8 days (black), no contact co-culture at 8 day (red) and monoculture conditioned at 8 days (blue). (b). Apparent permeability of contact co-culture at 8 days (black), no contact co-culture at 8 days (red) and monoculture conditioned at 8 days (blue).

Phalloidin staining of cells fixed on filter shows the distribution of cytoskeletal F-actin on HBMEC (Figure 3.11). The HBMEC on well (control) show stronger fluorescence in comparison with HBMEC on filter. In the control cells were spread out uniformly. Also, actin filaments are detectable as a network on control (Figure 3.11a). On filter, we can observe morphological alterations on monolayer with the presence of vacuole on the contact co-culture (Figure 3.11b), the non contact co-culture (Figure 3.11c) and the monoculture conditioned (Figure 3.11d).

The presence of these holes can explain the low TER and high permeability of HBMEC.

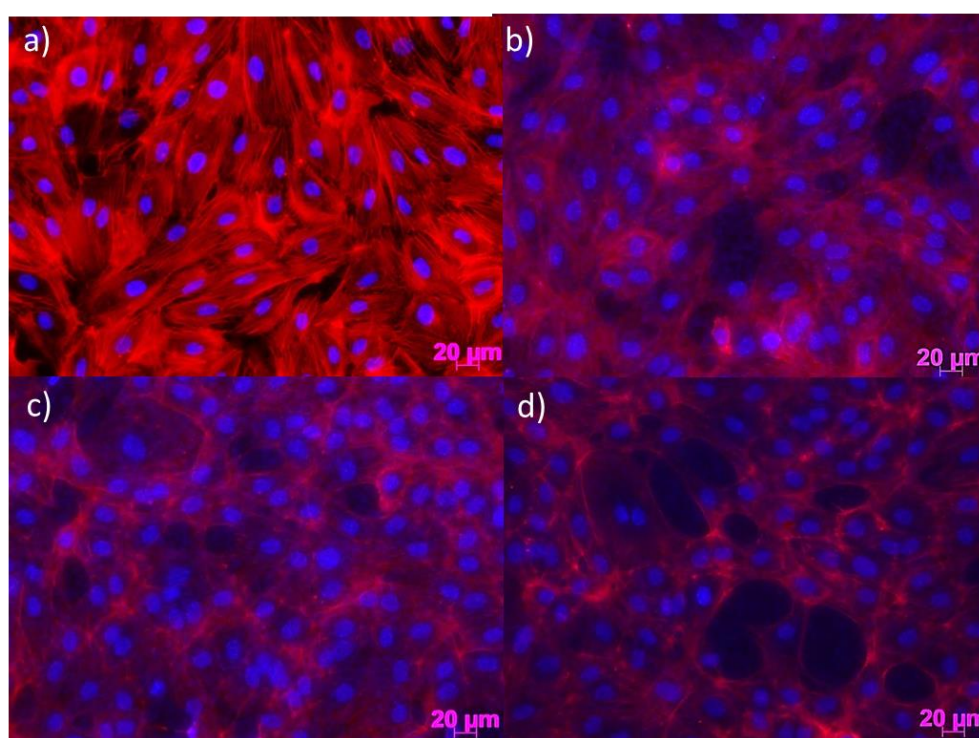


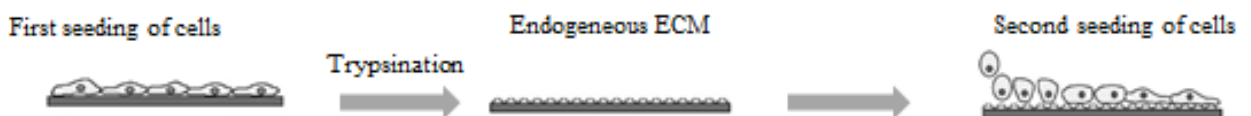
**Figure 3.11:** Actin staining by phalloidin examined by fluorescence microscopy. Nuclei were counterstained with DAPI. (a) Control of HBMEC cultured in monoculture in well. (b). HBMEC cultured in contact co-culture on filters. (c) HBMEC cultured in non contact co-culture on filters. (d). HBMEC cultured in monoculture with HA's conditioned media on filters.

### 3.3.3.4 Experiment 4: Impact of Endogenous Extracellular Matrix on the Integrity of Monoculture Conditioned, Contact and No Contact Co-culture of HBMEC.

In the previous experiment, we observed the presence of holes in HBMEC monolayer. We supposed that these holes appear by a lack of extra cellular matrix (ECM) on the filter. The ECM is known to have an impact on the barrier function of brain endothelial cells [8].

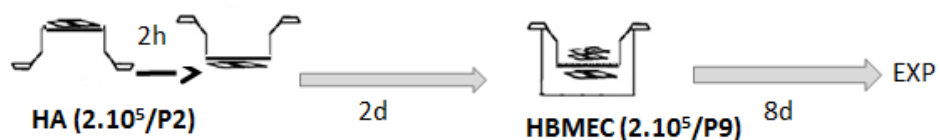
To assess the role of ECM on the integrity of HBMEC, cells were first seeded on fibronectin pre coated filters to promote adhesion by depositing endogenous extracellular matrix. Then cells are removed using trypsination (Figure 3.12a). Finally, a second seeding of cells was done and two conditions are tested: the contact co-culture and the monoculture conditioned media (Figure 3.12b). The contact co-culture (N=2) is composed with HA at passage 2 (P2) seeded ( $2 \cdot 10^5$  cells/filter) in the bottom of 24 filter with  $8 \mu\text{m}$  pore size (Millipore) and HBMEC at passage 9 (P9) seeded ( $2 \cdot 10^5$  cells/filter) under the filter. The monoculture conditioned (N=2) is composed with HBMEC at passage 9 (P9) seeded ( $2 \cdot 10^5$  cells/filter) in HA's media on the basal side.

a)

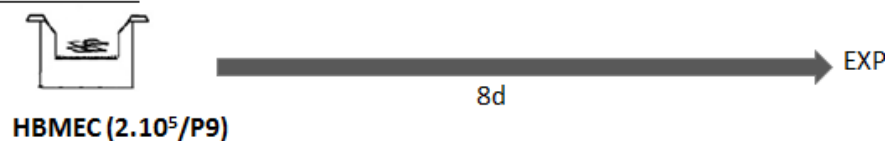


b)

#### COCULTURE CONTACT



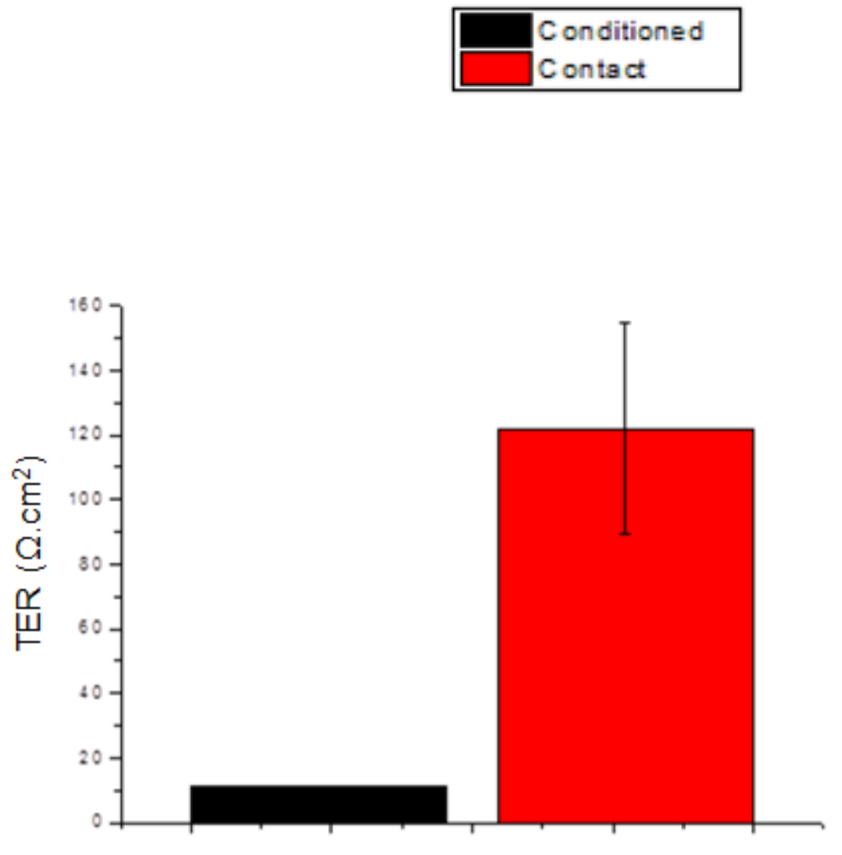
#### MONOCULTURE CONDITIONED



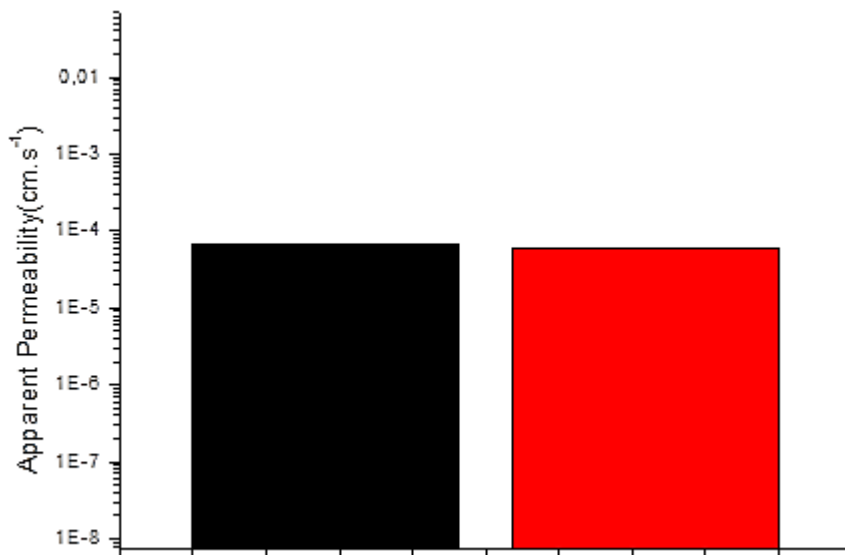
**Figure 3.12:** Schedule organization of the HBMEC experimentation 4. (a). Establishment of endogenous extracellular matrices derived from HBMEC and HA, adapted from experimental cell research, Hartmann C *et al.*, [8]. (b). Organization of the experiment.

Figure 3.13 provides the TER and Papp data recorded after deposition of endogenous extracellular matrix of monoculture conditioned and contact co-culture condition. For TER, we reported a significant difference on resistance between the two conditions. The monoculture conditioned model show a low TER around  $10 \Omega \cdot \text{cm}^2$  while the contact co-culture reveals a high TER around  $120 \Omega \cdot \text{cm}^2$ . The contact co-culture looks like a tighter model than the monoculture conditioned. The Papp data displayed a permeability around  $1 \cdot 10^{-4} \text{ cm} \cdot \text{s}^{-1}$  for both conditions.

a)



b)



**Figure 3.13:** (a).TER recorded after deposition of endogenous extracellular matrix by the CellZscope system of monoculture conditioned (black), and contact co-culture

(red). (b). Apparent permeability of monoculture conditioned (black), and contact co-culture (red).

The experiment suggests the importance of endogenous ECM on the resistance of HBMEC in contact with HA. Nevertheless, the TER and Papp results are not consistent, possibly due to issues related to a malfunctioning of some for the cellZscope electrodes. This experiment would need to be repeated for confirmation.

### 3.3.3.5 Experiment 5: Impact of Hydrocortisone on Integrity of Monoculture Conditioned, Contact and No Contact Co-culture of HBMEC

In this experiment, hydrocortisone, known to enforce the tightness of BBB, [9] was used to increase the integrity of HBMEC (Figure 3.14). The contact co-culture model (N=3) is composed with HA at passage 2 (P2) seeded ( $2 \cdot 10^5$  cells/filter) in the bottom of filter and HBMEC at passage 6 (P6) seeded ( $2 \cdot 10^5$  cells/filter) under the filter. The non contact co-culture (N=3) model is with HA at passage 2 (P2) seeded ( $2 \cdot 10^5$  cells/well) in the bottom of well and HBMEC at passage 6 (P6) seeded ( $2 \cdot 10^5$  cells/filter) under the filter. The monoculture conditioned (N=3) model is with HBMEC at passage 6 (P6) ( $2 \cdot 10^5$  cells/filter) cultured in HA's media on the basal side.

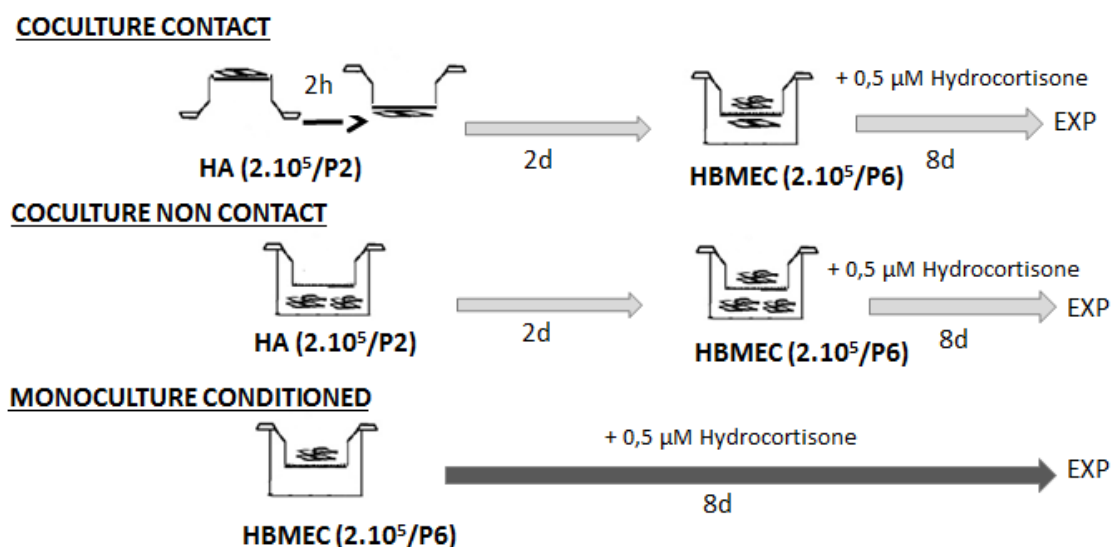


**Figure 3.14:** Details of the HBMEC experiment 5.

Addition of hydrocortisone did not change the resistance of the HBMEC except on the monoculture conditioned model where it changed slightly from 6 to 12  $\Omega \cdot \text{cm}^2$  (Figure 3.15a). But this TER value is still negligible compare to that measured *in vivo*. Papp show better data for the monoculture conditioned model with values between  $7 \cdot 10^{-4}$  and  $1 \cdot 10^{-5} \text{ cm} \cdot \text{s}^{-1}$  (Figure 3.15b).

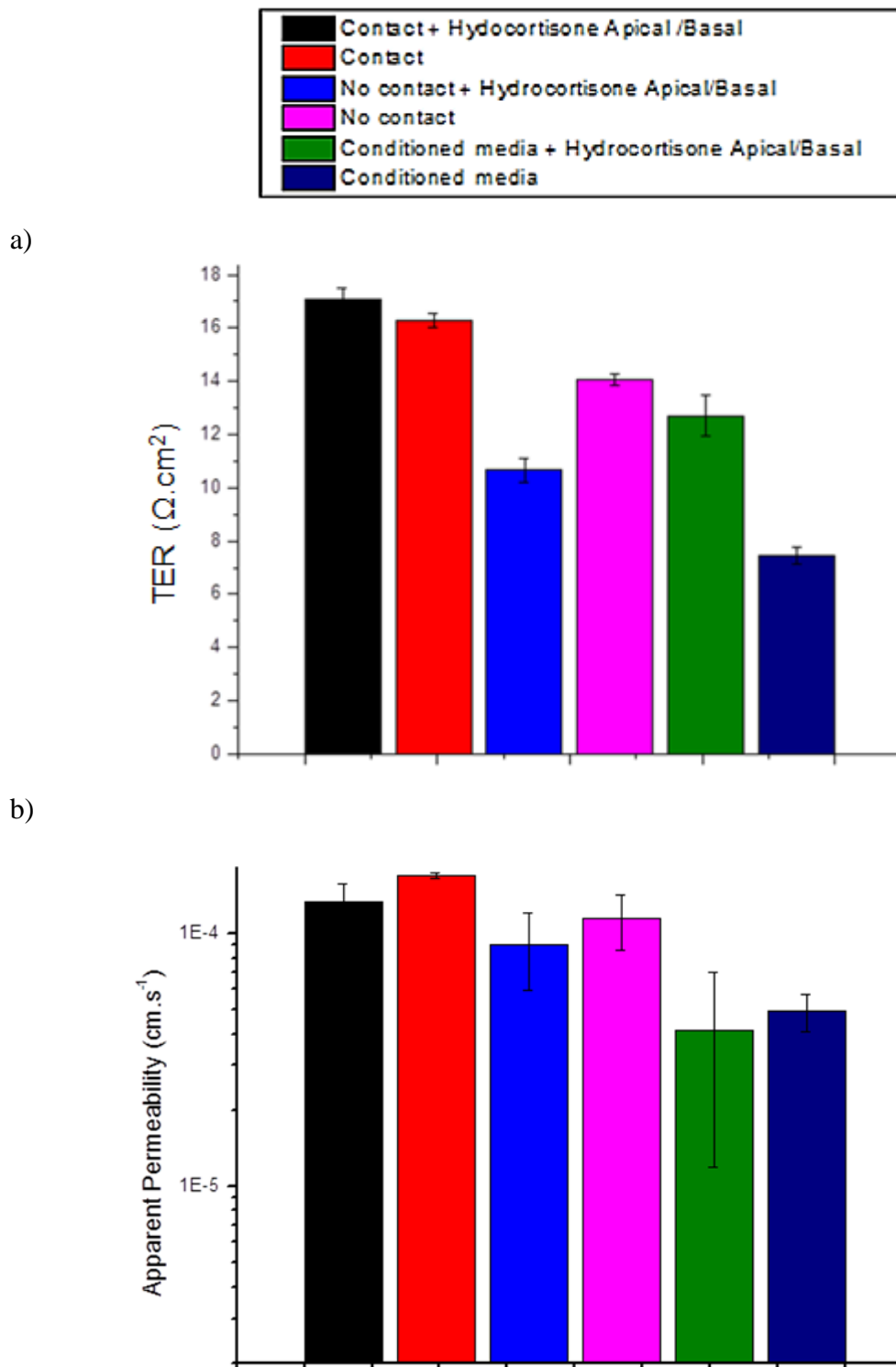


**Figure 3.15:** (a).TER recorded by the CellZscope system of contact co-culture supplemented with hydrocortisone at 8 days (black), contact co-culture at 8 days (red), no contact supplemented with hydrocortisone at 8 days (blue), no contact co-culture at 8 days (purple), monoculture conditioned supplemented with hydrocortisone at 8 days (green) and monoculture conditioned at 8 days (dark blue). (b). Apparent permeability of system of contact co-culture supplemented with hydrocortisone at 8 days (black), contact co-culture at 8 days (red), no contact supplemented with hydrocortisone at 8 days (blue), no contact co-culture at 8 days (purple), monoculture conditioned supplemented with hydrocortisone at 8 days (green) and monoculture conditioned at 8 day (dark blue).

### 3.3.4 Conclusion

HBMEC show promising results in contact or monoculture with conditioned media model. Also, the presence of endogeneous ECM seems to improve the integrity of the monolayer. However, this would need to be repeated in future experiments. A major problem however with this model is the high cost and their inconstancy after a limited number of passages. The filter format suggests the difficulty of cells to grow properly on porous membrane compare to planar substrate like well. Further investigation is needed to validate the HBMEC cell line for a human *in vitro* BBB model in terms of barrier tightness and paracellular permeability in order to integrate it with electronic devices.

## 3.4 *In vitro* BBB Model Using Immortalized Human Cerebral Microvascular Endothelial Cells (hCMEC/D3)

### 3.4.1 Generality on Immortalized Human Cerebral Microvascular Endothelial Cell (hCMEC/D3)

The immortalized human cerebral microvascular endothelial cell line hCMEC/D3 presents a more stable phenotype than primary human brain microvascular endothelial cells (HBMEC's) for use in constructing *in vitro* models of the BBB [10]. hCMEC/D3

were generated by transducing primary human endothelial cells with lentiviral vectors incorporating human telomerase and SV40-LT [11]. These cells have shown promising results in term of integrity even in absence of co-culture with glial cells, and can be constitute a valuable *in vitro* model of human BBB [12].

### 3.4.2 Materials and Methods

**Cell Culture:** hCMEC/D3 cells were a gift from Dr. Pierre-Olivier Couraud of the Institut Cochin, INSERM, Paris. The hCMEC/D3 cells used for the experiments were between passage 26 and 28. All culture was coated with rat-tail collagen type I solution at a concentration of 0.1 mg.ml<sup>-1</sup> into 24 filter 0.8 µm pore size (Millipore), and was incubated for 1 h at 37°C. hCMEC/D3 grown in endothelial basal medium-2 (EBM-2; Lonza Group Ltd., UK) supplemented with 1 ng.ml<sup>-1</sup> bFGF (Sigma Aldrich), 5% FCS (Invitrogen), 1.4 µM hydrocortisonee (Sigma Aldrich), 5µg.ml<sup>-1</sup> Acid ascorbic (Sigma Aldrich), 1/100 Chemically Defined Lipid concentrate (Invitrogen), 10 mM HEPES (Sigma Aldrich), and 1% penicillin-streptomycin (Invitrogen). Cells were cultured in an incubator at 37°C in a humidified atmosphere of 5% CO<sub>2</sub>. Cell culture medium was changed every 2 days.

Human Astrocyte (HA, ScienceCell) and Cortical Neurons (CN, Neurosys) were carried out as in section 3.3.2

**Permeability assay** was carried out as in section 3.3.2.

**CellZscope Measurements** were carried out as in section 3.2.2.

**Immunofluorescence of tight junction** was carried out as in section 3.2.2.

**Actin staining** was carried out as in section 3.3.2.

### 3.4.3 Results and Discussion

#### 3.4.3.1 Experiment 1: Immunofluorescence Time Course of hCMEC/D3

For this experiment, hCMEC/D3 cells were seeded ( $5 \cdot 10^4$  cells/well) on wells at passage 26. The time course of immunofluorescence of ZO-1 and Claudin 5 proteins at day 2, 4 and 6 of hCMEC/D3 cells show that the ZO-1 protein is found in early stages at day 2 (Figure 3.16). The protein is well staining localized on cells and shows a uniform presence on the confluent monolayer at day 6. For the claudin 5 protein formation on hCMEC/D3 cells, we observed that this protein is formed at later stages. At day 4, we saw a diffuse claudin 5 localization with occasional punctate staining. Finally at day 6, a well localization of claudin 5 is observed, but the organization of this protein is not homogeneous.

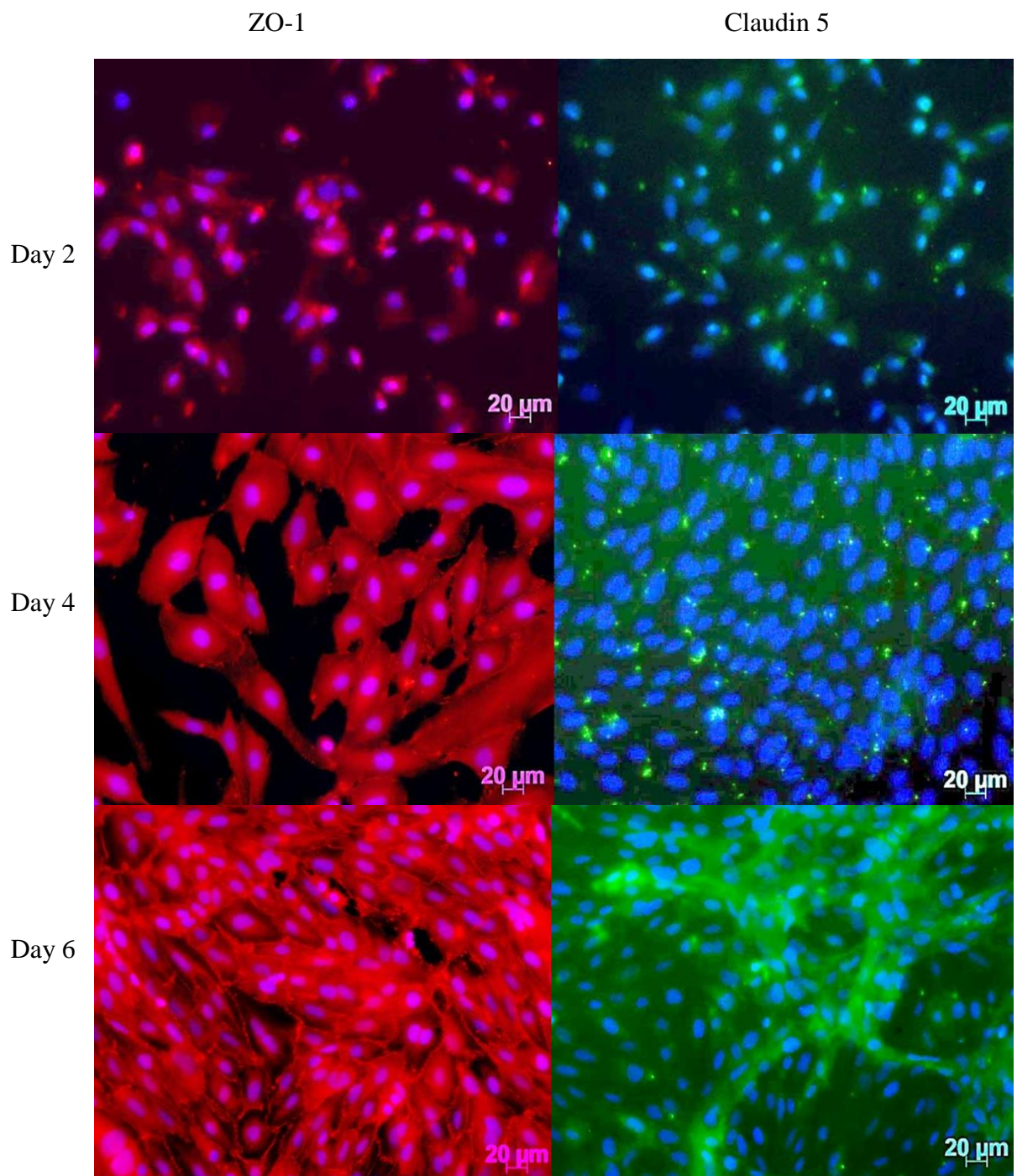


**Figure 3.16:** Immunofluorescence of hCMEC/D3 of ZO-1 (red) and claudin 5 proteins (green) at day 2, 4 and 6.

The immunofluorescence time course experiment allowed confirmation that from the day 6 cells possess the important protein for BBB integrity. Therefore, we considered it optimal to measure the integrity of the barrier after day 6.

### 3.4.3.2 Experiment 2: Integrity of Monoculture Conditioned, Contact and No Contact Co-culture of hCMEC/D3

In this experiment, hCMEC/D3 is cultured in contact co-culture and non contact co-culture with HA and in monoculture with conditioned HA media (Figure 3.17). The contact co-culture (N=3) is composed with HA at passage 3 (P3) seeded ( $2.10^5$  cells/filter) in the bottom of 24 filter,  $8\mu\text{m}$  pore size (Millipore) and hCMEC/D3 at passage 26 (P26) seeded ( $2.10^5$  cells/filter) under the filter. The non contact co-culture (N=3) is composed with HA at passage 3 (P3) seeded ( $2.10^5$  cells/well) in the bottom of well and hCMEC/D3 at passage 26 (P26) seeded ( $2.10^5$  cells/filter) under the filter. The monoculture conditioned (N=3) is composed with hCMEC/D3 at passage 26 (P26) ( $2.10^5$  cells/filter) cultured in HA's media on the basal side.

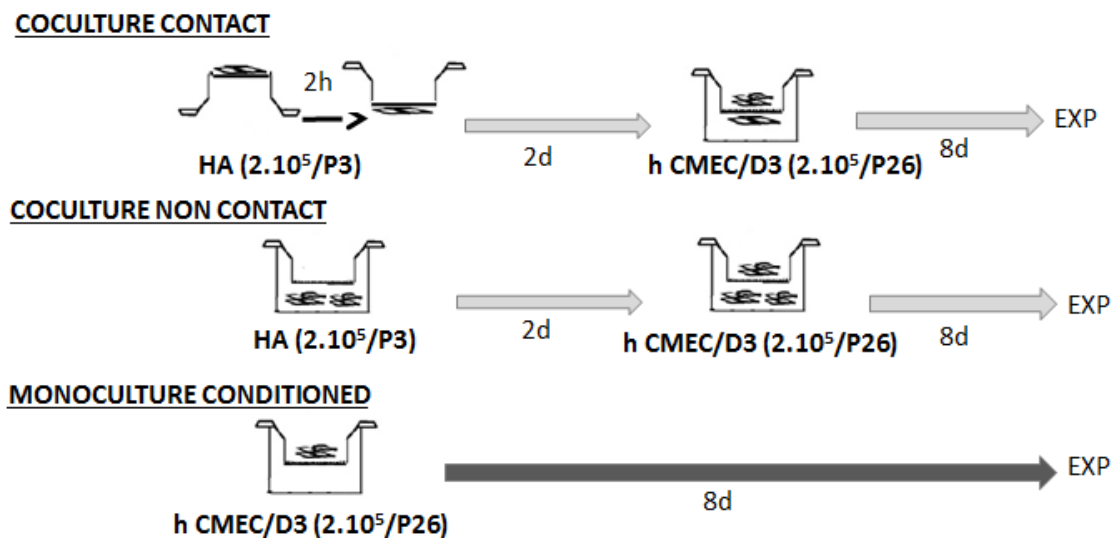


**Figure 3.17:** Details of the hCMEC/D3 experiment 2.

hCMEC/D3 cells have a higher TER results ( $20 \Omega \cdot \text{cm}^2$ ) than HBMEC ( $13 \Omega \cdot \text{cm}^2$ ). Contact and monoculture conditioned show the higher resistance (Figure 3.18a) around  $30 \Omega \cdot \text{cm}^2$  whereas the non contact model display a lower resistance at  $20 \Omega \cdot \text{cm}^2$ . The Papp results (Figure 3.18b) demonstrated that all model are not differentiated, the value for the three conditions stay approximately at  $10^{-4} \text{ cm} \cdot \text{s}^{-1}$ .

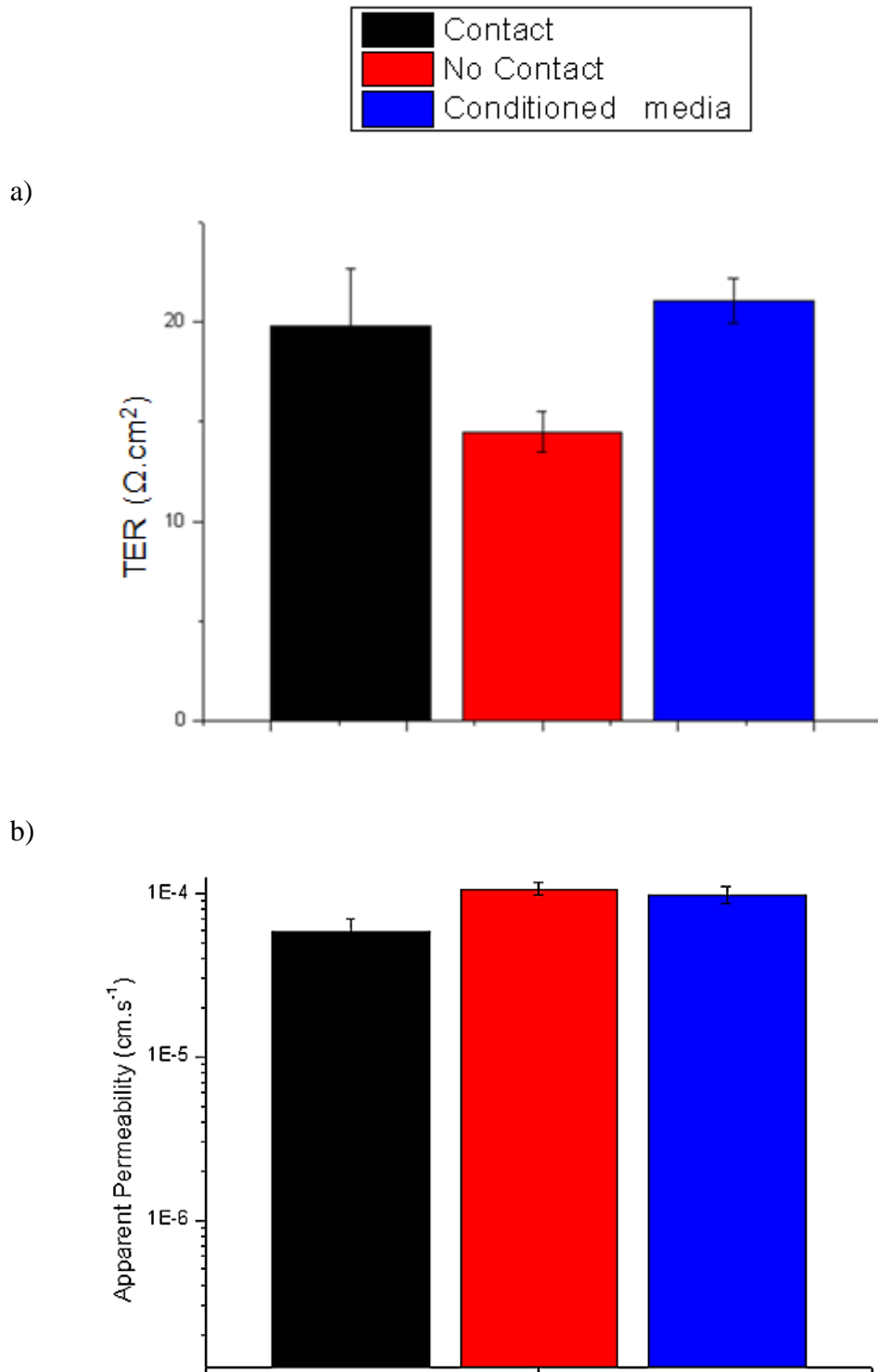


**Figure 3.18:** (a).TER recorded by the CellZscope system of contact co-culture at 8 days (black), no contact co-culture at 8 days (red) and monoculture conditioned at 8 days (blue). (b). Apparent permeability of contact co-culture at 8 days (black), no contact co-culture at 8 days (red) and monoculture conditioned at 8 days (blue).

Figure 3.19 demonstrate the organization of cytoskeleton of cells. In the contact model, hCMEC/D3 actin form a homogeneous network, we can observe a monolayer with hole and constituted of elongated cells. Whereas in the non contact model, a disorganization of hCMEC/D3 cells is detected. Cells are round and do not form a confluent monolayer. The monoculture cultured with conditioned HA media show elongated cells but the actin staining do not form a homogeneous monolayer.

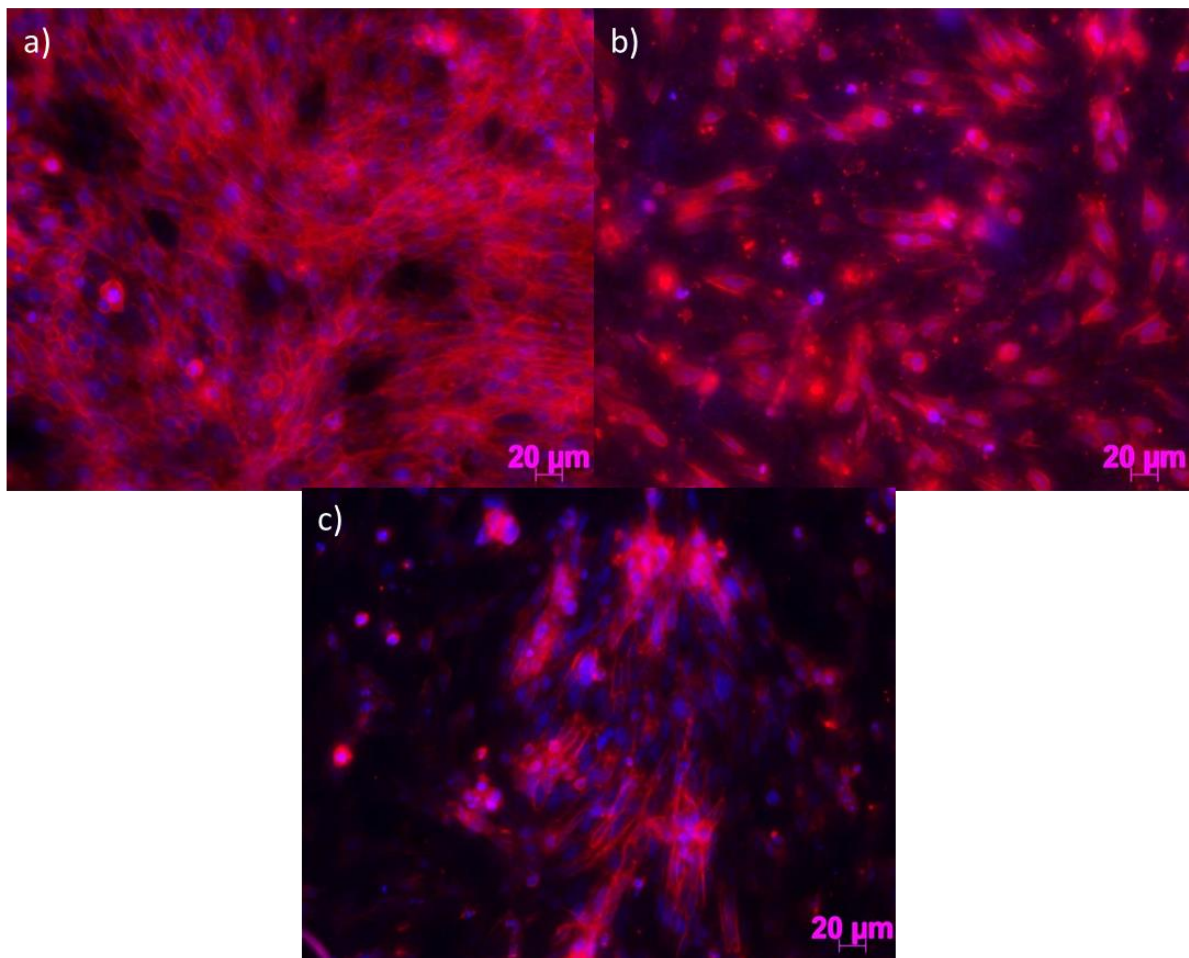


**Figure 3.19:** Actin staining by phalloidin examined by fluorescence microscopy. Nuclei were counterstained with DAPI. (a). hCMEC/D3 cultured in contact co-culture. (b) hCMEC/D3 cultured in non contact co-culture. (c). hCMEC/D3 cultured in monoculture with HA's conditioned media.

### .3.4.3.3 Experiment 3: Impact of Neuron on Integrity of Monoculture Conditioned, Contact and No Contact Co-culture of hCMEC/D3

To improve results on barrier tightness, we decided to culture hCMEC/D3 with HA and CN (Figure 3.20). Neurons have recently shown promising results in presence of brain endothelial cell by increasing the resistance of these cells [13]. For this experiment, the contact co-culture (N=3) is composed with HA/CN at passage 2 (P2) seeded ( $2.10^5$ cells/filter /  $3.10^5$ cells/filter) in the bottom of 24 filter with 8  $\mu$ m pore size (Millipore) or CN and hCMEC/D3 at passage 27 (P27) seeded ( $2.10^5$ cells/filter) under the filter. The non contact co-culture (N=3) is composed with HA/CN at passage 2 (P2) seeded ( $2.10^5$ cells/well /  $3.10^5$ cells/well) in the bottom of well and hCMEC/D3 at passage 27 (P27) seeded ( $2.10^5$ cells/filter) under the filter. The monoculture conditioned (N=3) is composed with hCMEC/D3 at passage 27 (P27) ( $2.10^5$ cells/filter) cultured in HA's media on the basal side.

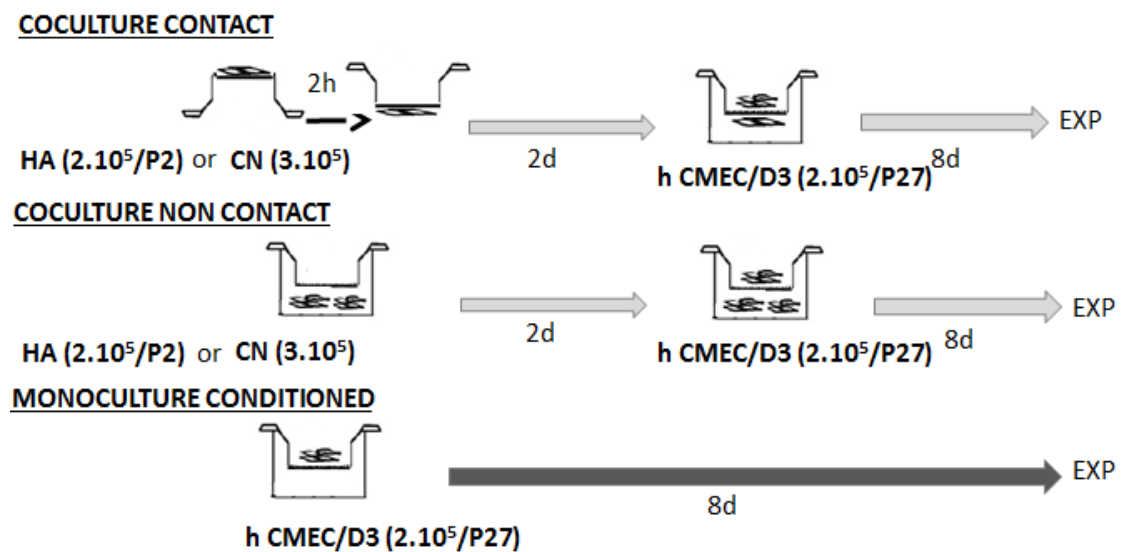


**Figure 3.20:** Details organization of the hCMEC/D3 experimentation 3.

In this experiment, global TER results were lower. However, a slight increase was seen. The TER of contact co-culture with HA, no contact with CN and monoculture conditioned HA media show results around 15  $\Omega \cdot \text{cm}^2$  (Figure 3.21a). The Papp results reveal a good permeability for the no contact with CN model compare to the other model (Figure 3.21b). The presence of neuron seems to modify cell differentiation.

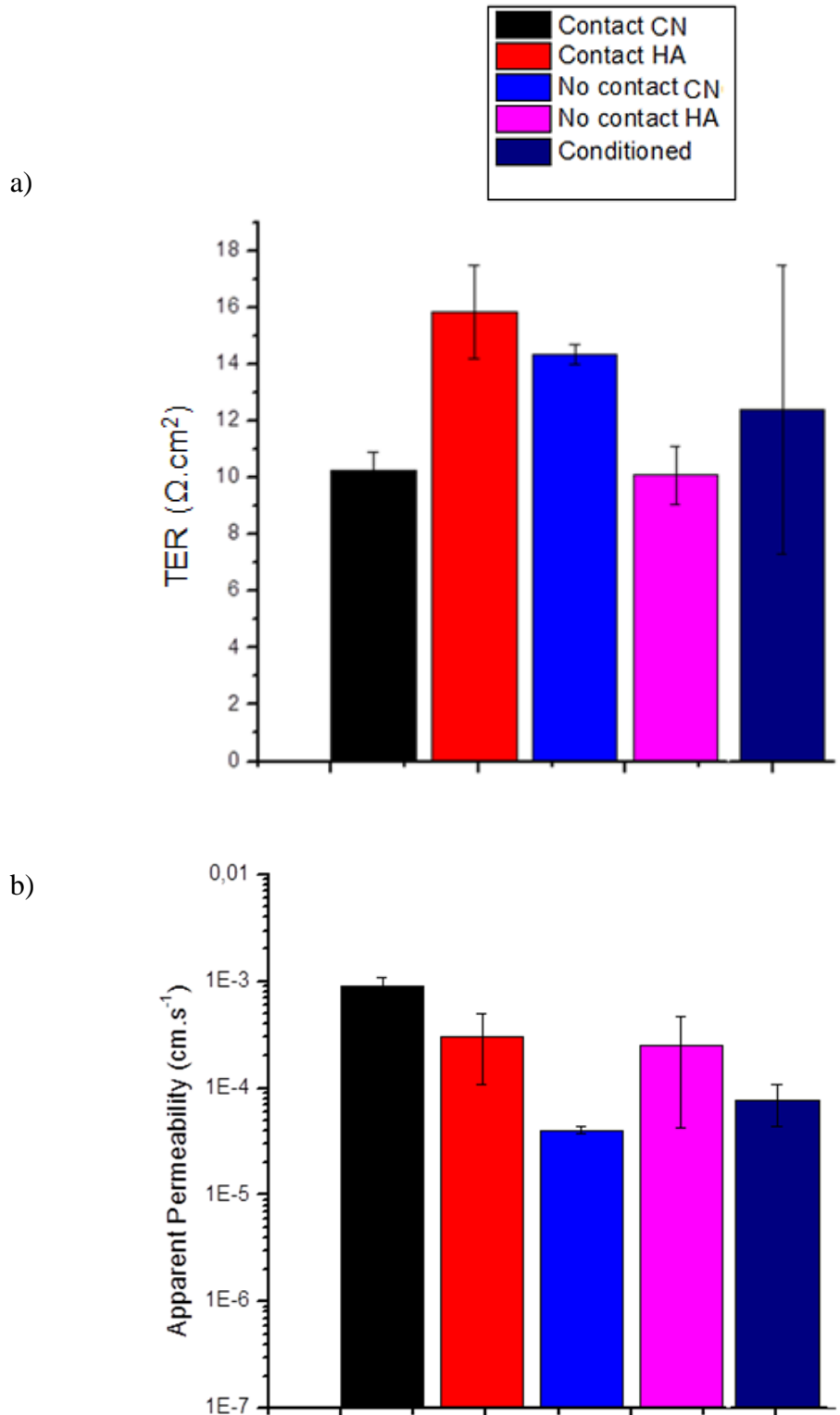


**Figure 3.21:** (a).TER recorded by the CellZscope system of contact co-culture with CN (black), contact co-culture with CN (red), no contact co-culture with CN (blue), no contact co-culture with HA (purple) and monoculture conditioned HA media (dark blue). (b). Apparent permeability of contact co-culture with CN (black), contact co-culture with CN (red), no contact co-culture with CN (blue), no contact co-culture with HA (purple) and monoculture conditioned HA media (dark blue).

### 3.4.4 Conclusion

Compared to HBMEC, the h CMEC/D3 cells seem to be a tighter barrier (Table 3.7). hCMEC/D3 cell line show encouraging results co-cultured with HA or CN and in monoculture with HA conditioned media. Although to increase the tightness and the barrier properties, the filter format appears not to be the better configuration for studying human BBB function.

		CONDITION		
		Contact with HA	Non contact with HA	Monoculture with HA conditioned media
TER ( $\Omega \cdot \text{cm}^2$ )	HBMEC	13	11	15
	h CMEC/D3	20	15	22
Papp ( $\text{cm} \cdot \text{s}^{-1}$ )	HBMEC	$1 \cdot 10^{-4}$	$8 \cdot 10^{-5}$	$4 \cdot 10^{-5}$
	h CMEC/D3	$5 \cdot 10^{-5}$	$1 \cdot 10^{-4}$	$8 \cdot 10^{-5}$

**Table 3.7:** Summarize TER and Papp data obtained on *in vitro* BBB model.

## 3.5 Integration of hCMEC/D3 with OECT

### 3.5.1 Materials and Methods

**OECT Measurement:** PEDOT:PSS (Heraeus, Clevios PH 1000) was used as the conducting polymer. Ethylene glycol (Sigma Aldrich) was added in a volume ratio of 1:4 (ethylene glycol to PEDOT:PSS) to increase conductivity. Dodecylbenzenesulfonic acid (DBSA) ( $0.5 \mu\text{L} \cdot \text{mL}^{-1}$ ) was added as a surfactant to improve film formation, and 3-glycidoxypropyltrimethoxysilane (GOPS) ( $10 \text{ mg} \cdot \text{mL}^{-1}$ ) was added as a cross-linker to improve film stability. Thermally evaporated gold

source and drain contacts were defined via lift-off lithography. Channel dimensions were patterned using a parylene peel-off technique, resulting in a channel active area width and length of 100  $\mu\text{m}$  and 10  $\mu\text{m}$ , respectively. Following PEDOT: PSS deposition, devices were baked for 1 h at 140  $^{\circ}\text{C}$  in atmospheric conditions. For electronic measurements; an Ag/AgCl was used as the gate electrode. All measurements were made using a National Instruments (NI) PXIe-1062Q system with a NI PXI-4071 Digital MultiMeter (DMM) for the AC current measurement. Cell media was used as the electrolyte. Measurements were performed at ambient temperature.

**Cell Culture of hCMEC/D3** was carried out as in section 3.4.2.

### 3.5.2 Results and Discussion of Integrity of hCMEC/D3 Using OECT Measurement

From all three models tested, the hCMEC/D3 model seems the best, so we decided to test it with the OECT. A no contact co-culture of hCMEC/D3 cells with CN was used. In this case, CN were cultured ( $3 \cdot 10^5$  cells/well) in the bottom well, and hCMEC/D3 at passage 28 (P28) are seeded ( $2 \cdot 10^5$  cells/filter) on the 24 filter 8  $\mu\text{m}$  pore size (Millipore) 24 hours after for 8 days. The measurement was first performed on filter without cells, then with hCMEC/D3 non contact co-culture with CN. A scratch on filter with cells was done at the end, to mechanically destroy the monolayer.

Figure 3.22 show the results of OECT transconductance response versus frequency. As described in chapter 1, transconductance is a key figure of merit for OECT and represents ratio between the drain current ( $I_{\text{DS}}$ ) divide by the gate voltage ( $V_{\text{g}}$ ). We noted, that there were no differences in the OECT behavior in presence of cells or not. hCMEC/D3 in filter format appears to be insufficiently sensitive to distinguish the barrier properties of hCMEC/D3. In agreement with the TER results obtained using the CellZscope, the BBB model appears to be non-functional with respect to blocking ion flow.

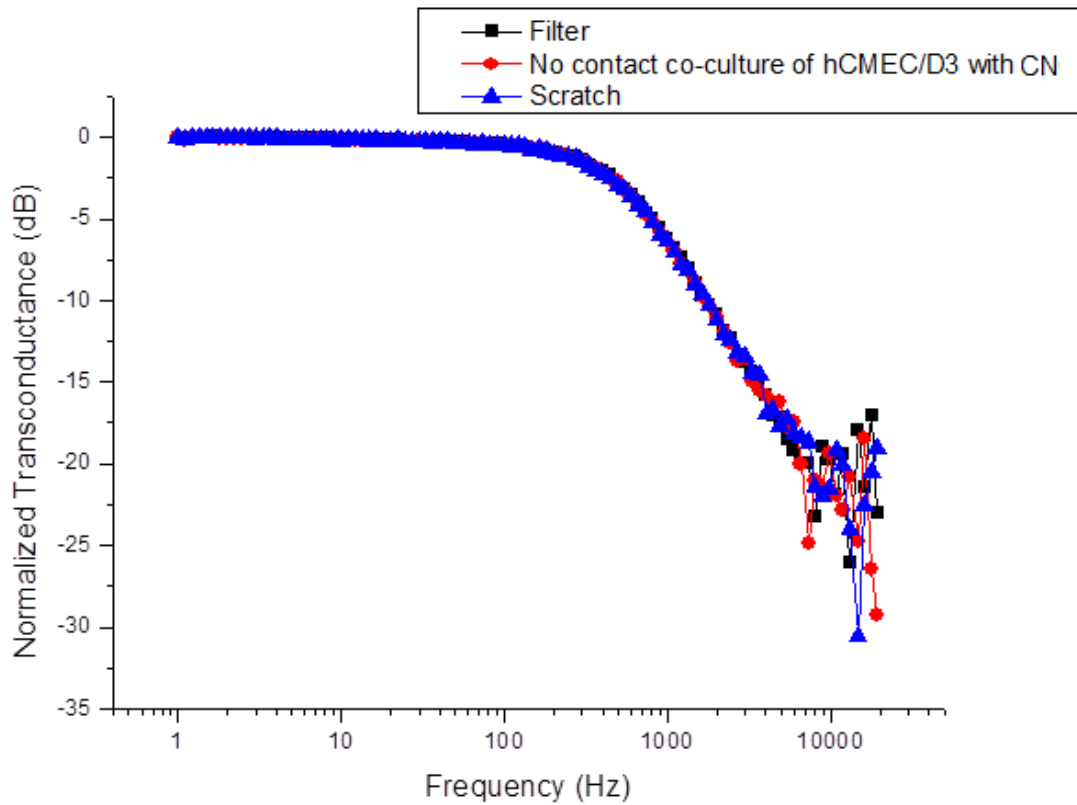


**Figure 3.22:** OECT transconductance response versus frequency, of the device alone (black), the hCMEC/D3 cells co-cultured in contact with HA (blue), after scratch the filter (red).

### 3.5.3 Conclusion

OECT assays, known to be very sensitive do not permit to detect cells on filter. There is no difference on the measurement with or without cell. One possible reason is that cells are not correctly forming homogenous monolayers on the filters and that a solution would be to seed directly BBB cells on OECT in planar configuration.

### 3.6 Conclusion

In this chapter, we investigated the relevance of the different type of BBB culture model for use as an *in vitro* BBB model. Biological methods that we used are generally use in academic laboratories to assess barrier integrity. On the basis of this study, the following specific conclusions can be drawn: the standard methods are not the most appropriate way to estimate the integrity of BBB tissue. These methods use a porous membrane of filter which appear not adaptable to a good growth of BBB endothelial cells.

The use of OECT in this configuration does not show encouraging results. One promising way is to perform an inverted model culture seeding the brain endothelial cells directly on OECT planar configuration without filter [14]. For that, the next step, will to evaluate the biocompatibility of BBB cell with OECT material especially the conducting polymer PEDOT.

### 3.7 Bibliography

1. Davila, J.C., et al., *Predictive value of in vitro model systems in toxicology*. Annu Rev Pharmacol Toxicol, 1998. **38**: p. 63-96.
2. Deli, M., et al., *Permeability Studies on In Vitro Blood–Brain Barrier Models: Physiology, Pathology, and Pharmacology*. Cellular and Molecular Neurobiology, 2005. **25**(1): p. 59-127.
3. Culot, M., et al., *An in vitro blood-brain barrier model for high throughput (HTS) toxicological screening*. Toxicol In Vitro, 2008. **22**(3): p. 799-811.
4. Siddharthan, V., et al., *Human astrocytes/astrocyte-conditioned medium and shear stress enhance the barrier properties of human brain microvascular endothelial cells*. Brain Res, 2007. **1147**: p. 39-50.
5. Gaillard, P.J., et al., *Establishment and functional characterization of an in vitro model of the blood-brain barrier, comprising a co-culture of brain capillary endothelial cells and astrocytes*. Eur J Pharm Sci, 2001. **12**(3): p. 215-22.
6. Hatherell, K., et al., *Development of a three-dimensional, all-human in vitro model of the blood-brain barrier using mono-, co-, and tri-cultivation Transwell models*. J Neurosci Methods, 2011. **199**(2): p. 223-9.
7. Demeuse, P., et al., *Compartmentalized coculture of rat brain endothelial cells and astrocytes: a syngenic model to study the blood-brain barrier*. J Neurosci Methods, 2002. **121**(1): p. 21-31.
8. Hartmann, C., et al., *The impact of glia-derived extracellular matrices on the barrier function of cerebral endothelial cells: an in vitro study*. Exp Cell Res, 2007. **313**(7): p. 1318-25.

9. Forster, C., et al., *Differential effects of hydrocortisone and TNFalpha on tight junction proteins in an in vitro model of the human blood-brain barrier*. J Physiol, 2008. **586**(7): p. 1937-49.
10. Daniels, B.P., et al., *Immortalized human cerebral microvascular endothelial cells maintain the properties of primary cells in an in vitro model of immune migration across the blood brain barrier*. J Neurosci Methods, 2013. **212**(1): p. 173-9.
11. Weksler, B.B., et al., *Blood-brain barrier-specific properties of a human adult brain endothelial cell line*. FASEB J, 2005. **19**(13): p. 1872-4.
12. Weksler, B., I.A. Romero, and P.O. Couraud, *The hCMEC/D3 cell line as a model of the human blood brain barrier*. Fluids Barriers CNS, 2013. **10**(1): p. 16.
13. Xue, Q., et al., *A novel brain neurovascular unit model with neurons, astrocytes and microvascular endothelial cells of rat*. Int J Biol Sci, 2013. **9**(2): p. 174-89.
14. Sansing, H.A., N.A. Renner, and A.G. MacLean, *An inverted blood-brain barrier model that permits interactions between glia and inflammatory stimuli*. J Neurosci Methods, 2012. **207**(1): p. 91-6.

# Chapter 4

---

## PEDOT:gelatin Composites Mediate Brain Endothelial Cell Adhesion

---

One option for OECT device configuration is to coat filter directly with PEDOT(TOS) and integrate this into the device. The following chapter describes the optimization of the adhesion of brain endothelial cell on PEDOT(TOS) coated filters. Adhesion to substrate or to neighboring cell is an essential process in epithelial/endothelial cell growth. BBB adhesion is built upon on the synergy between cells and the basement membrane. To mimic this basement membrane, gelatin, an extracellular matrix (ECM) protein is used. Here we incorporate gelatin with PEDOT using a new method: Vapor Phase Polymerisation (VPP). We prepared PEDOT(TOS):gelatin composites as a new biocompatible substrate, to promote brain capillary endothelial cell adhesion and growth in order to increase the sensitivity of the system for future use in an *in vitro* model of the BBB with integrated organic electronic devices for measuring tissue layer integrity. This remains a promising option for future integration of BBB models with OECT.

In this manuscript my roles were the following: I did the cell culture, the characterisation of cell growth, the preparation of PEDOT films and the characterization of these film using immunofluorescence, scanning electron microscope, contact angle and atomic force microscopy.

***This chapter corresponds to the following published article:***

Manuelle Bongo, Orawan Winther-Jensen, Scott Himmelberger, Xenofon Strakosas, Marc Ramuz, Adel Hama, Eleni Stavrinidou, George G. Malliaras, Alberto Salleo, Bjorn Winther-Jensen and Roisin Owens. *PEDOT:gelatin composites mediate brain endothelial cell adhesion*. Journal of Materials Chemistry B, 2013. **1**(31): p. 3860-3867.

## 4.1 Introduction

The use of conducting polymers (CPs) in biological applications is becoming increasingly widespread[1]. Many studies have now shown the interaction of CPs with living tissue[2, 3], neurons[4] and proteins[5]. Poly(3,4 ethylenedioxythiophene) (PEDOT)-based CPs are emerging as champion materials for interfacing with biology, with good film-forming properties and excellent chemical stability[6, 7]: for example, PEDOT doped with the water dispersible polystyrenesulfonate (PEDOT(PSS)) and PEDOT doped with tosylate anion (PEDOT(TOS)). Both these polymers, PEDOT(PSS) and PEDOT(TOS), have good biocompatibility with biological elements, but the ability of cells to adhere and grow on these materials is still not completely understood.

Cellular adhesion is an important process, both for adhesion to substrates and adhesion to adjacent cells. Cells generate contractile forces through interactions with their supporting microenvironment which are transmitted through the substrate by mechanotransduction [8, 9]. The surface of the substrate can also change the interactions and induce an internal reorganization of cellular architecture. The behaviour of cells on surfaces of varying rigidity or ‘hardness’ can be indicative of a particular phenotype: for example, the growth of cells on “soft”gels is now used as a means to identify cancer cells [10]. Cell–cell interactions are mediated by tight contacts and are crucial for cell morphology, function and growth. However, this adhesion is dependent on the interaction between cells and extracellular matrix (ECM) proteins which are known to support cell attachment and growth [11]. Examples of extracellular matrix proteins include fibronectin, laminin and collagen. Gelatin is a derivative of collagen, one of the most well-known ECM proteins.

A wide variety of bio-materials are used in tissue engineering and it is known that the choice of materials can influence the behaviour of cells [12]. CPs have frequently been studied as a potential new material in tissue engineering due to their ability to conduct ions and electrons, with potential applications in electrically controlled drug release [13], release of cells from surfaces [14], controlled alignment of muscle fibres [15] and many more [16]. For example, Schmidt and Nickels demonstrated that the CP polypyrrole created topographical cues for neuronal cells and had an effect on axon orientation [17]. Several groups have made composites of CPs and biomolecules, frequently via electropolymerisation, through incorporation of the desired species in the electrolyte solution [18]. Often, the goal for incorporation of the biospecies is to improve the interface with the CP. Although certain cell types have been demonstrated to grow directly on CPs including epithelial cells [12], endothelial cells[19], human breast cancer cells and fibroblasts [180], often extracellular matrix proteins are coated onto the substrates to enhance adhesion. Certain cells adhere very poorly even to tissue culture treated plastic substrates, a surface that has been specially treated (by a corona discharge) to encourage cell growth, therefore

necessitating the addition of an exogenously added ECM protein. When adding biospecies to CPs, two concerns must be addressed. First, the functionality of the biospecies should not be damaged during the polymerisation process or during subsequent processing steps. Second, the electrical properties of the CP should not suffer due to the incorporation of the biomolecule. Previous incorporation of proteins such as growth factors or ECM proteins into PEDOT films via electropolymerisation has been shown to result in both decreased electroactivity and poor mechanical properties [20, 21] attributed to changes in the rate of polymerisation. Incorporation of the ECM component hyaluronic acid into polypyrrole by electropolymerisation encouraged angiogenesis, but the resulting film was brittle with a four orders of magnitude lower conductivity [22].

One cell type known to require gelatin for adhesion is capillary endothelial cells of the blood–brain barrier (BBB) [23]. The BBB is a dynamic, physiological and metabolic barrier separating the blood from the central nervous system and is essential for maintaining brain homeostasis and enabling proper neuronal function. The BBB consists of endothelial cells lining the blood vessels (or capillaries) in the brain [24]. This barrier is very selective and impermeable. However when this barrier is altered, diseases such as multiple sclerosis, Alzheimer’s, Parkinson’s and other neurodegenerative disorders can occur [25]. The limitation of current treatments can help for understanding the complex functioning of the central nervous system and its interaction with the BBB. Thus, as in other tissue engineering strategies, the ability to develop an *in vitro* BBB model environment becomes a key element to successful tissue engineering [26]. In this study, we set out to determine if CP composites can be a suitable substrate for bovine brain capillary endothelial cell (BBCEC) adhesion, for future use in an *in vitro* model of blood–brain barrier with integrated organic electronic devices for measuring the integrity of this tissue layer [27]. Herein, we show a new method for preparation of PEDOT(TOS) composites with the biomolecule gelatin to promote BBCEC adhesion and growth on composite films. The method was designed not only to maintain the electrical properties of the CP, but also to retain the functionality of the biomolecule.

## 4.2 Materials and Methods

### 4.2.1 Materials

Anhydrous iron(III) para-toluenesulphonate (Fe(III)TOS) was obtained by vacuum drying of a 40% solution in butanol (ex. Yacoo Chemical Co., Ltd.) for 48 h at 50 °C. Gelatin (G2500) was purchased from Sigma Aldrich. Pyridine was from BDH Chemicals and acetic acid (glacial) was purchased from Ajax Chemicals.

#### 4.2.2 Vapor Phase Polymerisation of PEDOT(TOS) and PEDOT(TOS) Composite Films

To promote adhesion between the final PEDOT film and the substrate, glass slides were coated with plasma polymerised maleic anhydride prior to deposition of the oxidant solution. PEDOT(TOS):gelatin composites were prepared by dissolving 419 mg of Fe(III)TOS in 0.80 mL of 1 : 1.67 water : acetic acid (v/v) mixture in a vial and 24 mL of pyridine was added and vigorously stirred. In a separate vial, gelatin (35.4 mg and 70 mg for PEDOT(TOS):gelatin 1 : 1 and 1 : 2 ratios, respectively) was dissolved in 0.625 mL of 1 : 1.5 water : acetic acid (v/v). Gelatin was used at 1 : 1 and 1 : 2 for the CV experiments but otherwise the ratio was maintained at 1 : 1 throughout. Gelatin was omitted for PEDOT(TOS). The oxidant mixture was then added to the gelatin solution and stirred to mix thoroughly. The oxidant solution was spun onto the substrates (either glass slides or 96-well tissue culture treated plastic plates) at 1500 rpm for 30 s and placed directly in the vapor phase polymerisation chamber without a drying step. The vaporization chamber, containing an EDOT monomer (HD Stark or Yacoo Chemical Co., Ltd.), was kept in an oven at 70 °C, at ambient pressure. EDOT was allowed to polymerise on the coated substrates for 30 min to about an hour. After polymerisation the film was cooled to room temperature and washed with ethanol three times to remove excess Fe(III)TOS and unpolymerised EDOT monomer. Protein coated substrates were prepared by depositing gelatin (2 ug . mL<sup>-1</sup>) or BSA (5 ug . mL<sup>-1</sup>) onto substrates (either glass slides or 96-well tissue culture treated plastic plates or already prepared PEDOT(TOS) films) and incubating for 1 hour at 37 °C. For contact angle experiments alternative samples were prepared by spin-coating the protein samples onto the substrate and then baking at 70 °C for 30 minutes.

#### 4.2.3 Characterisation of PEDOT(TOS) and PEDOT(TOS) Composite Films

**XPS.** PEDOT(TOS) or PEDOT(TOS):gelatin 1 : 1 composites were coated on glass slides. XPS measurements were carried out on a SSI S-Probe XPS Spectrometer.

**NanoSIMs.** PEDOT(TOS) or PEDOT(TOS):gelatin 1 : 1 composites were coated on glass slides. Secondary ion mass spectrometry was performed using Cs<sup>+</sup> ion bombardment and negative ion detection on a Cameca NanoSIMS 50L.

**Cyclic voltammetry (CV).** PEDOT(TOS) or PEDOT(TOS):gelatin coated Au mylar was scanned in 0.05 M NaTOS, Ph 6.9 (bubbled with nitrogen for about 10 min prior to scanning) at 20 mV s<sup>-1</sup>. Ag/AgCl (3 M NaCl) and Pt wire were used as reference and counter electrodes, respectively.

**Swelling measurement.** PEDOT(TOS):gelatin 1 : 1 was coated on a quartz crystal microbalance (QCM) crystal. The composite coated crystal was immersed into water or Dulbecco's Modified Eagle's Medium (DMEM). The change in mass was monitored for 7 days.

**Conductivity measurement.** PEDOT(TOS) or PEDOT(TOS):gelatin composites were coated on glass slides. Sheet resistance was measured using Jandel four point probes. The thickness of the films was measured using a Veeco Dektak 150 Profilometer. The conductivity was then calculated from  $\sigma$  ( $\text{S cm}^{-1}$ ) = 1/thickness (cm)/sheet resistance (ohm).

**Contact angle.** In order to discriminate the nature of polar or apolar interactions at the solid–liquid interface, a contact angle (Apollo Instruments) measurement was conducted. Water is used in measuring the liquid contact angle to deduce the hydrophobicity (wide angle, low surface energy) or hydrophilicity (small angle, high surface energy) of the surface. 5  $\mu\text{L}$  drops were used and three measurements were taken for each sample. Contact angle images were analysed by SCAN 20 software.

**Atomic force microscopy.** To determine the roughness of the surfaces, an atomic force microscope (AFM, Veeco, Autoprobe SP II) was applied to scan three different areas of surface for each sample with an area of 1  $\mu\text{m}^2$ , and then to take the image of the surface in tapping mode. The tapping images were analysed by Windows Scanning X Microscope software to obtain the topography of the surface and the roughness parameters.

**Scanning electron microscopy.** To assess the film morphology, a scanning electron microscope (SEM, Ultra 55, Carl Zeiss) was used.

#### 4.2.4 Cell Culture and Characterisation of Cell Growth and Proliferation

Bovine Brain Endothelial Cells (BBECs) were a kind gift of the University Lille Nord de France, U. Artois, BBB Laboratory (LBHE). The BBECs were cultured at 37 °C in 5% CO<sub>2</sub> humidified incubators, in DMEM supplemented with 10% heat inactivated new-born calf serum (CS) (Invitrogen), 10% heat inactivated horse serum (HS) (Invitrogen), 2 mM glutamine (Glutamax<sup>TM</sup>-1, Invitrogen), 50  $\mu\text{g mL}^{-1}$  gentamicin and 1  $\text{ng mL}^{-1}$  basic fibroblast growth factor (bFGF) (Sigma Aldrich). The cells were detached by trypsinisation (0.05% trypsin–EDTA 1X, Invitrogen) and the numbers were determined by a cell counter (Scepter handheld automated cell counter, Millipore).

**Cell adhesion and proliferation tests.** A 96-well cell culture dish (approximate area: 0.3  $\text{cm}^2$ ) was coated with the CP composites according to the procedure described above. Each coated substrate was sterilized for 20 min in 70% ethanol and rinsed twice with PBS. Cells were seeded at a concentration of 10<sup>3</sup> cells per well. An

additional 0.4 mL of DMEM was added to each well. Cell adhesion was observed 3 hours after seeding (Primovert, Carl Zeiss). Adhesion and proliferation were evaluated after 4 days. A calcein-AM–propidium iodide assay was carried out to determine the cell viability (calcein-AM, Sigma) at  $1 \text{ mg mL}^{-1}$  and propidium iodide (propidium iodide solution, Sigma) at  $2 \text{ mg mL}^{-1}$ . To perform these tests, the media in the dishes were discarded and the cells were gently rinsed two times with PBS. 0.3 mL of the calcein-AM–PI mixture was added to each well and incubated for 30 min at  $37 \text{ }^{\circ}\text{C}$ . Fluorescence images were taken (Axio Observer Z1, Carl Zeiss, calcein-AM 485 nm/535 nm, PI 530 nm/620 nm) and cells were counted to determine viability.

**MTT assay.** The MTT assay (MTT Cell Proliferation Assay Kit, Cayman Chemical) was carried out according to the manufacturer’s instructions. Four replicates were evaluated. After 4 days, the media were aspirated and replaced with 100 mL of fresh media supplemented with 10 mL of MTT reagent and the plate was incubated at  $37 \text{ }^{\circ}\text{C}$  for 3 hours. Then 100 mL of crystal dissolving reagent was added to dissolve formazan crystals and the absorbance ( $A_{570 \text{ nm}}$ ) was measured with a spectrophotometer (Infinite, M1000, Tecan). For comparison, the absorbance of the formazan solution measured from gelatin was carried out as a control. The ratio of the differences in absorbance of the formazan solution between the several groups and the gelatin control was defined as the relative cell growth rate.

**Immunofluorescence assay.** To investigate the distribution of gelatin throughout the film and surface availability, an anti-gelatin antibody was used. The blocking step was done with PBS-T (0.05% Tween 20 in PBS) and 5% non-fat dry milk during 30 min at room temperature. A rabbit polyclonal anti-gelatin antibody (Mybiosource) was added to PBS for 1 h at room temperature and then Alexa Fluor 568 goat anti-rabbit (Molecular Probes) was added for 1 h at room temperature. Finally, samples were examined with a fluorescent microscope (Axio Observer Z1 Carl Zeiss).

## 4.3 Results and Discussion

### 4.3.1 Preparation and Characterisation of PEDOT(TOS):gelatin Composites

To improve the interface between CPs and biorecognition elements, we adopted a previously described procedure to incorporate biomolecules by vapour phase polymerisation (VPP) [203]. PEDOT(PSS) is commercially available as a liquid formulation, however, it has limitations in terms of tunability of the polymer, and since it is a finely balanced solution, addition of additional molecules does not seem feasible [28]. VPP prepared PEDOT(TOS) films have been shown to be a good substrate for cell adhesion as compared to PEDOT(PSS) [29]. We previously described the use of VPP to make PEDOT(TOS):PEG composites, in a manner that

not only did not decrease the electrical properties of the CP, but actually increased the conductivity [30]. A particular difficulty to overcome, when using iron(III) as an oxidant for PEDOT VPP in combination with a hydrophilic polymer with a large number of active groups, is to avoid the coordination of Fe(III) to these groups and thereby avoiding the formation of a gel during the mixing of the VPP precursors. This was overcome by changing the solvent system to a combination of water and acetic acid, where the acetic acid preferably coordinated to Fe(III) and thereby prevented gelation. As acetic acid is a weak acid, it was thought to be a good choice to avoid denaturation of biomolecules included in the oxidant solution.

To fully characterise PEDOT(TOS):gelatin composites, a variety of substrates were prepared, including PEDOT(TOS), PEDOT(TOS) overlays (coated) with either gelatin or a control protein bovine serum albumin (BSA): PEDOT(TOS) + gelatin, PEDOT(TOS) + BSA, and PEDOT(TOS) polymer composites with either gelatin or BSA: PEDOT(TOS):gelatin and PEDOT- (TOS):BSA. For cell culture experiments, films or proteins alone were coated onto 96-well tissue culture plates and therefore an additional control was included of the plastic well alone (well).

Gelatin is a polypeptide that consists of different protein fractions resulting from the degradation of the inter- and intramolecular hydrogen bonds that constitute collagen molecules. The particular type of gelatin used was from porcine skin, prepared from acid cured tissue, with an estimated molecular weight of 50–100 kDa. The molecular weight of the EDOT monomer is 142 Da. To verify the presence of gelatin in the composite films, X-ray Photoelectron Spectroscopy (XPS) and Secondary Ion Mass Spectroscopy (NanoSIMS) analysis were performed. Representative traces from XPS are shown in Figure 4.1. The appearance of a nitrogen peak, present in the multiple amine groups of gelatin, is obvious in the PEDOT(TOS):gelatin trace, but is absent in the PEDOT(TOS) trace. The percentage of the individual elements taken from multiple spots on the composite films is shown in Table 4.S1 in the ESI.† The average percentages in the PEDOT(TOS) film were 28%, 64%, and 7% for oxygen, carbon, and sulphur respectively, with negligible nitrogen present. The average percentages in the PEDOT- (TOS):gelatin films were 28%, 62%, 4% and 5% for oxygen, carbon, sulphur and nitrogen, respectively.

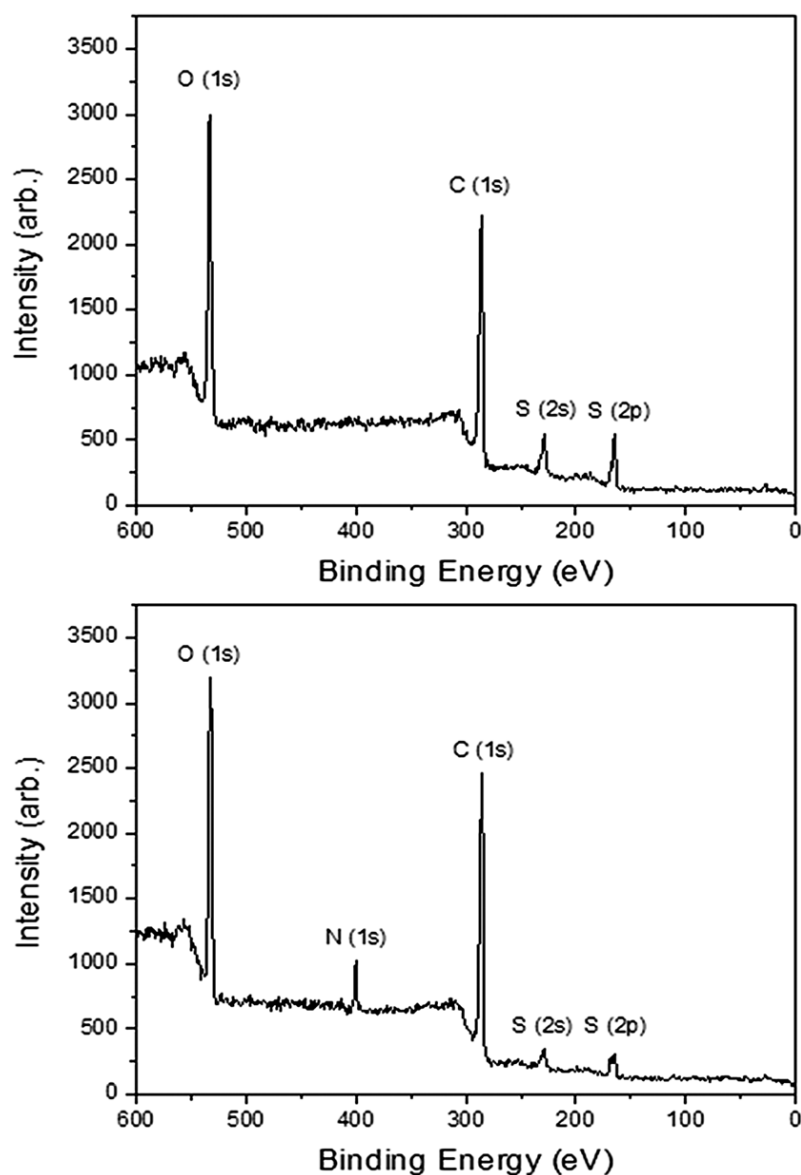


**Figure 4.1:** XPS of PEDOT(TOS) top and PEDOT(TOS):gelatin (bottom) films.

**Table S1. XPS of PEDOT(TOS) films**

Element	PEDOT(TOS)		PEDOT(TOS):Gelatin		
	Spot 1	Spot 2	Spot 3	Spot 1	Spot 2
O	27.48%	29.07%	29.23%	28.43%	28.87%
C	65.16%	63.26%	63.17%	62.37%	62.92%
S	7.36%	7.67%	7.59%	4.04%	3.45%
N	negligible	negligible	negligible	5.15%	4.76%

Table 4.S1: XPS of PEDOT (TOS) films.

A mass-spectrometric technique, NanoSIMS, was used to show the lateral distribution of gelatin in the films as indicated by representative images in Figure 4.2. NanoSIMS is an ultra-high sensitivity chemical imaging technique which optimizes SIMS analysis at high lateral resolution. The elemental maps for nitrogen, carbon, and sulfur in panels A, B, and C respectively indicate a uniform lateral distribution of gelatin within the PEDOT- (TOS):gelatin film.

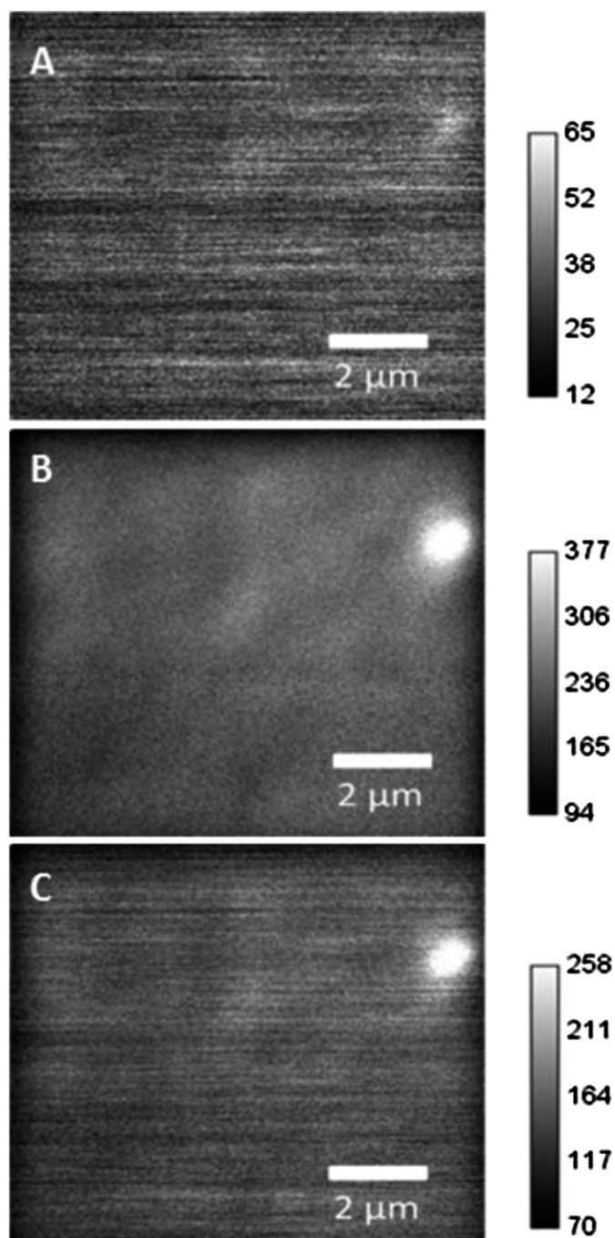


**Figure 4.2:** NanoSIMS of PEDOT(TOS):gelatin films. Panels A, B and C show elemental analysis for nitrogen, carbon and sulphur respectively.

A final confirmation of the presence of gelatin in the composite films was carried out using immunofluorescence. This was done using an anti-gelatin antibody which was hypothesised to bind to epitopes on surface exposed gelatin molecules. This was deemed of relevance since for tissue engineering applications on two dimensional substrates, it is the surface exposed gelatin which is seen by the cells and mediates potential adhesion. Figure 4.3 shows the results of the immunofluorescence staining of PEDOT(TOS) composite films in comparison with controls. In panel A, PEDOT(TOS) alone, no gelatin presence is observed, as expected. Panel 3B shows a well coated with gelatin and shows that the protein is relatively evenly distributed over the whole sample although there is some evidence of protein aggregation which might explain the bright points in the images. The same appears to be true for panels 3C and 3D whether the gelatin is coated on top of the film (3C) or present in a composite (3D).

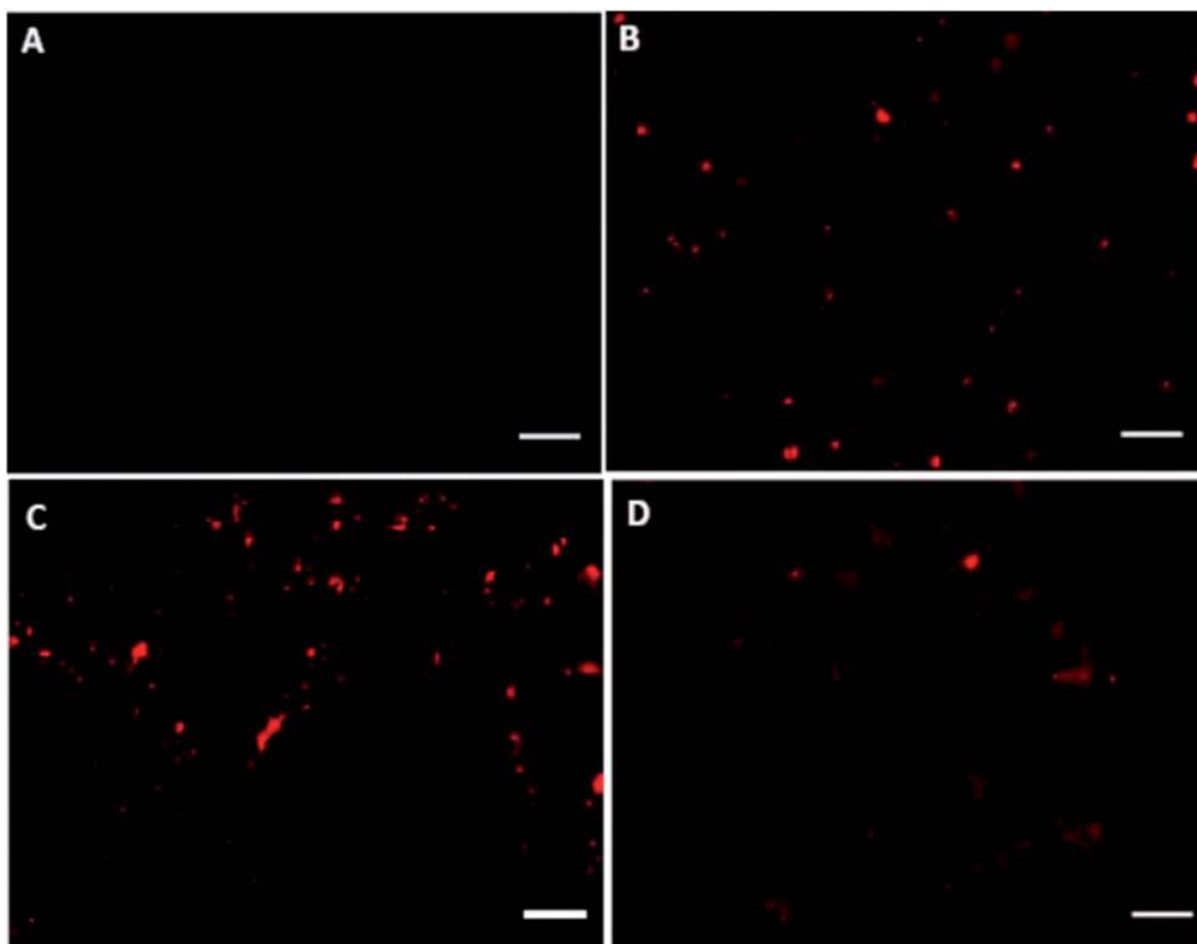


**Figure 4.3:** Immunofluorescence images of substrates stained with anti-gelatin antibodies (red). (A) PEDOT(TOS), (B) gelatin coated on well, (C) PEDOT(TOS) + gelatin, and (D) PEDOT(TOS):gelatin. Scale bar = 100  $\mu\text{m}$ .

Although in this instance the electrical properties of the PEDOT(TOS):gelatin films were not used for modulating adhesion of mammalian cells, an evaluation of the electrochemical properties of the films was carried out to ensure that there was no adverse effect on the CP through the introduction of the gelatin protein. CVs of PEDOT(TOS):gelatin 1 : 1 and 1 : 2 (Figure 4.4) showed typical electrochemical characteristics for PEDOT [30, 31] indicating that the incorporation of gelatin, for these ratios, did not significantly change the electrochemical properties of PEDOT. The conductivity of PEDOT(TOS):gelatin 1 : 1 was in the same range as the PEDOT(TOS) which was about  $310 \text{ S cm}^{-1}$ . The dilution effect was obvious with PEDOT-(TOS):gelatin 1 : 2 where the conductivity was about  $200 \text{ S cm}^{-1}$ . This trend is apparently different from PEDOT(TOS)poly-(ethylene glycol) ((PEDOT(TOS):PEG)) where the conductivity increased with higher quantities of PEG in the composites [30, 32].

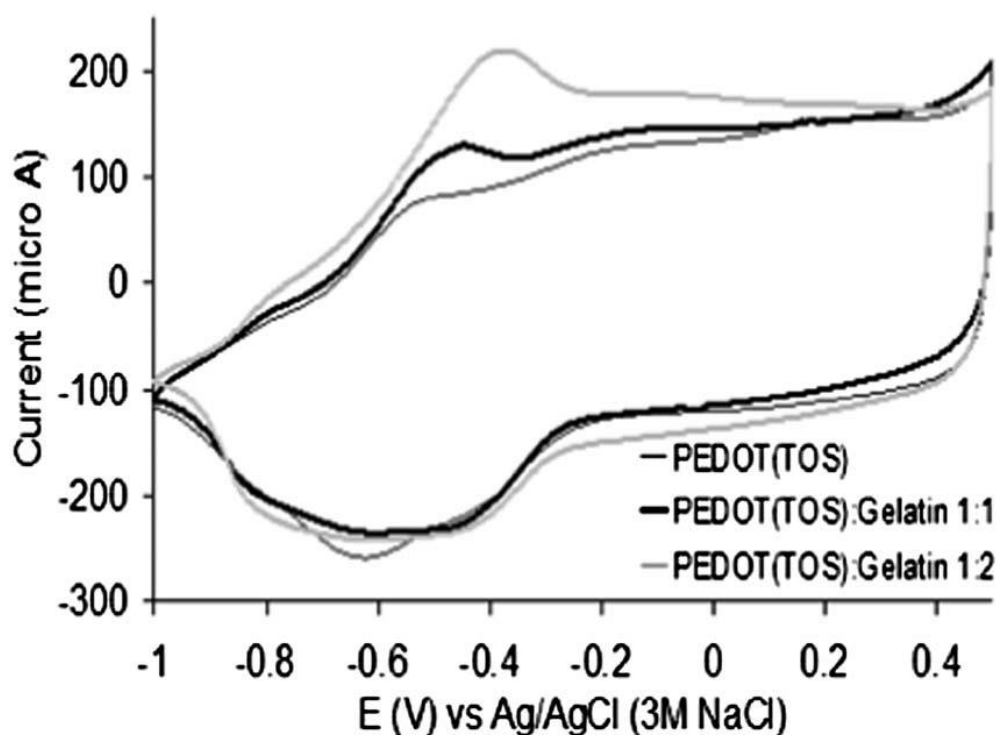
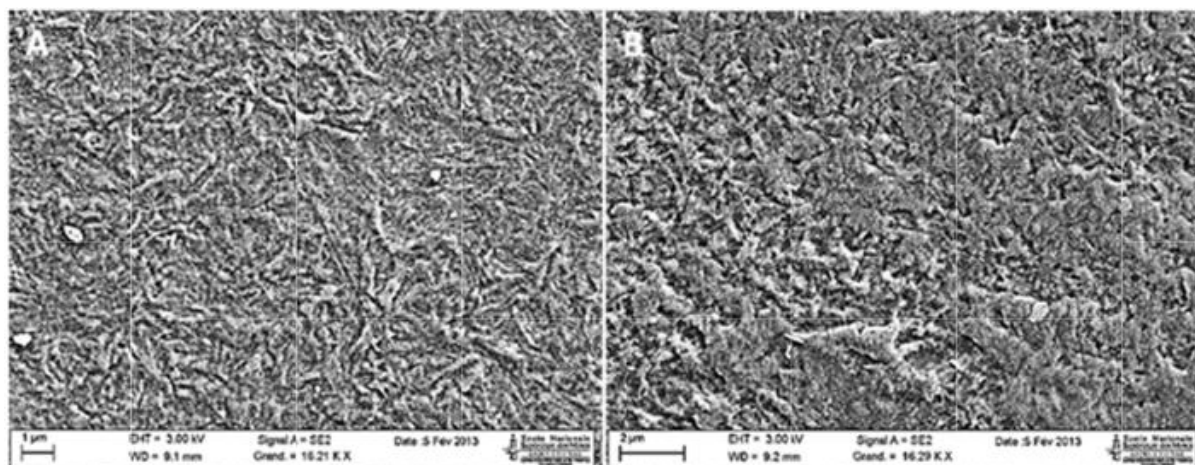


**Figure 4.4:** CVs of PEDOT(TOS), PEDOT(TOS):gelatin 1 : 1 and PEDOT(TOS):gelatin 1 : 2 in 0.05 M NaTOS, pH 6.9 at 20 mV s<sup>-1</sup>.

A variety of different factors are known to mediate cellular adhesion to substrates. It is known that the surface morphology of the substrate can have a significant influence on the adhesion, proliferation and function of cells in addition to the surface chemistry [33]. Since the primary mechanism of adhesion to the composite films in this study is expected to be via the mediation of an extracellular matrix protein, PEDOT(TOS) films were characterised in terms of surface chemistry (contact angle measurements) and roughness (AFM analysis). BSA, a 66 kDa globular protein, was used as a control. The results are summarized in Table 4.1. We observed that the roughness values of gelatin and BSA films are 1.7 nm ± 0.9 nm and 2.2 nm respectively. The roughness of PEDOT(TOS) films averaged at 17.7 nm ± 1.8 nm. When PEDOT(TOS) is layered with gelatin and BSA, the roughness decreases (12.7 nm ± 1.7 nm for PEDOT(TOS) + gelatin and 7 nm ± 0.5 nm for PEDOT(TOS) + BSA), appearing to indicate that gelatin and BSA smooth out the films when coated on top. Roughnesses of 20.7 nm ± 1.6 nm for PEDOT(TOS):gelatin and 23.7 nm ± 3.2 nm for PEDOT(TOS):BSA indicated that the morphology of the films did not change greatly as compared with PEDOT(TOS) when the proteins were combined as a composite. SEM images (ESI, Figure 4.1) indicate that there is not a large difference in morphology between PEDOT(TOS) and PEDOT(TOS):gelatin films.



**ESI, Figure 4. 1:** SEM of PEDOT(TOS) and PEDOT(TOS):gelatin

Surfaces with contact angle values > 90° are generally considered to be hydrophobic [34]. Contact angle results (Table 4.1) established that PEDOT(TOS) films have surfaces that can be considered relatively hydrophilic with contact angles of 49.3° ± 6°, compared to glass slides which can be considered very hydrophilic. Due to a

potential difference in humidity depending on whether substrates were prepared by baking (in the case of the PEDOT(TOS) composites) or by incubation at 37 °C in a humidified incubator (in the case of the BSA or gelatin overlaid samples), controls were measured of protein coated samples prepared in both ways, by baking or incubation. No significant difference was seen in the contact angle values. Films with BSA, either alone, overlaid on PEDOT(TOS) or in a composite with PEDOT(TOS), had invariant contact angles all around 60°. Interestingly, films of gelatin alone or gelatin overlaid on PEDOT(TOS) had contact angles similar to PEDOT(TOS) alone, however, the PEDOT(TOS):gelatin composite was significantly more hydrophobic. Gelatin is often considered a hydrogel and therefore could be expected to be hydrophilic. It has been reported that due to the relative freedom of randomly coiled gelatin molecules, there is a reorganization of hydrophilic moieties at the surface, resulting in a consistently higher contact angle (50–70°) than might be expected from a hydrogel (~ 10 to 20°) [35]. At 67.4° the contact angle value of the PEDOT(TOS):gelatin composite suggests that there may be an additional molecular reorganisation at the surface of this film resulting in an even higher contact angle than the coated films.

	Glass slide	PEDOT(TOS)	Gelatin	PEDOT (TOS) + gelatin	PEDOT(TOS): gelatin	BSA	PEDOT (TOS) + BSA	PEDOT(TOS): BSA
Contact angle (°)	20.8 ± 1.5	49.3 ± 6	47.9 ± 6.0	41.8 ± 6.7	67.4 ± 1.4	62.2 ± 0.1	59.4 ± 1.4	60.9 ± 2.1
Roughness (nm)	0.6 ± 0.5	17.7 ± 1.8	1.7 ± 0.9	12.7 ± 1.7	20.7 ± 1.6	2.2 ± 0.0	7.0 ± 0.5	23.7 ± 3.2

**Table 4.1:** Contact angles and roughness values (obtained from AFM measurements) for PEDOT(TOS) and PEDOT(TOS) composite films. Data presented are mean SD, n = 3

#### 4.3.2 Growth of Bovine BBCEC on PEDOT(TOS) Composite Films

To address the biocompatibility of the prepared composite films, bovine brain capillary endothelial cells (BBCECs) were observed 3 hours after cell seeding (Figure 4.5 (1)). On all substrates, the cell seeding concentration was identical. The number of cells in each well was relatively constant; cells were isolated and well distributed. We observed a difference in cell morphology depending on the coating used. In the case of the wells alone or coated with gelatin, PEDOT(TOS) + gelatin or PEDOT(TOS):gelatin, the cells are elongated which is a good indication for initial adhesion, a necessary step for future proliferation [36, 37]. In the case of all other

wells, cells remained round and non-elongated. To determine the viability of the BBCEC on the polymer composites, a calcein-AM–propidium iodide assay was carried out (Figure 4.5 (2)). Calcein-AM stains the live cells green and propidium iodide stains the dead cells red. Again to control rigorously the effects that might be due to a non-specific protein interaction, BSA was included as a control. It is clear from Figure 4.5 that BSA does not support cell adhesion and therefore cell viability.

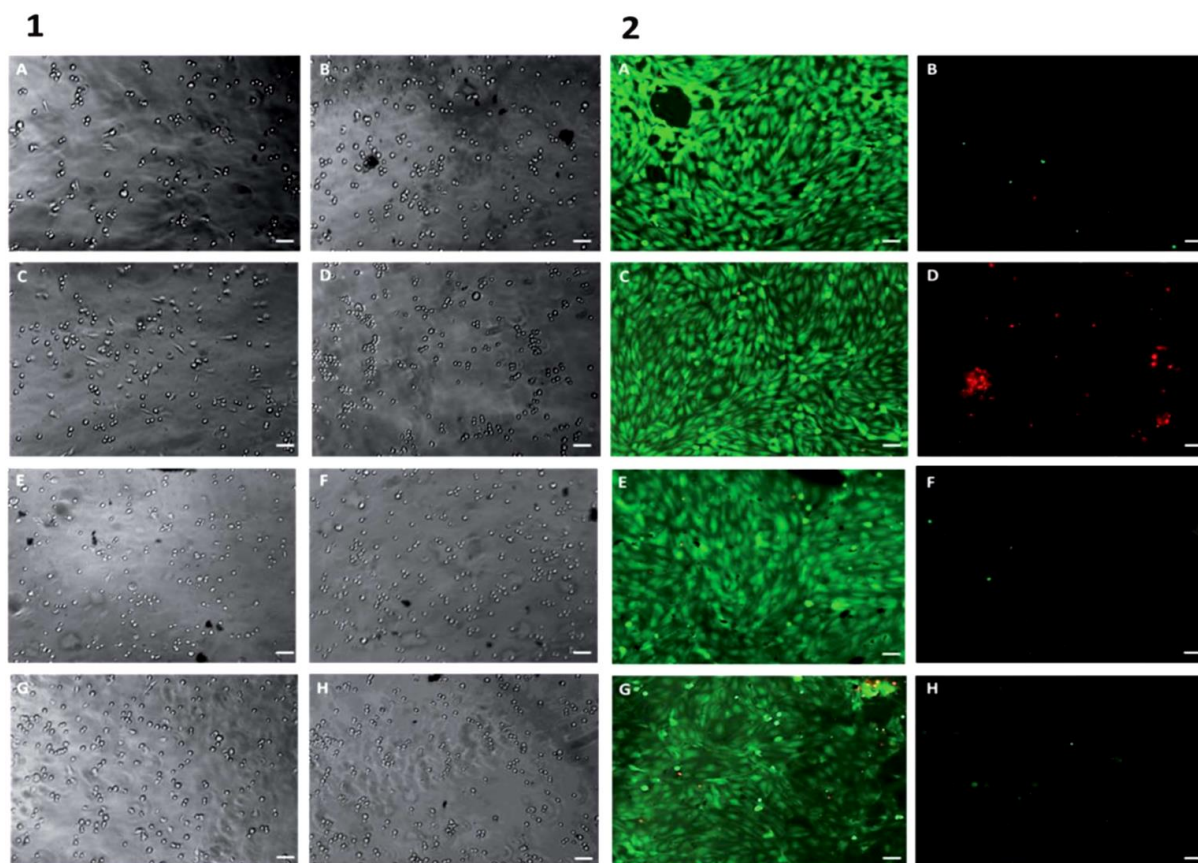
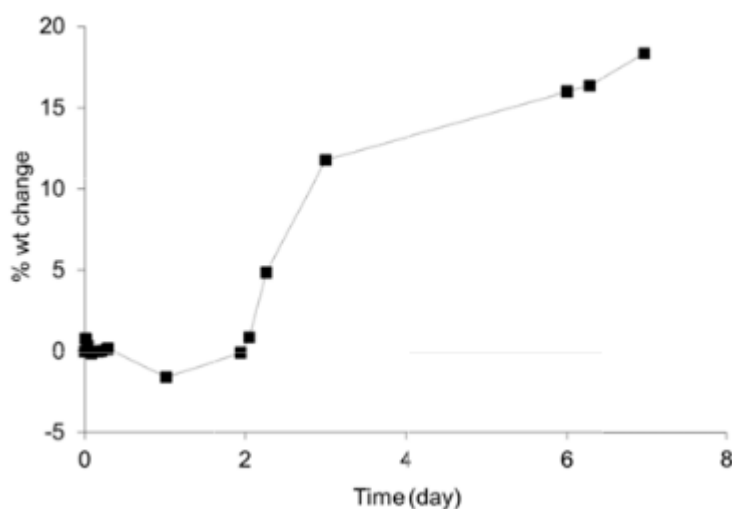


**Figure 4.5:** Initial adhesion (1) and viability (2) of BBCECs observed 3 hours and 5 days after seeding on 96-well plates  $\pm$  polymer composite coating. Wells are as follows: (A) well, (B) PEDOT(TOS), (C) gelatin, (D) BSA, (E) PEDOT(TOS) + gelatin, (F) PEDOT(TOS) + BSA, (G) PEDOT(TOS):gelatin, and (H) PEDOT(TOS):BSA. For the initial adhesion study images were taken by phase contrast microscopy. For viability assays, the live cells are stained with calcein-AM (green) and dead cells are stained with propidium iodide (red). Scale bar = 50  $\mu$ m.

In all wells containing BSA, either coated directly on the well (D), overlaid on PEDOT(TOS) (F) or in a composite with PEDOT(TOS) (H), cells died and formed

clusters. This result was expected, as there is no evidence to suggest that BSA can support the adhesion of cells. In the case of the control well and the PEDOT(TOS) films either with overlaid gelatin or with gelatin as a composite, cells were alive and evenly spread out. PEDOT(TOS) alone was also unable to support cell growth. This result shows a similar trend to the initial adhesion data. Although exogenously added ECM proteins are thought to be important specifically during the adhesion process, after which cells usually produce their own adhesion proteins, the stability of the gelatin within the film was also determined by a QCM swelling experiment. The results show that the composite films had a water uptake in the same level as PEDOT(TOS):PEG (ESI, Figure 4.2†).



ESI, Figure 4.2: water uptake.

The MTT assay reflects the level of cell metabolism [38]. The results for the MTT assay for viability of growth of BBECs on the tested films are shown with the relative cell growth rates (Figure 4.6). Although multiple wash steps are carried out in both ethanol and PBS, this quantitative assay was designed to investigate changes in cell metabolism caused by substances that may leach out of the PEDOT(TOS) films (such as gelatin fragments, tosylate ions and unpolymerised EDOT monomers). The viability for the growth rate of BBECs is determined by measuring the absorbance of the formazan solution. Substrates coated with PEDOT(TOS) +/- biomolecules were seeded with BBCEC as before. Results shown in Figure 4.6 indicate that although the well alone (tissue culture treated plastic (2)) supports the growth of BBCECs, wells coated with gelatin (1) have a greater relative growth rate. In addition, when gelatin was added to PEDOT(TOS) either by overlaying (5) or in a composite (7), the viability of cells cultured decreased only slightly compared to that of control cells grown on the tissue culture well coated with gelatin. However as was noted for the adhesion and viability assays in Figure 4.5, BSA was unable to support cell growth either coated directly onto the well, or integrated with PEDOT(TOS) as an overlay or as a composite. As before, PEDOT(TOS) alone did not support cell growth.

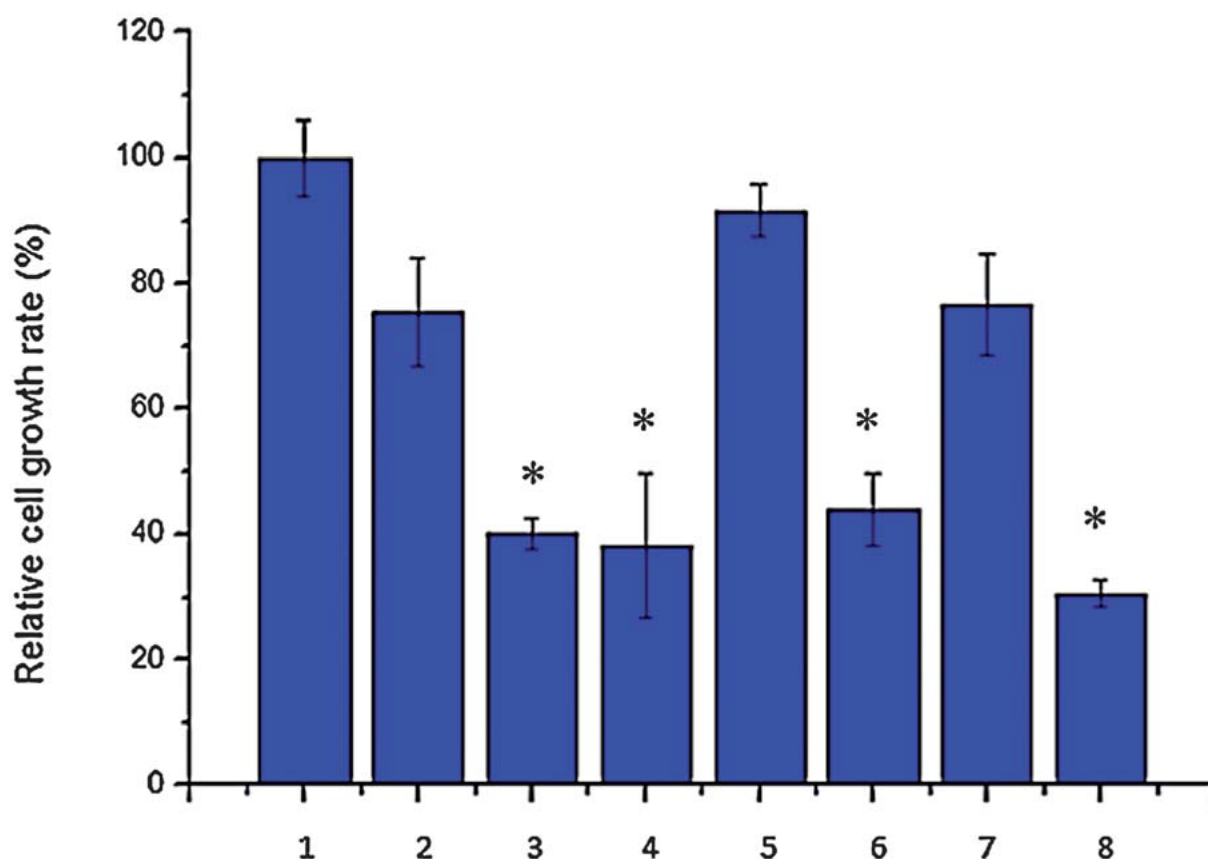


**Figure 4.6:** Viability of BBCECs grown on (1) gelatin, (2) well, (3) BSA, (4) PEDOT(TOS), (5) PEDOT(TOS) + gelatin (6) PEDOT(TOS) + BSA, (7) PEDOT(TOS):gelatin, and (8) PEDOT(TOS):BSA. Gelatin represents the positive control and is used to determine 100% viability.

#### 4.4 Conclusions

Our results clearly show that PEDOT(TOS):gelatin composites not only maintain electrochemical properties of the CP, but also retain the functionality of the incorporated biomolecule. We demonstrate that the gelatin composite materials had

relatively little change in characteristics with respect to roughness, contact angle and morphology of PEDOT(TOS). The PEDOT-(TOS):gelatin composite materials allowed the growth of BBECs while the PEDOT(TOS) films did not. The cell growth on PEDOT(TOS):gelatin composite films was shown to be specific to the gelatin protein, as PEDOT(TOS):BSA films used as a control could not support cell growth. This demonstrates that the mediation of cell adhesion was as a result of the specific functionality of the gelatin protein, and not a non-specific protein effect, implying that the VPP method used was nondestructive to the protein. In this study we have demonstrated for the first time a method for preparation of CP-biomolecule composite films which not only retain the functionality of the biospecies but also maintain the electrical properties of the CP. Although a complete characterisation of molecular interactions between the cells and the polymer surface is warranted, our results support the use of CP composites in tissue engineering and open the possibility of controlling cell behaviour electrically using such composites.

#### 4.5 Bibliography

1. Owens, R.M. and G.G. Malliaras, *Organic Electronics at the Interface with Biology*. MRS bulletin, 2010. 35(06): p. 449-456.
2. Wan, A.M.D., et al., *Electrical control of cell density gradients on a conducting polymer surface*. Chemical Communications, 2009(35): p. 5278-5280.
3. Tria, S.A., et al., *Validation of the organic electrochemical transistor for in vitro toxicology*. Biochim Biophys Acta, 2013. **1830**(9): p. 4381-90.
4. Khodagholy, D., et al., *Highly conformable conducting polymer electrodes for in vivo recordings*. Adv Mater, 2011. **23**(36): p. H268-72.
5. Wan, A.M., et al., *Electrical control of protein conformation*. Adv Mater, 2012. **24**(18): p. 2501-5.
6. Nikolou, M. and G.G. Malliaras, *Applications of poly(3,4-ethylenedioxythiophene) doped with poly(styrene sulfonic acid) transistors in chemical and biological sensors*. Chem Rec, 2008. **8**(1): p. 13-22.
7. Winther-Jensen, B. and K. West, *Stability of highly conductive poly-3,4-ethylene-dioxythiophene*. Reactive & Functional Polymers, 2006. **66**(5): p. 479-483.
8. Hynes, R.O., *Integrins: bidirectional, allosteric signaling machines*. Cell, 2002. **110**(6): p. 673-87.
9. Lim, J.Y., et al., *The regulation of integrin-mediated osteoblast focal adhesion and focal adhesion kinase expression by nanoscale topography*. Biomaterials, 2007. **28**(10): p. 1787-97.
10. Discher, D.E., P. Janmey, and Y.L. Wang, *Tissue cells feel and respond to the stiffness of their substrate*. Science, 2005. **310**(5751): p. 1139-43.
11. Engler, A.J., et al., *Matrix elasticity directs stem cell lineage specification*. Cell, 2006. **126**(4): p. 677-89.

12. Svennersten, K., et al., *Electrochemical modulation of epithelia formation using conducting polymers*. *Biomaterials*, 2009. **30**(31): p. 6257-64.
13. Abidian, M.R., D.H. Kim, and D.C. Martin, *Conducting-Polymer Nanotubes for Controlled Drug Release*. *Adv Mater*, 2006. **18**(4): p. 405-409.
14. Persson, K.M., et al., *Electronic control of cell detachment using a self-doped conducting polymer*. *Adv Mater*, 2011. **23**(38): p. 4403-8.
15. Gilmore, K.J., et al., *Skeletal muscle cell proliferation and differentiation on polypyrrole substrates doped with extracellular matrix components*. *Biomaterials*, 2009. **30**(29): p. 5292-304.
16. Guimard, N.K., N. Gomez, and C.E. Schmidt, *Conducting polymers in biomedical engineering*. *Progress in Polymer Science*, 2007. **32**(8-9): p. 876-921.
17. Nickels, J.D. and C.E. Schmidt, *Surface modification of the conducting polymer, polypyrrole, via affinity peptide*. *J Biomed Mater Res A*, 2013. **101**(5): p. 1464-71.
18. Cosnier, S., *Biomolecule immobilization on electrode surfaces by entrapment or attachment to electrochemically polymerized films. A review*. *Biosens Bioelectron*, 1999. **14**(5): p. 443-56.
19. Gumus, A., et al., *Control of cell migration using a conducting polymer device*. *Soft Matter*, 2010. **6**(20): p. 5138-5142.
20. Asplund, M.L.M., et al., *Stability of Poly(3,4-ethylene dioxythiophene) Materials Intended for Implants*. *Journal of Biomedical Materials Research Part B-Applied Biomaterials*, 2010. **93B**(2): p. 407-415.
21. Green, R.A., N.H. Lovell, and L.A. Poole-Warren, *Impact of co-incorporating laminin peptide dopants and neurotrophic growth factors on conducting polymer properties*. *Acta Biomater*, 2010. **6**(1): p. 63-71.
22. Collier, J.H., et al., *Synthesis and characterization of polypyrrole-hyaluronic acid composite biomaterials for tissue engineering applications*. *J Biomed Mater Res*, 2000. **50**(4): p. 574-84.
23. Culot, M., et al., *An in vitro blood-brain barrier model for high throughput (HTS) toxicological screening*. *Toxicol In Vitro*, 2008. **22**(3): p. 799-811.
24. Bernacki, J., et al., *Physiology and pharmacological role of the blood-brain barrier*. *Pharmacol Rep*, 2008. **60**(5): p. 600-22.
25. Saha, A., et al., *The blood-brain barrier is disrupted in a mouse model of infantile neuronal ceroid lipofuscinosis: amelioration by resveratrol*. *Hum Mol Genet*, 2012. **21**(10): p. 2233-44.
26. Ma, S.H., et al., *An endothelial and astrocyte co-culture model of the blood-brain barrier utilizing an ultra-thin, nanofabricated silicon nitride membrane*. *Lab Chip*, 2005. **5**(1): p. 74-85.
27. Jimison, L.H., et al., *Measurement of barrier tissue integrity with an organic electrochemical transistor*. *Adv Mater*, 2012. **24**(44): p. 5919-23.
28. Winther-Jensen, B., et al., *Vapor Phase Polymerization of Pyrrole and Thiophene Using Iron(III) Sulfonates as Oxidizing Agents*. *Macromolecules*, 2004. **37**(16): p. 5930-5935.
29. Karagkiozaki, V., et al., *Bioelectronics meets nanomedicine for cardiovascular implants: PEDOT-based nanocoatings for tissue regeneration*. *Biochim Biophys Acta*, 2013.
30. Jimison, L.H., et al., *PEDOT:TOS with PEG: a biofunctional surface with improved electronic characteristics*. *Journal of Materials Chemistry*, 2012. **22**(37): p. 19498-19505.

31. Winther-Jensen, B. and D.R. MacFarlane, *New generation, metal-free electrocatalysts for fuel cells, solar cells and water splitting*. Energy & Environmental Science, 2011. **4**(8): p. 2790-2798.
32. Winther-Jensen, B., et al., *Conducting Polymer Composite Materials for Hydrogen Generation*. Advanced Materials, 2010. **22**(15): p. 1727-1730.
33. Zhu, Y., et al., *Layer-by-layer assembly to modify poly(l-lactic acid) surface toward improving its cytocompatibility to human endothelial cells*. Biomacromolecules, 2003. **4**(2): p. 446-52.
34. Rios, P.F., et al., *The effect of polymer surface on the wetting and adhesion of liquid systems*. Journal of Adhesion Science and Technology, 2007. **21**(3-4): p. 227-241.
35. Yasuda, T., T. Okuno, and H. Yasuda, *Contact Angle of Water on Polymer Surfaces*. Langmuir, 1994. **10**(7): p. 2435-2439.
36. Lakard, S., et al., *Adhesion and proliferation of cells on new polymers modified biomaterials*. Bioelectrochemistry, 2004. **62**(1): p. 19-27.
37. Pierres, A., et al., *How Cells Tiptoe on Adhesive Surfaces before Sticking*. Biophys J, 2008. **94**(10): p. 4114-4122.
38. HuvencersOorsprong, M.B.M., L.A.P. Hoogenboom, and H.A. Kuiper, *The use of the MTT test for determining the cytotoxicity of veterinary drugs in pig hepatocytes*. Toxicology in Vitro, 1997. **11**(4): p. 385-392.

# Chapter 5

---

## Integration of an *in vitro* Model of the Blood Brain Barrier with the OEECT

---

Parallel development of OECT devices by members of the Owens-Malliaras group focused on miniaturization of these devices. However as explained in chapter 2, section 2.4.1, these miniaturized devices are not compatible with a non-planar, filter format. The following chapter is a manuscript in preparation describing results obtained combining two main points: 1) cells were grown directly on the PEDOT:PSS channel to improve homogeneity of cell viability and reduce defects in the cell layer, and 2) the use of a miniaturized device resulted in increased sensitivity.

In this manuscript my role consisted of the following: I did the cell culture and I learned how to set up the OECT experiment. I performed the monitoring of BBB cells with the microscale OECT and I analyzed the data.

***This chapter corresponds to an article in preparation:***

Manuelle Bongo, Marc Ramuz, Jonathan Rivnay, Pierre Leleux, Roisin Owens.  
*Organic electrochemical transistors for measuring Blood Brain Barrier tissue integrity.*

*In preparation for submission to Toxicology In vitro*

### 3.1 Introduction

The BBB is a specialized endothelial tissue which consists of a very selective barrier formed of brain microvascular endothelial cells which restrict the passage of substances from the blood to the brain [1]. The BBB expresses a high number of ion channels and transporters, has a low rate of pinocytosis, and forms intercellular tight junction (TJ) protein complexes which limit paracellular permeability [2]. The BBB is capable of simultaneously restricting neurotoxic substances while ions and nutrients are selectively allowed to cross the endothelium from the blood into the brain [3]. This dynamic transport system is necessary for maintaining Central Nervous System homeostasis [4]. It is known that the functional homeostasis of the brain is compromised in numerous disease states, and it has previously been shown that disruption of the BBB is associated with several diseases like stroke, hypoxia [5]. This barrier is very effective at protecting the brain against the passage of foreign substances, however it also means that it often prevents life-saving drugs from being able to repair the injured or diseased brain [6]. In looking at the numerous ongoing activities in the area of BBB research, the validity of the models used is still a subject of debate. One of the issues in BBB research is the difficulty in monitoring the integrity of the barrier, and in particular for drug development to assess the passage of molecules from the blood into the brain. For many years, the conventional techniques of evaluating membrane integrity has been performed by measurement of the flux of a standard molecule across the barrier or the measurement of TER [7]. In general, a direct correlation between the solute flux of a cell layer and its electric resistance exists; tight cell layers exhibit high electrical resistance and low permeability [8, 9]. An over-reliance on permeability methods using fluorescent molecules may be problematic due to issues with specificity, and introduction of artefacts, besides being time consuming and expensive.

The ability to accurately assess barrier tissue integrity is a starting point to provide valuable information about barrier function and cellular integrity in general. Electronic methods for monitoring cells have the advantage of being label free, non-invasive, and can additionally provide real-time measurements. Electronic methods for live-cell sensing refer to a broad range of measurements such as membrane potential probing, impedance monitoring of cells, extracellular recording of electrical activities from neurons and myocytes through both electrodes and transistors, and more. Until recently, the majority of methods for electrically monitoring cell health *in vitro* have been for use in basic research. However, there is increasing demand for reliable techniques for high throughput screening, with a preference for label free methods. In non-electrically active cells, electronic measurements can be used as a measure of cell coverage and differentiation, and thus as a measure of cell viability.

More subtle effects may also be discerned such as receptor binding, cell morphology etc. although this relies on a more complex interpretation of the signal generated. The advent of organic electronics has created a unique opportunity to interface the worlds of electronics and biology, using devices such as the OECT, which provide a very cheap and sensitive way to detect minute ionic currents, in an electrolyte, as the transistor amplifies the gate current [10].

Previous studies in the department of bioelectronics have demonstrated the use of the OECT to monitor the integrity of barrier tissues, specifically of epithelial tissues, and were demonstrated to be an efficient and cost-effective means of sensing barrier tissue integrity [11, 12]. In these studies case, cells were grown on a transwell filter, in a top gate configuration [13]. A further study demonstrated that cells could be grown directly on the channel of the transistor with a planar format, with both the channel and the gate patterned on the same surface.

In this study, we want to use the OECT as an alternative technology to assess the barrier integrity of BBB [19]. Here, a hybrid configuration was used, cells were seeded directly on the OECT channel to maximize the contact between cell and the device, with the aim to improve the sensitivity and the limit of detection of the sensor. In order to maintain a high level of measurement sensitivity, Ag/AgCl was used in a top gate configuration. As Ag/AgCl is a non-polarizable gate, it brings superior performance compare to gold or PEDOT:PSS gate for acute measurements We demonstrate for the first time the integration of OECTs with Immortalized Human Brain Endothelial Cell line hCMEC/D3, for assessing barrier tissue layer integrity. We developed a co-culture of hCMEC/D3 with cortical neurons (CN), known to increase the resistance of the brain endothelial cells [14]. The immortalized cell-line used here has the significant advantage of being readily available, without the cost and sourcing problems associated with primary human brain endothelial cells. The integration of this model of the BBB allowed us to measure sensitively minute variations in ionic flux induced by toxic or pathogen compounds in real time, with high sensitivity and high temporal resolution.

## 3.2 Materials and Methods

### 3.2.1 OECT Fabrication

The active conducting polymer formulation is based on PEDOT:PSS (Heraeus, Clevios PH 1000), supplemented with ethylene glycol (0.25 mL for 1 mL

PEDOT:PSS solution; Sigma–Aldrich), 4-dodecylbenzenesulfonic acid ( $0.5 \mu\text{L.mL}^{-1}$ ), and 3-glycidoxypropyltrimethoxysilane ( $10 \text{ mg.mL}^{-1}$ ). Gold source and drain contacts were patterned via lift-off lithography on a clean glass substrate ( $75 \text{ mm} \times 25 \text{ mm}$ ), and thermally evaporated. Photoresist S1813 (MicroChem Corp.) was spin coated at 3000 rpm for 30 s on the glass substrate. Patterns were defined by photolithography (Chrome mask and Mask Aligner). MF-26A was used as developer. After that, 5 nm and 100 nm of chromium and gold were evaporated. At the end, the photoresist was lifted-off under sonication in an acetone bath for 1 h, which left the substrate with the source and drain Au contacts only. PEDOT:PSS channel dimensions were patterned using a parylene-C peel-off technique described previously [15]. Two layers of Parylene C of  $2 \mu\text{m}$  each were deposited – with in between, a spin-coated film of 2% soap solution at 1000 rpm for 30s. Then AZ-9260 photoresist was spin coated at 3000 rpm for 30s. After a soft bake for 2 minutes at  $110^\circ\text{C}$ , substrate was exposed to UV-light for patterning the PEDOT: PSS area. AZ developer was used to remove the targeted photoresist. With the plasma etcher, areas without photoresist were removed. It resulted in a channel active area width and length of  $100 \mu\text{m}$  and  $10 \mu\text{m}$ , respectively. Following PEDOT:PSS deposition at 3000 rpm for 30s, devices were baked for 1 h at  $140^\circ\text{C}$  under atmospheric conditions. A glass well of  $0.5 \text{ cm}^2$  (hole diameter of  $0.8 \text{ cm}$ ) was sonicated 10 min in water to clean it, then fixed to the device using PDMS to defined the cell growth area (Figure 5.1).

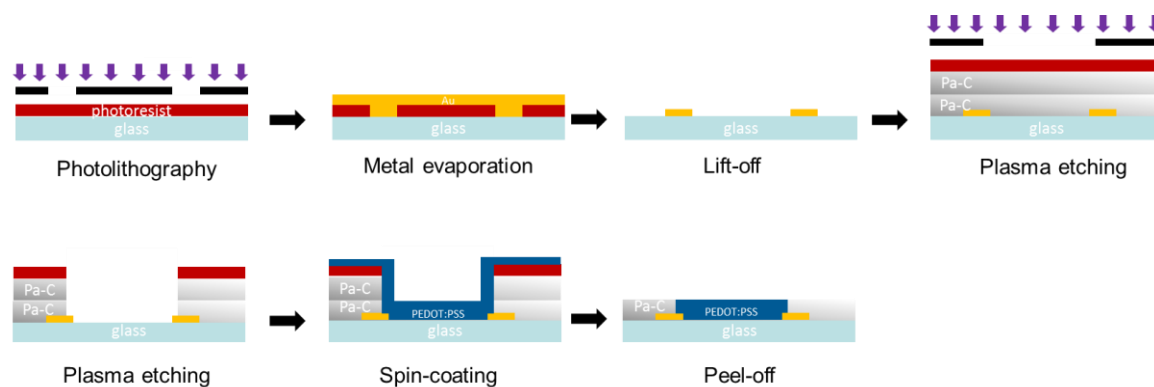


**Figure 5.1:** Schematic of the fabrication process for the OEET.

### 3.2.2 OECT Measurement

All of the measurements were done using a Ag/AgCl pellet as a gate electrode (Harvard apparatus) and cell medium (as described below) was used as the electrolyte. Experiments were performed outside of incubator but cells were on a hotplate at 37°C. Measurement parameters were chosen to avoid exposing the cell layers to a voltage drop above 0.5 V, as high voltages have been shown to damage bilayer membranes. The recording of the OECTs was performed using a National Instruments (NI) PXIe-1062Q system with a NI PXI-4071 Digital MultiMeter (DMM) for the AC current measurement. A Data Acquisition (DAQ) from NI (BNC-2110) was used as gate voltage wave generator. A Labview script was used to pilot the recording equipments. The recorded signals were saved and analyzed using customized Matlab script. The channel of the OECT was biased at  $V_{DS}=-0.6V$ . The modulation between the gate and the source ( $V_{GS}$ ) – generated by the DAQ - was a sinusoidal signal with 10mV amplitude, swept between 1Hz to 20 kHz. The recording consisted of the channel current measurement ( $I_{DS}$ ), in response to the  $V_{GS}$  modulation. To avoid the effect of noise on analysis data, filtering is necessary. For that an appropriate cut off frequency is essential. The cut off frequency is the frequency either above or below which the power output of a circuit. This parameter determines the amount of signal distortion and it is taken at -3 decibels. To determine the integrity of BBB, we expected a high frequency cut off without cell, a low frequency cut off with cell and the difference of frequency cut off between no cells and cells have to be high.

### 3.2.3 Cell Culture

**Cell Culture of hCMEC/D3:** Immortalized human brain capillary endothelial cells (the hCMEC/D3 cell line) were kindly donated by Dr. Pierre-Olivier Couraud of the Institut Cochin, INSERM, Paris. The hCMEC/D3 cells used for the experiments were between passage 25 and 35. All culture was coated with rat-tail collagen type I solution at a concentration of  $0.1 \text{ mg.ml}^{-1}$  and was incubated for 1 h at 37°C. The cells were directly seeded on the device in a concentration of  $3.10^5 \text{ cells.cm}^{-2}$ . hCMEC/D3 grown in endothelial basal medium-2 (EBM-2; Lonza Group Ltd., UK) supplemented with  $1 \text{ ng.ml}^{-1}$  Fibroblast growth factors (bFGF, Sigma Aldrich), 5% FCS (Invitrogen),  $1.4 \text{ }\mu\text{M}$  hydrocortisone (Sigma Aldrich),  $5 \text{ }\mu\text{g.ml}^{-1}$  Acid ascorbic (Sigma Aldrich), 1/100 Chemically Defined Lipid concentrate (Invitrogen), 10 mM HEPES (Sigma Aldrich), and 1% penicillin-streptomycin (Invitrogen). Cells were cultured in

an incubator at 37°C in a humidified atmosphere of 5% CO<sub>2</sub>. Cell culture medium was changed every 2 days.

**Cell Culture of Cortical Neurons :** Neurons from rat, were kindly donated by Dr. Noelle Callizot of the Neurosys company, Gardanne. These cells were seeded in inserts at a density of  $3.10^5$  cells/insert (24 insert, Millipore). All inserts were coated with 2 µg/cm<sup>2</sup> poly-l-lysine (Sigma Aldrich) for 1 h at 37 °C. Neurons were routinely maintained at 37 °C in a humidified atmosphere of 5% CO<sub>2</sub> in culture medium containing neurobasal medium (Invitrogen) supplemented with 2% B27 nutrient supplement (Invitrogen), 2 mM l-glutamine (Invitrogen), 1% of Penicillin-Streptomycin (Invitrogen) and 10 ng/ml of Brain-Derived Neurotrophic Factor (BDNF, Invitrogen).

***In vitro* BBB Models:** Monoculture models were seeded directly on the OECT device pre-coated with rat-tail collagen type I. Co-culture models were set up as follows. Neuron cells were seeded on the apical side of a 0.4 cm<sup>2</sup> polycarbonate membrane pre-coated with poly-l-lysine. After 24 h incubation, hCMEC/D3 cells were seeding on the basal side, directly on the device OECT coated with rat-tail collagen type I. All experiments were performed at day 8.

**Monitoring BBB Toxicology: EGTA:** Ethylene glycol-bis(beta-aminoethyl ether-*N,N,N',N'*-tetra acetic acid, is a calcium chelator , known to have dramatic effects on paracellular permeability and transepithelial resistance (TEER) in barrier tissue. After rinsing with PBS without Ca<sup>2+</sup> and Mg<sup>2+</sup> for 10min, hCMEC/D3 cells were exposed for 15 min at 40mM of EGTA. This EGTA solution is from a stock solution of 0.2 M EGTA in DI water, pH adjusted to 8 with 1 M Tris-HCl. **Trypsin:** Trypsin is a proteolytic enzyme which cleaves the cell-cell and cell-substrate bonds. hCMEC/D3 cells were exposed to 0.25% of trypsin-EDTA.

**Immunofluorescence:** After exposure to EGTA, hCMEC/D3 cells grown on device were fixed with 4% paraformaldehyde in PBS pH 7.4, for 15 min at room temperature. Permeabilization was done using 0.25% Triton in PBS, for 10 min at room temperature and with a blocking step consisting of 1% BSA in PBST (0.05% Tween 20 in PBS), for 30 min at room temperature. Mouse monoclonal anti-claudin 5 and rabbit polyclonal anti-ZO1 were used at 5 µg/mL (Invitrogen), in 1% BSA in PBST for 1 h at room temperature. Monolayers were then incubated for 1 h at room temperature with the secondary antibodies Alexa Fluor 488 goat anti-mouse IgG and Alexa Fluor 568 goat anti-rabbit (Molecular Probes). Finally, the cells were incubated for 5 min at room temperature with Fluoroshield with DAPI (Sigma Aldrich), mounted and examined with a fluorescent microscope (Axio Observer Z1, Carl Zeiss).

**CellZscope Measurements:** were carried out as in chapter 3 section 3.2.2.

### 3.3 Results and Discussion

#### 3.3.1 / Microscale OEET for monitoring toxicity to BBB

In an OEET, the drain current ( $I_{DS}$ ) between the source and drain electrodes is modulated by the application of a gate voltage. The mechanism for current modulation relies on the electrochemical doping and dedoping of a degenerately doped conducting polymer film in contact with an electrolyte [11]. A positive gate voltage between the gate and the source induces a flux of positive ions into the transistor channel, dedoping the polymer film and reducing conductivity (Figure 5.2a, 5.2b). The  $I_{DS}$  response to a sinusoidal gate voltage pulse is directly correlated with the magnitude of ionic flux into the conducting polymer. In the present device architecture (Figure 5.2c), the barrier properties of the cell layer grown directly on OEET modify this ionic flux.

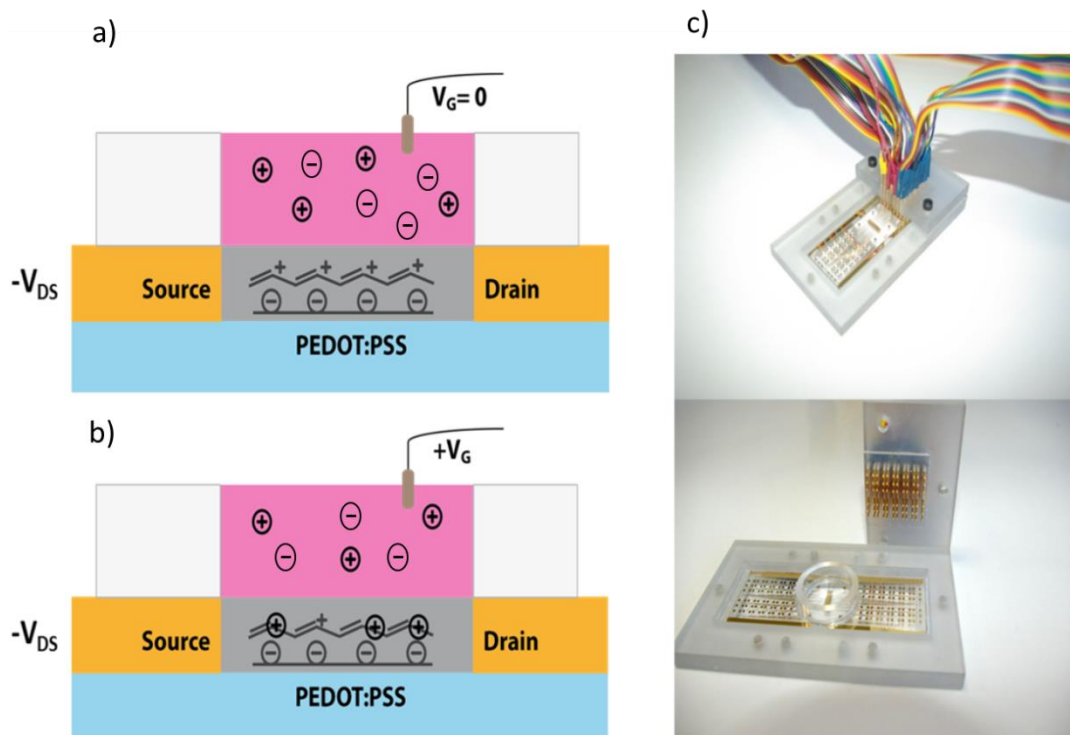


**Figure 5.2:** (a). Schematic of the OEET at  $V_g=0$ . PEDOT:PSS conducting polymer is connected by gold source and drain contacts. Ions are present and stay in the biological media (in pink). (b) At  $V_g > 0$ , the electric field push the positive ions from the media into the PEDOT:PSS. The measured source drain current ( $I_{DS}$ ) is thus decreased. (c). Pictures of the OEET made on a 3 x 1 inches glass substrates. A dedicated 3D printed holder with embedded pogo pins was used to probe the OEETs.

The OEET can be modeled by an association of resistances and capacitance as described in Figure 5.3. As already described by Bernards and coworkers [16], OEETs may be represented by a resistance ( $R_s$ ) and a capacitance ( $C_d$ ) in series. Another resistance ( $R_{med}$ ) for the media and a capacitance ( $C_p$ ) for the gate electrode / electrolyte interface were used.

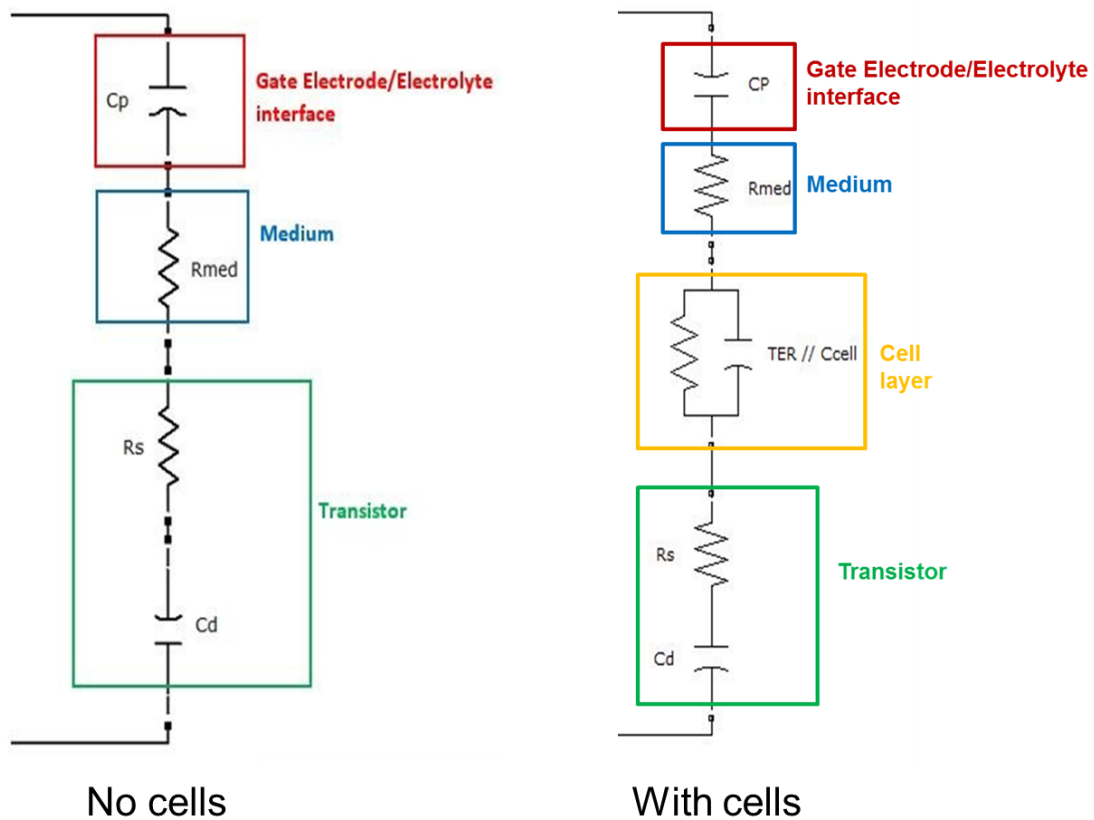
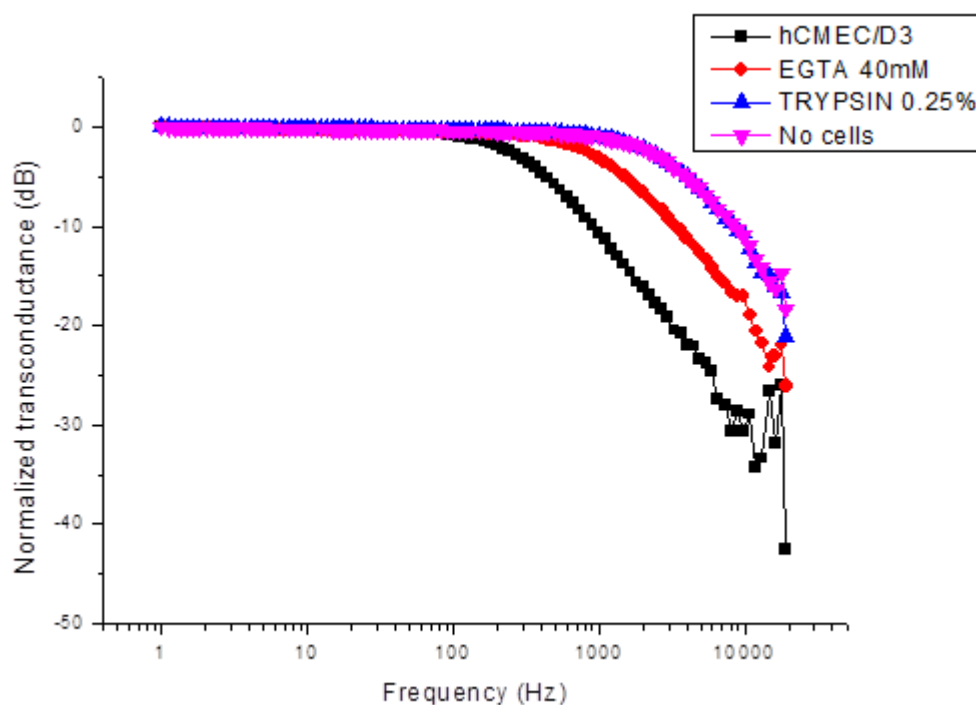


**Figure 5.3:** Electrical modeling of the OEET with (right) and without (left) cell layer.

The presence of the cell layer between the gate and the conducting polymer is represented by a resistance and a capacitance in parallel ( $TER // C_{cell}$ ) as seen in Figure 5.3. The addition of this RC module will modify the frequency response of the system when subject to  $V_{GS} = 0.01 \sin(\omega t)$ . It will act as a low pass filter that will reduce the recorded cut off frequency. This impedance technique has already been used for barrier tissue characterization [17]. In contrast to current impedance techniques based on electrodes only, we use a transistor configuration in order to benefit to the inherent amplification of such devices. It improves the signal quality and thus the signal to noise ratio.

Figure 5.4 shows the OECT normalized response as a function of frequency in the presence and absence of a cell layer. Without BBB cells, the OECT frequency cut-off response is around 2380 Hz, which is associated with a high ionic flux through the electrolyte and into the polymer channel (Figure 5.4a). Indeed, in the absence of a cell layer, ions are not hampered from dedoping the conducting polymer. The cut-off frequency is thus only attributed to the intrinsic property of the OECT which stays constant over the full experiment. However, when we measure the OECT with BBB cells, the frequency cut-off response is reduced 285 Hz, because in this case, the presence of the cells slows down the ionic flux. On introduction of 40 mM EGTA onto the BBB cell monolayer, the frequency cut response of the OECT changes, returning to a value of 737 Hz. When EGTA is added to healthy BBB cells, the frequency cut-off response is higher, indicating a disruption of functional components in the cells that block ion flow, which we attribute to the cell barrier properties (Figure 5.4b).

a)



b)

Frequency Cut (Hz)	
No Cells	2380 ± 354
h CMEC/D3	285 ± 73
h CMEC/D3 + EGTA	737 ± 302
h CMEC/D3 + Trypsin	2572 ± 152

**Figure 5.4:** OECT frequency response. (a) Monitoring of frequency, without cells (purple), with cells (black), on addition of 40mM of EGTA (red), on addition of 0.25% of trypsin (blue). (b) Table of frequency cut off values.

Videomicroscopy observation of BBB cell monolayer carried out during the experiment in Figure 5.5 does not show any difference with and without EGTA, in both cases, we can observe a nice confluent monolayer of BBB cells (Figure 5.5b, 5.5c), confirming that the cells are present on the surface of the device even with EGTA treatment. Complete disruption of the BBB cell monolayer was achieved by treating with Trypsin-EDTA, solution known to detach cell layers as evidenced in Figure 5.5d. A slight increase in the frequency cut off value was observed, indicating that the detachment of the cells did not further alter ion flow to the device.

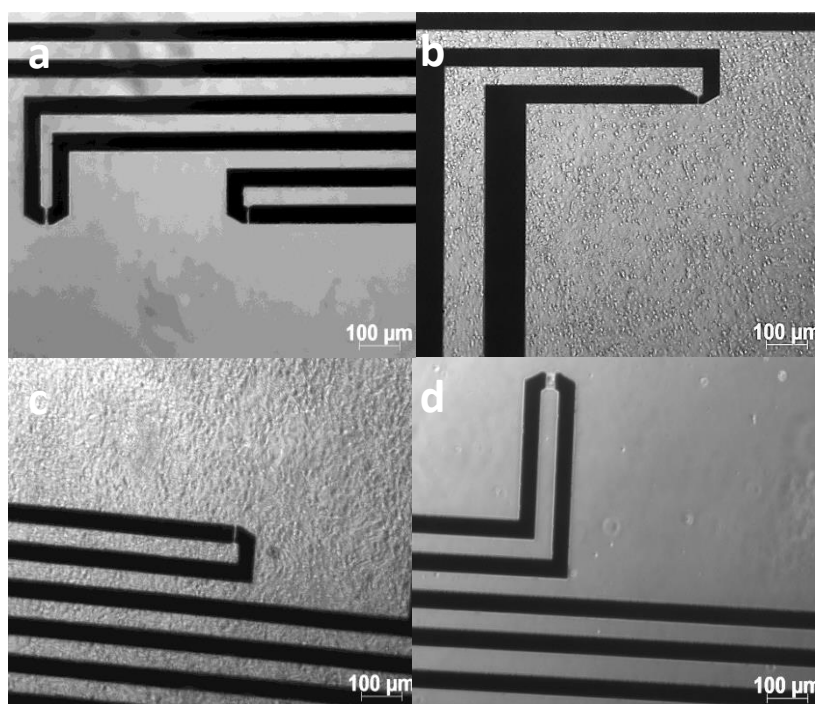


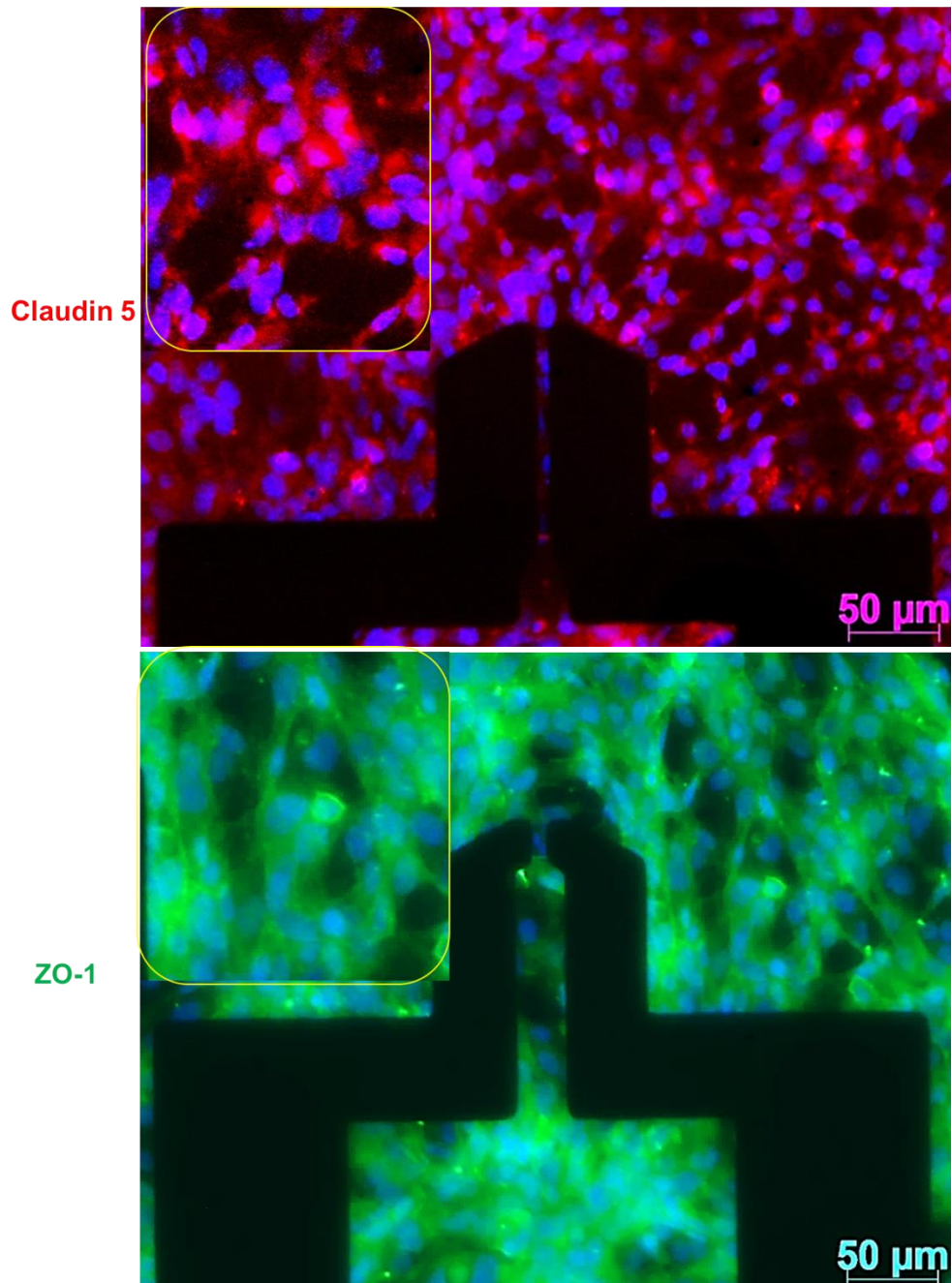
**Figure 5.5:** Light microscope images of device at day 8 (a). Without h CMEC/D3 cells (b). With healthy h CMEC/D3 cells (c). After EGTA (d). After Trypsin.

OECT results were compared to barrier tissue assessment using a standard biological technique: immunofluorescence staining. Immunofluorescence staining of junctional proteins, although not a technique adaptable with high throughput screening, is still a reference technique for assessing barrier tissue integrity since it allows localization of key proteins known to be essential for the barrier properties. Figure 5.6 shows the immunofluorescence staining of tight junction proteins carried out after 15 min of exposure to EGTA using antibodies against claudin-5 and ZO-1. Cell nuclei were

stained with DAPI. Control staining on h CMEC/D3 cells without EGTA exposure shows a clear localization of claudin-5 and ZO-1 around the cellular periphery (Figure 5.6a). In presence of EGTA, there was a disorganization of proteins and a diffuse pattern of claudin-5 and ZO-1 (Figure 5.6b).

a)

Without EGTA



b)

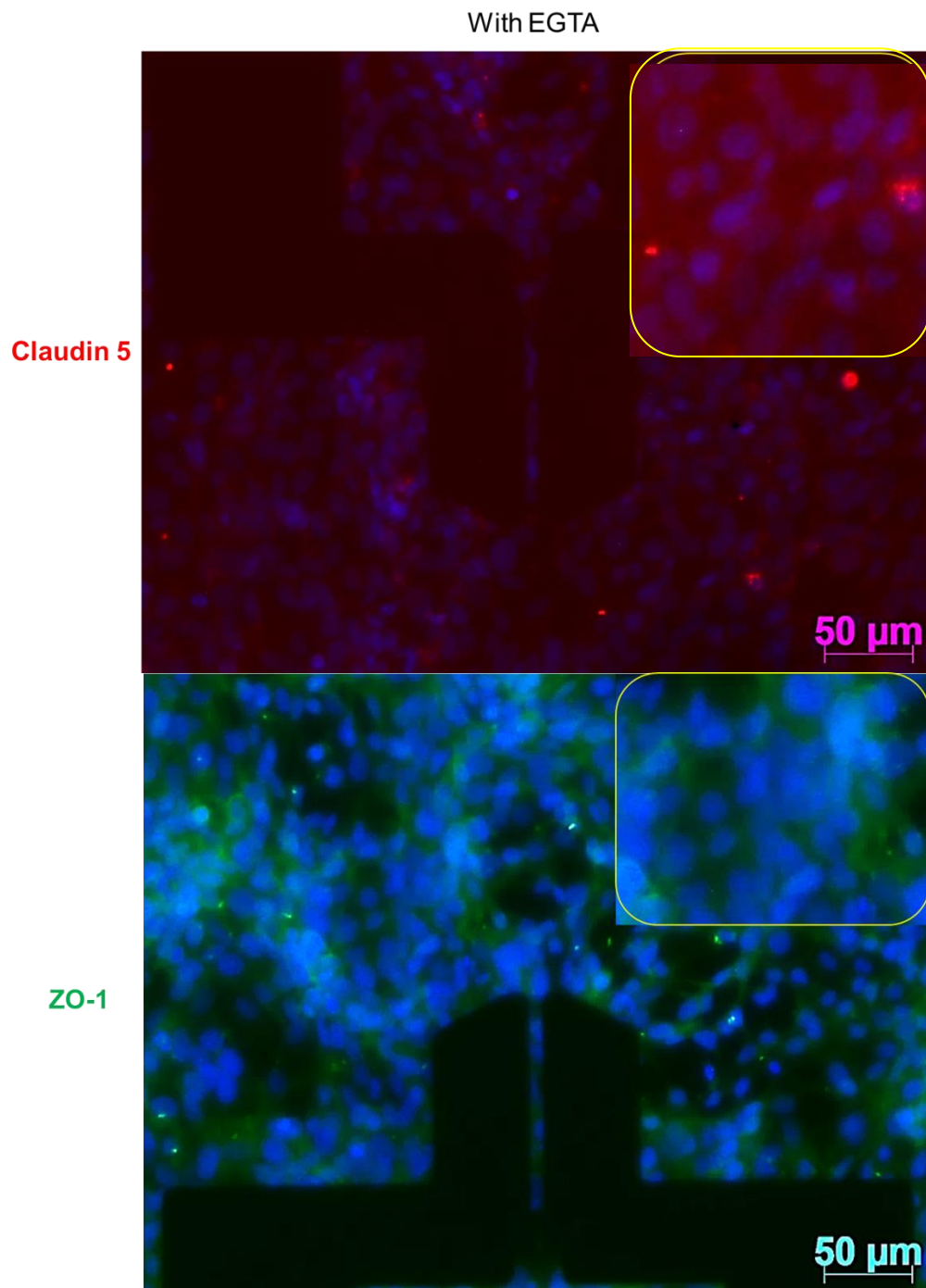
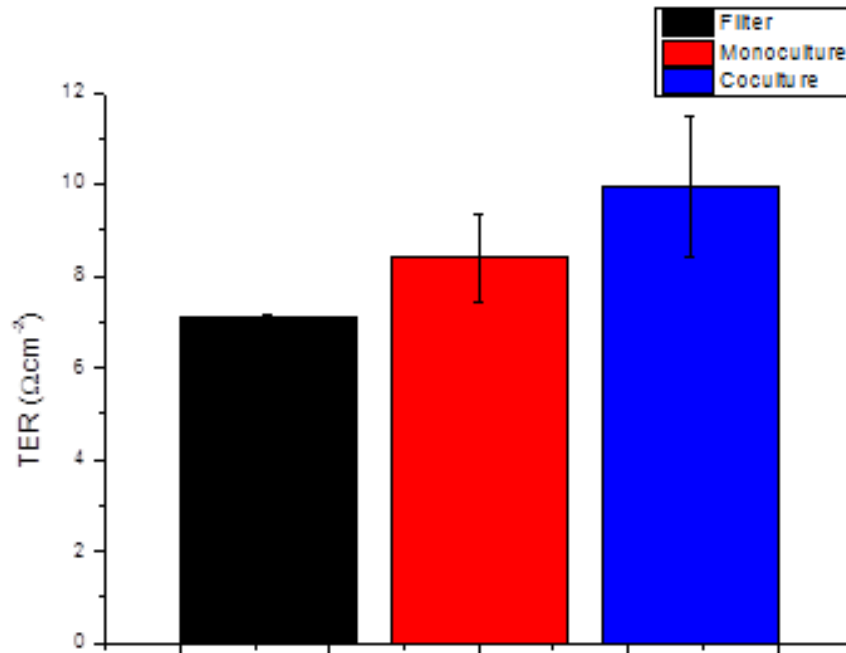


**Figure 5.6:** Immunofluorescence of proteins in BBB monolayer upon exposure to EGTA. (a) Monolayers were exposed to 40mM of EGTA for and then stained with antibodies against apical junction proteins. (b) Monolayers non exposed to EGTA.

### 3.3.2 OECT as a Better Sensing method for monitoring BBB Cells

Although the BBB has been reported to have high TER in some *in vivo* measurements [18], many of the current models used have considerably lower TER values. Improvement of the models will be required and a large number of research groups are devoted to exploring different parameters including cell type, cell environment, co-cultures etc. In the meantime however, it is necessary to have a method to assess and evaluate the *in vitro* models with sufficient dynamic range to monitor both high and low TER values. As seen in Figure 5.7a, the commercially available CellZscope setup (NanoAnalytics GmbH) poorly detects the BBB barrier properties with an average maximum measured TER of  $10 \Omega \cdot \text{cm}^2$ . This value is close to the value of filters alone ( $7 \Omega \cdot \text{cm}^2$ ). The values are in the noise range of the setup and are thus not reliable. The CellZscope data does not show any difference in presence or absence of BBB cells, and further, there is no difference when cells are in monoculture or co-cultured with neurons (Figure 5.7b). In contrast, our approach showed a large difference between cells and no cells. One explanation is our use of a transistor – which amplifies the measured signal - instead of simple electrodes as in the CellZscope. The other explanation comes from the device geometry / measurement principle. For the CellZscope, cells were grown on biological filters. As it is difficult to obtain high quality optical images of live cells on filters, it was hard to confirm or invalidate the appropriate and confluency of the BBB cells. The roughness of the filter membrane or the pore size could influence – in a detrimental manner – the cell layer quality and tightness; which results in a low TER measurement. With a filter configuration, a small inhomogeneity or hole in the cell layer is enough to have most the ions going through and thus short cut the measurement.

a)



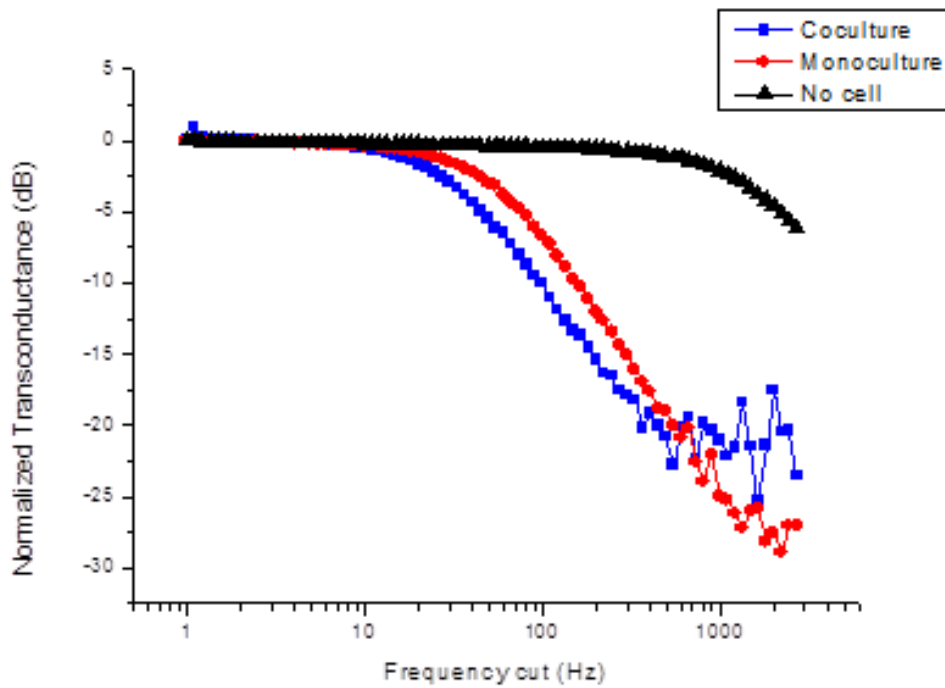
b)

TER (Ω.cm <sup>2</sup> )	
No Cell	7 ± 0.0
Monoculture hCMEC / D3	8 ± 0.9
Co-culture hCMEC / D3 + CN	10 ± 1.5

**Figure 5.7:** TER of h CMEC/D3 cells and the filter alone using the CellZscope at day 8 (N=3). (a) TER at day 7 for monoculture (red), co culture with neuron (blue) and without cells (black). (b) Table of TER values.

Figure 5.8 shows the OECT normalized response as a function of frequency in the presence of monoculture and co-culture with CN. The frequency cut-off of the co-culture model is slower than the monoculture model. In this case, the presence of CN, improved h CMEC/D3 barrier properties; hCMEC/D3 cultured with CN, slowed down more efficiently the ionic flux.

a)



b)

Frequency Cut (Hz)	
No Cell	2000
Monoculture hCMEC / D3	74
Co-culture hCMEC / D3 + CN	45

**Figure 5.8:** OECT frequency response at day 8. (a) Monitoring of frequency, without cells (black), in monoculture condition (red), in co culture with neuron (blue). (b) Table of frequency cut off values.

With the OECT device, cells were in direct contact with the flat and smooth substrate [19]. The optical images (Figure 5.5) prove the proper cell growth and the layer formation. Another possible aspect is the close vicinity of the cells to the sensing area

which improves the sensitivity of the measurement. Even in the presence of some dead cells or not fully confluent layer, the OECT will still detect a change in measurement. Overall, growing cells directly onto the OECT turns out to be a better system configuration, especially for BBB cell which present a low TER and are very sensitive to growing environment / condition. OECT's results show an important difference without cell (2000Hz) and with BBB cells (74Hz) (Figure 5.8a). In addition the system is capable of detecting changes in culture, going from 74Hz in monoculture to 45 Hz in co-culture (Figure 5.8b). Further experiments are necessary to validate these results.

The ability to take micro-optical images allows keeping track of the cells growth. In contrast to other electrical monitoring techniques, the OECT is compatible with high resolution optical imaging, both for bright-light images and fluorescence images. On top of the inherent amplification, the easy fabrication and geometry versatility of the OECT results in a larger dynamic range of barrier properties characterization.

### 3.4 Conclusion

We have demonstrated for the first time the ability to use OECT in an impedance configuration in order to characterize BBB tissue. We propose that the measurement of resistance across the membrane provides a robust measurement of BBB integrity. Compared to conventional electrode-based systems, the OECT offers the advantage of a direct amplification of the recorded current. This device provides a better resolution than commercially available setups. It is a cheap and disposable device. The biocompatibility of the PEDOT: PSS enables direct growth of the cells allowing an increase in the sensitivity of the measurement.

It must be cautioned that this is a novel concept that requires further investigation and potentially, to reach high dynamic measurement range (measure low to high ion flux through the cell layer) some optimization of the OECT is required.

### 3.5 Bibliography

1. Ballabh, P., A. Braun, and M. Nedergaard, *The blood-brain barrier: an overview: structure, regulation, and clinical implications*. *Neurobiology of Disease*, 2004. **16**(1): p. 1-13.
2. Hawkins, B.T. and T.P. Davis, *The blood-brain barrier/neurovascular unit in health and disease*. *Pharmacol Rev*, 2005. **57**(2): p. 173-85.

3. Stamatovic, S.M., R.F. Keep, and A.V. Andjelkovic, *Brain endothelial cell-cell junctions: how to "open" the blood brain barrier*. *Curr Neuropharmacol*, 2008. **6**(3): p. 179-92.
4. Hawkins, R.A., et al., *Structure of the blood-brain barrier and its role in the transport of amino acids*. *J Nutr*, 2006. **136**(1 Suppl): p. 218S-26S.
5. Brown, R.C. and T.P. Davis, *Calcium modulation of adherens and tight junction function: a potential mechanism for blood-brain barrier disruption after stroke*. *Stroke*, 2002. **33**(6): p. 1706-11.
6. Janigro, D., *Are you in or out? Leukocyte, ion, and neurotransmitter permeability across the epileptic blood-brain barrier*. *Epilepsia*, 2012. **53 Suppl 1**: p. 26-34.
7. Prozialeck, W.C., et al., *Epithelial barrier characteristics and expression of cell adhesion molecules in proximal tubule-derived cell lines commonly used for in vitro toxicity studies*. *Toxicol In Vitro*, 2006. **20**(6): p. 942-53.
8. Balda, M.S., et al., *Functional dissociation of paracellular permeability and transepithelial electrical resistance and disruption of the apical-basolateral intramembrane diffusion barrier by expression of a mutant tight junction membrane protein*. *J Cell Biol*, 1996. **134**(4): p. 1031-49.
9. Eigenmann, D.E., et al., *Comparative study of four immortalized human brain capillary endothelial cell lines, hCMEC/D3, hBMEC, TY10, and BB19, and optimization of culture conditions, for an in vitro blood-brain barrier model for drug permeability studies*. *Fluids Barriers CNS*, 2013. **10**(1): p. 33.
10. Tria, S.A., et al., *Sensing of barrier tissue disruption with an organic electrochemical transistor*. *J Vis Exp*, 2014(84): p. e51102.
11. Jimison, L.H., et al., *Measurement of barrier tissue integrity with an organic electrochemical transistor*. *Adv Mater*, 2012. **24**(44): p. 5919-23.
12. Tria, S.A., et al., *Validation of the organic electrochemical transistor for in vitro toxicology*. *Biochim Biophys Acta*, 2013. **1830**(9): p. 4381-90.
13. Tria, S., et al., *Sensing of EGTA Mediated Barrier Tissue Disruption with an Organic Transistor*. *Biosensors (Basel)*, 2013. **3**(1): p. 44-57.
14. Xue, Q., et al., *A novel brain neurovascular unit model with neurons, astrocytes and microvascular endothelial cells of rat*. *Int J Biol Sci*, 2013. **9**(2): p. 174-89.
15. Khodagholy, D., et al., *High transconductance organic electrochemical transistors*. *Nat Commun*, 2013. **4**: p. 2133.
16. Bernardis, D.A. and G.G. Malliaras, *Steady-state and transient behavior of organic electrochemical transistors*. *Advanced Functional Materials*, 2007. **17**(17): p. 3538-3544.
17. Benson, K., S. Cramer, and H.J. Galla, *Impedance-based cell monitoring: barrier properties and beyond*. *Fluids Barriers CNS*, 2013. **10**(1): p. 5.
18. Grant, G.A., N.J. Abbott, and D. Janigro, *Understanding the Physiology of the Blood-Brain Barrier: In Vitro Models*. *News Physiol Sci*, 1998. **13**: p. 287-293.
19. Marzocchi, M., et al., *Conducting polymer thin films as substrates for cell cultures*. *MRS Online Proceedings Library*, 2014. **1624**: p. null-null.

# Chapter 6

---

## Conclusion and Outlook

---

In this thesis, three different BBB models were evaluated in order to be integrated with OECT device. First, we attempted to develop a BBEC model known to fully differentiate with respect to barrier properties in 4 day. While, these cells appear to form a confluent layer, the TER and Papp value with and without cell show little or no difference and in fact it may be argued that this barrier does not possess functional (tight) barrier properties. Nonetheless, we proceeded to use BBEC for further investigation of biocompatibility of the PEDOT based conducting polymers with these cell types. We show for the first time the possibility to combine CPs with an ECM in order to improve cell adhesion to the device.

In a renewed effort to develop an *in vitro* model of the BBB, we decided to focus on a human brain endothelial model, reported to reach high TER and have low permeability. To assess barrier property of these human BBB model, cells were co-cultured with astrocytes or neurons. The second model used was a commercial HBMEC primary cell. In this case, the ideal barrier function was not observed, possibly due to inhomogeneities in the cell coverage. The last model developed used an immortalized human brain endothelial cell, h CMEC/D3. As with the HBMEC model, inhomogeneities in coverage of cells seeded on filters can be an interpretation of the non-ideal results for this model. The integration of hCMEC/D3 with OECT in the filter configuration does not permit to detect the presence of cell and confirmed to us that the filter format was not the appropriate way to assess BBB integrity for our purposes.

The use of an inverted model where h CMEC/D3 are directly cultured on OECT device showed for the first time a robust measurement of BBB integrity. This hybrid configuration with planar OECT configuration and top gate, is able to distinguish the presence of BBB cell but also the disruption of this barrier in presence of EGTA. Further, preliminary data shows that the OECT is able to discriminate when BBB cells are in monoculture or co-cultured conditions.

Future work will be required to solidify the OECT results in hybrid configuration. Moreover, the flexibility of the device permits some optimization in order to increase the potential of high-throughput screening and the device operation time for the use with sensitive cell like BBB cell. In summary the results presented here represent a great future potential of the OECT as a diagnostics method for integration with models of the BBB.